# FIBRE-COMPATIBLE MODELOCKED LASERS AT 1.5MM

David Burns

A Thesis Submitted for the Degree of PhD
at the
University of St Andrews

1991

Please use this identifier to cite or link to this item:
http://hdl.handle.net/10023/14158

# FIBRE-COMPATIBLE MODELOCKED LASERS AT 1.5μm

Thesis submitted for the degree of Doctor of Philosophy to the University of St.Andrews

by

David Burns, B.Sc.

J.F.Allen Physics Research Laboratories
Department of Physics and Astronomy
University of St.Andrews
North Haugh
St.Andrews, Fife
Scotland. KY16 9SS

## Declaration

I, David Burns, hereby certify that this thesis has been composed by myself, that it is a record of my own work, and that it has not been accepted in partial or complete fulfilment of any other degree or professional qualification. I was admitted to the Faculty of Science of the University of St.Andrews as a candidate for the degree of Ph.D on October 1986.

In submitting this thesis to the University of St.Andrews I understand that I am giving permission for it to be made available for use in accordance with the regulations of the University Library for the time being in force, subject to any copyright vested in the work not being affected thereby. I also understand that the title and abstract will be published, and that a copy of the work may be made and supplied to any *bona fide* library or research worker.

David Burns
February 1990

I hereby certify that the candidate has fulfilled the conditions of the Resolution and Regulations appropriate to the Degree of Ph.D.

W. Sibbett
Research Supervisor
February 1990

# Abstract

This thesis describes techniques for the generation of ultrashort optical pulses using semiconductor lasers. Active modelocking through gain modulation is applied to 1.5μm InGaAsP semiconductor lasers which utilise microlensed optical fibres as external-cavity components, and tunable optical pulses of ~5ps duration have been generated. Particular attention has been given to suppression of the noisy subpulse features associated with low-frequency modelocked semiconductor lasers. This has led to two suppression methods applicable to symmetric (or balanced) and asymmetric cavity configurations, allowing the generation of clean, single feature short pulses of 7-10ps duration with peak powers in excess of 300mW. The physical phenomena relating to such processes will be outlined. Further amplification of these pulses using an erbium-doped fibre amplifier has resulted in output peak powers in the 5W range.

A study of the phase-noise characteristics of these modelocked laser systems was undertaken using a high-speed photodetector and wide-band spectrum analyser arrangement. This characterisation allowed improvements in the rms pulse timing jitter from >2ps to below 300fs in the frequency range 50-5000Hz.

Novel modelocked laser configurations were also constructed where the cavity components included both a semiconductor amplifier and an erbium-doped fibre amplifier. Linear and ring hybrid lasers were investigated with resultant pulse durations as short as 3ps with high peak power and excellent stability.

CW and mechanical Q-switched doped fibre lasers were configured in diffraction grating tuned cavities with high output coupling (R=4%). Unprecedented output powers of up to 700mW tunable over ~100nm around 1.55μm, and 800mW tunable around 1.08μm were obtained. Also the value of 800W peak power for the 80ns output pulses from the Q-switched erbium-doped fibre laser amounts to the most intense pulse created thus far from any fibre laser device. Optimisation of the total tuning range attainable from erbium-doped fibre lasers via length tuning resulted in a variety of nonlinear phenomena, namely self Q-switching and optical bistability at the long wavelength tail of the tunable range.

Heather and Julie

# FIBRE-COMPATIBLE MODELOCKED LASERS AT $1.5\mu m$

1. INTRODUCTION

2. EXTERNAL-CAVITY SEMICONDUCTOR LASERS

3. ACTIVE MODELOCKING OF InGaAsP SEMICONDUCTOR LASERS

4. SUBPULSE SUPPRESSION IN MODELOCKED InGaAsP SEMICONDUCTOR LASERS

5. PHASE NOISE MEASUREMENTS OF AN ACTIVELY MODELOCKED InGaAsP SEMICONDUCTOR LASER SYSTEM

6. AMPLIFICATION OF ULTRASHORT PULSES USING AN ERBIUM-DOPED FIBRE AMPLIFIER

7. THE CONTROLLED AMPLIFIER MODULATOR

8. RARE EARTH, DOPED FIBRE LASERS

9. CONTROLLED AMPLIFIER MODELOCKED LASERS

10. GENERAL CONCLUSIONS

Appendix A. ERBIUM-DOPED FIBRE FLUORESCENCE MEASUREMENTS

# CHAPTER 1

# INTRODUCTION

## 1.1 Introduction

The main accent of this thesis is the generation of ultrashort pulses from semiconductor lasers for use in single-mode, silica-optical fibre telecommunications systems. This introductory chapter has therefore been devoted to the principles of laser oscillation in semiconductor materials, and the major developments in device structure designs that are implemented to provide optimised performance. The basic principles and techniques of laser modelocking and the diagnostic systems used to evaluate such sources will also be outlined.

## 1.2 Semiconductor theory

### 1.2.1 Band structure of solids

The nearly-free electron model[1] of matter in the solid state leads to the introduction of energy gaps in the continuum of electronic energy states implied by simpler theories in which the periodic potential of the ion cores in the lattice has been neglected. The electron population of such allowed bands determine the electrical and optical properties of solids. All the low-lying energy bands have fully occupied states and hence do not play a major role in the physical properties of the material. Such properties are essentially determined by the two highest bands which are designated the valence and conduction bands. A general consideration of the populations of these two highest energy bands allows categorisation of the elements of the periodic table, in their solid state, into one of four types. These classes are denoted metals, semi-metals, semiconductors, and insulators. In a metal the conduction band is highly populated with electrons (somewhere between 10 and 90%), whereas an insulator has a completely full valence band and an empty conduction band, thus the electrons of the insulator are immobile, resulting in high values of electrical resistivity. At absolute zero pure semiconductors will normally behave as insulators, their distinctive properties[2] being revealed in the main by thermal excitation and the addition of impurities into the crystal lattice. The energy band diagram of a semiconductor at a given temperature will show either small, but significant, population of the conduction band, or alternatively a small proportion of unoccupied states at the top of the valence band.

The parabolic band approximation can be used to understand the essential physics of laser operation in semiconductors, and from this the energy versus wavevector and density of states curves of figure 1.1 are obtained. The electron, and hole, distributions within the energy bands are defined by Fermi-Dirac statistics, which give the occupation probability of an allowed electron state of energy E as;

$$f_e(E) = \frac{1}{\exp\frac{(E-F_e)}{kT} + 1}$$

where $F_e$ is the Fermi energy, k is Boltzmann's constant and T is temperature. Figure 1.1b shows the conduction band electron distribution at 0K and at some finite temperature T.

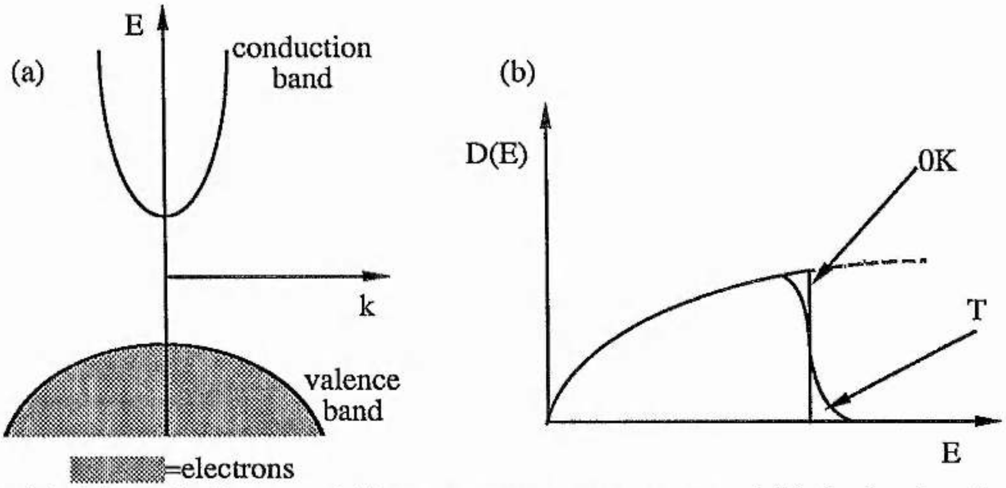

Figure 1.1 Schematic diagram of (a) energy versus wavevector and (b) the density of states for a semiconducting medium

The Fermi energy, $F_e$, is located at an energy where the electron (or hole) occupation probability equals 0.5. Also the concept of a quasi-Fermi level is frequently used in reference to the principles of semiconductor lasers, and is defined in the same manner as the Fermi level but relates to the distributions in each band rather than for the system as a whole.

### 1.2.2 Basic semiconductor laser theory

It is believed that Johann Von Neumann was the first person to treat the idea of a semiconductor light amplifier essentially correctly in 1953[3]. Several individuals were working independently on the concept of the semiconductor laser during the middle and late 1950's and early 1960's, prior to the first demonstration of the semiconductor injection laser. This occurred almost simultaneously by four research groups[4] in late 1962 and historical reports by the leaders of the four groups can be found in reference 3.

The details pertinent to laser action in semiconductor materials can be understood from consideration of simplified energy band diagrams. Figure 1.2 represents the energy band populations for three extreme cases of semiconductor, that is (a) with no doping, and with high concentrations of n and p type dopants (b and c). A semiconductor with such a high doping level is termed degenerate.

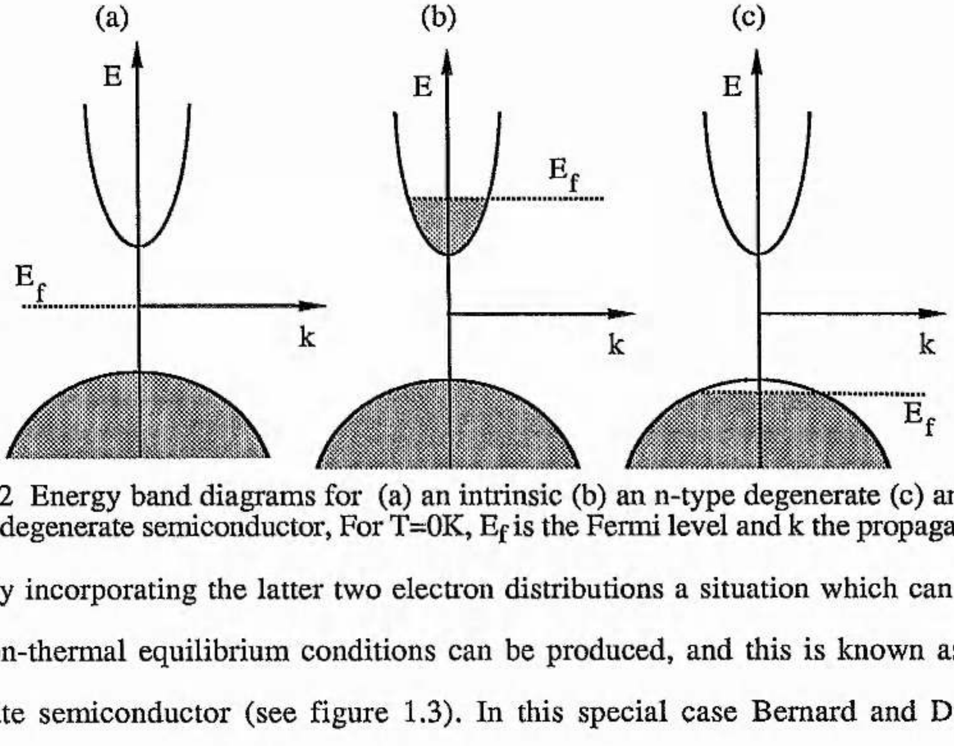

Figure 1.2 Energy band diagrams for (a) an intrinsic (b) an n-type degenerate (c) and a p-type degenerate semiconductor, For T=0K, $E_f$ is the Fermi level and k the propagation vector

By incorporating the latter two electron distributions a situation which can only exist under non-thermal equilibrium conditions can be produced, and this is known as a doubly degenerate semiconductor (see figure 1.3). In this special case Bernard and Duraffourg[5] established that if an incident photon satisfies the condition;

$$E_g < h\nu < E_{FC} - E_{FV}$$

where $E_{FC}$ and $E_{FV}$ are the quasi-Fermi levels of the conduction and valence bands respectively, and $h\nu$ is the photon energy, then it can induce stimulated radiative recombination of conduction band electrons with valence band holes. Thus optical gain can occur for all transitions with energies less than the separation of the quasi-Fermi levels. Within this gain medium it is only required that a suitable resonator be provided for laser oscillation to be possible. Figure 1.3 also indicates that the semiconductor laser can be represented as a four-level laser system. The Fermi levels exist well into the bands so the resultant optical gain is exhibited over an extended wavelength range.

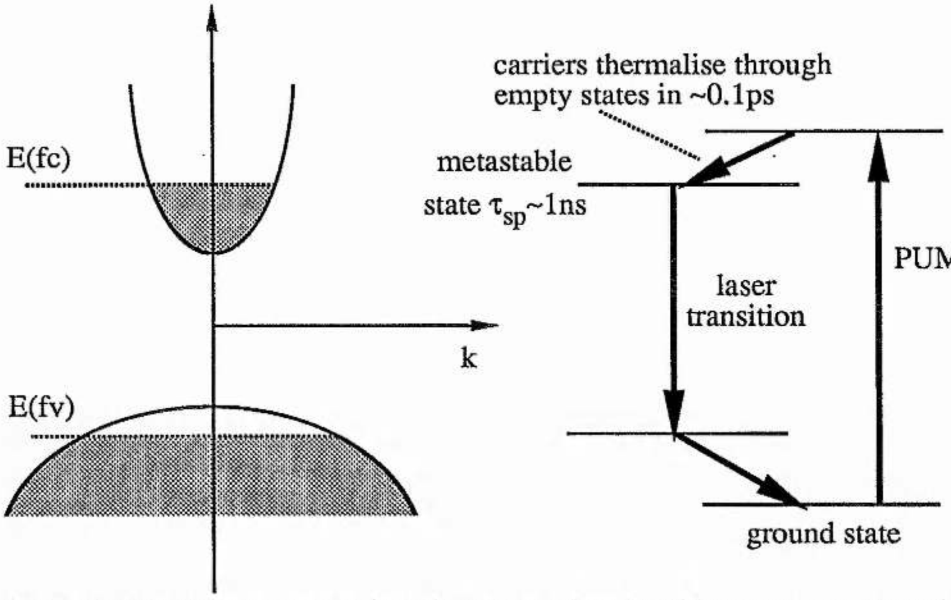

Figure 1.3 The doubly degenerate semiconductor as a four-level laser system. Note that the laser states are not the discrete states indicated but are smeared in energy.

The doubly degenerate semiconductor gain medium can be prepared in various ways, the most simple being by optical pumping. In this case incident short wavelength light can promote valence band electrons high into the conduction band, where they relax to the band minimum via lattice scattering. Holes also accumulate at the top of the valence band through similar scattering processes. With sufficient pumping the doubly degenerate case can be created and further pumping will allow a significant degree of population inversion by which the laser oscillation threshold can be established. This laser oscillation threshold being a function of the reflectivities of the resonator mirrors used. Optically pumped semiconductor lasers have been successfully demonstrated[6] but the most convenient method of creating the situation of figure 1.3 is by forward biasing a pn junction as shown in figure 1.4. Such a laser is commonly referred to as a semiconductor diode laser, or alternatively an injection laser[7].

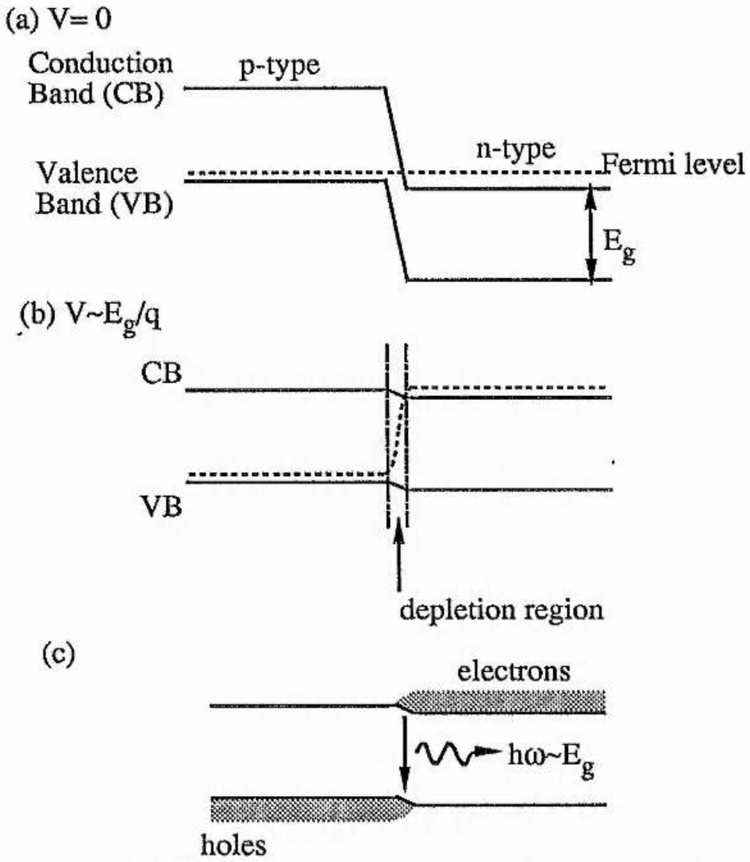

Figure 1.4 Energy diagram of a pn junction with (a) zero bias, and (b) forward-biased. (c) With the correct bias applied a doubly degenerate region, exhibiting optical gain can be produced.

Of the many semiconductors available, it is only in direct bandgap materials that laser action is possible. This is because in an indirect bandgap semiconductor the transition probability is small due to the requirement that the crystal momentum should be conserved. Therefore phonon involvement is necessary for interband recombination in indirect semiconductors and this can be regarded as parasitic. Additionally, reabsorption of the laser radiation would be approximately as strong as the induced emission[8]. The direct bandgap semiconductor GaAs was used for the first injection lasers[4]. However, these early lasers had very high threshold current densities and hence could only operate continuously at cryogenic temperatures, and were thus impractical devices.

### 1.2.3 Heterojunction semiconductor lasers

The semiconductor diode laser came of age when heterojunctions[9] and stripe geometry contacts[10] were employed to confine the current flow and the subsequent optical radiation produced to a small active region. By employing such confinement techniques the current density necessary for laser operation was reduced and continuous-wave operation at room temperature was achieved[11]. The energy-band diagram of a double heterojunction (DH) laser is illustrated in figure 1.5.

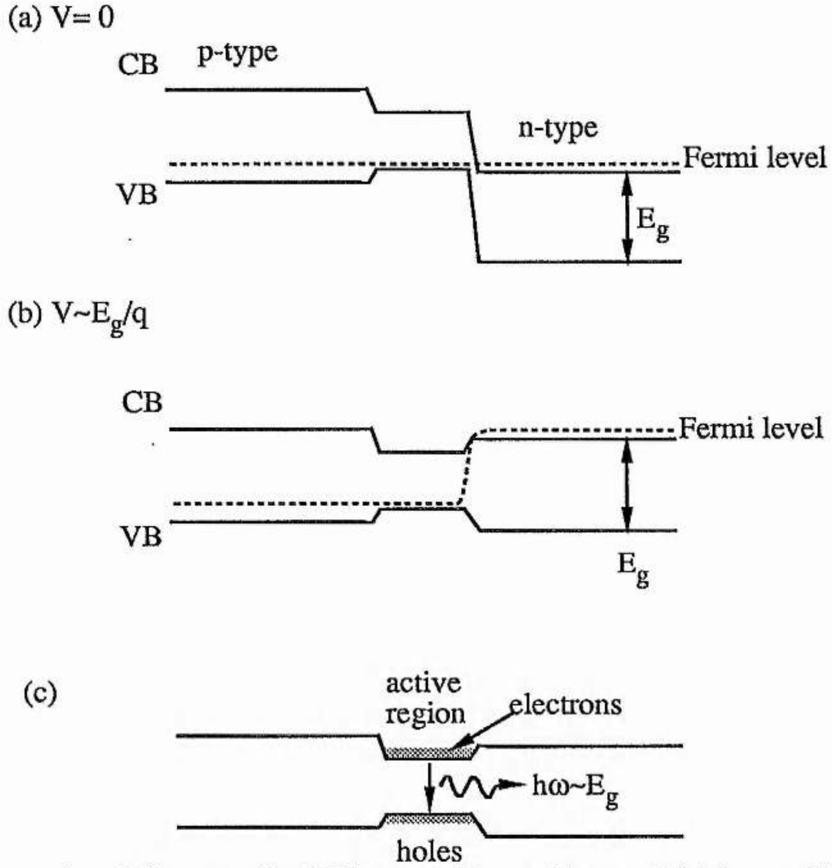

Figure 1.5 Energy-band diagram of a DH laser at (a) zero bias, and (b) forward bias.
(c) Heterobarriers confine the carriers to the active region where they can recombine radiatively .

With forward biasing, electrons and holes are injected into, and confined between the heterojunctions such that optical gain can be exhibited within a localised region (the active region). Prepared in this way the device can act as a laser amplifier, or a broadband spontaneous emission source (LED). To form a laser oscillator positive optical feedback must be introduced to the system. Although for most lasers this is normally achieved using highly reflective cavity mirrors, in the case of the semiconductor material another resonator option is available. By cleaving the semiconductor along the (110) crystal plane a perfectly parallel resonator can be formed, and owing to the large refractive index of GaAs, the facet has a reflectivity of;

$$R = [\ (n-1)\ /\ (n+1)\ ]^{2} \sim 30\%$$

for n=3.5, with a similar value being obtained for InP system lasers. This degree of facet reflectivity is sufficient for oscillation in most semiconductor lasers since the material gain can be very high and thus the large output coupling can be accommodated.

Since the refractive index of a semiconductor is inversely proportional to the magnitude of the energy gap, the refractive index profile in the direction perpendicular to the junction (see figures 1.6(a) and (b)) gives the DH laser the optical features of a slab waveguide. The difference in refractive indices of the active region and the cladding regions is usually ~5% and so the confinement of the optical field to the active region can be very good (see figure 1.6(c)).

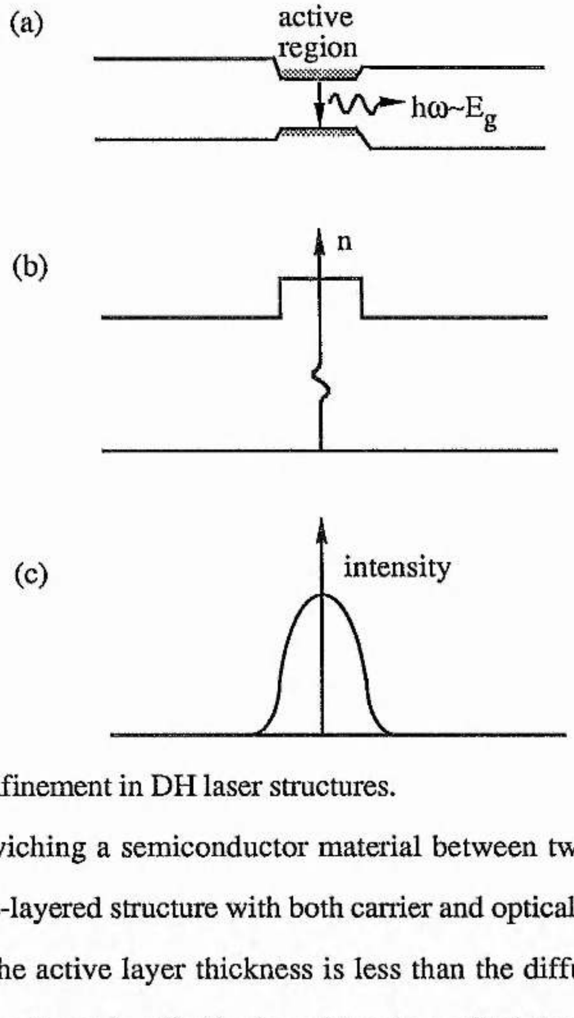

Figure 1.6 Optical confinement in DH laser structures.

Thus by sandwiching a semiconductor material between two layers of material with a larger bandgap, a three-layered structure with both carrier and optical confinement in a thin plane can be produced. [If the active layer thickness is less than the diffusion length of the injected carriers, then the active layer is effectively uniformly excited throughout its thickness.] The materials used to form such a structure have to be chosen carefully to ensure that the crystalline lattice parameter is constant across the heterojunction. This lattice matching prevents production and propagation of dislocations that result from the stress and strain in the crystal which would cause non-radiative recombination of injected carriers. In mismatched DH structures the radiative quantum efficiency is reduced and the threshold current density is increased. For acceptable laser media a mismatch of 0.1% is acceptable. This lattice matching condition places a restriction on the materials from which good heterojunction lasers can be produced, and Table 1 gives details of two alloy semiconductors from which room temperature CW lasers have been made.

| Active Region | Cladding Region | Useful Wavelength Range (μm) | Minimum Threshold Current Density, $J_{th}$ ($kA/cm^2$) | Substrate |
|---|---|---|---|---|
| $Ga_yAl_{1-y}As$ | $Ga_xAl_{1-x}As$ | 0.65 - 0.9 | 0.5 | GaAs |
| $In_{1-x}Ga_xAs_yP_{1-y}$ | InP | 1.1 - 1.6 | 0.5 | InP |

Table 1.1 Two alloy semiconductor lasers. For $In_{1-x}Ga_xAs_yP_{1-y}$ the lattice matching condition to InP is y=2.197x. $Ga_xAl_{1-x}As$ is lattice matched to GaAs for all x values (although it only has a direct gap for $0<x<0.38$).

### 1.2.4 Stripe-geometry DH lasers

To further improve device efficiency stripe-geometry contacts[12] can be employed to provide carrier confinement in the plane parallel to the junction. A stripe contact is etched into an insulating layer of $SiO_2$, so that the injected carriers are restricted to a narrow path through the laser structure. The stripe widths vary from 2 - 30 μm, where the narrower stripes are preferred to allow oscillation on a single transverse resonator mode. It is the narrow strip through the laser structure where the electron path intersects the confinement plane defined by the heterojunctions which constitutes the active laser volume. The area outwith this region sees no gain, and so the optical field is attenuated in this region, such that the light is confined to the stripe region where gain is available. This condition is normally referred to as gain guiding.

By using a stripe-geometry, double heterojunction structure the threshold current density necessary for laser oscillation is reduced. In addition the small rectangular aperture thus created is more suitable for efficient coupling of the radiation into external cavities and optical fibres, single filamentary laser action occurs, and single transverse mode operation can be achieved. One disadvantage due to diffraction from the very different dimensions of the exit aperture (typically 2μm x 0.2 μm) is that the beam can be highly elliptical.

The features outlined above are the basic characteristics of most semiconductor lasers, and in the next two sections a description of the key fundamental characteristics utilised to optimise the performance of modern semiconductor lasers is given.

### 1.2.5 Quantum well lasers

The predominant dependence of threshold current on active layer thickness is found to be $\frac{d}{\Gamma(d)}$, where d is the active layer thickness, and $\Gamma(d)$ is the confinement factor. For a thick active layer, $\Gamma \sim 1$ and the threshold is linearly dependent on d, because of the dependence of the gain on carrier density rather than the total number of carriers. It therefore follows that the active layer should be made as thin as possible to minimise the threshold current. However, for very thin active regions the threshold current begins to increase very rapidly because the confinement factor decreases as $d^2$. Thus for any DH laser there is a specific layer thickness which will minimise the threshold current. To affect further improvements in threshold current a set of separate confinement heterostructures[13] can be used such that the carriers and photons have separate means of confinement, and a constant confinement factor can be maintained whilst allowing the active layer thickness to be further reduced.

The technique of separate confinement heterostructures allows fabrication of active layers sufficiently thin that they give rise to quantum size effects[14]. In these so called 'quantum well' lasers the confinement of electrons in one dimension results in a quantisation of the allowed energy levels. The density of states is changed from the usual parabolic dependence to a step-like function, as illustrated in figure 1.7. The threshold current density of 'state of the art' QW lasers[15] can be as low as 0.1kA/cm$^2$, which is equivalent to threshold currents of the order of a milliampere.

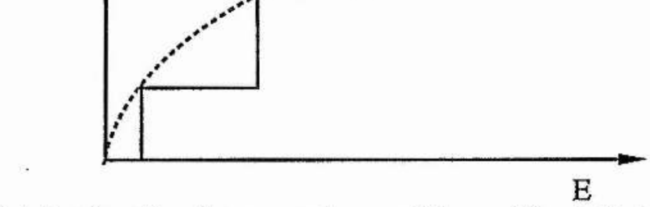

Figure 1.7 Density of states function for a quantum well laser. The dotted line indicates the density of states for a bulk semiconductor.

Quantum well lasers have now become the standard type of commercial GaAs/AlGaAs laser where usually a multiple quantum well active region is employed. Quantum well lasers have also been demonstrated in InGaAsP/InP[16]. It is clear that these technologies will become increasingly widespread and are being implemented in the development of quantum wire and quantum box devices. For these structures threshold currents in the region of microamps have been projected[17].

### 1.2.6 Lateral confinement-index guided lasers

The simplest practical semiconductor laser structure is the double heterostructure laser utilising stripe-geometry contacts as mentioned previously. In this 'archetype' laser structure current diffusion from under the contact defines the active region and gain guiding of the optical field in the plane parallel to the junction plays a crucial role. As a consequence these lasers have high threshold currents and are prone to excitation of multiple transverse modes in the plane of the junction. Also astigmatism, self-pulsations, and restricted high temperature performance are problems associated with gain guided lasers.

All of the detrimental features of stripe geometry lasers can be substantially reduced by the introduction of some form of imposed refractive index variation in the lateral structure of the device. Such index guided lasers are usually classified, dependent on the method inducing the index step, as weak or strong index guided lasers. Weak index guiding is achieved by introducing lateral variations of refractive index in the confinement, or cladding layers whereas strongly index guided lasers have an active volume which is completely buried in wide band-gap, low index material (hence the term buried-heterostructure laser). Many examples of such structures are detailed in the literature[18] so only the two structures used in this work will be described here.

#### 1.2.6.1 The ridge waveguide laser - weak index guiding

The structure of a 1.5μm InGaAsP/InP ridge waveguide laser[19] is shown in figure 1.8(a). In this structure the ridge provides the loading for weak index guiding and also acts as a narrow current confining stripe. Due to coupling of the optical field generated in the active region to the ridge the effective lateral refractive index profile across the active region exhibits a step index profile. Although the induced effective index variation is small it has been shown that an index step of $>5\times10^{-3}$ is sufficient for complete index guiding[20], figure 1.8(b). This device is popular since it requires no regrowth and hence gives good layer quality and reproducibility in production.

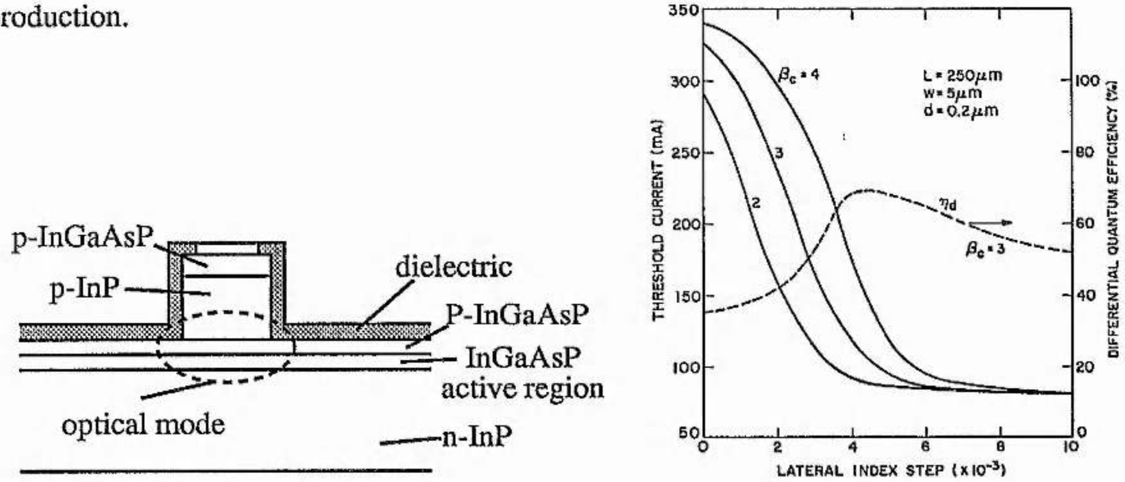

(a) (b)

Figure 1.8 (a) The ridge waveguide laser structure (b) onset of index guiding with an increase in the lateral refractive index step. (After reference 20).

The ridge waveguide structure has been used extensively in this work since the ridge can be oriented at an angle to the cleaved facets thereby permitting the facet reflectivity to be significantly suppressed. This cannot, in general, be done on strong index lasers since the etching of mesas is crystal axis dependant and angled facets have to be polished rather than cleaved.

### 1.2.6.2 The double-channel planar buried heterostructure laser (DCPBH) - strong index guiding

In general, index guiding and current confinement are provided by separate parts of the structure in weakly guided lasers, and so they have a larger mode volume, a weaker mode confinement, and also appreciable current spreading can take place. This results in a higher threshold than in their strong index guided counterparts. A representative example of a strong index laser is the double channel planar buried heterostructure (DCPBH) laser[21] as shown in figure 1.9. Here two channels are etched to form a mesa which constitutes the active region. A current confining p-n-p-n structure is then grown and the capping layers are subsequently applied. The reduced carrier leakage current and the enhanced optical confinement result in a low threshold current (of typically less than 20mA), high output power (>10mW), and high temperature operation.

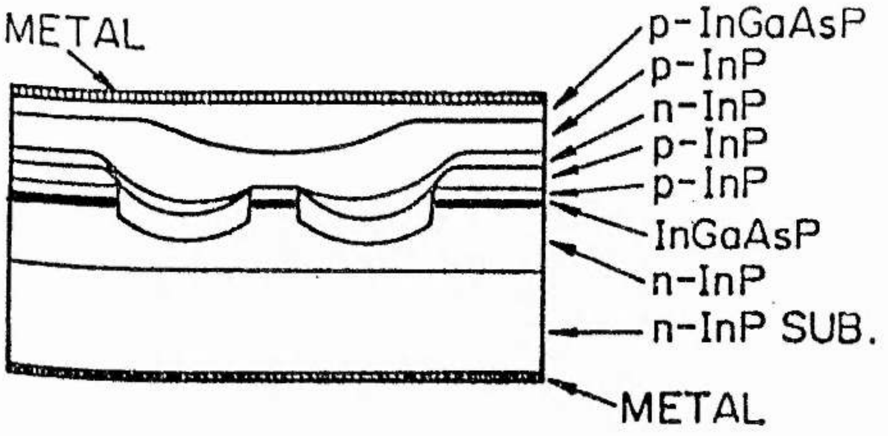

Figure 1.9 Structure of a double channel planar buried heterostucture laser.

The output from buried heterostructure lasers is typically more symmetrical than in weakly guide lasers since the lateral active region dimension is much reduced, hence allowing for efficient coupling (>50%) to lensed single-mode optical fibres.

## 1.3 InGaAsP semiconductor lasers and optical fibre communications

$In_{1-x}Ga_xAs_yP_{1-y}/InP$ semiconductor lasers are preferred for optical fibre communications due to the wavelength range of the emission that can be accessed by varying the composition of the active region. By this means $In_{1-x}Ga_xAs_yP_{1-y}$ lasers can be made to emit from 1.1µm to 1.6µm. This range includes the highly desirable wavelengths of 1.3µm and 1.5µm which correspond to the lowest attenuation windows in the loss spectrum of silica-based optical fibre, fig 10(a). Propagation loss at 1.5µm can be as low as 0.2dB/km[22].

The broadening of an optical pulse, on propagating a length L of optical fibre, due to material dispersion can be expressed as,

$$\Delta t = \left| -\frac{L\lambda}{c} \frac{d^2n}{d\lambda^2} \Delta\lambda \right|$$

The variation of the dispersion parameter ($\frac{d^2n}{d\lambda^2}$) with wavelength for pure silica[23] is shown in figure 1.10(b). It can be seen from this graph that at wavelengths around 1.3µm the value of $\frac{d^2n}{d\lambda^2}$ becomes zero and and so in this spectral region the material dispersion term becomes very small indeed. Thus an optical pulse at 1.3µm will have the minimum pulse broadening during propagation along the fibre such that higher bit rates could be transmitted over longer distances before the pulses start to overlap with each other. Although material dispersion of silica becomes zero at 1.27µm the total dispersion will now be dominated by other dispersive effects such as waveguide dispersion, and higher order dispersion effects.

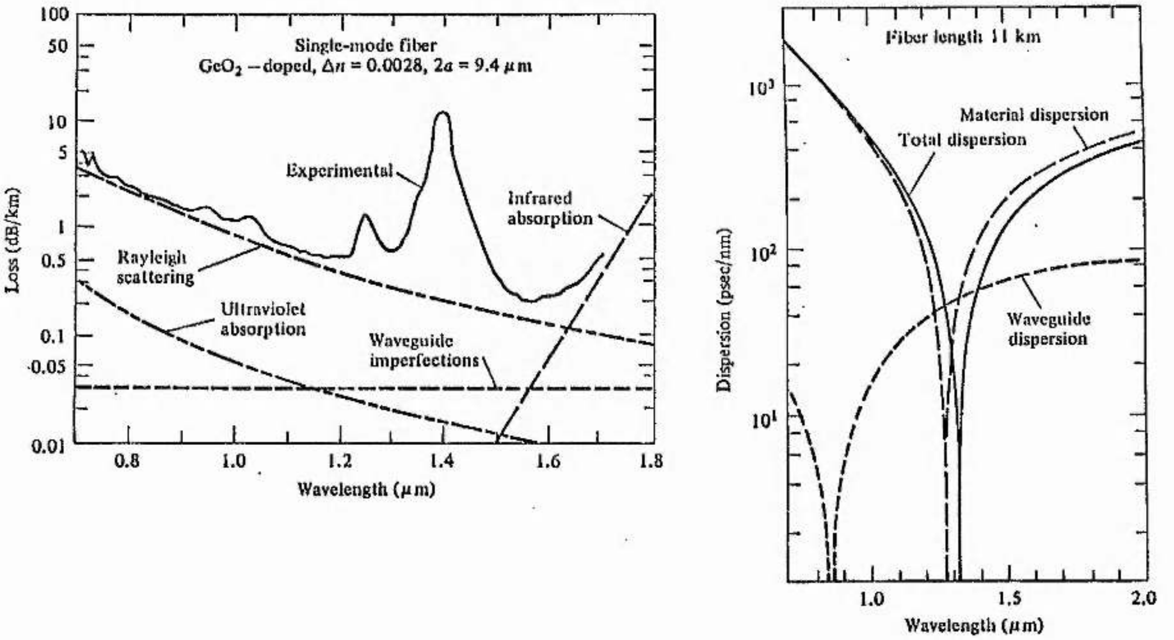

Figure 1.10 (a) Loss spectrum and (b) dispersion characteristics of silica optical fibre. (After reference 22)

An alternative approach to fibre telecommunications systems is to operate at the wavelength region of lowest loss around 1.5µm. Here the sign of $\frac{d^2n}{d\lambda^2}$ is negative and this can be favourable when combined with the self-phase modulation which arises from the intensity-dependent refractive index effects in the fibre, and under suitable conditions solitonic pulse shaping can to be exploited to dramatically extend the possible transmission distance[24]. Much effort has been dedicated to this subject with the conclusion that to maximise the bandwidth-length product of the communications system then soliton propagation is necessary, and becomes more so the longer the transmission span.

## 1.4 Modelocking

The following simple analysis will show that by controlling the relative phases of the oscillating axial modes of a laser resonator that a well ordered periodic sequence of ultrashort pulses can be produced. The subject of laser modelocking is based on producing such an output from practical laser sources, and a wide variety of techniques been developed to achieve this objective[25].

### 1.4.1 Modelocking theory

Consider a laser oscillating on many longitudinal cavity modes. The electric field E(t) as a function of time is then,

$$E(t)=A\sum_{m=0}^{M-1} e^{i(\omega_m t+\delta_m)}$$

where M is the the number of oscillating modes, $\omega_m$ is the angular frequency of the m^th^ mode, and $\delta_m$ is the phase of the m^th^ mode. For simplicity all modes are assumed to have the same amplitude A. The axial cavity modes differ in frequency by $\Delta\omega$, where

$$\Delta\omega = \omega_m - \omega_{m-1} = 2\pi \frac{c}{2nL}$$

n is the refractive index, and L is the length of the resonator.

In the case of a free-running laser the relative phases of all the oscillating modes are random thus the total intensity is found by adding all the individual modal intensities,

$$I = MA^2$$

If we can insert some device into the cavity to make the laser modes interact such that they all have the same relative phase then the laser is said to be modelocked. The total intensity must now be found by adding the individual electric fields of all the oscillating modes and then taking its square. The total intracavity electric field is therefore,

$$E(t)=A\, e^{i\delta} \sum_{n=0}^{M-1} e^{i\omega_m t}$$

By writing $\omega_m = \omega - m\Delta\omega$, where $\omega$ is the angular frequency of the highest frequency mode, then this equation can be restated as,

$$E(t)= A\, e^{i(wt+\delta)}\, [1+ e^{-i\phi} + e^{-2i\phi} + \dots\dots\dots + e^{-(m-1)i\phi}]$$

where $\phi = \Delta\omega t = \pi \frac{ct}{nL}$. The term in brackets is a sinc function, and thus the total field intensity may be expressed as;

$$I(t) = E(t)^2 = A^2 \frac{\sin^2 \frac{M\phi}{2}}{\sin^2 \frac{\phi}{2}}$$

This function is the description of a train of pulses separated by $\frac{2nd}{c}$ (the round-trip time of the laser resonator), and of peak intensity $I_m = M^2A^2$ (see figure 1.11). The duration of the pulses is $\frac{2nd}{cM}$, or equivalent to the reciprocal of the oscillating bandwidth of the laser.

This description of modelocked lasers is directly applicable to the case where initially many cavity modes are oscillating, and so it is only satisfactory for inhomogeneously broadened laser media. In the case of a homogeneously broadened laser medium the picture is substantially different, and the significant differences will be outlined after some brief definitions concerning the broadening mechanism of the laser medium.

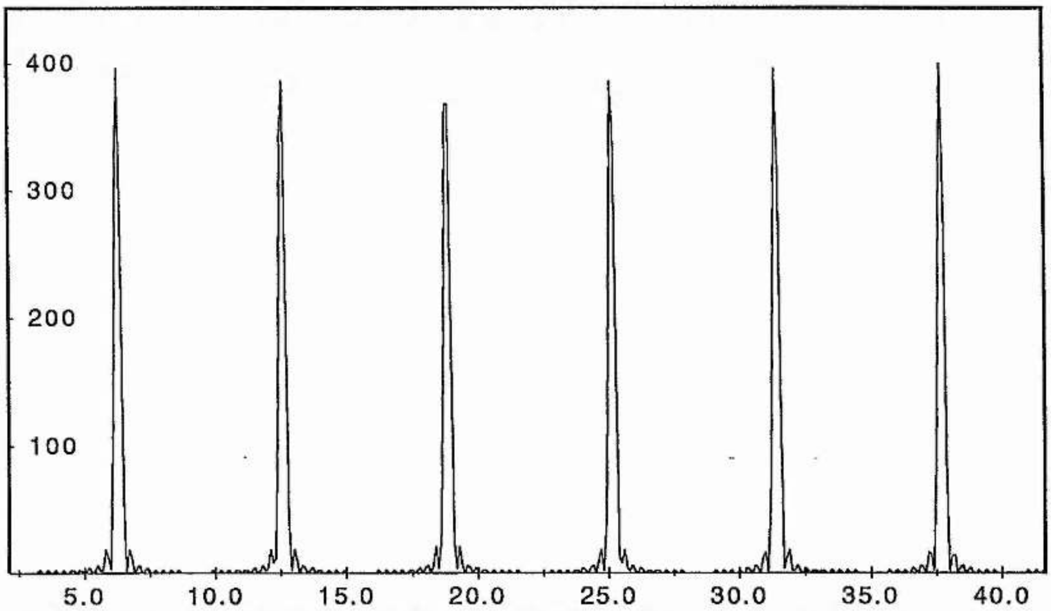

Figure 1.11 Plot of the derived total field intensity of a modelocked laser, where A=1, M=20. The ordinates represent intensity and the abscissae represent $\phi$ (which corresponds to time).

### 1.4.2 Homogeneous and Inhomogeneously broadened laser transitions

In a homogeneously broadened laser, neglecting the effects of spatial hole burning, the output consists of only one longitudinal cavity mode[26]. This situation arises due to two phenomena, firstly in an oscillating laser the gain is clamped at a value which is equal to the cavity losses. Secondly, the gain spectrum of any individual atom residing in the upper laser level is the same as the gain spectrum of the total inverted ensemble. Thus when the pumping is such that the laser oscillates at the peak of the gain, the total upper state population is clamped, at the threshold value, and oscillation elsewhere is inhibited since the population inversion is not sufficient to satisfy the threshold condition.

In an inhomogeneously broadened laser there exist different groups of inverted atoms each with different gain spectra. Thus this laser can be thought of as a group of homogeneously broadened lasers with slightly different emission frequencies. Hence the laser can emit a highly multimode spectrum the width increasing with higher pumping.

As already mentioned modelocking is the process whereby the longitudinal cavity modes of the laser are made to oscillate with a definite phase relationship. Therefore in the inhomogeneously broadened laser since many modes will normally be oscillating the only requirement for modelocking is that they be forced into possessing a definite phase relation. In the perfect homogeneously broadened laser the initially oscillating mode is modulated at a frequency coincident with the intermode spacing, and induces energy transfer to its nearest neighbour modes which can then oscillate. These can then promote further mode generation and the process continues until some steady state evolves where the pulse-duration remains constant. The duration of the pulse is limited, for example, by low modulation depth of the modulator or by the available laser gain spectrum. Hence in this case in the pulse build-up period (typically a few tens or hundreds of round trip times) a dramatic spectral broadening will be seen. Since the mode generation arises, albeit indirectly, from an applied modulation signal the 'new' modes must, in principle, possess a definite phase relationship.

In conclusion it can be said that modelocking is obtained by phase locking oscillating modes in inhomogeneously broadened lasers and by mode generation in homogeneously broadened lasers. In practice, homogeneously broadened lasers are never usually single mode, largely due to spatial hole burning, hence these modes must firstly be phase locked before the further mode generation can take place.

### 1.4.3 Active and passive modelocking

There are two basic types of modelocking, namely active and passive. The passively modelocked system involves a saturable absorber (normally a dye solution) for which absorption decreases with higher incident light intensity[27]. Passively modelocked lasers generate the shortest pulses due to their efficient use of the available bandwidth, the pulsewidth being proportional to the inverse linewidth of the laser. Table 1.2 gives the functional dependence of some pulse shapes; the Gaussian and hyperbolic secant squared shapes are frequently assumed to describe those emitted from modelocked lasers. The bandwidth-duration product values corresponding to Fourier transform limited pulses are also included in Table 1.2.

| Pulse shape | Intensity profile | $\Delta\nu\Delta t$ |
|---|---|---|
| square | 1 $t < t_p/2$<br>0 $t > t_p/2$ | 0.866 |
| Gaussian | $\exp\left(\frac{4\ln 2t^2}{t_p^2}\right)$ | 0.441 |
| $\mathrm{sech}^2$ | $\mathrm{sech}^2\left(\frac{1.71t}{t_p}\right)$ | 0.315 |

Table 1.2 Ultrashort pulse shapes

In an actively modelocked system a periodic change in the gain (or loss) is applied in synchronism with the cavity round-trip time. For a sinusoidal modulation of a homogeneously broadened gain media, Haus[28] derived that the pulses produced are Gaussian with durations given by;

$$\Delta t \sim [\, M^4 \,( f_m \,\Delta\nu\, )^{1/2}]^{-1}$$

Where M is the modulation depth, $\Delta\nu$ is the gain bandwidth and $f_m$ is the modulation frequency. Active modelocking cannot fully utilise the potential gain bandwidth and so broader pulses are produced than for its passive modelocking counterpart. The reason for this can be seen from the dependence of the pulse duration on the modulation frequency. Because the modulation in the passively modelocked laser is induced by the intracavity flux the $f_m$ term is essentially the gain bandwidth ($\Delta\nu$). ie. the modulation created is unlimited (except by that imposed by the gain bandwidth). Thus the two techniques, at least theoretically, are the same, the passive case reducing to active due to the modulation frequency limitation. In practice, for active modelocking modulation frequencies around 100MHz are used, due mainly to cavity length and electronics considerations in large-frame laser systems. This limitation on the modulation frequency is not as severe for semiconductor lasers for which the practicalities of modelocking will be considered in section 1.4.4.

### 1.4.4 Modelocking of semiconductor lasers

A convenient and popular method of modelocking a semiconductor laser in an external cavity is to superimpose a radio frequency (RF) signal on a subthreshold DC bias. The RF signal is chosen to be equal to (or a multiple of) the external cavity mode spacing. The first successful modelocked operation of a semiconductor laser was in 1978[29], where an uncoated AlGaAs laser chip was combined with a spherical mirror in an external cavity configuration. A similar cavity configuration was used for the first modelocked InGaAsP laser[30]. The pulse durations recorded for these experiments were 20ps and 18ps respectively. Since then semiconductor lasers have been modelocked in more refined cavities, and pulse durations of ~5ps have been recorded[31].

Semiconductor lasers have also been passively modelocked using aged[32] and proton bombarded[33] laser diodes, and more importantly by utilising the saturable absorption properties of a multiple quantum well structure[34] (MQWS). Passive modelocking using aged or proton bombarded lasers has produced the shortest pulse durations, although this method is unattractive since the laser is intentionally damaged and thus its lifetime is severely reduced.

The main problem encountered in the optimisation of modelocked semiconductor lasers is the suppression of the diode facet reflectivity. This is important since in an external cavity configuration the external cavity modes tend to lock together with a definite phase relation, but there is no phase relation between each cluster of external cavity modes defined by the Fabry Perot modes of the diode resonator (see figure 1.12). This is known as modelocking in clusters, and has been treated theoretically by Haus[35], who concluded that for bandwidth-limited pulse production with durations less than 20ps then the internal Fabry-Perot effect must be eliminated, or at least significantly reduced.

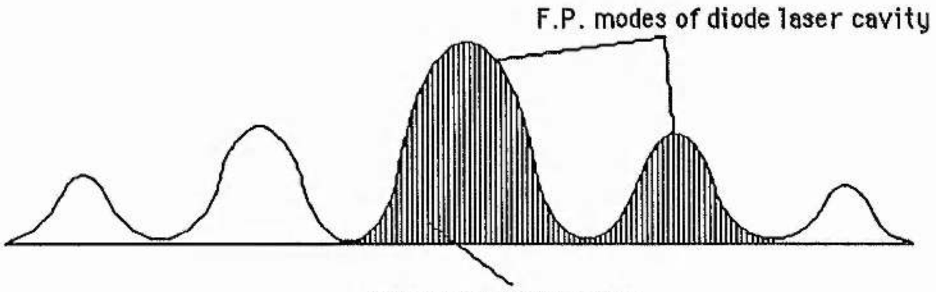

Figure 1.12 Mode structure of a laser diode in an external cavity, where there is no suppression of the facet reflectivity.

If the facet reflectivity is not satisfactorily frustrated then a pulse exhibiting temporal substructure is produced, and a second-harmonic generation (SHG) intensity autocorrelation trace for such pulses[30] is illustrated in figure 1.13. Facet reflectivity suppression can be achieved by using either anti-reflection coatings[36] or angled-stripe[37] amplifier structures and in chapter 2 these techniques will be detailed and contrasted.

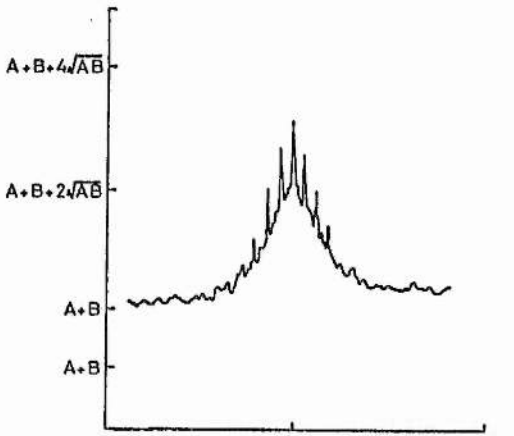

Figure 1.13 SHG autocorrelation function of pulse produced from a laser exhibiting appreciable internal facet reflectivity. (After reference 30).

## 1.5 Ultrashort pulse diagnostics

Investigations into the operating characteristics of ultrashort pulse lasers have closely followed the developments leading to increased temporal resolution in the measurement diagnostics. Direct linear-response detection systems have given way to nonlinear measurement techniques which have substantially better temporal resolution. In this section the most practical and useful (and most frequently used) ultrashort pulse detection systems will be described and their relative advantages and disadvantages will be highlighted.

### 1.5.1 Direct detection using photodiode/oscilloscope combinations.

The most convenient method for the detection of laser pulses is to use photodiodes and ultrafast oscilloscopes. In most circumstances it is the oscilloscope bandwidth which places the main limitation on this measurement technique because ultrafast photodiodes have been demonstrated with bandwidths in excess of 100GHz[38], and devices with bandwidths of ~20GHz are now commonplace. High speed oscilloscopes with up to 500MHz bandwidth are both expensive and bulky, but can be replaced with a sampling oscilloscope (with effective detection bandwidths of many gigahertz) if a periodic laser signal is used. A state-of-the-art sampling unit will be capable of a temporal resolution of ~20ps[39]. When combined with ultrafast photodiodes the typical current state-of-the-art performance is ~25ps where cable and connector bandwidth limitations must be considered.

The modelocked laser sources that are presently available produce optical pulses with typical durations from 10ps down to several tens of femtoseconds cannot be adequately monitored with photodiode/oscilloscope detection systems. Therefore such diagnostics are only used in a qualitative capacity in the modelocked laser output optimisation procedure, and as a monitor of the long-term stability of the pulse sequence.

### 1.5.2 Linear-response electron-optical streak camera

Streak cameras[40] were designed to improve the time resolution of ultrashort pulse diagnostics over that available from photodiode/oscilloscope systems. A schematic of an electron-optical streak image tube is shown in the figure 1.14. The incident laser pulse liberates a packet of photoelectrons at the photocathode of the streak camera and the temporal distribution of the electron packet essentially follows that of the laser pulse temporal intensity distribution. The electrons are then accelerated by the voltage applied to the mesh electrode and enter the main drift region of the streak tube at a relatively high velocity. Electron lenses focus the electron packet onto the phosphor screen of the image tube. The electron packet is deflected by a linear ramp voltage which is applied to the deflection plates. When the electrons strike the phosphor coated screen the luminosity is proportional to the number of electrons present. By ramping the voltage applied to the deflection plates the electron packet is streaked; that is the electrons are deflected at an angle that is directly related to the time at which they enter the deflection zone. The temporal distribution of the electrons (and hence the incident optical pulse) is thus transformed into a spatial distribution which can be detected from the phosphor screen by subsequent imaging onto a detector such as an optical multichannel analyser. The detection sensitivity of the streak camera can be very high and can be enhanced with a microchannel plate intensification stage which provides electron gain.

A particularly relevant design of streak camera is the synchronously operating[41] (or Synchroscan) system which is used for repetitive input signals and is ideal for monitoring pulses from modelocked lasers. In this camera an RF voltage signal is applied to the deflection plates in synchronism with the incident laser pulse sequence. The sinewave deflection signal is adjusted to ensure that the electron packet is deflected when the scan is linear (the deflection signal deviates less than 5% from linear over the centre 1/6th of the sinewave period). In this way the streaked image of each pulse is superposed so that the output signal can accumulate over many incident pulses giving an enhanced sensitivity and signal-to-noise ratio. By using an optical multichannel analyser (OMA) a quasi-real-time output can be obtained.

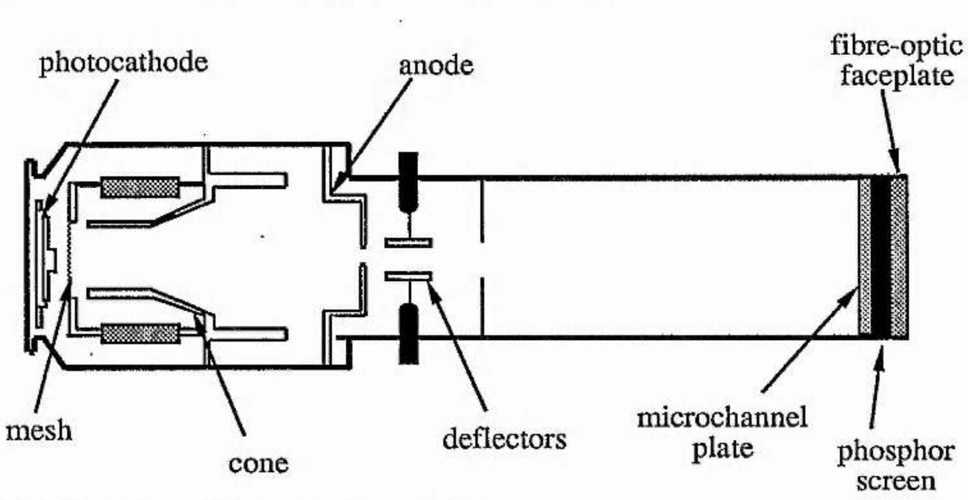

Figure 1.14 Photochron IIA streak image tube.

The limit of temporal resolution of streak camera systems has been reduced to ~300fs in the single-shot mode of operation[42], whereas in the synchroscan mode 1ps represents the best resolution to date[43]. In synchroscan cameras the measured pulse duration is also exaggerated by any pulse-to-pulse timing jitter present on the incident pulse train. Thus observation of the recorded pulse duration versus integration time will reveal the frequency dependence of inherent phase noise and this will be discussed later in chapter 6. Such information is especially relevant if the laser is to be used for timing and electro-optic sampling applications for example. This is because with low phase noise laser sources longer data acquisition periods can be used leading to enhanced measurement sensitivity.

### 1.5.3 Nonlinear detection by SHG autocorrelation

Pulse duration measurement techniques of the linear-response type described above, although attractive for certain applications, are not capable of resolving timescales sufficiently less than a picosecond. Therefore nonlinear techniques must be utilised. The most widely used nonlinear pulse measurement technique utilises second harmonic generation (SHG) to obtain the second-order autocorrelation function[44] of the ultrashort pulse train. There are a various ways of experimentally obtaining this function such as non-colinear (or background free), single pulse autocorrelators, or the more common colinear approach (shown in figure 1.15). All these methods give the desired correlation function from which information about the pulse duration can be extracted after an assumption is made regarding the specific input pulse shape. The detailed pulse shape cannot, however, be inferred due to the symmetry of the intensity autocorrelation function. By using detection electronics of sufficient bandwidth the fringe-resolved, second-order autocorrelation function can be obtained and this approach provides additional useful, although qualitative, information with regard to the frequency chirp of the pulse. For more comprehensive duration, shape and phase analysis crosscorrelation techniques[45] are required which are considerably more complex and are not widely used as yet.

The standard, colinear, 'real-time' autocorrelator of figure 1.15 comprises a Michelson interferometer to split the input pulse into two components, which are retroreflected by corner cube mirrors and recombined. These signals are focussed onto a nonlinear optical crystal and the second harmonic signal thus generated is detected by a photomultiplier tube. A variable delay is introduced into one beam (in this real-time case by a speaker mounted mirror) so that one pulse can 'walk through' the other such that the autocorrelation function can be derived. For perfectly modelocked pulses the autocorrelation function is bell-shaped with a 3:1 contrast ratio. When the pulses are not overlapped the background signal (level 1) is obtained whereas when the pulses are overlapped an enhanced SHG signal is produced (since the SHG signal is quadratically related to the peak intensity). When the pulses are fully overlapped the SHG signal is a maximum and this level is 3 times the background level if the two beams are of equal intensity. When the mirror is scanned the autocorrelation can be observed in quasi-realtime on an oscilloscope, and the entire autocorrelation trace can be obtained for each sweep of the moving mirror which is translated at a typical frequency of ~25Hz.

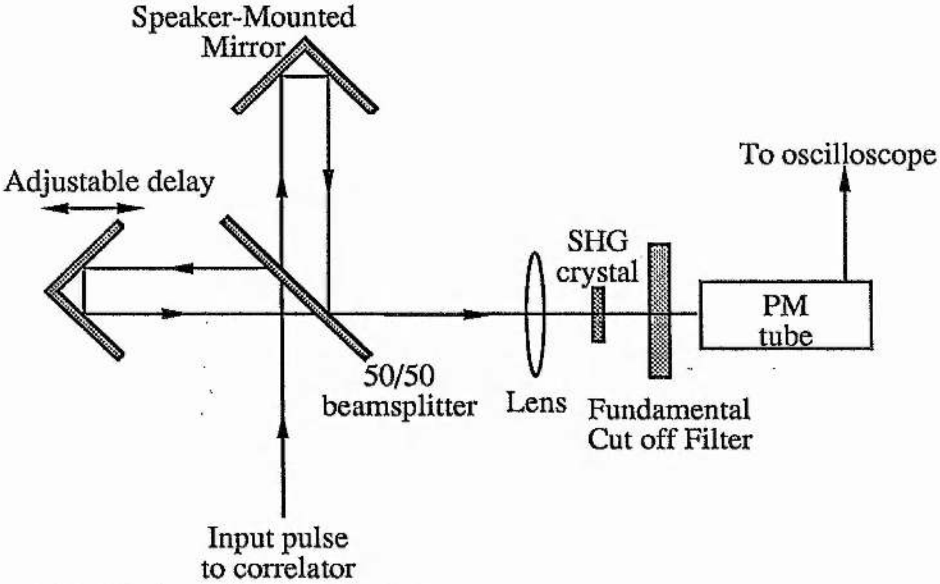

Figure 1.15 SHG intensity autocorrelator

### 1.5.4 Spectral measurements

Another useful source of information indicating the quality of the pulses produced from modelocked lasers is by monitoring the oscillating spectral output. Traditionally scanning grating monochromators have been utilised for such measurements due to the large bandwidths normally encountered, but present day needs are for spectral analysis on a timescale similar to the integration time that applies to the temporal measurement schemes. For example, the acquisition of an autocorrelation trace typically takes around 20ms. One method of fast spectral analysis is to employ a CCD array detector at the exit of a monochromator thus allowing a constantly updated monitor of the spectral characteristics of the laser. This technique can be expensive and requires quite elaborate electronic control circuitry for data acquisition. Also, the limited availability of acceptable quality germanium-based CCD arrays has limited this technique to wavelengths detectable using silicon devices (<1.1μm).

The scanning Fabry-Perot interferometer[46] (SFPI) normally associated with narrow wavelength features (it is more usual to quote bandwidth in terms of frequency when using a SFPI) can be easily converted to record relatively broad spectral features from modelocked laser sources. A full scan across a few free-spectral ranges of the SFPI can be acquired in a time comparable to, or much less than, any of the previously discussed temporal measurement techniques. Moreover the necessary component parts of the SFPI are readily available and reasonably cheap and in-house designed and built interferometers have been used in this project work.

## 1.6 Summary

In this chapter a description of laser oscillation in semiconductor materials has been given. Details of the operating principles and characteristics of two types laser structure, the ridge waveguide and the DCPBH, were also outlined. These efficient laser structures have been used extensively throughout this work.

By applying the technique of active modelocking to semiconductor lasers the potential exists for highly efficient digital optical sources applicable to silica-based optical fibre telecommunications systems. Characterisation of these ultrashort pulse laser sources require diagnostics capable of resolving events on a picosecond timescale. Both linear and nonlinear response measurement techniques have been developed to achieve this, and have been extensively applied to ultrashort pulse semiconductor lasers in the subsequent chapters of this work. The relative merits of these systems have been contrasted here.

# CHAPTER 2

# EXTERNAL-CAVITY SEMICONDUCTOR LASERS

## 2.1 Introduction

In chapter 1 the principles of laser oscillation in semiconductor media were outlined. The semiconductor laser exhibits features such as small physical dimensions, high efficiency, low power electrical pump, single transverse mode operation, large gain bandwidth, and high speed modulation capability. These features are attractive in any laser system and for some of the noted features the semiconductor laser is unrivalled. However, as will now be discussed, the semiconductor laser is far from the ideal source for many applications. In this chapter the problematic characteristics of the output from standard semiconductor lasers will be outlined along with some proposed solutions.

### 2.1.1 Output beam profile

The most obvious problem with semiconductor lasers is the astigmatic, elliptical output beam which is the result of diffraction from the rectangular cross-section of the active region (figure 2.1). The degree of ellipticity can be very high in some laser structures, but it is minimised in the strongly index-guided buried heterostructure lasers. Fortunately the elliptical output beam can be readily transformed into one of circular symmetry by using suitable lensed optical fibre pigtails and this particular topic will be considered later in section 2.8.1.

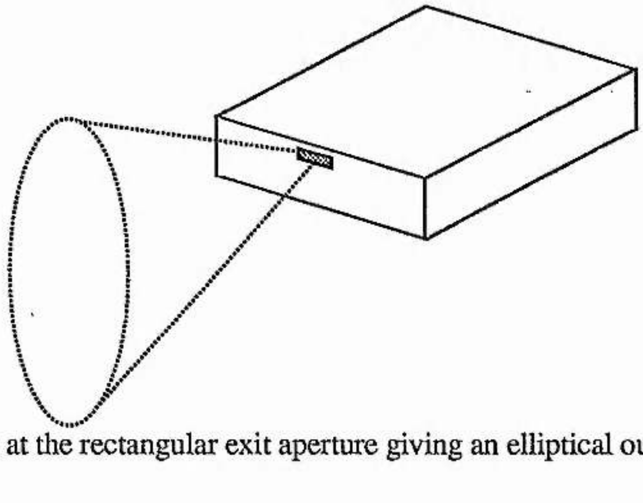

Figure 2.1 Diffraction at the rectangular exit aperture giving an elliptical output beam

### 2.1.2 Multi-axial mode output

Another major deficiency in the output is that the spectrum of almost all semiconductor lasers is highly multimode[47, 18]. Even though the resonator length is short (<500μm), and hence the axial mode spacing is large, the gain bandwidth is large enough (>50nm for InGaAsP lasers) that multiple longitudinal mode emission is inevitable as evidenced in figure 2.2 for a 1.5μm ridge waveguide laser oscillating at a drive current of $1.2xI_{th}$. Moreover, due to the integrated nature of this solid laser bandwidth limiting elements cannot be used.

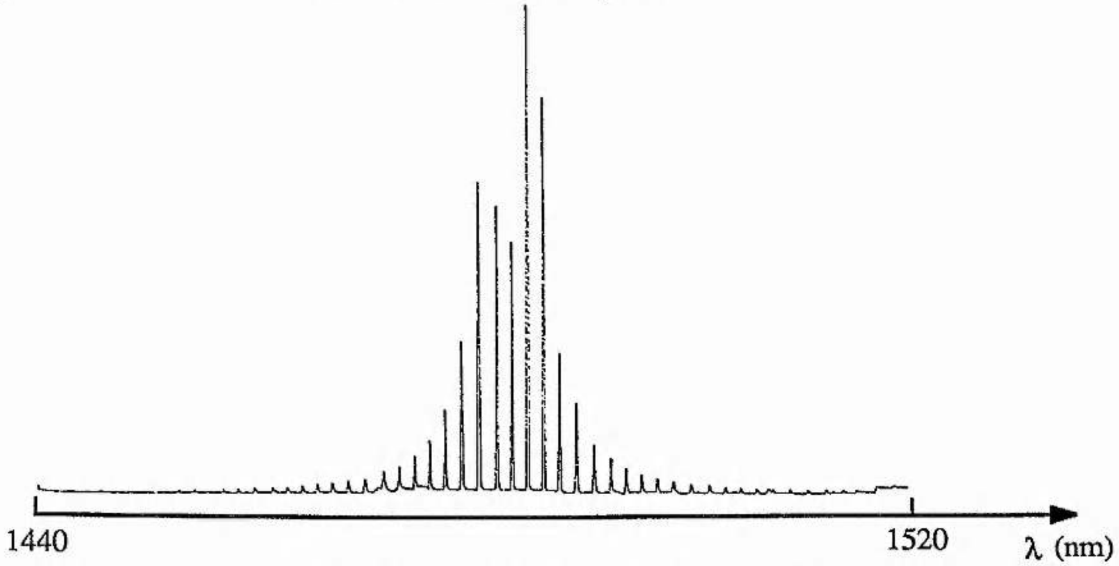

Figure 2.2 Spectrum recorded for 1.5μm ridge waveguide laser at $1.2xI_{th}$.

One novel solution to this problem termed distributed feedback, first developed for single longitudinal mode dye lasers[48], has been successfully applied to semiconductor lasers[49]. These lasers utilise a corrugated region close enough to the active region to affect the propagating optical field (see figure 2.3(a)). At each corrugation a small portion of the field is backscattered. Each reflection can only add in phase with all other reflections at one precise wavelength, the Bragg wavelength, which is defined by the corrugation period. No mirrors are required for oscillation, and DFB lasers can give a single longitudinal mode output with linewidths of typically 10MHz under strong pumping conditions. A spectrum obtained from a 1.5μm InGaAsP phase-shifted DFB laser[50] is shown in figure 2.3(c) where the excellent mode selectivity can be clearly seen. Further linewidth reduction is not possible in DFB lasers, and only short range wavelength tunability can be achieved (through current or temperature changes). Another narrow linewidth integrated laser configuration is the distributed Bragg reflector[51] (DBR). This device is similar to the DFB but here the gain region and the distributed reflector are separate (see figure 2.3(b)).

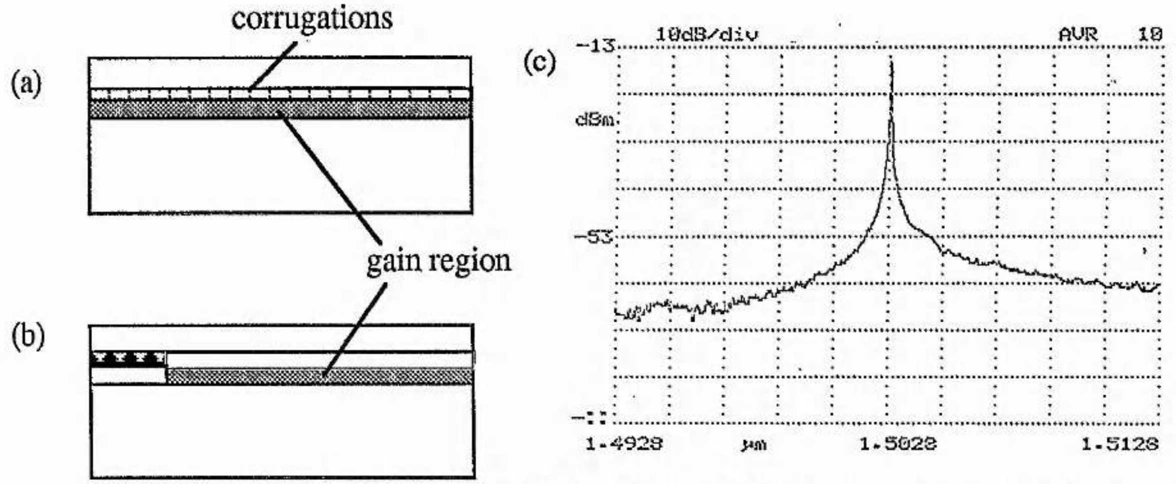

Figure 2.3 Lasers with integral mode control; (a) Distributed feedback laser, (b) Distributed Bragg reflector laser, (c) Spectrum of 1.5μm DFB laser.

## 2.2 The simple external-cavity semiconductor laser

By selecting specific values of x (and hence y) mole fractions in the active $In_xGa_{1-x}As_{1-y}P_y$ layer using laser design curves[52] such as that in figure 2.4, the laser output can be compositionally tuned to the desired operational wavelength regime. This coarse tuning allows laser oscillation to be achieved over the wavelength range of 1.1 - 1.6μm for InGaAsP active regions lattice-matched to InP. Any single laser chip has a potential tuning range on the order of ~50nm for 1.3μm devices and >70nm for 1.5μm lasers.

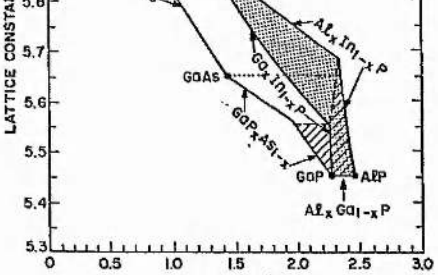

Figure 2.4 Compositional tuning of laser oscillation wavelength. (After reference 52).

Some degree of tunability can be achieved by varying the injection current level or the device temperature. Both of these tuning mechanisms are undesirable since the laser output, and hence the injection current would normally be used as a control parameter in most applications. Although temperature is acceptable between room temperature and $0^0$C, outside this range the problems of accelerated device degradation and condensation exist respectively. Hermetically sealed laser packages allow significant extension of the temperature tuning range but at the expense of design flexibility. Thus, if long-range wavelength tunability and improved mode control could be added to the characteristics already mentioned then semiconductor laser applications would be dramatically increased. To this end the semiconductor laser can be combined with a passive resonator to form a composite-cavity laser[53]. In the remainder of this chapter will discuss the operational and necessary conditions for optimal performance of such external cavity semiconductor laser configurations will be discussed. Various forms of integrated fibre resonators will also be described.

The basic format of an external-cavity semiconductor laser[47] is shown in figure 2.5. In general a lens is used to collect and collimate the divergent beam from the semiconductor laser, and a mirror to reflect the beam back into the active region of the diode. Hence a three-mirror compound resonator is formed which is typically about two orders of magnitude longer than the diode chip length. Elements such as Fabry-Perot etalons, birefringent plates, and prisms can therefore be included between the mirror and the lens to control the spectral characteristics of the output laser beam. The output beam is derived from either the external diode facet (M1 in the figure) which has a reflectivity determined by the coating applied during chip manufacture. This can range from R(AR)<0.01 to R(uncoated)=0.35 to R(HR)>0.95. Alternatively the output beam can be taken as the intensity transmitted through the external cavity bulk mirror.

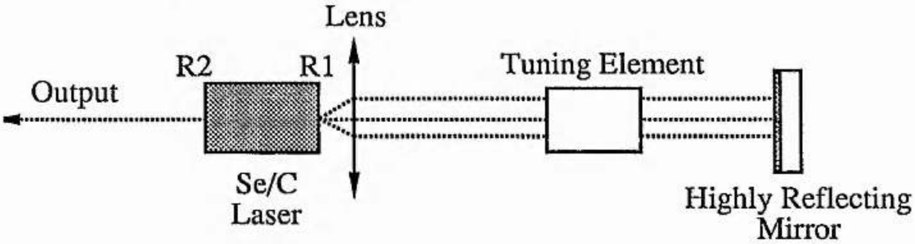

Figure 2.5 The basic components of an external-cavity semiconductor laser

The internal diode facet (M2) usually has some form of reflectivity suppression in an attempt to eliminate the subcavity formed between the two reflective surfaces of the diode (gain media). These subcavity effects serve to modulate the laser gain spectrum such that a larger internal reflectivity gives rise to a larger gain ripple. This has deleterious effects in tunable narrow linewidth[54] and modelocked operation of external-cavity semiconductor lasers[55]. In the former the output power versus wavelength is modulated and its continuous tuning range is limited, and in the latter, pulse substructure is evident. Experimental continuous-wave external-cavity lasers will be discussed in section 2.6, and modelocked versions will be detailed in chapter 3. The key topic of residual internal facet reflectivity will be addressed here since in the external cavity laser, and also for semiconductor amplifiers, performance is closely related to the degree of facet reflectivity suppression.

## 2.3 Anti-reflection coated semiconductor amplifiers

The optical field in the semiconductor laser is not a plane wave but an allowed mode of the waveguide so the facet reflectivity is not exactly the value calculated from the simple Fresnel formula (previously quoted in section 1.2.3). The modal reflectivity of the guided mode is considerably more complicated, and has been treated theoretically by Reinhart et al[56] and Ikegami[57]. The main results of this treatment were that the reflectivity is higher for the TE modes (hence these are the normal laser modes), and increases with an increased dielectric constant step (in the plane perpendicular to the junction for the case of the DH laser). In some particular cases the reflectivity was found to increase by as much as 20% over the plane wave value.

Numerous attempts to frustrate diode facet reflectivity have been undertaken with varying degrees of success. The most popular technique is to deposit a single-layer anti-reflection (AR) coating[58] directly onto the diode laser facets. With antireflection coatings exceptionally low facet reflectivities are achievable although complete suppression has not yet been demonstrated. Lasers with single-layer coatings of $SiO_x$[59] and $Si_3N_4$[60] have been reported to have modal facet reflectivities of approximately $10^{-4}$ (0.01%) although such low reflectivities are only exhibited over a narrow bandwidth. Broadband low-reflectivity characteristics have been achieved using multi-layer AR coatings[61], although optimised design of such coatings is an extremely complex task. It can be concluded that although very low modal facet reflectivities can be produced by AR coatings it will be some time yet before a perfect coating can be demonstrated because of the design difficulties and tight deposition tolerances required.

Many indirect techniques[62] have been devised to measure the facet reflectivity of diode amplifiers but their efficiencies have been variable. It is only by measuring the gain spectrum that the modal facet reflectivity of good (ie low R) semiconductor amplifiers can be properly determined. Some idea of the quality of the coating can be given by a knowledge of the threshold current increase after the coating process, and also from the current for the onset of spectral modulation observed on the fluorescence spectrum of the diode chip.

## 2.4 Angled-stripe semiconductor amplifiers

Another increasingly popular approach to facet reflectivity suppression of semiconductor amplifiers is to use an 'angled-stripe' geometry[63, 64]. The term 'angled-stripe' is defined in figure 2.7. The angled-stripe diode structure is more difficult to fabricate because for good facet quality the bars of devices sawn from the wafer are cleaved along the (100) crystal plane. Therefore the active region of diodes with complicated index guiding structures (eg. BH, DCPBH) which exhibit more attractive properties than simpler designs (eg. ridge waveguide) are difficult to make at an angle to the cleaved facet. This is because the techniques used in their construction (etching in particular) are crystal axis dependent. Facets of diodes with complex structures can be polished to produce an angled-stripe amplifier, but this process is difficult, wasteful and laborious, and facet quality will always be suspect[65].

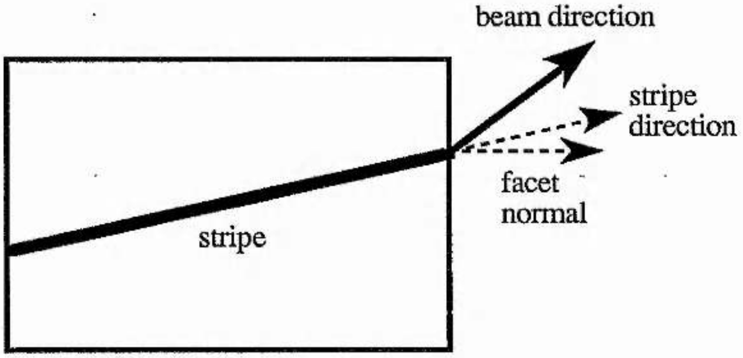

laser chip (as viewed from top)

Figure 2.7 An angled-stripe semiconductor amplifier; the stripe angle is defined as the angle between the stripe direction and the facet normal.

To produce angled-stripe diode amplifiers with any reproducibility a simpler diode structure must be used. Fortunately, the previously developed ridge waveguide laser structure is an ideal candidate for angled-stripe amplifier production. For this reason angled-stripe ridge waveguide semiconductor amplifiers were used in this work, and these will be referred to as angled-ridge amplifiers[66]. The ridge waveguide laser is similar to the stripe geometry laser discussed earlier in the respect that the epitaxial layers forming the active and cladding regions are grown in one stage. A ridge is then etched on the top layer at a preselected angle, the wafer is then metallised, sawn into bars and finally cleaved into individual devices. The device thus produced, unlike stripe-geometry lasers exhibits index guiding in the plane of the active region. This is due to the influence of the ridge on the refractive index as seen with respect to the optical mode in the active region (see section 1.2.6.1 in chapter 1). One residual production problem with this device is that the wet chemical etch used to form the ridge is crystal axis dependent and tends to undercut the top layer causing difficulties in achieving good metalisation on the side walls of the ridge[67]. The result of this can be degradation of the thermal contact between the diode and the heatsink. However, dry chemical etching techniques have been identified to overcome this failing. It follows therefore that it should be possible to produce an angled-ridge amplifier with little extra effort than in the production of standard Fabry-Perot laser devices without any compromise in device quality.

The facet reflectivity of ridge amplifiers is suppressed with respect to the guided mode in the active region and not for the beam incident on the facet from the coupling lens. Therefore it is commonplace to deposit a low quality (R~1%) antireflection coating onto the angled facet. The effect of this coating is twofold, since apart from minimising the coupling losses it has been shown to further reduce the facet modal reflectivity[68].

## 2.5 A comparison of AR-coated and angled-ridge semiconductor amplifiers

There are a few characteristics which differ from AR-coated and angled-ridge amplifiers. The first and most obvious difference is evident on examination of the fluorescence spectrum of the diode amplifiers (see figure 2.8). The large period modulation on the fluorescence spectrum of the AR-coated diode is due to feedback from either the microlens surface or the cleaved end (R=-14dB) of the output coupling microlensed fibre-pigtail. This modulation is a purely feedback dependent effect[69]. The retroreflected beam is focussed onto the active region of the diode where a portion of the beam propagates within the surrounding cladding region which has a different refractive index from that of the active region. Consequently, there is an interferometric interaction between the two optical components that propagate in the diode structure and gives rise to the spectral modulation observed on the fluorescence spectrum.

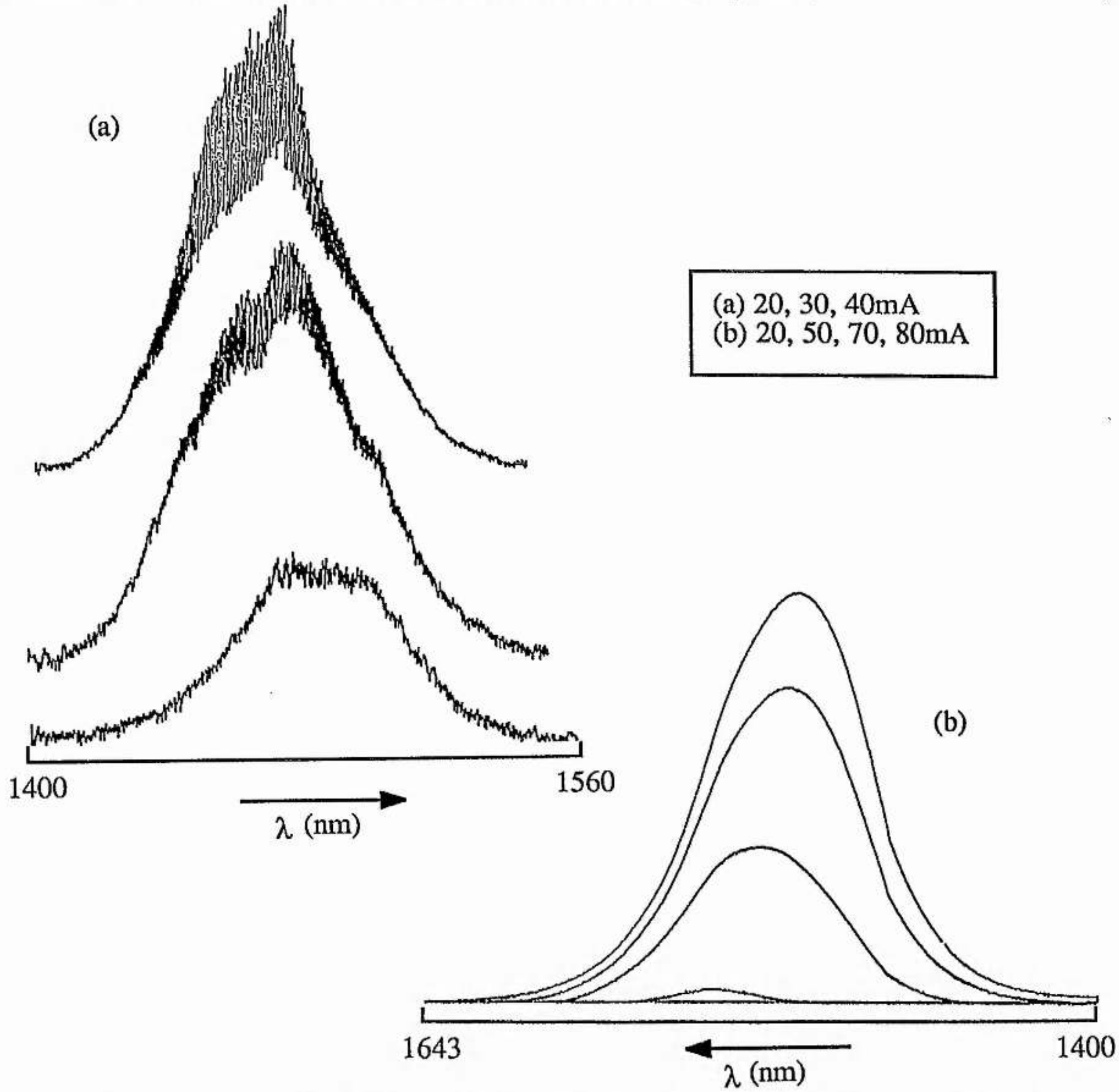

Figure 2.8 Fluorescence spectra of (a) an AR-coated [spectra have been displaced vertically for clarity], and (b) an angled-ridge semiconductor amplifier

The modulation period was measured to be ~11nm which is in good agreement with the period observed with Brewster-angled AlGaAs amplifiers (~3.5nm) when the oscillation wavelength is taken into account (850nm to 1500nm). The absence of this modulation on the angled-ridge amplifier spectrum is probably due to the reduced facet reflectivity. Hence any feedback entering the amplifier is not reflected off the other facet and so cannot influence the output fluorescence (gain) spectrum. When angled-ridge amplifiers are used as the gain media in external fibre resonators the feedback induced modulation is present on sub-threshold fluorescence spectra (see figure 3.11). Therefore this phenomenon is present in all semiconductor laser systems where feedback reflections are focussed onto the active region.

The spectral modulation associated with the Fabry-Perot resonances due to the residual facet reflectivity are clearly displayed on the spectra of the AR coated amplifier. The threshold current of similar uncoated devices are in the range of 15-20mA, and the modulation evident at currents as low as 30mA would indicate the poor quality of the antireflection coatings. From higher resolution measurements, and a knowledge of the gain levels present a value for the facet reflectivity of ~0.1% was calculated. However, in the case of the angled-ridge amplifiers the spectral modulation cannot be resolved for currents greater than 2.5 times that of a standard Fabry-Perot device of the same structure. This indicates an improvement in the facet reflectivity suppression, although since no ripple is evident the reflectivity cannot be obtained from these measurements. For a similar device Zah et al measured the gain ripple to be ~5dB at 25dB small-signal gain which amounts to a facet reflectivity of $\sim 10^{-3}$. More recently[37], reflectivities of less than $10^{-4}$ have been obtained from angled-ridge waveguide structures where a narrow ridge was used to eliminate the effect of higher order modes.

The best value of gain ripple for AR-coated amplifiers[36] was 0.2dB (ie. a few percent) for a peak gain of 27.5dB which translated into a reflectivity of $3 \times 10^{-5}$. This was observed for a single layer AR coated InGaAsP amplifier, but the spectral region over which this extremely low value was obtained was very narrow. Over the rest of the bandwidth the gain ripple increased to 2-3dB. This result should be typical for all high quality single layer AR-coated amplifiers because there will be a wavelength band, albeit narrow, where the facet reflectivity is dramatically reduced. This wavelength of 'zero' reflectivity is not easily controllable since the required layer thickness and its refractive index can only be approximated. Through the added complication of multilayer coatings the bandwidth of the antireflection coating can be extended. However, the reflectivity of angled-ridge amplifiers does not suffer this sensitivity with wavelength[37].

### 2.6 External-cavity InGaAsP lasers

### 2.6.1 Description and cavity optimisation

In this section the operational parameters of a simple grating-tuned, external-cavity InGaAsP laser are described. The external cavity laser shown in figure 2.9 was constructed. The semiconductor laser was an InGaAsP ridge-waveguide device which had one cleaved facet and one anti-reflection coated facet. The threshold current for the solitary diode chip was 105mA. The output from the AR coated facet was coupled onto a 1.6μm blazed diffraction grating using a x20 microscope objective. The grating was oriented in the Littrow configuration such that the diffracted beam was directed back along the incident beam and focussed onto the active region of the laser chip. In figure 2.9(b) the relative power efficiency curve for the diffraction grating used is illustrated[71].

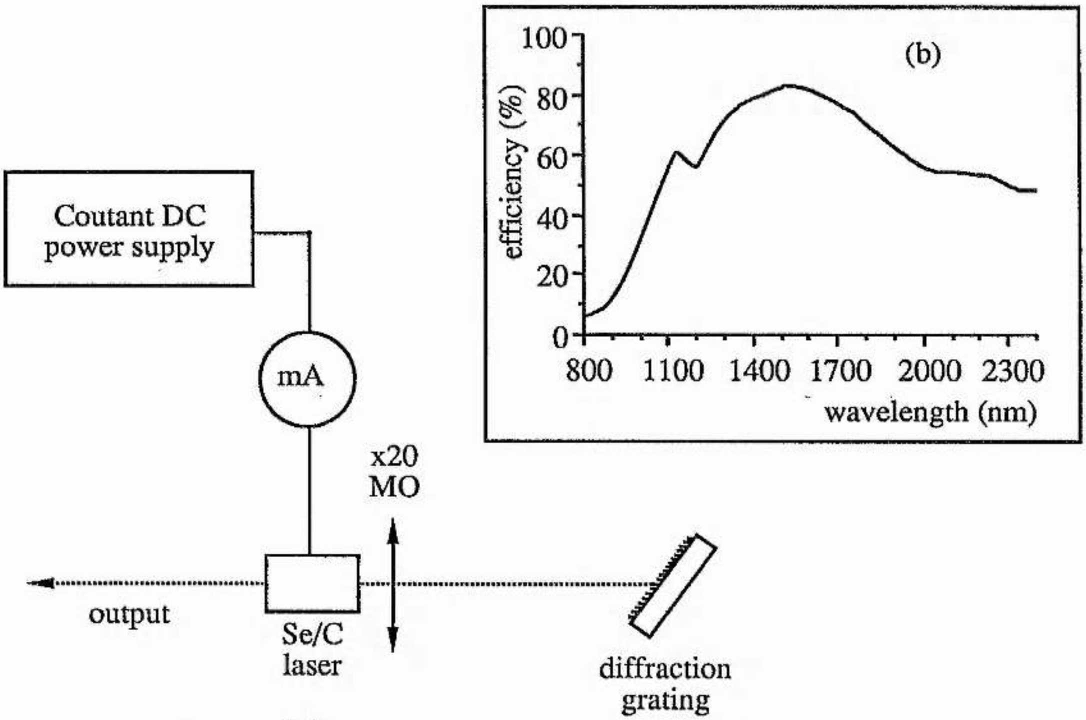

(a)

Figure 2.9 (a) Grating-tuned, external-cavity semiconductor laser. (b) Relative power efficiency curve for a typical 1.6μm blazed grating.

The output from the cleaved facet (R=35%) was directed onto a germanium photodiode to record the L/I characteristic of the external-cavity laser. The output was also coupled into a length of multimode fibre which served as the input to an optical multichannel analyser (the resolution limit for 50 micron core input fibre was 0.2nm).

The L/I characteristic for the external-cavity laser when the system was optimised for minimum threshold current is shown in fig 2.10. The condition of minimum threshold current was met by ensuring that the intracavity beam between the objective and the grating was collimated. This criterion was met by using an IR phosphor card[72] placed directly in front of the grating and adjusting the microscope objective until the diode chip emission was focussed. The diffracted beam from the grating was then aligned back into the microscope objective, and the cavity was optimised for maximum output power without altering significantly the distance between the objective and the diode facet. This configuration (focussed beam operation) does not give minimum threshold current, but is particularly stable. To achieve the collimated beam condition the objective was then moved towards the diode facet until a maximum in output power was found, where further small re-alignments were generally required to fully optimise the cavity. The collimated beam configuration is the configuration of minimum threshold current, but is more sensitive to alignment than the focussed beam cavity.

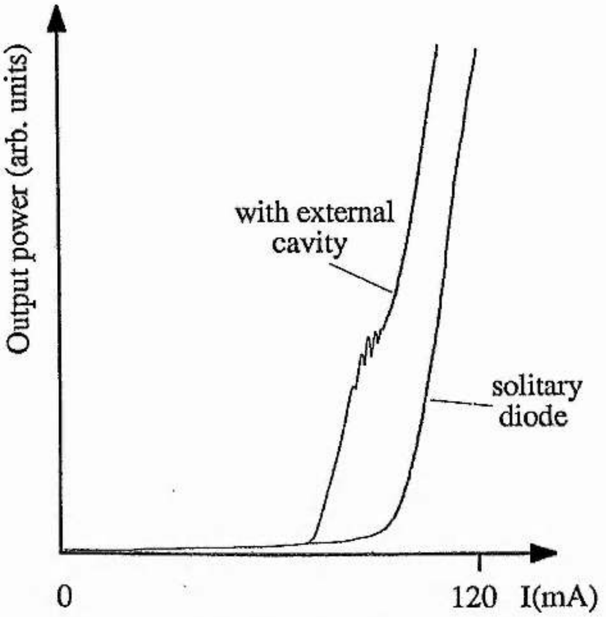

Figure 2.10 Light-current characteristics for the grating-tuned, external-cavity laser.

### 2.6.2 Tuning performance

The output from the laser consists of a narrow band of wavelength defined by the wavelength of the diffracted beam from the grating which are focussed onto the active region of the diode chip. Hence, by rotating the grating about an axis perpendicular to the optical axis of the laser, the output can be tuned. In this way the external-cavity laser was tuned over a wavelength range of 65nm whilst oscillating on a single resolution limited line (see figure 2.11).

The fundamental limit on the tunability is governed by the bandwidth of the diode chip over which the gain can exceed the cavity losses. This value is larger than the FWHM of the fluorescence bandwidth which can exceed 70nm[54]. The limit on the tunability in the case of the external-cavity laser is determined by the quality of the antireflection coating on the diode facet and the quality factor of the composite resonator in the following manner. If the threshold current for an external-cavity mode is lower than the solitary diode threshold current then this mode can oscillate and will be the only oscillating mode. If the threshold current of an external-cavity mode is greater than that of the solitary diode then this mode cannot oscillate and the output spectrum will jump back to that obtained from the solitary diode (see figure 2.12). Therefore the criterion for maximising the tunable range is to maximise the difference between the solitary diode laser threshold and the composite-cavity minimum threshold. In experiments using diodes with extremely good AR coatings tuning ranges of up to 90nm have been demonstrated[54].

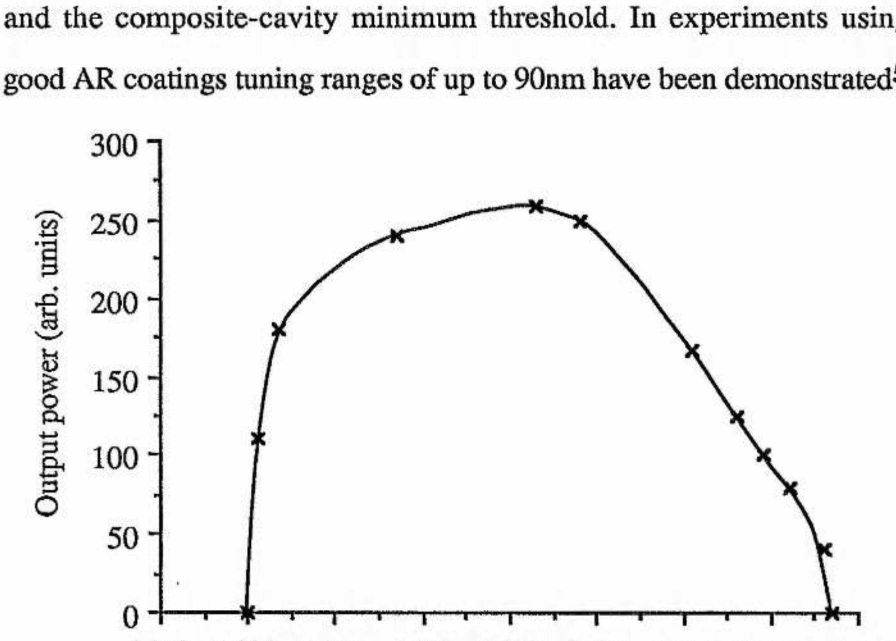

Figure 2.11 Tuning range of the external-cavity laser configuration. (Not continuous, see text).

The wavelength tuning across the tunable range of the laser is discontinuous, since no oscillation can be sustained in the troughs of the Fabry-Perot mode structure of the solitary diode spectrum. This does not imply that the laser stops oscillating when tuned to such a trough, but instead would jump to the next Fabry-Perot mode or oscillate simultaneously on both adjacent modes (see figure 2.13).

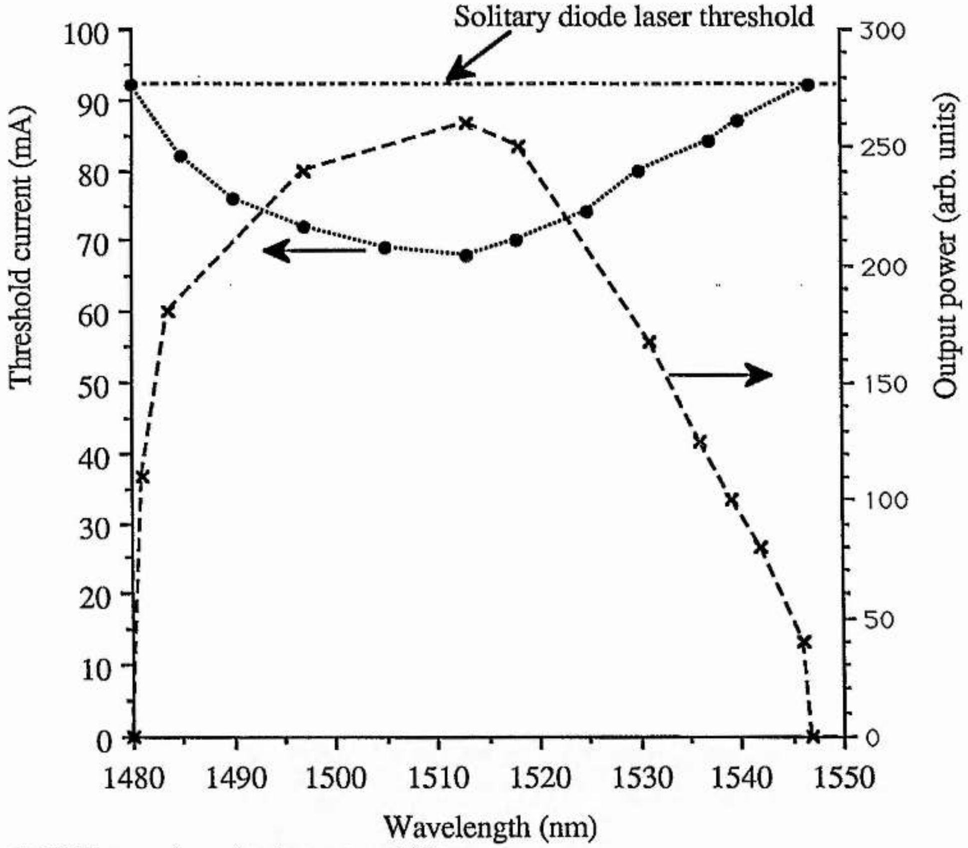

Figure 2.12 External-cavity laser tunability.

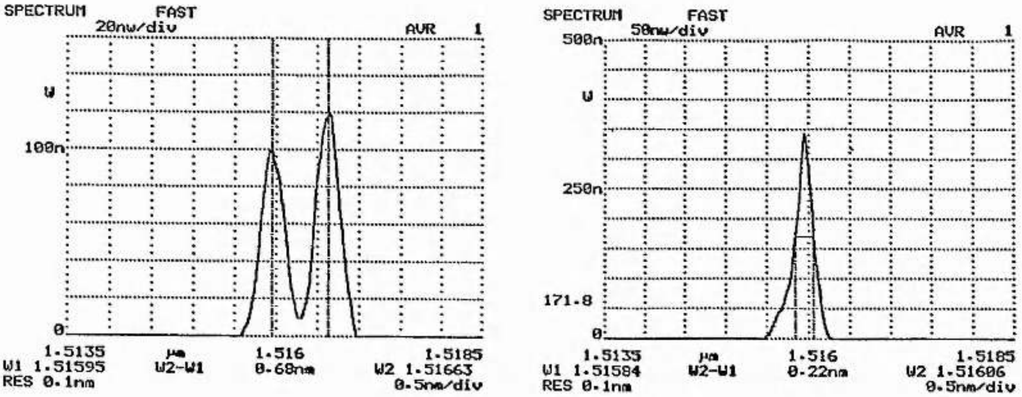

Figure 2.13 Discontinuous tuning.

Within each Fabry-Perot mode of the solitary laser chip the tuning can be continuous and can exhibit a very narrow linewidth[73]. The width of the Fabry-Perot mode will to some extent be a function by the residual reflectivity of the coated facet because this determines the gain modulation. Since the resolution of the spectrum analyser used was not sufficient to resolve the individual external cavity modes no study of intramode tuning could be attempted. Intramode oscillation on narrow linewidths with continuous tuning has been reported by various authors[74]. Furthermore, it has been demonstrated that the linewidth of the external-cavity laser configuration is sensitive to the effective power reflectivity of the external cavity and the reflectivity of the internal diode facet[75]. The condition for narrow linewidth operation of <100kHz can be expressed as[76],

$$\xi = \frac{(1-r_2)^2 \eta^2 R}{r_2} > 4.6$$

where $\xi$ is the extended-cavity coupling parameter, $r_2$ is the residual facet reflectivity, $\eta$ is the coupling efficiency to the external cavity, and R is the power reflectivity of the external feedback element. For the case studied here the value of $\xi$ was found to be between 6 and 11. The linewidth of the external-cavity laser will be reduced by the square of the ratio of the total external-cavity length to that of the diode chip[77]. Oscillation linewidths of ~10kHz have been demonstrated for similar grating loaded external-cavity lasers[74]. Coupling parameters of less than 4.6 can result in one of four distinct situations ranging from stable narrow line operation with very small feedback levels (<40dB), to a region of coherence collapse with moderate degrees of feedback. Such regimes are defined and detailed in reference 78. Side-mode suppression ratios of greater than 30dB were readily recorded for the external-cavity laser (see figure 2.14) and this demonstrated the exceptional wavelength selectivity of this simple laser configuration.

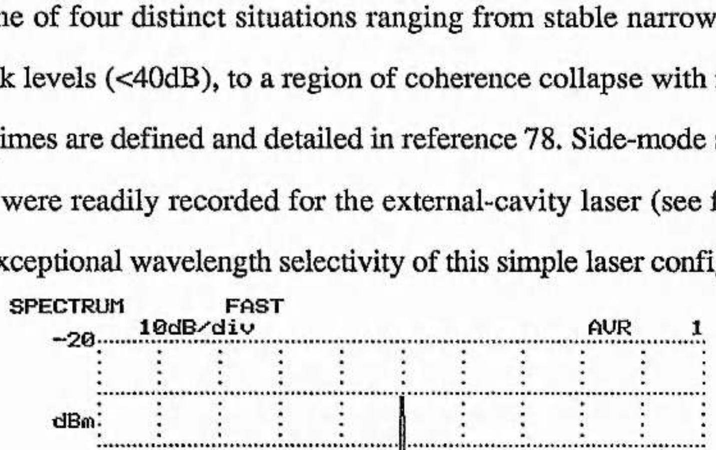

Figure 2.14 Spectrum of the output from the external cavity laser.

### 2.6.4 Limit to single-mode operation

If an external-cavity mode satisfies the oscillation condition previously discussed then the available power in the mode is limited only by the maximum output power of the diode and not by the solitary diode threshold current. It was observed that the L/I characteristic for the external-cavity laser exhibited a strange oscillatory behaviour close to the turning point of the solitary diode L/I characteristic (see figure 2.10). However no change in the spectrum was observed at least to the resolution limit of the optical multichannel analyser. This strange behaviour has been attributed elsewhere to the onset of chaotic emission[79]. (Since this does not occur in all external cavity systems further investigation was not attempted, although details can be found in, for example, reference 79). Thus although the quality of the anti-reflection coating determines the tuning range of the laser it does not limit the power available in narrow line operation.

A further example of the wavelength selectivity of the grating-loaded cavity is indicated in figure 2.15. Here the laser was tuned to one extreme of the tuning range, and the current was increased to above that of the solitary diode threshold. On blocking and unblocking the external cavity the following behaviour was observed. With the cavity blocked the emission was that of the solitary diode laser. On unblocking the cavity the output immediately jumped back to the preselected external cavity mode, and the modes of the solitary diode disappeared. This represents an excellent demonstration of the influence of the external cavity on the output of the laser, and further confirms the homogeneous nature of the semiconductor laser gain[80].

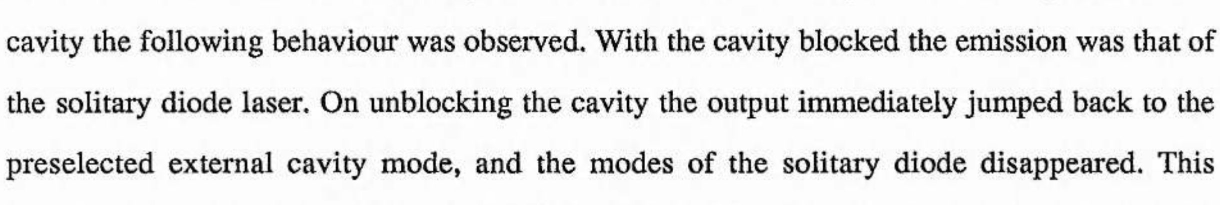

Figure 2.15 Transition from (a) multimode oscillation of the solitary diode laser to (b) narrow band oscillation under the influence of the external cavity.

### 2.6.5 Applications

The grating-tuned, external-cavity semiconductor laser provides a useful and cheap alternative to the KCl:Tl and NaCl:OH$^-$ colour-centre lasers for low power tunable laser applications at wavelengths around 1500nm. The system requires few components and can in principle be extremely compact and stable, with the major advantage of electrical excitation. The potential lifetime of an external-cavity laser is in principle only a function of the longevity of the laser chip employed. For quality InGaAsP telecommunications lasers continuous lifetimes of greater than 25 years have been demonstrated[81]. Potential applications would include for instance, a signal source for silica-based optical fibre systems, gain versus wavelength measurements of fibre amplifiers, and as a pump/signal source for Brillouin fibre amplifiers. Additionally a simpler external-cavity configuration consisting of a lensed fibre directional coupler can be employed to reduce the linewidth of DFB diode lasers through weak optical feedback[82] to the more acceptable kHz regime. Thus the external-cavity laser could also provide a broadly-tunable, narrow-linewidth local oscillator for coherent communications systems. High-power GaAlAs external cavity lasers can be exploited around 800nm for applications ranging from, for example, spectroscopy to probing nonlinear and other optoelectronic devices.

The only compromise in external cavity lasers is the inevitable increase in total system size. Nevertheless, through dedicated engineering endeavour, a miniaturised external-cavity laser package[83] has been developed at BTRL where the end product measured only 30mm x 30mm x 50mm (approximately the size of a matchbox). This package, which is not much bigger than a hermetically sealed, pigtailed semiconductor laser, retained mechanically-controlled long-range wavelength tuning and piezoelectric transducers for short-range scanning. Although the study of more advanced external cavity lasers will continue, these lasers can already meet most of the demands for commercial applications.

## 2.7 Tuning range attainable

As shown previously, the typical tuning range of a 1.5μm InGaAsP external-cavity laser featuring a single-layer, anti-reflection coating is about 65nm, and similar results are also obtained with angled-ridge devices. Although large, this figure is by no means the maximum that can be obtained from semiconductor lasers. The first route to an enhanced tuning range is to use multi-layer AR coatings and in figure 2.16 the details of the 120nm tuning range obtained from a three-layer coated buried heterostructure device when configured in the grating-loaded cavity geometry are shown[84]. Two-layer coated devices[85] with 90-100nm tuning ranges have also been demonstrated[86]. Therefore it is evident that the enhanced tunability of multilayer-coated lasers is due to a "flatter" facet modal reflectivity across the gain spectrum, albeit the minimum reflectivity is usually not as low as for single-layer coatings.

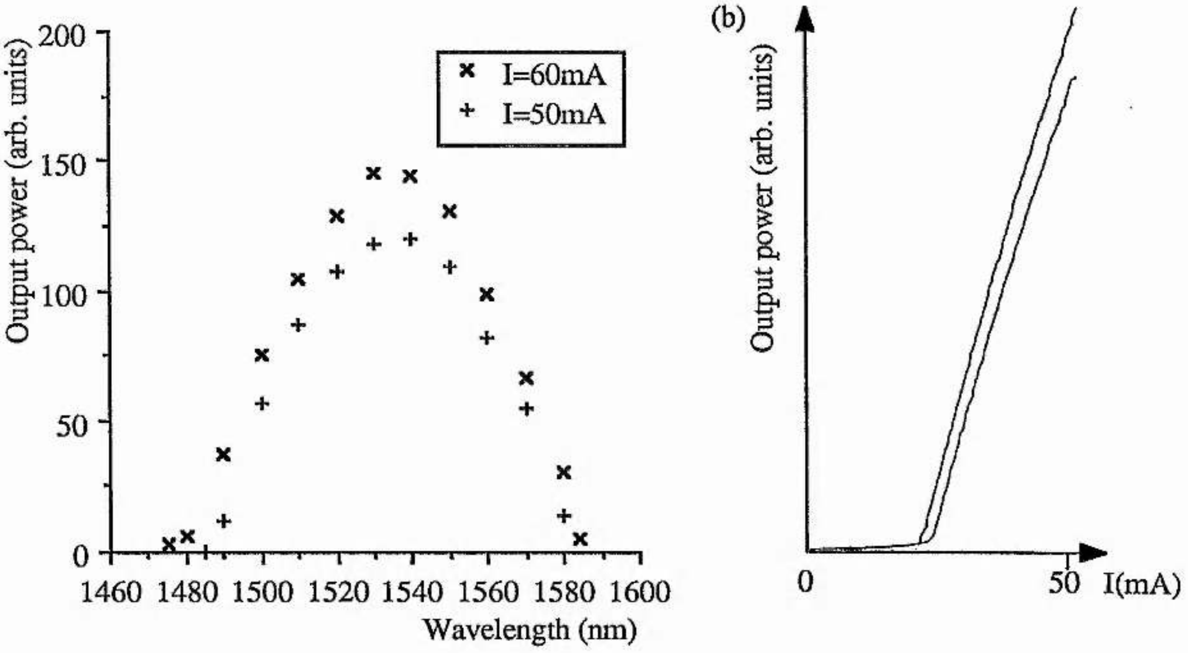

Figure 2.16 (a) Tuning range of the external cavity configuration utilising a multilayer AR coated diode chip. (b) L/I characteristic at $\lambda$=1540nm.

The 110-120nm tuning ranges obtained from conventional laser structures by using triple-layer coatings is not expected to increase significantly by further refinement to the coating because the range becomes limited by the available gain bandwidth. However, remarkable improvements on this figure have been obtained recently by optimisation of the gain spectrum of quantum-well semiconductor lasers. An unprecedented 110nm tuning range around 800nm has been demonstrated from a grating-tuned uncoated AlGaAs laser[87]. In a similar fashion, tuning from 1320 to 1562nm was shown for an InGaAsP quantum-well laser system[16]. This single laser is therefore capable of operation within the second and third telecommunications windows of silica-based optical fibres. This feature has not been achieved with any other laser source to date. It is expected that both these figures will increase to some degree, and that the quantum-well technology which has replaced almost all AlGaAs semiconductor lasers will be the dominant structure for future InGaAsP lasers.

## 2.8 Integrated fibre components

The external cavity configurations considered thus far have all utilised bulk optic components for beam collimation, wavelength selectivity and retroreflection. In this section some integrated fibre-based components will be considered for use with semiconductor lasers in external-cavity geometries.

### 2.8.1 Drawn-tapered, microlensed fibre

Coupling to and from semiconductor lasers and amplifiers is now normally achieved using microlensed optical fibre pigtails. The lenses can be fabricated using a variety of methods[88] with one such technique producing the so called 'the drawn-tapered microlensed fibre'[89]. This type of lensed fibre was used extensively in this work. The lens is produced by pulling a length of fibre within an electrical arc formed between two electrodes where an applied force results in the fibre tapering before snapping occurs. The fibre end is then heated again in the arc to allow a meniscus of predetermined curvature to form. A schematic of such a lensed fibre is shown in figure 2.17. The tapering of the fibre core region allows the guided mode to fill the aperture of the lens thus giving a spot size diminution of ~2:1. The coupling efficiency to a standard laser structure is normally higher than 50%, and so can successfully replace microscope objectives as coupling elements to semiconductor lasers.

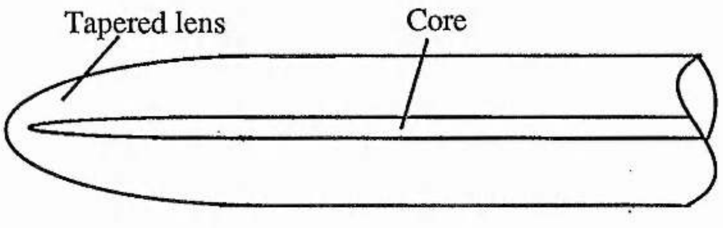

Figure 2.17 Schematic of a drawn-tapered, microlensed fibre.

The positional tolerances of a typical microlensed fibre were measured by optimally coupling to a 1.5μm DCPBH laser and noting the misalignment to reduce the output signal by one half. The values found were; 1μm in the horizontal (x) plane, 0.6μm for the vertical (y), and was oscillatory with a period of ~0.8μm along the optic axis (z axis). (These values had an estimated error of 0.1μm.) The oscillation of the coupling in the z direction is due to interference between the fields within the facet/fibre subcavity, and the value obtained agrees well with the expected λ/2 dependence. The ripple in the output power was <1/6 of the maximum output, and the average coupling was a slow function of position and hence was beyond the range of the piezo-electric transducer used. A crude estimate of the optimum fibre/facet distance of ~50μm was determined by comparison with the known length of the laser chip by using an eyepiece grid on the microscope.

Finally, the coupling coefficient of the microlensed fibre was compared to that obtained using x10 and x20 microscope objectives. Efficiencies around 50% were obtained for both the fibre lens and the x20 objective, the only significant difference between these two coupling lenses is that the fibre lens suppresses the amount of spontaneous emission output.

### 2.8.2 The fibre grating

The fibre grating[90] is a wavelength selective reflection filter suitable for incorporation as a bandwidth-limiting mirror in external-cavity semiconductor lasers (see figure 2.18). The device is produced by etching a periodic Bragg grating onto the core of the fibre which has been exposed by polishing. A thin (80nm) $Al_2O_3$ layer is deposited onto the grating which distorts the fibre mode profile to increase the overlap of the field to the corrugations hence promoting efficient coupling. A cladding layer of oil of specified refractive index is then placed on top of these experimental devices. (A production device would of course use a more robust cladding layer, such as silica, rather than the oil drop.)

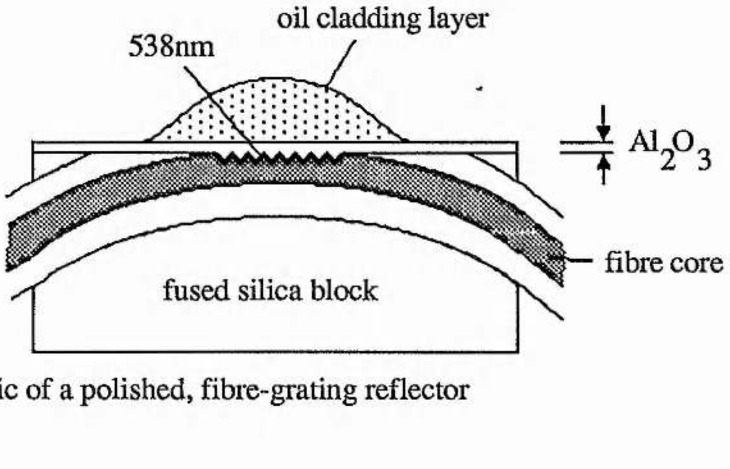

Figure 2.18 Schematic of a polished, fibre-grating reflector

The incident light undergoes partial reflection at each period of the grating and these subreflections can add in phase to give a large reflection at only one wavelength defined by the first-order Bragg condition,

$$\lambda_R = 2n_e\Lambda$$

where $n_e$ is the effective index of the fibre mode, and $\Lambda$ is the corrugation period.

The reflection and transmission functions of the grating reflector used in this work (kindly provided by C.J. Rowe of Plessey Research (Caswell) Ltd) are shown in figure 2.19. The reflectivity was 60% with a bandwidth of 1.2nm at 1.53μm. In producing these devices the reflectivity and bandwidth are determined by the interaction length of the grating. The peak of the reflection function could be altered to a degree by changing the refractive index of the capping oil. A tuning range of greater than 1nm was obtained for a change in index from 1.448-1.454. Tunable fibre gratings have been demonstrated[91] with tunable ranges in excess of 60nm around 1.3μm, but these devices are delicate and prone to damage. The transmission function of the device was >30% within the reflection band (see figure 2.19(b)).

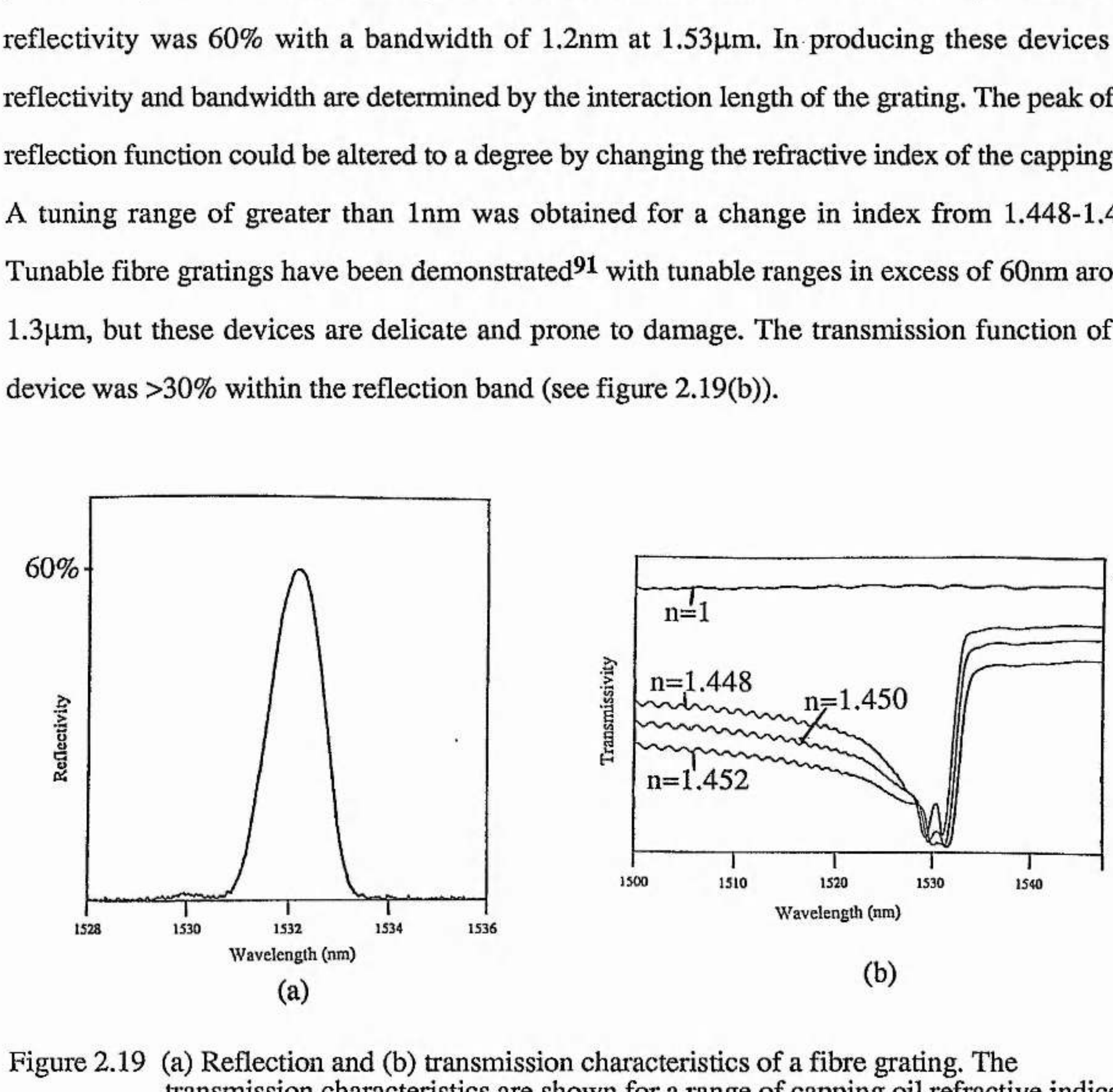

(a)

(b)

Figure 2.19 (a) Reflection and (b) transmission characteristics of a fibre grating. The transmission characteristics are shown for a range of capping oil refractive indices

Fibre gratings have been used to promote single-mode oscillation in external-cavity semiconductor lasers[92], and have also been employed in fibre-Raman oscillators[93] and high-power CW fibre lasers (see chapter 8). The CW characteristics of the external cavity InGaAsP semiconductor laser configuration of figure 2.20 incorporating a fibre grating reflector will now be detailed. (The modelocked performance of this laser will be assessed in chapter 3.)

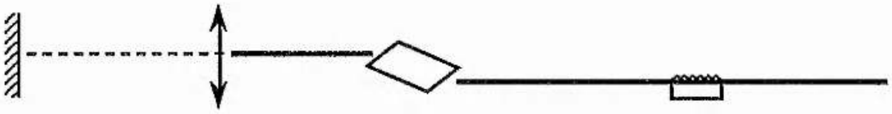

Figure 2.20 Fibre-grating, external-cavity laser.

One fibre pigtail of the grating reflector was spliced onto a length of microlensed fibre thus forming one arm of the external cavity laser. The other arm utilised a similar lensed fibre, a collimating microscope objective and a highly reflecting plane mirror. The cavity alignment was optimised using piezo-electrically controlled micropositioners and the resulting L/I characteristic is presented in figure 2.21(a). The transmitted light from the grating was directed via a mechanical chopper onto a scanning monochromator. The output was detected by a large-area germanium photodiode and a lock-in amplifier. Laser spectra corresponding to the crosses on the L/I curve were recorded (see figure 2.21(b)). It should be noted that the oscillating laser peak is suppressed relative to the fluorescence background because the oscillating bandwidth was small. Also, due to the large scans involved, a fast scanning speed was used to minimise the recording time, thereby reducing stability effects. The detection time constant was also kept relatively high to increase the sensitivity.

At low injection currents the fluorescence spectra are simply the convolution of the grating transmission function and the amplifier fluorescence spectrum. With increasing current the laser begins to oscillate and this is characterised by the emergence, and subsequent domination, of the narrow peak centred at the wavelength of maximum reflectivity. The oscillating bandwidth was measured to be 0.18nm using a 1m monochromator, which was resolution limit of the measurement system.

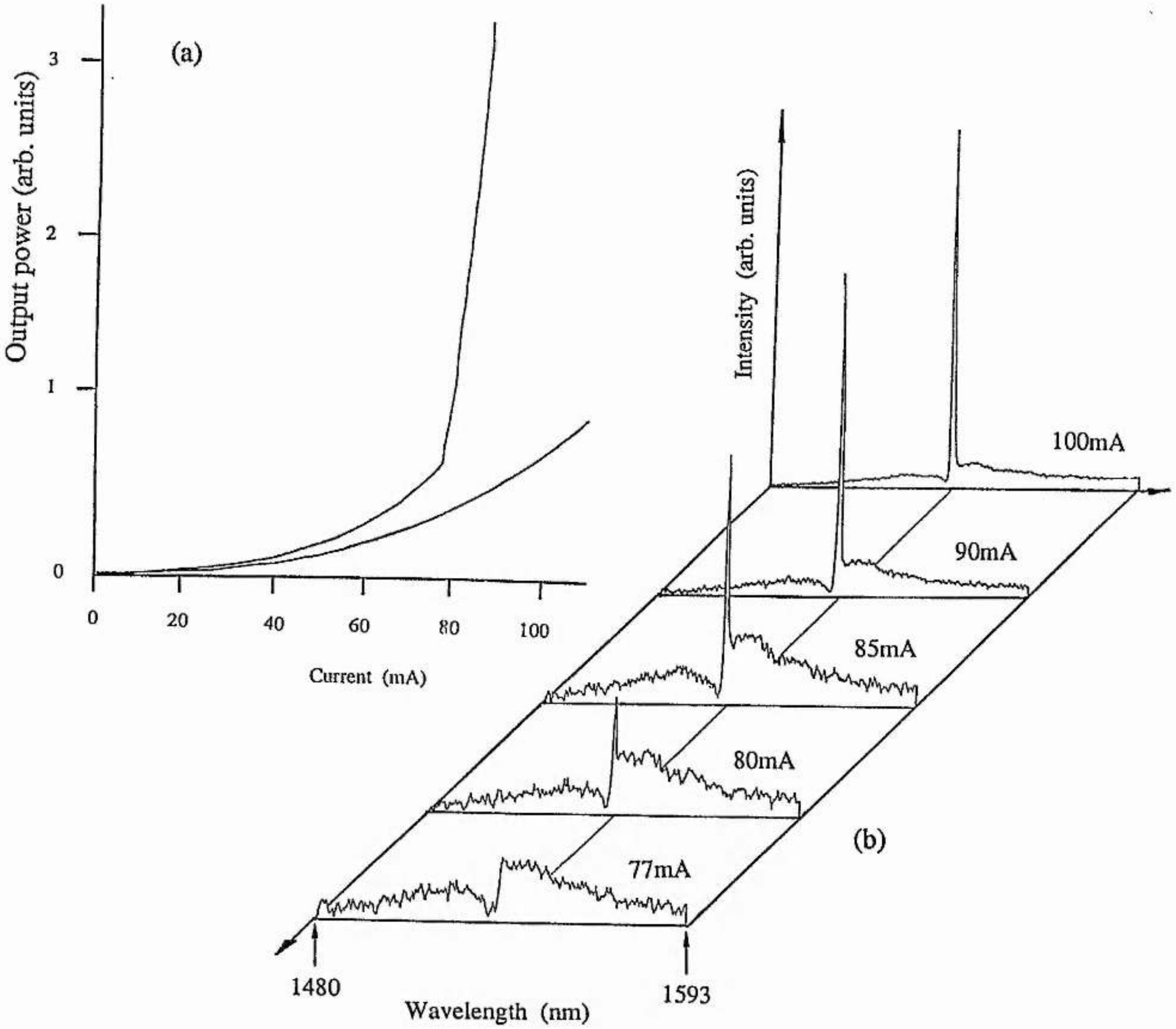

Figure 2.21 CW characteristics of a fibre-grating loaded, external-cavity laser (a) L/I characteristics and (b) spectra.

The laser exhibited good output power stability on a timescale of the order of a few minutes, with small adjustments of the fibre lenses being required to restore the power loss. The main source of the power loss was the temperature instability of the laboratory environment which resulted in misalignment due to the difference in thermal expansion of the diode header and lens positioners. Creep in the piezo-electric elements also contributes to this problem. This was more of a nuisance rather than a serious problem because previously developed thermally-compensated diode-to-fibre coupling headers which are both static and mechanically stable could be used$^{94}$. In this case, to maximise the laser stability a box enclosure was placed over the diode/fibre coupling arrangement. This relatively primative measure did indeed reduce the problem without imposing any restrictions on the flexibility of the experimental configurations.

### 2.8.3 The fibre directional coupler

An attractive degree of flexibility in design of fibre cavities can be introduced by incorporating fibre directional couplers. Indeed, for active fibre devices (see chapter 5, 8, and 9) their use is essential. The couplers used in this work were produced at STL using the fused tapering technique[95]. A schematic of a fused coupler is shown in figure 2.22(a). In the coupler the zero-order symmetric mode and the first-order antisymmetric mode are excited. The power in one arm of the device is given by,

$$I = I_0 \sin^2(\beta_0-\beta_1)z$$

where z is the coupling length and $\beta_0$ and $\beta_1$ are the propagation constants of the two modes. The term $(\beta_0-\beta_1)$ results in power transfer between the two fibres, with complete power transfer occurring every beat length. Through careful fabrication the desired cross-coupling coefficient can be obtained at the required operating wavelength. By this means 3dB splitters or low-tap monitors can be produced with excess losses below 0.1dB. A typical spectral response of a 1.5μm, 3dB coupler is shown in figure 2.22(b). Multiplexors and polarisation beamsplitters can also be made by increasing the interaction length, and various NxN and 1xN devices have also been demonstrated[96].

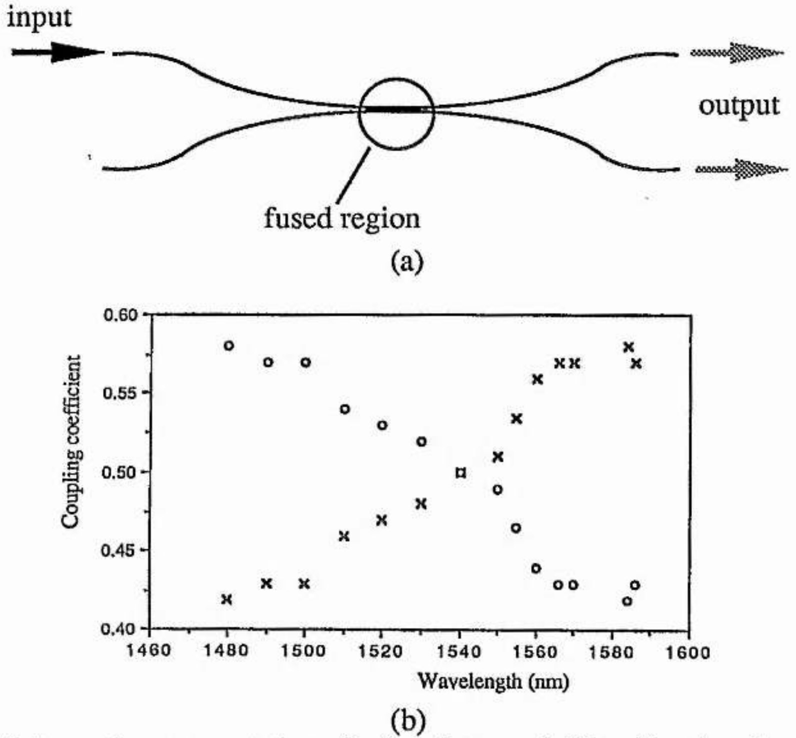

Figure 2.22. (a) Schematic representation of a fused-tapered, fibre directional coupler, and (b) the spectral response of a 1.5μm, 3dB coupler.

### 2.8.4 The fibre loop mirror

The fibre loop mirror is fabricated by splicing together the two output ports of a standard fibre directional coupler[97] (see figure 2.23). The resulting device has the power reflectivity and transmission functions,

$$T = (1-2K)^2\,(1-\gamma)^2 \exp[-2\alpha L]$$

$$R = 4K(1-K)\,(1-\gamma)^2 \exp[-2\alpha L]$$

K is the coupling coefficient, $\gamma$ is the excess loss of the directional coupler, $\alpha$ is the propagation loss in the loop and L is the loop circumference. Therefore the total loss in the loop mirror is,

$$A = 1 - (T+R)$$

These equations are obtained from a simple superposition of the counterpropagating optical fields in the device, noting that there is a $\pi$ phase change on crossing from one fibre to the other in the coupling region. The reflected component has a $\pi/2$ phase change with respect to the incident field for all values of K, whereas the transmitted signal is in phase with the input for $K<0.5$, or in antiphase for $K>0.5$.

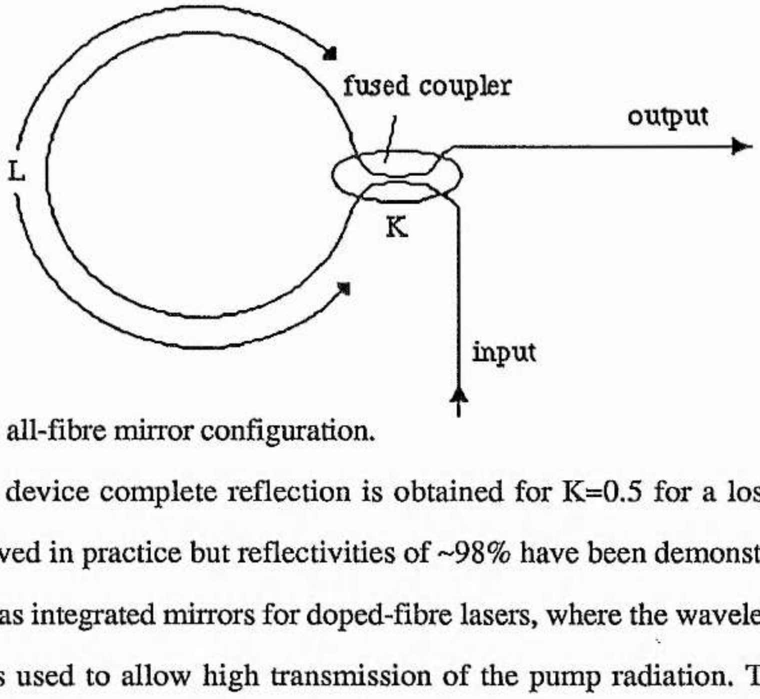

Figure 2.23 The all-fibre mirror configuration.

For this device complete reflection is obtained for $K=0.5$ for a lossless coupler. This cannot be achieved in practice but reflectivities of ~98% have been demonstrated. Loop mirrors have been used as integrated mirrors for doped-fibre lasers, where the wavelength dependence of the coupler was used to allow high transmission of the pump radiation. The device can thus effectively act as a dichroic mirror. Alternatively by using long asymmetric loops the intrinsic nonlinearity of the fibre can be accessed to enable switching of short optical pulses. This latter feature may also have ramifications in modelocked laser studies as a noise suppressor or indeed as a passive modelocking element[98].

## 2.8 Summary

In this chapter the continuous wave behaviour of external-cavity semiconductor lasers has been outlined. Emphasis has been placed on the importance of the suppression of the facet reflectivity to enhance the available tuning range obtained from these laser sources. In chapter 3 it will be shown that the effect of residual facet reflectivity plays just as important a role in the output characteristics of modelocked external-cavity lasers. Through the use of optimised anti-reflection coatings and quantum well structures the tuning ranges from external-cavity semiconductor lasers have reached unprecedented values. Various fibre components have also been outlined which will allow for additional, interesting flexibilities to be introduced into cavity design for specific systems. Therefore in general terms this type of laser arrangement can be seen to offer very considerable potential for future implementations.

# CHAPTER 3

# ACTIVE MODELOCKING OF InGaAsP SEMICONDUCTOR LASERS

## 3.1 Gain modulation

Modelocking of semiconductor lasers[99] can be achieved in a variety of ways of which the most convenient involves gain modulation[100]. In this case a radio frequency signal that is synchronous with the external-cavity mode separation is superposed onto the direct current injection level. This combination of drive signals is applied to the laser chip via a conventional microwave bias tee, which effectively isolates the DC supply from the RF signal generator. The practical aspects of impedance matching radio frequency signals to semiconductor lasers will be described together with the response of semiconductor lasers to radio frequency signals and then the modelocking performance will be addressed

## 3.2 RF power matching

To allow for maximum flexibility the laser submount (which was designed to allow optical access to both facets) was fixed to the connectorised mount illustrated in figure 3.1. The diode chip exhibits a low series electrical resistance along with significant shunt capacitance[101] and the bond wires add an appreciable inductance. Because the output impedance of the signal generator was 50Ω, the load presented by the laser header is far from ideal so power matching circuitry is a necessity. A simple matching network has been developed by assuming reasonable values for the load impedance. Frequency agility was built into the matching network thereby allowing for correction of reasonable errors in the assumed impedance of the package.

The experimental configuration was assumed to be composed of a terminal load (the diode amplifier) exhibiting a series resistance of 8Ω in parallel with a capacitance of 20pf. The operating frequency was chosen to be 900MHz ($\lambda$=33.3cm in standard coaxial cable). The inductance introduced by the bond wires was calculated to be ~6.5nH[102], as indicated in figure 3.2(a). This load was transformed into that of figure 3.2(b) using a straightforward series-to-parallel conversion. The complete system can then be represented as shown in figure 3.2(c). At this stage it is more helpful to derive the necessary matching components with the use of a Smith's chart. Figure 3.3 shows the solution plotted on such a chart, and the details are described in the following points 1-5.

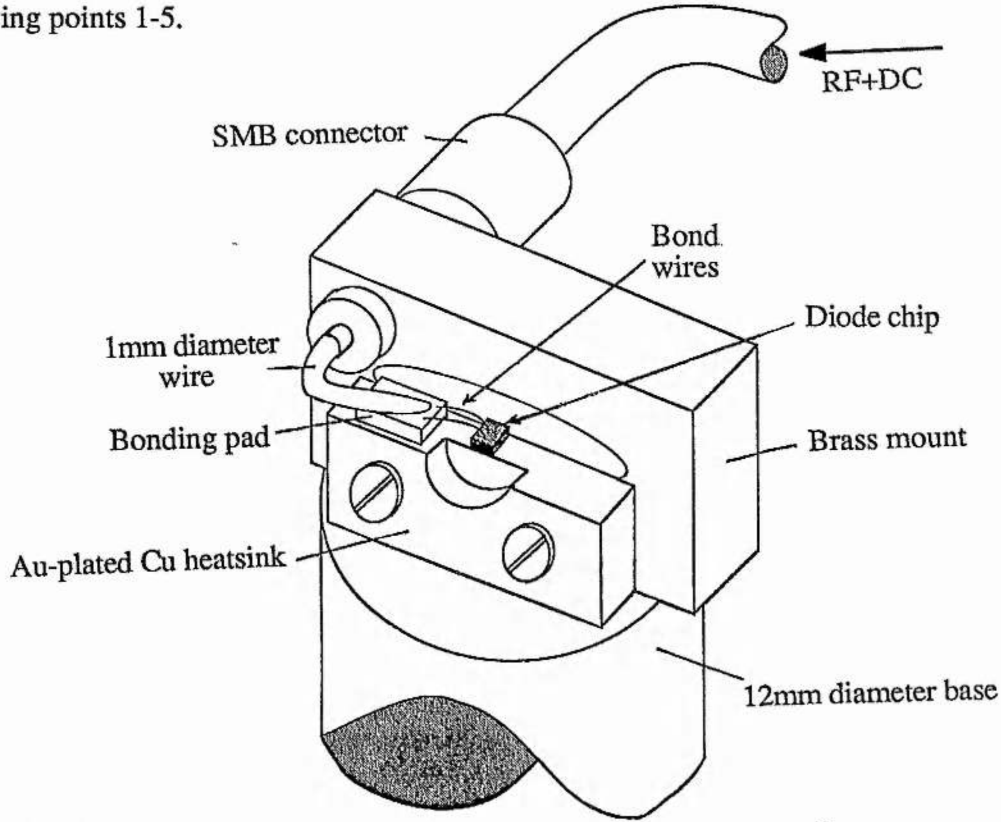

Figure 3.1 Connectorised mount for semiconductor devices used in this work. The long 12mm brass base allows the mount to be securely fixed to the fibre coupling jig.

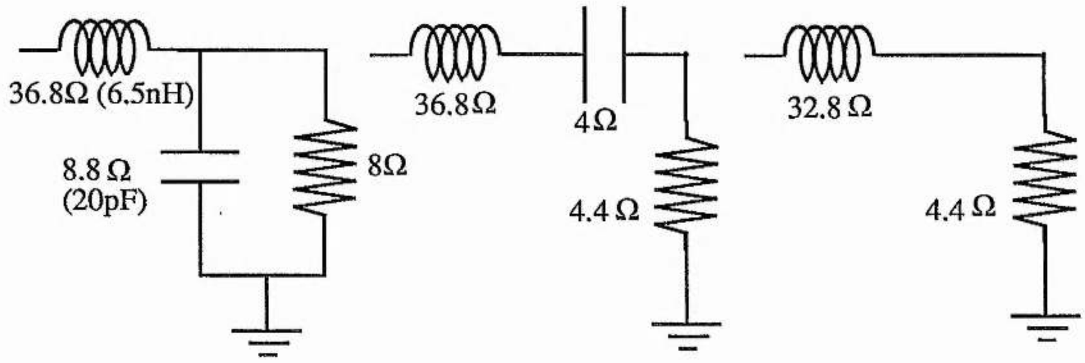

(a) (b) (c)

Figure 3.2 Terminal load diagrams representing (a) the connectorised laser package. (b) and (c) are obtained after a series-to-parallel conversion

(1) Initial condition as illustrated in figure 3.2(c). Note that the chart uses units normalised to the characteristic impedance of the transmission line which in this case was 50Ω.

(2) A clockwise rotation about the centre point to the R=1 (50Ω) contour. To achieve this requires the addition of 3.95cm of cable, and the load is now represented by (50+j195)Ω. The series inductance can be cancelled by insertion of a series capacitor with an impedance of 195Ω, but this is undesirable since the load requires to be DC biased.

(3) A line is drawn from point 2 through the centre point to intersect the previously drawn large circle. This amounts to a series to parallel conversion, and the load is now 6Ω (resistive) in parallel with 13Ω (inductive).

(4) A further clockwise rotation of $\frac{1}{3}\lambda$ again gives a 50Ω match but with an excess parallel inductance of 200Ω.

(5) A capacitor of the order of 1pf is then required in parallel to cancel the reactive impedance. This amounts to moving along the R=1 contour to the centre point. The load now lies on the centre point which represents a perfect 50Ω resistive match.

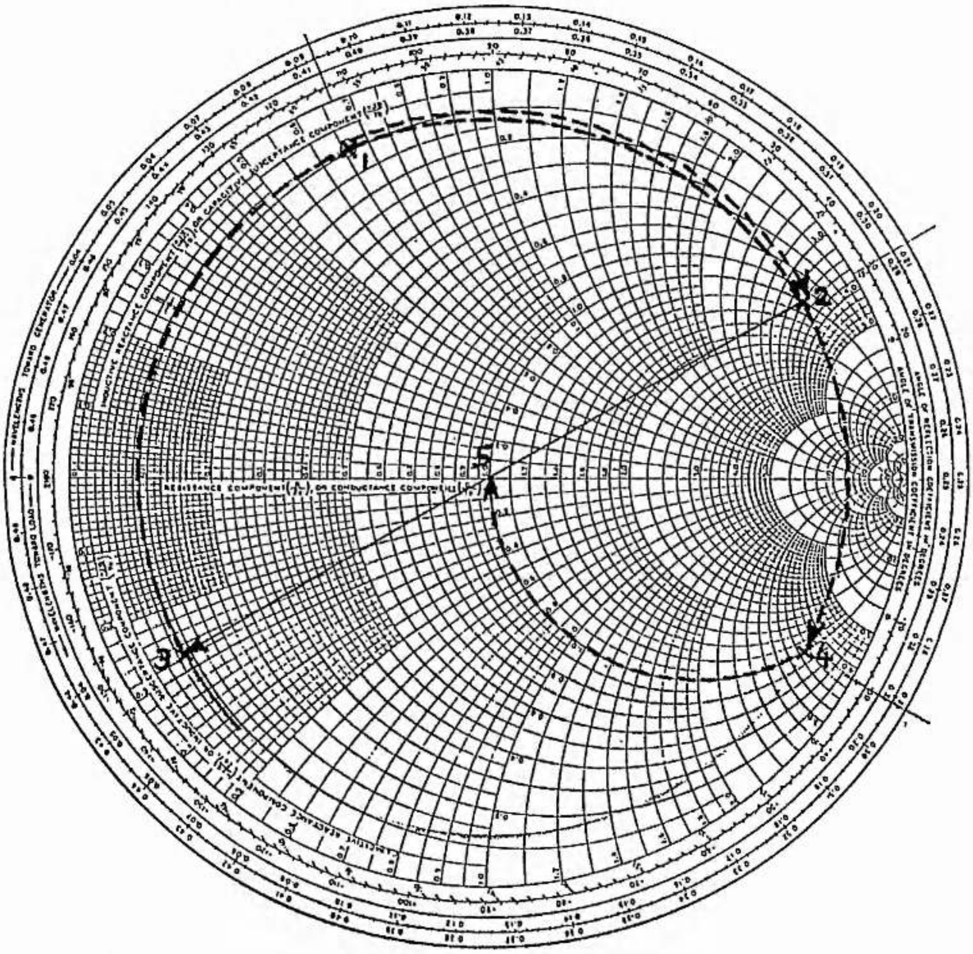

Figure 3.3 Smith's chart solution of the impedance matching problem.

The complete impedance matching network is detailed in figure 3.4(a). The delay line enabled the cable length to be adjusted, and the trimming capacitor had a range of 0-20pf. This network acts as an RF resonator in which the quality factor, Q, is maximised by adjusting the variable elements. The resonator extends from the trimming capacitor to the laser diode. The resonating RF field can reach high values and excess cable lengths (that is any extra half wavelengths) which cause power loss implies that high quality cabling is required. It is useful to consider this system as the RF analogue of a resonant optical Fabry-Perot interferometer (see figure 3.4(b)). For a lossless resonator on resonance there is no reflected wave and the output equals the input. In this arrangement the power transmitted to the laser diode is compromised due to loss in the network even if a perfect impedance match is obtained.

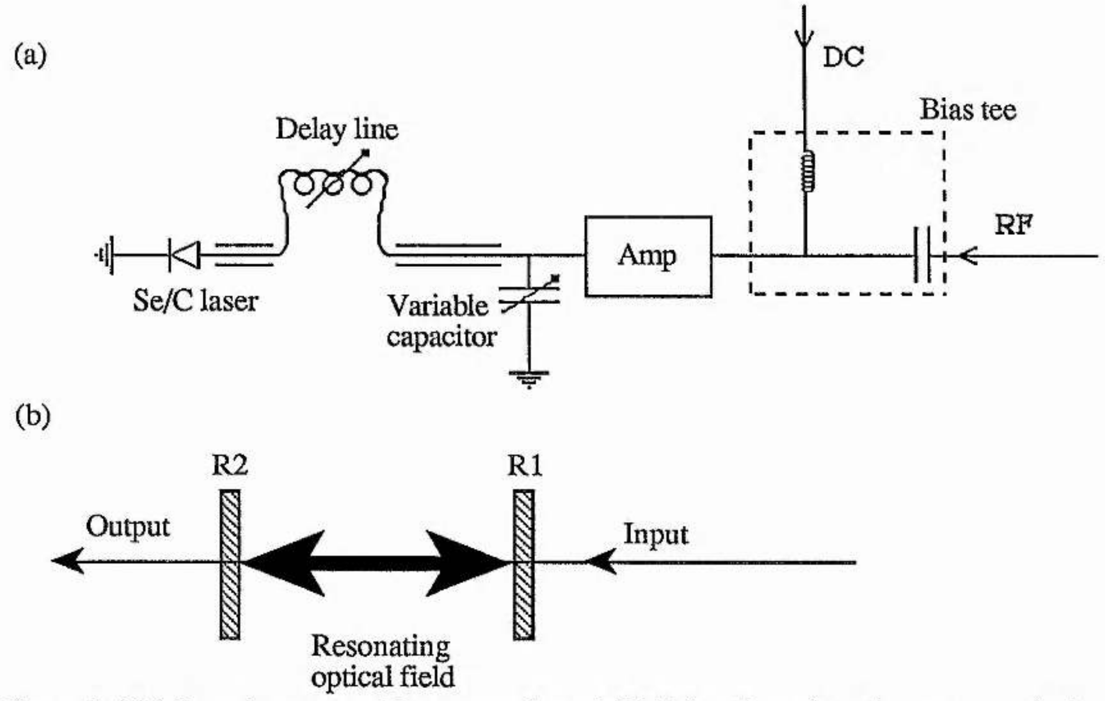

Figure 3.4 (a) Impedance matching network, and (b) Fabry-Perot interferometer optical analogue

With such an impedance matching network large-modulation active modelocking of semiconductor lasers can be achieved. Before a discussion of modelocking is presented the response of the semiconductor laser to a modulated current will be outlined. This will also serve as an introduction to the important topic of pulse production by gain-switching since the frequency dependence of the gain-switching process is important in the description of the initial transient stages of semiconductor laser modelocking.

## 3.3 Direct modulation of semiconductor lasers

The most direct way of modulating the output of a laser is to vary the strength of the laser excitation. This is useful in the case of semiconductor lasers because the light output is directly proportional to the injection current over a large current range, hence the conversion of the current modulation to light modulation is also linear. Very high repetition rates can be achieved since the photon lifetime within the laser cavity is on the order of picoseconds. Following analysis of the rate equations pertinent to semiconductor lasers the relaxation oscillation resonance can be determined[103]. The photon number within the laser responds to a step-like current excitation by exhibiting damped relaxation oscillations, or 'spiking' at an angular frequency,

$$\omega_R^2 = \omega_o^2 - \left(\frac{\gamma}{2}\right)^2$$

where $\gamma = \frac{1}{\tau_{sp}} + \tau_c \omega_o^2$

where $\tau_{sp}$ is the spontaneous emission lifetime, $\tau_c$ is the cavity (or photon) lifetime, and $\omega_o$ is the relaxation oscillation frequency. For continuous excitation, the presence of the relaxation oscillation resonance affects the modulation depth of the output laser signal. The modulation depth remains constant for frequencies well below the resonance, increases significantly in the vicinity of the resonance, then falls markedly at frequencies above the resonance. The resonant enhancement of modulation index can be ~10 times that of low frequency modulation indices, although electrical parasitics lead to a flatter small-signal modulation response and a smaller enhancement at resonance[104]. The relaxation oscillation frequency of typical semiconductor lasers is normally several gigahertz, and can be increased, for example, by reducing the photon lifetime by decreasing the laser length or by frustrating the facet reflectivity. Modulation at frequencies of up to 66GHz has been previously demonstrated experimentally[105] although only small modulation depths were obtained.

By applying a strong sinusoidal or short current pulse to the semiconductor laser the first 'spike' of the relaxation oscillation can be isolated[106]. This behaviour in semiconductor lasers is termed gain-switching and can generate pulses shorter than other laser systems due to the smaller time constants involved. In fact the output pulses can be significantly shorter than the applied drive waveform. The operating principle is considered in figure 3.5. The excitation pulse increases the gain above threshold where the laser turns on and the light builds up in the cavity.

The rapidly increasing light signal can saturate the gain through stimulated emission thus turning the laser off. Depending on the details of the excitation waveform (and hence the gain) the output can consist of multiple pulses due to gain recovery.

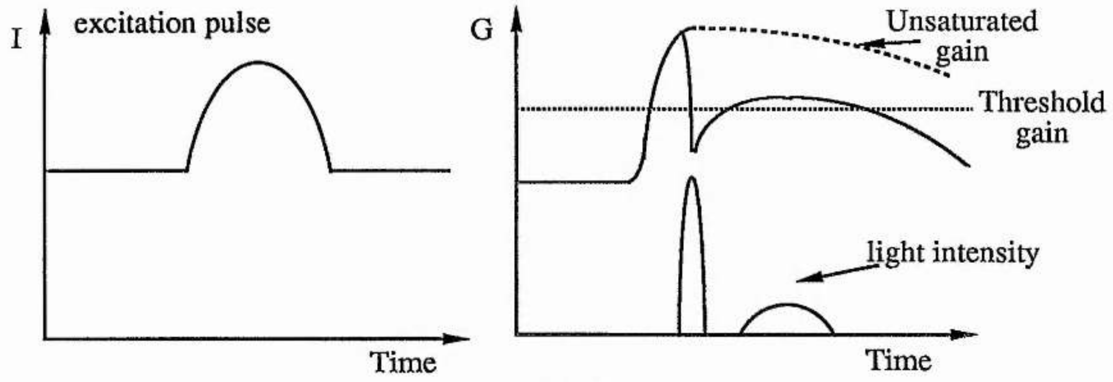

Figure 3.5 Pulse generation through gain switching.

In the case of single pulse outputs a rough estimate of the pulse duration can be made from the usual rate equations. Perturbation of the steady state laser emission[107] shows that the ringing period is,

$$\Delta t \sim (\tau_c \tau_{sp}/\eta)^{1/2}$$

where $\eta$ is the fractional excess gain above threshold. Since the width of the pulse in the isolated spike regime is much less than one period, then $\Delta t$ is an overestimate of the pulse duration. For the case of $\eta \sim 1$, $\tau_c = 3$ps, and $T_G = 1$ns, then $\Delta t \sim 60$ps.

Another theory[100] predicts that,

$$\Delta t \sim \left(\frac{\tau_c}{\eta f_m}\right)^{1/2}$$

where $f_m$ is the modulation frequency (which can be replaced by the inverse duration of the excitation pulse). From this a value of $\Delta t$ of around 50-60ps is found for a modulation frequency of 1GHz. Therefore both these approaches imply that the resultant gain-switched pulse duration should be of the order of a few tens of picoseconds.

Gain switching has the advantage of short pulse generation without any other optical components, and experimentally gain-switched pulses of ~20ps duration have been obtained, at multi-gigahertz repetition rates[108]. Analysis has indicated that for an inversion ratio, r, of 2 the pulsewidth is ~5 times the photon lifetime ($\tau_c \sim 2$-3ps), but in practice typical lasers can only be driven to r~1.5 resulting in pulse durations in the range 20-30ps. Short cavity lasers can further reduce the duration of the gain-switched pulses due to a decrease in the photon lifetime. Because the build-up starts from spontaneous emission noise, many axial modes are excited with random phases, and the output is essentially a noise burst. Therefore gain-switched pulses suffer from large amounts of amplitude and timing jitter, and the pulse duration and wavelength are normally ill-defined. In principle, relaxation oscillations can be a single mode event, and this situation can be promoted by injection seeding the pulsing laser[109], or alternatively by using a laser with inherent mode control such as a distributed feedback (DFB) laser[110].

Gain-switched laser pulses have a substantial frequency chirp across the pulse envelope originating through gain saturation produced by the strong optical field. Transmission through long lengths of dispersive optical fibre has been used to dechirp and reduce the duration of gain-switched laser pulses[111]. Such techniques tend to defeat the basic simplicity of these lasers and so the shorter, cleaner pulses produced by modelocking become a more attractive option. In the following section the active modelocking of semiconductor lasers will be described with particular emphasis being placed on quaternary InGaAsP devices that operate at wavelengths around 1.5μm.

### 3.4 Actively modelocked semiconductor lasers

A distinction can be made in the current-modulated active modelocking techniques as applied to semiconductor lasers between the high-frequency modulation and low-frequency modulation techniques. The high-frequency technique can be thought of essentially as a delayed, but synchronised, injection seeding of a gain-switched laser chip. Figure 3.6 shows the response of a semiconductor laser to a current waveform consisting of a strong sinusoidal component superimposed on a DC injection current[112]. As the modulation frequency increases the number of spikes decrease, and eventually a single pulse is generated around 1GHz. This can be considered as the initial conditions present in the high frequency modelocked semiconductor laser although the details of this situation will vary according to the particular semiconductor laser used. Subsequent filtering and re-injection of the pulse by the external cavity acts as a seeding signal, with the resulting pulse being more coherent, and also enhanced gain saturation promotes pulse shortening. This process continues to a steady state where coherent, although chirped, pulses of durations as short as ~5ps are produced[31].

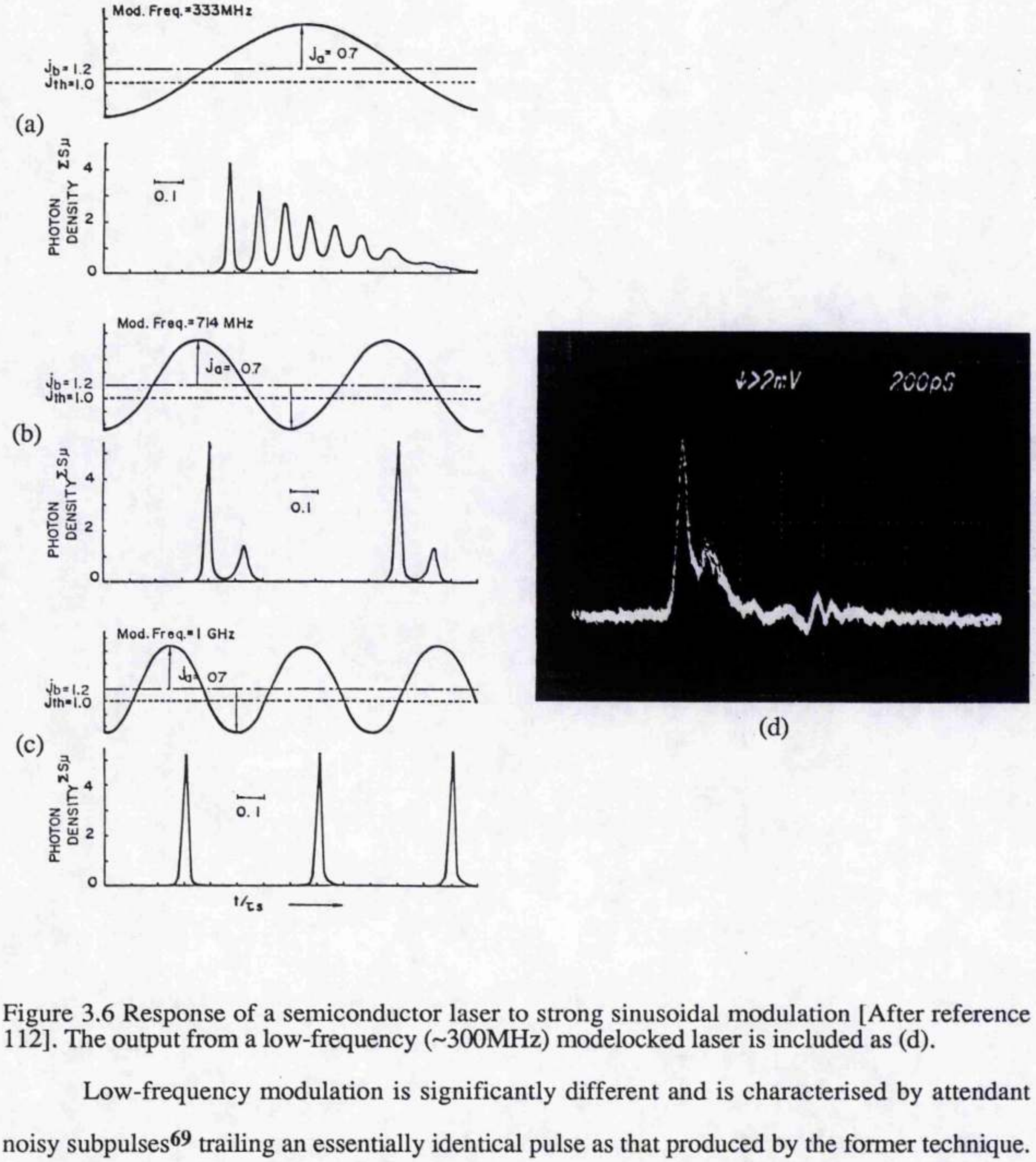

Figure 3.6 Response of a semiconductor laser to strong sinusoidal modulation [After reference 112]. The output from a low-frequency (~300MHz) modelocked laser is included as (d).

Low-frequency modulation is significantly different and is characterised by attendant noisy subpulses[69] trailing an essentially identical pulse as that produced by the former technique. The initial conditions being somewhat similar to that of figure 3.6(b). To illustrate this the oscillogram of figure 3.6(d) was obtained from a modelocked InGaAsP semiconductor laser operating at 300MHz. The degree of subpulsing was observed to diminish with increasing modulation frequency and this topic will be discussed in more detail in chapter 4. The remainder of this chapter will be devoted to the operational properties of low-frequency modelocked semiconductor lasers because these offer the attractive features of higher peak pulse powers.

### 3.5 Symmetrical linear external-cavity lasers

When angled-stripe semiconductor amplifiers are used as gain media in external-cavity laser configurations the amplifier must be coupled to two external cavity sections to allow laser oscillation. AR coated diodes require only one such section as do chips produced with only one angled facet[113]. The diode amplifier is highly absorbing to its own radiation when unpumped and a requirement for modelocking with this cavity type is that the diode is placed centrally between the two external-cavity mirrors. That is, the cavity should be symmetrical or balanced (see figure 3.8). The tuning element allows the laser output to be tuned over the large gain bandwidth of the amplifier, and also acts to restrict the oscillation bandwidth which is desirable for good modelocked performance. Possible tuning elements can be etalons, prisms and diffraction gratings. For modelocking the total cavity length is normally in the range of a few centimetres to ~1m. For experimental configurations, long cavity lengths are normally chosen to aid flexibility and harmonic modelocking is utilised to keep the repetition rate within acceptable limits.

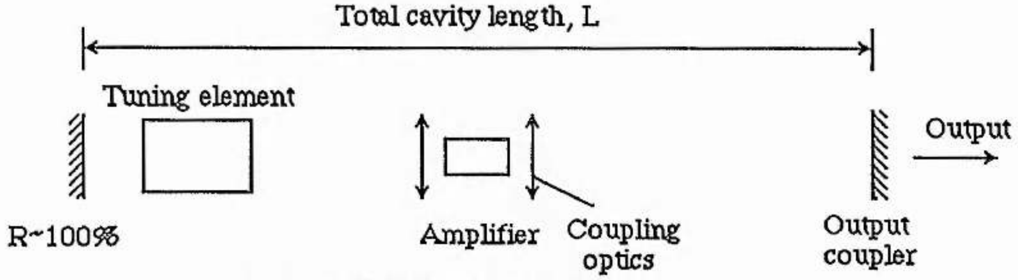

Figure 3.8 Symmetrical external-cavity semiconductor laser.

The standard modelocking technique for low frequency systems is to apply a subthreshold DC bias and superimpose onto this an RF signal of frequency equal to the external cavity mode spacing (or some multiple thereof). For a 1m long laser the cavity mode spacing ($\frac{c}{2L}$), where L is the optical path length) is 150MHz. However, in the case of a balanced cavity, modulation at 150MHz would mean that the intracavity pulse would experience gain only on alternate passes through the diode amplifier and hence the output pulses would be seriously degraded. For this reason the modelocking frequency ($f_m$) of the balanced cavity is chosen using the relation,

$$f_m = \frac{c}{nL}$$

where n is an integer indicating the harmonic number. It should be noted that this is the same resonance criterion as for modelocked ring lasers (L in this case defines the optical path length of the perimeter) where the pulses also collide in the gain medium.

### 3.5.1 Lensed fibre cavities

The laser configurations studied here utilised microlensed fibre external-cavities[114] instead of the more conventional microscope objective/bulk mirror (or diffraction grating) free-space external cavities. The reason for this is twofold; firstly the small dimensions of the fibre microlenses can allow access to the output from angled-ridge amplifiers without resorting to complicated heat-sink headers, and secondly, the fibre medium is more compact than free-space cavity sections because it can be wound into a reasonably tight coil (diameter >50mm) without affecting its transmission. Mirrors can be directly butted[115] onto the end of a cleaved fibre without the introduction of significant loss or alternatively some type of integrated fibre mirror/filter may be used. An integrated fibre-grating reflector was used in part of this work (see section 3.8) but in general the cavities incorporated a bulk-optics cavity section to facilitate tunability and more importantly bandwidth control (see figure 3.9). Prism and etalon tuned configurations will feature in this chapter along with the fibre grating cavity. The more attractive bulk diffraction-grating loaded external-cavity laser was also extensively used and will be described in chapter 4.

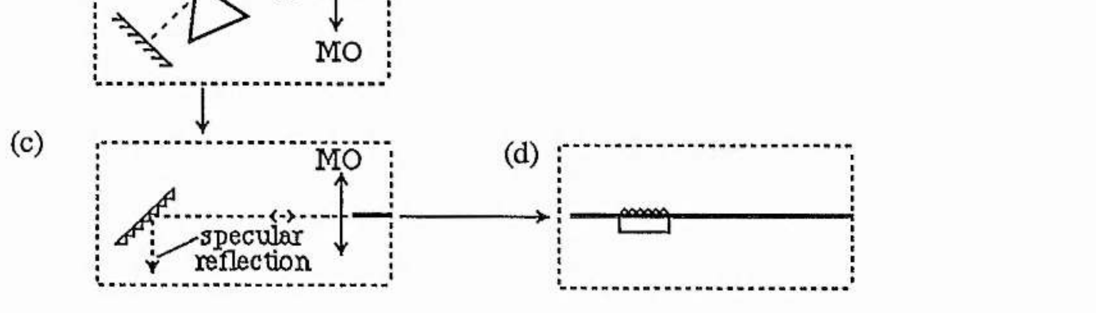

Figure 3.9 Experimental realisations of balanced external-cavity lasers incorporating (a) etalons, (b) prism, (c) diffraction grating, and (d) an integrated fibre grating reflector.

### 3.5.2 CW operating characteristics of symmetrical external-cavity lasers incorporating angled-ridge semiconductor amplifiers.

The laser cavity as illustrated in figure 3.9(a) was configured using an angled-ridge ($10^o$) waveguide InGaAsP amplifier. The light/current characteristics measured for the laser is shown in figure 3.10, where curve (a) was recorded with the external cavity blocked and curve (b) obtained for the unblocked cavity. The solitary angled-ridge amplifier could not sustain laser oscillation for current levels in excess of 6-7 times the threshold current of an identical Fabry-Perot device (~40mA). The fluorescence intensity as a function of injection current was typical of an ASE laser, but single-sided feedback was observed to affect the features of the fluorescence spectrum. Figure 3.11 shows such a fluorescence spectrum which is characterised by a large period spectral modulation which only appears when significant optical feedback is present as was described in section 2.5. This modulation influenced the free-running oscillation spectrum of the laser (see figure 3.12(a)) where oscillation on several peaks of the modulated gain spectrum were observed with finer detail being evident within each cluster.

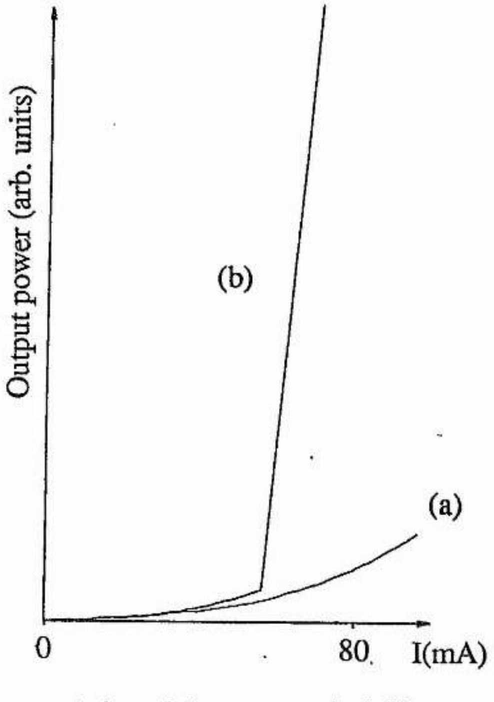

Figure 3.10 Light/current characteristics of the symmetrical fibre external-cavity laser for (a) the free-space section blocked, and (b) unblocked.

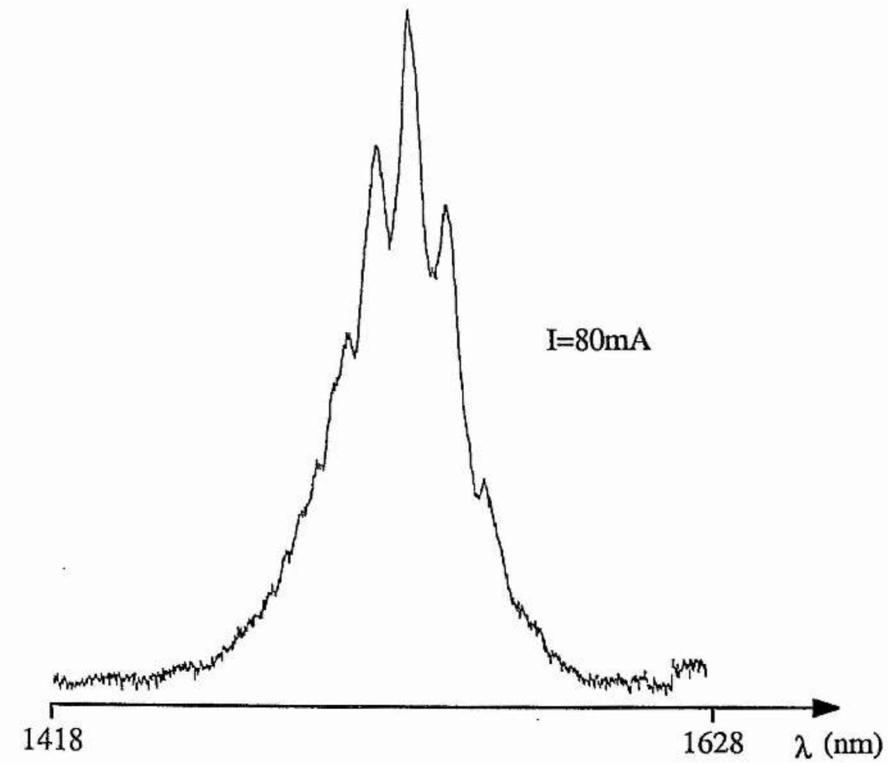

Figure 3.11 Fluorescence spectrum of angled-ridge amplifier with single-sided external-cavity feedback

Figure 3.12 (a) Free-running spectrum of symmetrical external cavity laser, and (b) after insertion of two etalons (0.5 and 0.2mm)

The total emission spectrum can be viewed as a superposition of a series of spectral modulations on the essentially bell-shaped material gain spectrum of the semiconductor amplifier.

These are (i) the ~11nm period feedback induced modulation, (ii) the Fabry-Perot modulation due to either the semiconductor amplifier and/or reflections from the fibre microlenses [The measured period was 0.66nm and the expected periodicity for the amplifier cavity and the cavity formed between the two fibre lenses was 0.67 and 0.65nm respectively therefore the measurement resolution was insufficient to provide an unambiguous source for this modulation], and (iii) the modulation due to the external cavity itself which would be ~150MHz and hence was unresolvable in these measurements.

By inserting two etalons into the free-space cavity section a single Fabry-Perot mode defined by the amplifier/fibre lens subcavity could be isolated (see figure 3.12(b)). The most suitable etalons were found to have thicknesses of 0.5 and 0.2mm, and by rotating the etalons some degree of wavelength tunability was provided.

## 3.6 Modelocked symmetrical external cavity semiconductor lasers

### 3.6.1 Modelocked etalon-tuned semiconductor laser

On application of a ~600MHz RF component (which relates to the second harmonic modelocking frequency for the 1m long cavity) onto a subthreshold DC current the position of the bulk cavity mirror and the modulation frequency were iteratively adjusted such that a pulsed output was observed on a PIN photodetector/sampling oscilloscope arrangement. The resolution-limited pulse durations observed demanded employment of a synchronously operating streak camera for further pulse characterisation. To achieve this a frequency multiplying network had to be constructed because the frequency of the streak camera deflection sinusoid was selected to be ~150MHz. [A frequency divider was initially used but the introduction of spurious timing jitter in the detection system warranted the use of a higher fidelity multiplier circuit.] The frequency multiplier circuit is detailed in figure 3.13, and the accompanying oscillograms indicate its performance characteristics.

The signal generator output of 0dBm at 150MHz (figure 3.13(b)) was transformed to the desired 600MHz output signal (figure 3.13(c)) with a harmonic gain of ~1dB [ie. from 150 to 600MHz]. The output signal power could be varied by adjusting the gain of the two in-line amplifiers, and the second harmonic suppression of the output signal was below 50dB for all outputs up to a power of ~3dBm. [The RF amplifiers used had a maximum output of 10mW, a gain of 20dB and a 3dB gain compression frequency of ~850MHz[116]. Figure 3.13(d) illustrates amplification of broadband noise (generated from a reverse biased diode) using such an amplifier]. The bandpass filters had a bandwidth of a few megaHertz which effectively suppressed the harmonics created in the multiplication process but allowed for reasonable tunability of the output signal frequency. The resultant ~600MHz signal was then amplified to ~1W and applied to the laser through the impedance matching network described previously.

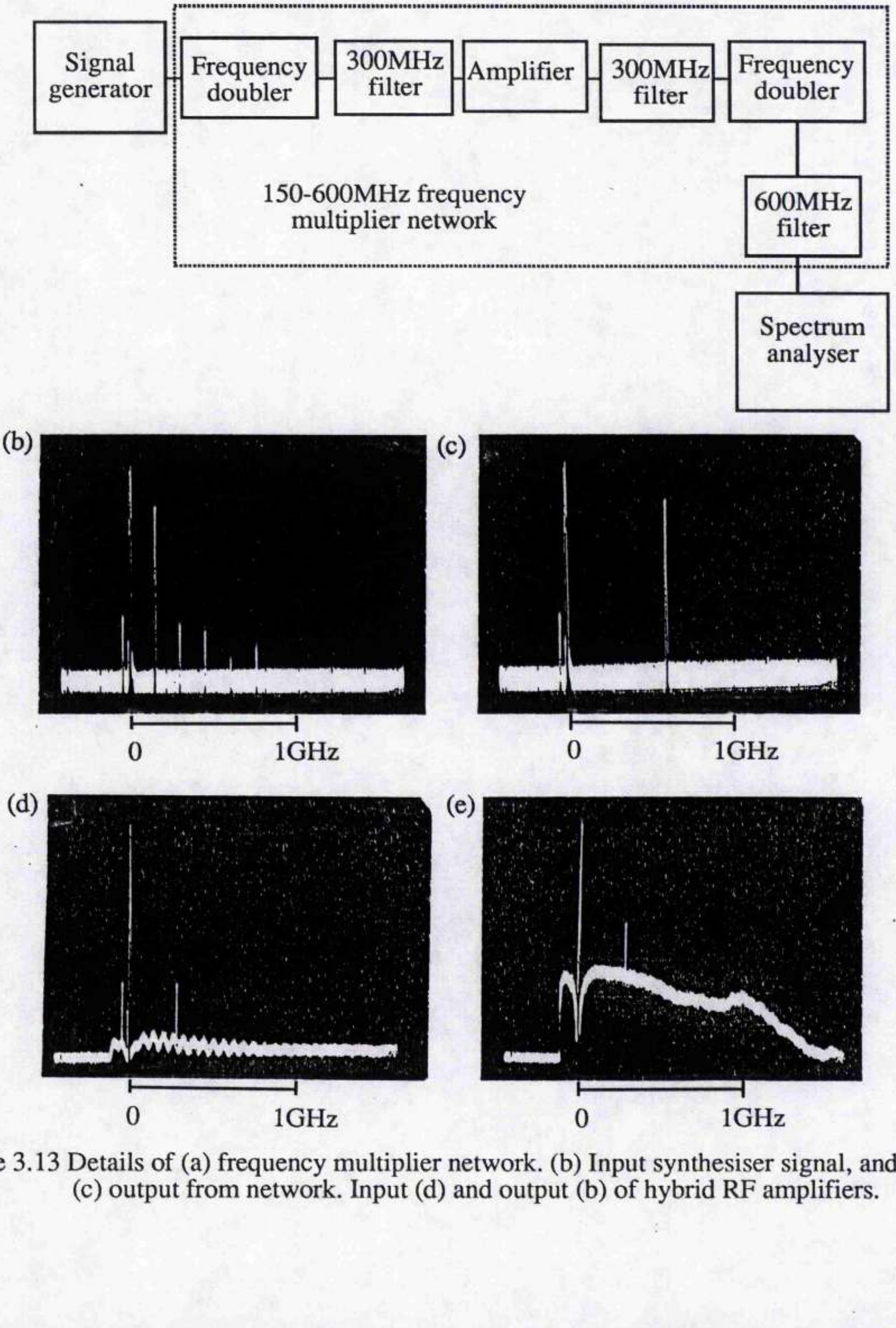

Figure 3.13 Details of (a) frequency multiplier network. (b) Input synthesiser signal, and (c) output from network. Input (d) and output (b) of hybrid RF amplifiers.

Using the frequency multiplier network the modelocked laser could be driven by the signal applied to the deflection circuitry of the streak camera. Thus the relative timing jitter of the diagnostic system was minimised so that of the temporal resolution of the camera was not severely compromising. A typical optimised streak intensity profile obtained from the laser is shown in figure 3.14(a). The measured FWHM pulse duration of 5.1ps corresponds to 3.7ps after the deconvolution of the temporal resolution (~3.5ps) of the measurement system. This implied that the main pulse peak power was approximately ~180mW.

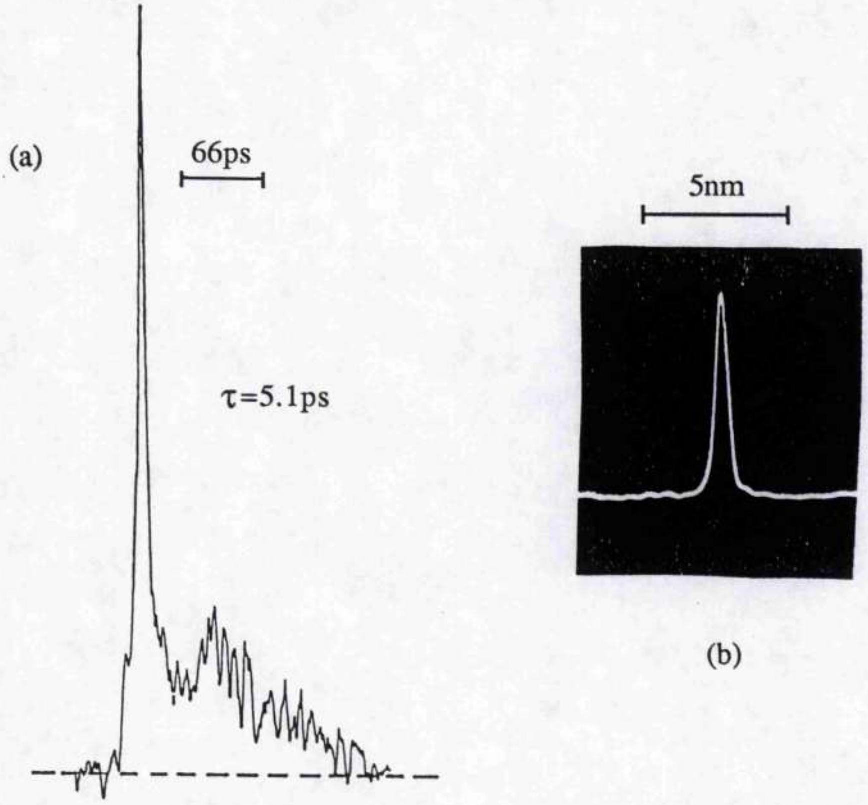

Figure 3.14 (a) Streak intensity profile of modelocked pulses from the etalon-tuned laser, and (b) corresponding output spectrum.

The spectral bandwidth of the modelocked pulses was obtained using a scanning Fabry-Perot interferometer and was 1.3nm (see figure 3.14(b)). It was evident that significant spectral broadening accompanied the modelocking process which is consistent with the concept of mode generation through the nonlinear interaction of the pulses with the semiconductor gain medium (see section 1.4.2). Moreover, the existence of frequency chirp across the pulse envelope further extends the bandwidth, and the ΔνΔt product of 0.64 for these pulses indicates that significant frequency chirp is present.

### 3.6.2 Frequency chirp

One problem that is frequently discussed and is especially relevant to modelocked semiconductor lasers is the existence of frequency chirp[117]. Frequency chirp is defined as the rate of change of the instantaneous frequency of the optical pulse. The presence of chirp can be established quite simply by calculating the duration-bandwidth product of the pulse and comparing the result with those obtained for bandwidth limited pulses of particular shape. The most commonly assumed pulse shapes are the bell-shaped Gaussian and $\text{sech}^2$, although it is reasonable to expect that pulses from most modelocked lasers would be assymetric. This is because the pulse shaping mechanisms acting on the leading and trailing edges of the pulse are usually different in origin.

There are also a variety of techniques which can give extra information about frequency chirp and these vary from strictly qualitative (eg. interferometric autocorrelation[44]) to quantitative measurements (eg. cross correlation[45] and spectro-temporal analysis[118]). Of these techniques the spectro-temporal analysis requires no ambiguous assumptions, is linear and is highly visual. Basically a calibrated dispersive element (usually a monochromator with the exit slit removed) followed by a streak camera with a two dimensional readout system (eg. a CCD array or a photographic plate) is used. The data is then represented by a two-dimensional streaked image where one axis defines the temporal extent of the pulse, and the other the instantaneous spectrum. The temporal data is therefore limited by the resolution of the streak camera (and also any delay introduced by the dispersive element), but the spectral data can usually be adequately resolved using most spectrographs.

Measurements of the chirp content of modelocked semiconductor laser pulses have been obtained in the above manner[119]. The chirp has been shown to be largely linear, with nonlinear components at the extremes of the pulses. This suggests that a simple linearly dispersive delay line could be employed to compensate for the main chirp content leading to the generation of shorter pulse durations. However, the peak wavelength of the instantaneous spectrum of modelocked semiconductor lasers shifts from shorter to longer wavelengths across the pulse envelope, and so positive group velocity dispersion is required for chirp compensation. This presents a problem at 1.5μm since most pulse compressors[120] introduce negative group velocity dispersion (GVD) as is the case for standard optical fibres. Optical fibres can be produced which exhibit positive GVD[121] at 1.5μm although these usually introduce substantial propagation loss since the magnitude of the dispersion is low and so long lengths are required (a few kilometres). The Treacy diffraction grating pair can be adapted to introduce large degrees of positive GVD[122] but this configuration is very lossy with, at best, 10-20% throughput efficiencies.

The primary source of frequency chirp in semiconductor lasers arises due to gain saturation across the duration of the pulse. It is also known that the refractive index of the active region of the semiconductor laser is dependent upon the carrier density. Olsson and Agrawal[123] showed that for a travelling-wave laser amplifier that changes in the carrier density resulting from gain saturation due to picosecond pulses directly affected the refractive index of the material. Their analysis also examined the spectral distortion produced by this gain saturation induced self-phase modulation, and showed that large spectral shifts and broadening were possible. Consideration can also be given to the quasi-Fermi levels of the carrier distribution during the passage of the optical pulse. Initially these levels extend far into the conduction and valance bands hence amplification over a broad spectral region is possible. On amplification, and subsequent saturation the carrier density is significantly reduced resulting in a smaller separation of the Fermi levels. This then restricts amplification to the red spectral region of the propagating pulse and so a redistribution of the instantaneous spectral content of the pulse would indeed be expected.

### 3.6.3 Pulse substructure

During the process of optimising the modelocked laser distinct types of substructure have been observed on the output pulses, as illustrated in figure 3.15. The first (figure 3.15(a)) is the primary subpulse that arises due to gain recovery within the pumping cycle. The second 'level' of substructure indicated by figure 3.15(b) is revealed by careful adjustment of the cavity length and the modulation frequency such that the gain medium is at the centre of the external cavity. This implies that for this effect the timing of the pulses with respect to their collision in the gain medium has to be very precise. A frequency detuning of 10kHz or a cavity arm imbalance of a few microns serves to destroy this timing. The period of the structure was consistently measured to be ~12ps when using the AR coated amplifier (L=350μm) and ~18ps for the longer angled-ridge amplifier (L=500μm). These figures do not relate in a simple way to the length of the subcavity, but in both cases are almost exactly three times longer than the transit time of the pulses within the amplifier. Although the origin of such features is not clear the records imply that energy transfer takes place between the counterpropagating pulses.

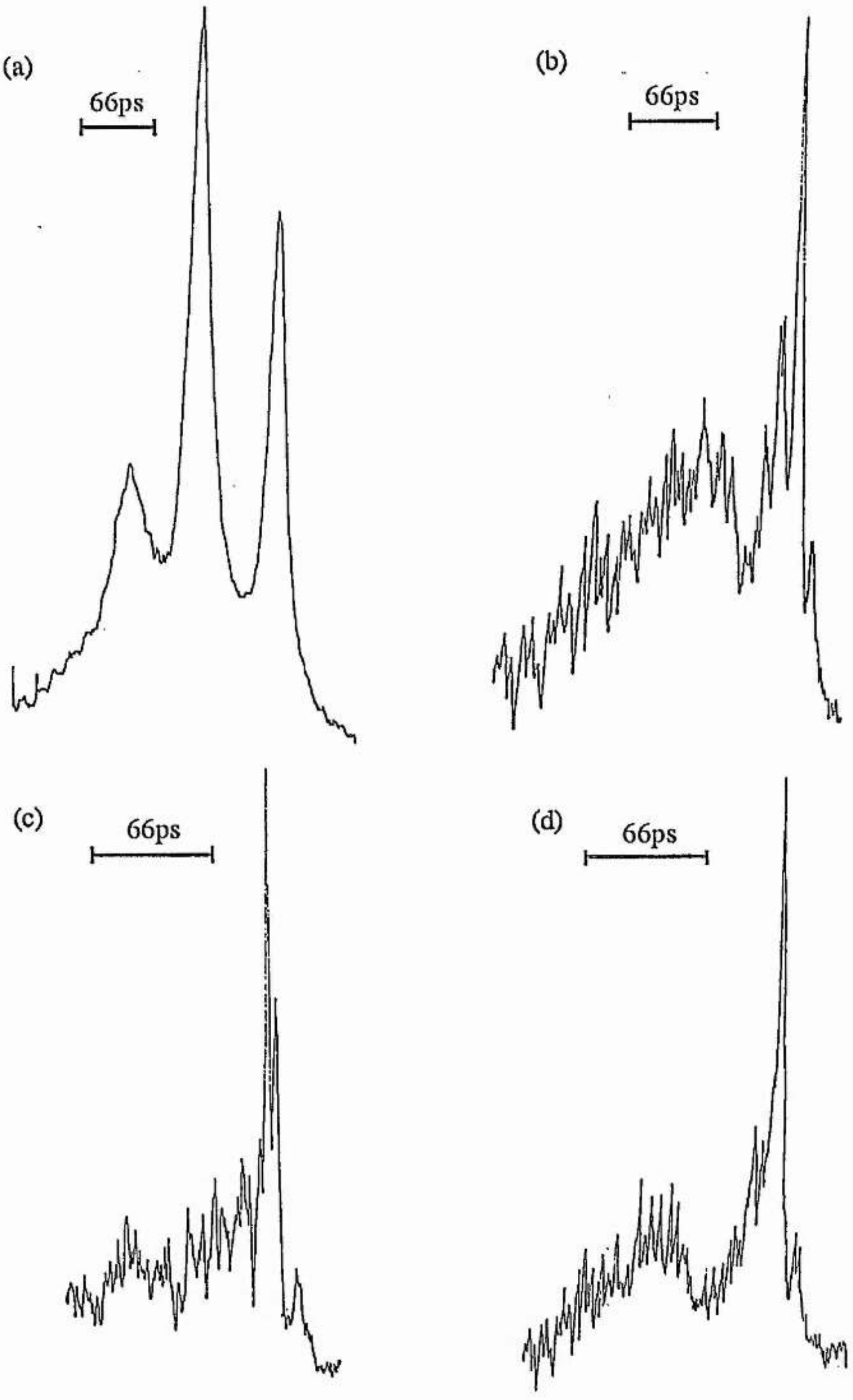

Figure 3.15 Modelocked pulse substructure. (a) details two pulses overlaid with a 66ps delay for calibration purposes, whereas (b), (c), and (d) are single output pulse profiles. In all cases the direction of propagation is from left to right.

When the streak camera resolution was carefully optimised (200 pixels of scan for a 66ps time delay) a further level of substructure could be observed (see figure 3.15(c)). The phase stability of this ~4.3ps period substructure for the AR coated amplifier was poor and could only be recorded using the fastest available accumulation time of the camera system, which was 33ms and corresponds to integration of about 20 million pulses. Each subpeak had a duration of ~3ps which was the absolute limit of the temporal resolution of the streak camera. In some measurements the total pulse duration (FWHM) would contain one such subpulse such that the pulse durations could be as short as 3.5ps (as reproduced in figure 3.15(d)) although in most cases (~90%) this was not so.

The origin of this substructure is believed to be due to the effect of the residual reflectivity of either the diode facets or reflections from the surface of the fibre microlenses. Hence this is then the fundamental substructure arising from the diode subcavity. The ~4.3ps periodicity relates to the optical path length of the 350μm long laser amplifier since the external cavity is 'double-armed'. Again there is energy transfer between the two pulses and it is obvious that the cavity balance condition will be very stringent for this transfer to produce an observable effect, as was evidenced during the experiment. By dephasing the arrival of the two counter-propagating pulses the subreflections cannot build-up to form appreciable structure on the output pulses, so smooth pulses are detected. This is normally the case in external cavities that have been configured with two arms since the balance must be maintained to within a few microns (which corresponds to a temporal delay of tens of femtoseconds).

The substructure observed here is similar in nature to that obtained by Morton et al[124] for their high-frequency, modelocked asymmetric-cavity laser where the measured ~10ps pulse exhibited substructure. In their case, under conditions of strong microwave modulation, very short (0.5ps) component pulses each separated by the round-trip time of the diode subcavity were observed. Their analysis revealed that even for very small residual facet reflectivities the subcavity effect can produce large changes in the pulse structure because the process can build-up over many round trips of the external cavity.

### 3.6.4 Initial conditions of semiconductor laser modelocking

It was suggested previously that the steady-state modelocked performance of the semiconductor laser was influenced by the initial conditions of the pulse build-up, and these were likened to that of a gain-switched laser. Using the modelocked laser described here [except that an AR coated amplifier was used] it was found that small changes in the initial gain conditions (affected by altering the fibre/facet distance) could significantly alter the output pulse features. Figure 3.16 illustrates two such output pulses, pulse (a) was obtained from an optimised cavity whereas pulse (b) was generated by increasing the laser threshold.

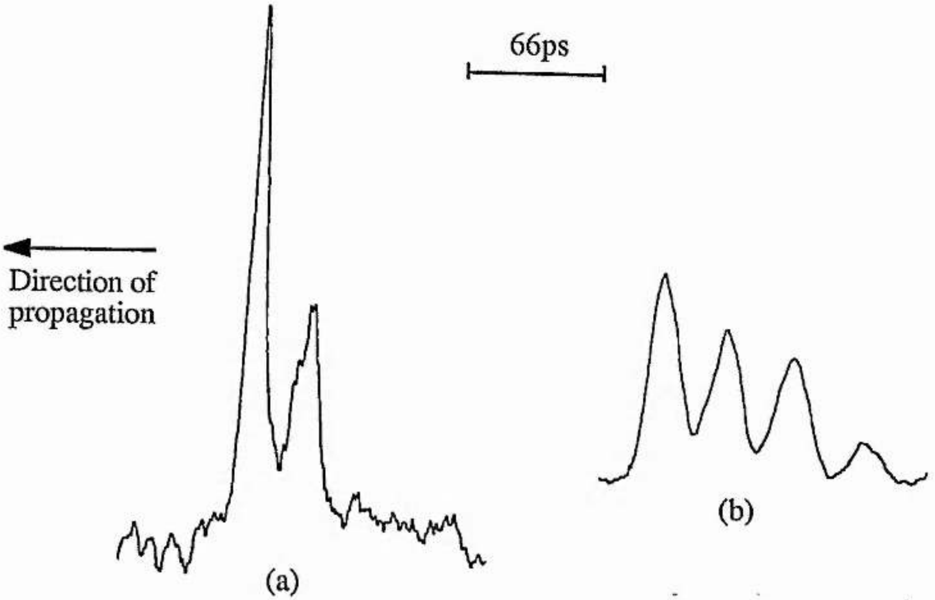

Figure 3.16 Variation of modelocked laser output pulse profiles.

It is believed that the reduced curvature of the gain present in case (b) promotes an initial gain-switching condition similar to that shown in figure 3.6(a) and case (a) to that of figure 3.6(b). Therefore to produce discrete pulses the slope and the temporal extent of the modulation signal must be reduced. This can be brought about by using a reduced DC current and increasing the RF signal component of the laser modulation signal. [An explanation of the details of this technique will be dealt with in section 4.3.3.] The etalon-tuned laser was modelocked under these conditions and it was found that subpulse-free pulse generation was indeed accessible (see figure 3.17). In fact the best output pulses were obtained when no DC current was applied to the laser, although rectification of the RF signal led to ~9mA being registered on the milliammeter used to monitor the DC current flowing through the laser. The deconvolved pulse duration obtained under conditions of zero DC bias was 8.2ps and so in discrete pulse production increased pulse durations were observed. [The peak power was 140mW in this case.]

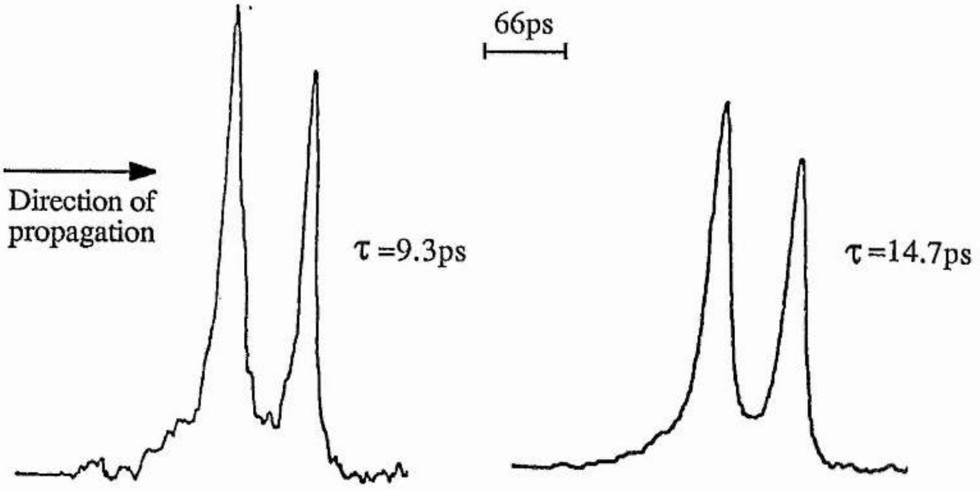

Figure 3.17 Subpulse-free modelocked pulses generated through the zero DC bias technique obtained over accumulation times of (a) 33ms, and (b) 3.3s. [Double pulses are shown to provide temporal calibration].

### 3.6.5 Prism-tuned modelocked laser

The etalon-tuned cavity allows sufficient bandwidth limitation such that good modelocked pulses can be obtained, but it has limitations in that wavelength tuning although possible is tedious when more than one etalon is required (as is usually the case). This procedure is made easier by using either intracavity prism tuning or by employing a diffraction-grating retroreflector. However, the bandwidth limitation is less stringent with prism tuning due to the low dispersion of silica at 1.5μm. The laser cavity of figure 3.9(b) incorporating a prism as the tuning element, was modelocked using the zero DC biasing technique described previously. The laser was tuned to obtain the maximum output power by rotating the highly reflecting mirror. The modelocked pulse properties were observed not to vary significantly across the tuning range of the laser, although the drive currents required some re-optimisation as the laser was tuned. The output pulse profiles were monitored as a function of modulation frequency around the optimum modelocking frequency. Where a long integration time of 3.3s was used for each streak camera record to ensure that any statistical fluctuations in either the pulse duration or the measurement apparatus was averaged out.

### 3.6.6 Detuning characteristics

Figure 3.18 summarises the detuning characteristics of the prism-tuned laser operated using the zero DC bias technique.

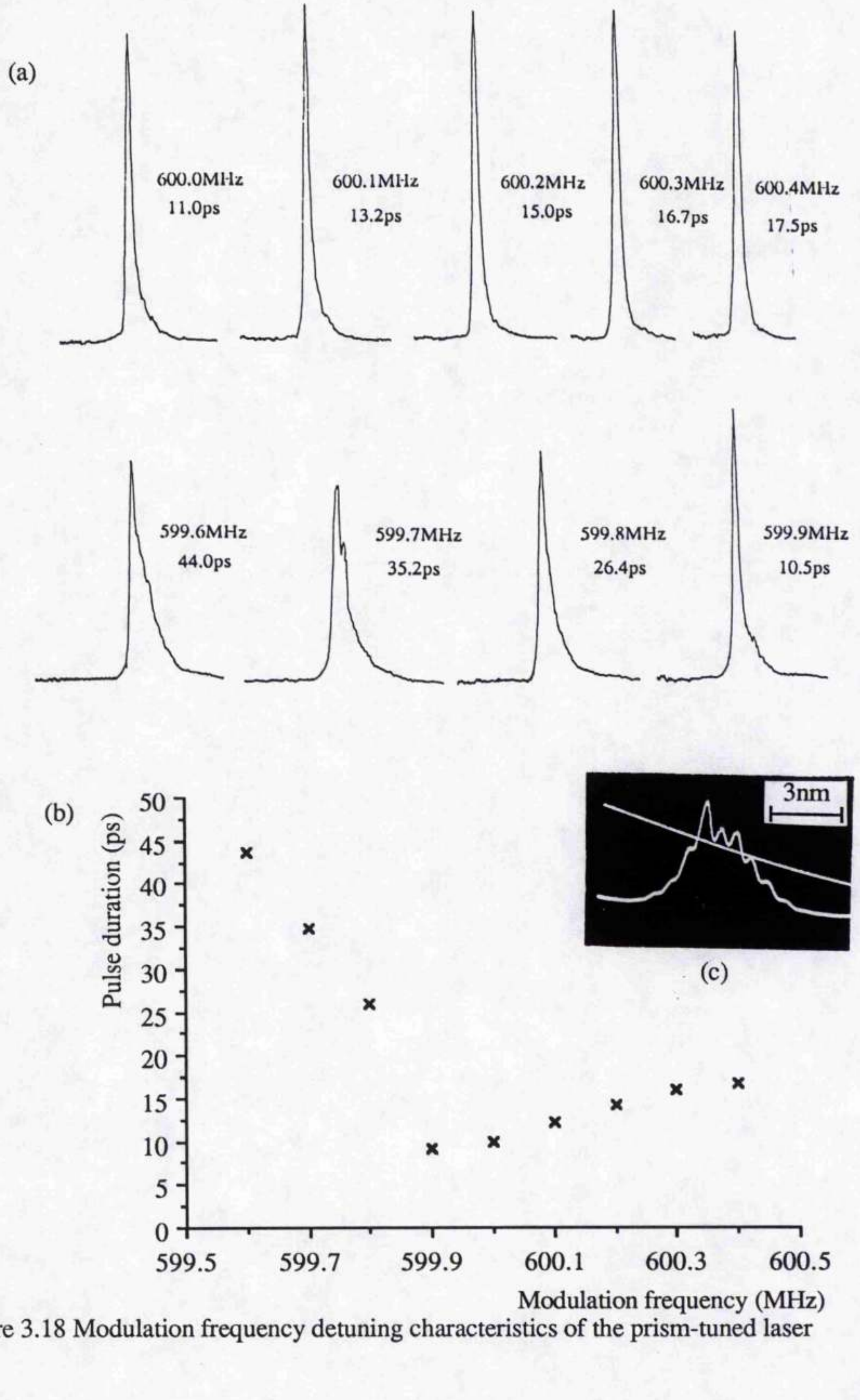

Figure 3.18 Modulation frequency detuning characteristics of the prism-tuned laser

At high frequencies the output consists of single pulses of >15ps duration, and the duration decreases slowly with decreasing modulation frequency until a minimum of ~9ps is reached at the optimum modelocking frequency (which was 599.9MHz). Further small reductions in frequency resulted in a marked increase in pulse duration, which was due mainly to the increasing energy content of the trailing edge of the pulse. The pulse broadening on negative frequency detuning is due to the same process of gain recovery which is involved in subpulse generation but here the 'subpulse' is not as well defined. Figure 3.18(c) illustrates an optimised, calibrated streak record for this laser (delay=60ps) and the corresponding output spectrum (where the spectral modulation due to the amplifier subcavity can be clearly seen). The broad spectral bandwidth of ~2.4nm indicates the limited bandwidth restriction imposed by the silica prism. However, this situation could be improved by using a prism possessing higher dispersion at the 1.5μm spectral region.

### 3.6.7 Modelocked fibre-grating, external-cavity laser

In this section a fully fibre-integrated, modelocked, external-cavity InGaAsP laser will be described. The cavity configuration is shown schematically in figure 3.9(d) and utilises a fibre-grating reflector[90] as both a cavity retroreflector and bandwidth-limiting filter. The amplifier used was a 500μm long, 1.55μm InGaAsP angled-ridge waveguide device where the ridge angle was ~10°. The CW performance characteristics of this laser were detailed previously in section 2.8.2.

For optimum modelocking performance the DC bias level was set in the 60-65mA range, and the RF signal was adjusted so that its frequency was harmonically related to the cavity mode separation. The laser output as monitored on an InGaAs PIN photodetector and sampling oscilloscope was optimised to determine the modulation frequency most suitable for the streak camera system. This was found to be ~650MHz which was the 12th harmonic of the fundamental modelocking frequency of 54MHz (the optical path length of the cavity was 2.76m). The pulses were then monitored using the streak camera and over an accumulation time of 33ms more than 20 million pulses were integrated to give a single streak record of which figure 3.19(a) is typical. The pulse duration was found to be 8.5ps but the energy contained within the main pulse is only approximately half of the total pulse energy. Therefore the main pulse peak power was calculated as 60mW. Although, as has been seen, modelocking was successful with this cavity configuration the relatively long pulse durations produced would suggest that the distributed nature of the fibre-grating reflector restricts the minimum pulse duration.

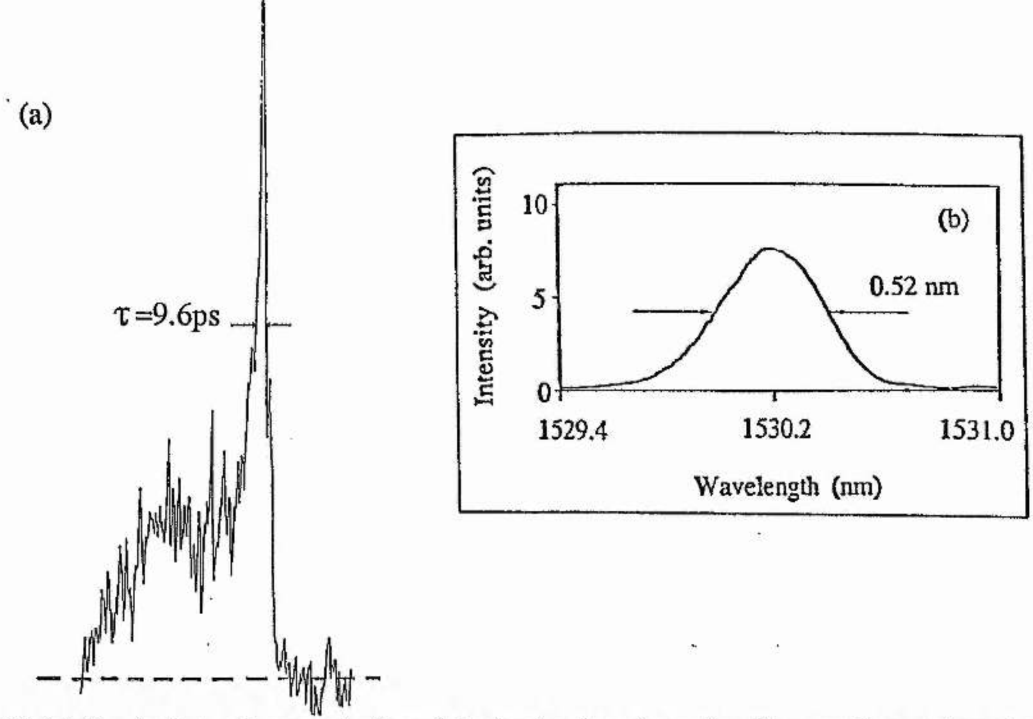

Figure 3.19 (a) Typical streak record of modelocked pulses from the fibre-grating external cavity laser, and (b) the associated output spectrum.

Spectra of the modelocked laser were observed to be very stable and exhibited typical bandwidths of up to 0.5nm (see figure 3.19(b)). [The duration-bandwidth product was therefore 0.54.] As described in section 2.8.2 the centre wavelength of the output could be tuned by varying the refractive index of the oil capping layer, and a shift of approximately 1nm was achieved for the available index range of 1.448-1.454. This fine tuning mechanism combined with the selective wavelength tunability arising from the choice of optical fibre grating characteristics could be used to exploit the large gain bandwidth of the InGaAsP amplifier. Thus an array of these lasers operating at slightly shifted centre wavelengths could provide a compact source for a wavelength division optical communications network.

### 3.7 Fibre ring laser

Many advantages can be gained by selecting a ring cavity configuration for modelocked lasers[125]. The requirement, for example in balanced linear cavities, of ensuring a centrally positioned gain medium is automatically achieved in ring lasers, since the counterpropagating pulses travel the same path, albeit in opposite directions. Ring configurations have been frequently employed in modelocked semiconductor lasers, where a sequence of mirrors[126] or optical fibres[127] have been used to define the resonator (see figure 3.20).

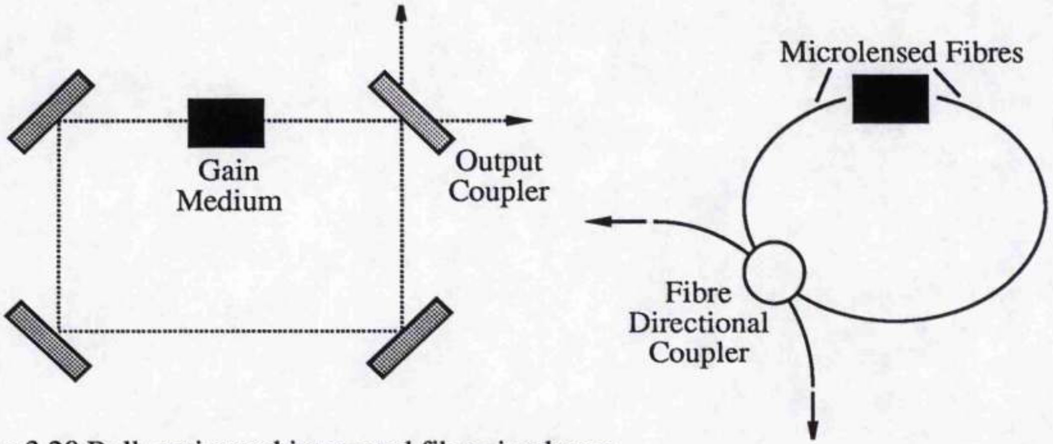

Figure 3.20 Bulk optics and integrated fibre ring lasers

In this work an integrated fibre ring cavity was constructed using a fibre directional coupler. Microlensed fibres allowed coupling to the angled-ridge semiconductor amplifier. The coupler exhibited a ~10dB coupling coefficient, so that 10% of the circulating energy was coupled out of both outputs. A fibre polarisation rotator[128] was used to optimise the L/I characteristics of the CW laser (see figure 3.21(a)) thus enabling the feedback to be launched into the highest gain mode (TE) of the amplifier. The perimeter of the ring laser was measured to be approximately 2.3m, hence the corresponding fundamental modelocking frequency was ~40MHz. The modulation frequency was chosen to be in the useful working range of the streak camera diagnostic which corresponded to the 10th harmonic (~600MHz) of the cavity mode separation. The output modelocked pulses (see figure 3.21(b)) were very similar to those obtained in the balanced-cavity configurations although the laser stability was noticeably improved.

The ring laser did not include any bandwidth limitation other than that imposed by the gain medium and was therefore not tunable. A novel technique using the birefringence of a polarisation preserving directional coupler has been demonstrated[129] to allow tuning of a similar ring laser. The polarisation axes of the fibre and the amplifier were oriented at 45° to each other, thus the fibre cavity acted as a Lyot filter. Wavelength division multiplexors or tunable fibre couplers could also be used to solve this problem. Such devices are essential for the optimisation of the modelocked ring laser but were not available during the course of this work.

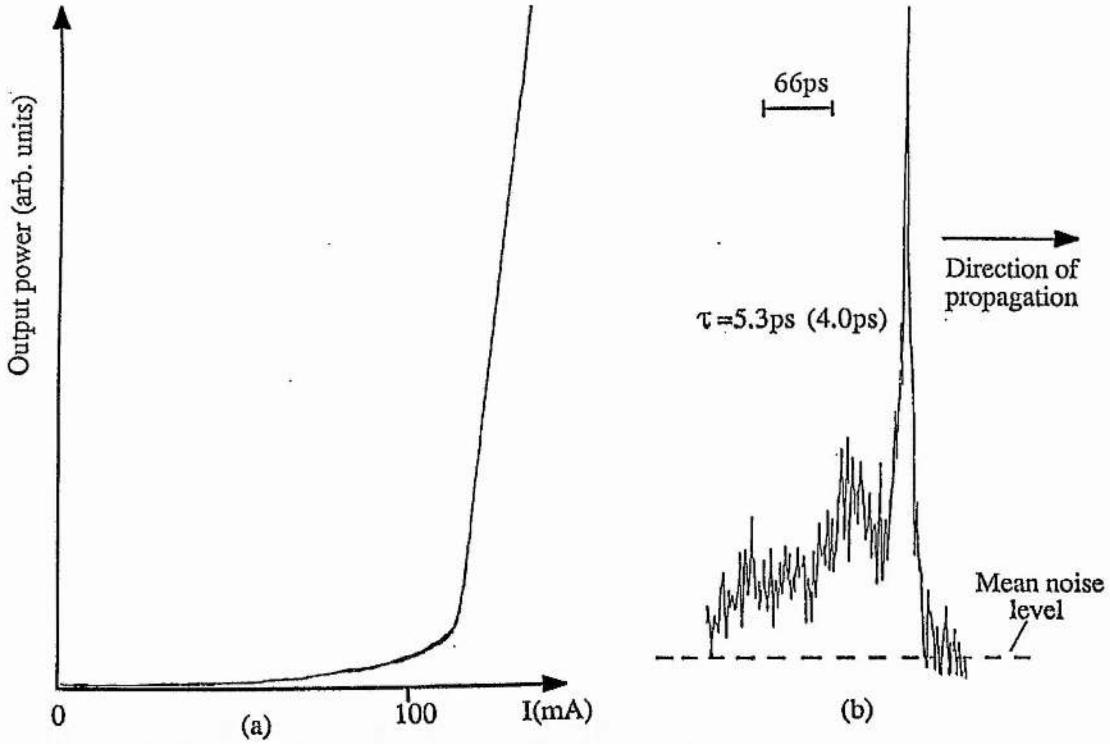

Figure 3.21 (a) CW, and (b) modelocked output from the fibre ring laser

### 3.8 Dynamic detuning

It has been suggested[130] that the limit to the pulse duration from modelocked semiconductor lasers is imposed by an effect termed dynamic detuning. This is best described in a time-frame travelling with the intracavity pulse. As the pulse undergoes multiple transits of the laser cavity the pulse duration is steadily reduced, and the peak power increases accordingly. As the peak power increases the pulse can saturate the gain at an earlier time, and the result of this is to push the peak of the pulse forward in local time, or in other words the pulse travels faster through the gain medium. This pulse shortening process cannot go on indefinitely because the pulse will eventually become dephased from the modulation signal so that the available gain is reduced. This leads to a decrease in the pulse energy such that the gain is then saturated at a later time and the pulse pulled backwards towards the higher gain region. A steady state is then approached where the motion of the pulse due to the two counteracting processes is balanced. As a result the pulse duration is stabilised through the gain saturation process and limited by the form of the gain modulation signal present.

## 3.9 Summary

The emphases of this chapter have been placed on the production of ultrashort optical pulses from semiconductor lasers. Practical consideration was given to impedance matching high frequency modulation signals to semiconductor lasers, and this led directly to an appraisal of the large modulation response of these lasers. A variety of modelocked symmetrical external-cavity InGaAsP lasers were detailed and the concept of modelocking as a form of synchronous injection-seeded gain-switching has been suggested. The problems of frequency chirp and subpulsing were also described and it is the latter problem which will be the centre of discussion in chapter 4.

# CHAPTER 4

# SUBPULSE SUPPRESSION IN MODELOCKED InGaAsP SEMICONDUCTOR LASERS

## 4.1 Introduction

In the previous chapter the technique of low-frequency gain modulation was applied in modelocking InGaAsP semiconductor lasers. In this chapter the long term properties of the temporal envelope of mode-locked pulses from InGaAsP semiconductor laser systems will be addressed. As already shown the main problem associated with ultrashort pulse generation from semiconductor lasers is the emergence of a noisy trailing subpulse when the system is tuned for optimum pulse duration. At the outset the origin and properties of this subpulsing must be investigated with a view to its subsequent elimination. Several techniques that have been developed to enable discrete, single feature ultrashort pulse sequences to be produced from these systems will be described.

## 4.2 Origin of subpulse

By considering the streak camera intensity record of figure 4.1 subpulse detail is clearly in evidence. These features were first observed by Chen during an extensive study of mode-locked, Brewster-angled GaAlAs laser systems in 1985[69]. The probable origin for the trailing subpulse features is suggested using figure 4.2. It is assumed that a short optical pulse is incident on the gain medium at a time $t_0$. At this point the carrier density (or gain) is substantial although it has not reached its peak value. Stimulated emission leads to a reduction of the inverted population of carriers, and this gain saturation performs the primary pulse shaping function. The pulse then exits the gain medium leaving a markedly reduced carrier density behind. Because the modulation applied to the semiconductor gain medium is in the form of a slow sinusoid, the carrier density can recover after the passage of the first pulse to a value capable of supporting a secondary pulse. The temporal extent of the overall pulse envelope (including the subpulse) therefore indicates the gain window produced by the applied modulation signal.

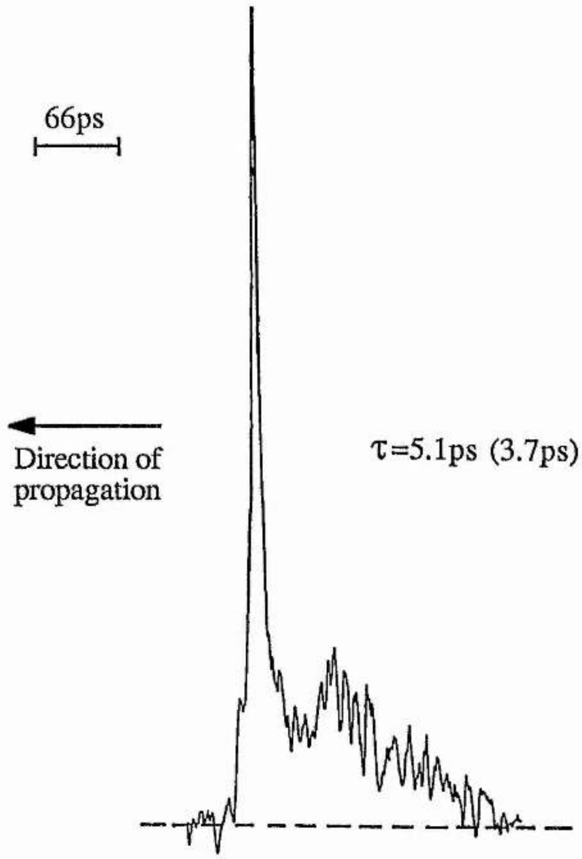

Figure 4.1 Streak intensity record of the output from a modelocked symmetrical external-cavity semiconductor laser. $f_m$=600MHz. The dotted line indicates the mean noise level.

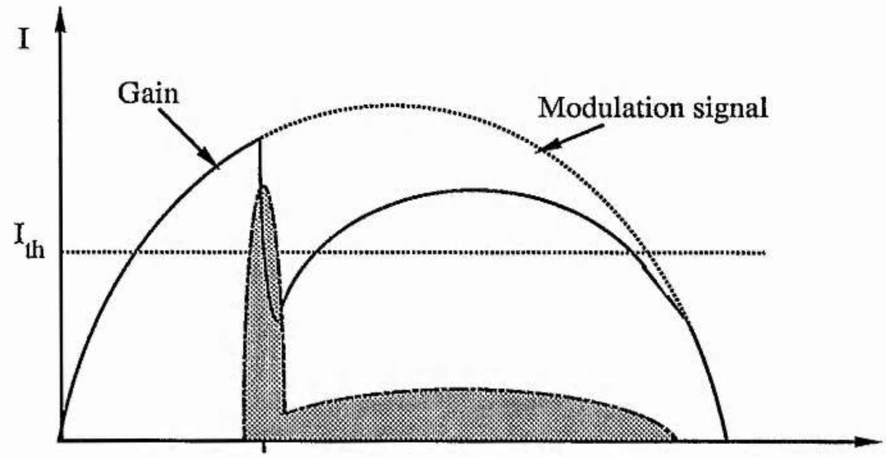

Figure 4.2 Origin of subpulsing in modelocked semiconductor lasers. [The shaded region ndicates the output pulse intensity spectrum.]

This indicates that there is sufficient gain recovery following the gain saturation due to the main pulse to support a secondary pulse although it does not imply how this pulse is formed. It could be due to the emission of spontaneous noise (and its subsequent amplification) during this time window which becomes the source of the subpulse. Alternatively, and more probably the initial long burst of noise created when the laser is turned on actually determines the detail of the modelocked pulse profile (see section 3.4). The leading part of the noise burst (or gain switched pulse) is amplified and shaped by gain saturation to form the main ultrashort pulse created by the laser. The trailing part is sustained due to the presence of residual gain but is not significantly shaped because both the light intensity and the available gain are low.

Another source (which will be described further in section 4.4) has been identified where a substantial subpulse is created on a single-pass through the semiconductor gain medium. This latter phenomenon can only occur however under the particular conditions of very high pumping.

## 4.3 Gain window reduction

It follows, therefore, that it is necessary to reduce the temporal extent of the gain window to eliminate the deleterious effects of gain recovery during the pump cycle. There are several methods in which this can be affected and these will be described in the following three subsections.

### 4.3.1 Short-pulse electrical drive

The most straightforward technique to provide a reduced gain window is to use a short-pulse electrical drive for the laser[131]. This can be achieved quite easily by using a commercially available step recovery diode (also known as a comb generator) which can produce short electrical pulses of ~100ps duration. These devices are unfortunately limited in operating frequency range and require broadband power matching into the diode package to avoid degradation of the short pulse characteristics of the electrical drive signal. The diode packages used in this work did not feature broadband power matching and so effort was made to achieve features equivalent to those of comb generators using single frequency RF signals.

### 4.3.2 High-frequency modulation

An alternative approach using sinusoidal modulation to reduce the gain window is based along similar lines to that of the comb generator, and this is to increase the modulation frequency to such an extent that the gain window can be reduced to any value desired, eg a 10GHz RF signal is equivalent to a 50ps pulsed signal. Figure 4.3 shows three sinusoidal modulation signals representing modulation frequencies of 300, 600 and 900MHz respectively. And the extent of the gain window reduction by increasing the modulation frequency in such a manner can be clearly seen. Using an InGaAs PIN photodiode as the detector, sampling oscilloscope traces of pulse profiles from the modelocked InGaAsP semiconductor laser with modulation frequencies of 300, 600 and 900MHz as shown in figure 4.4 were recorded for comparison purposes.

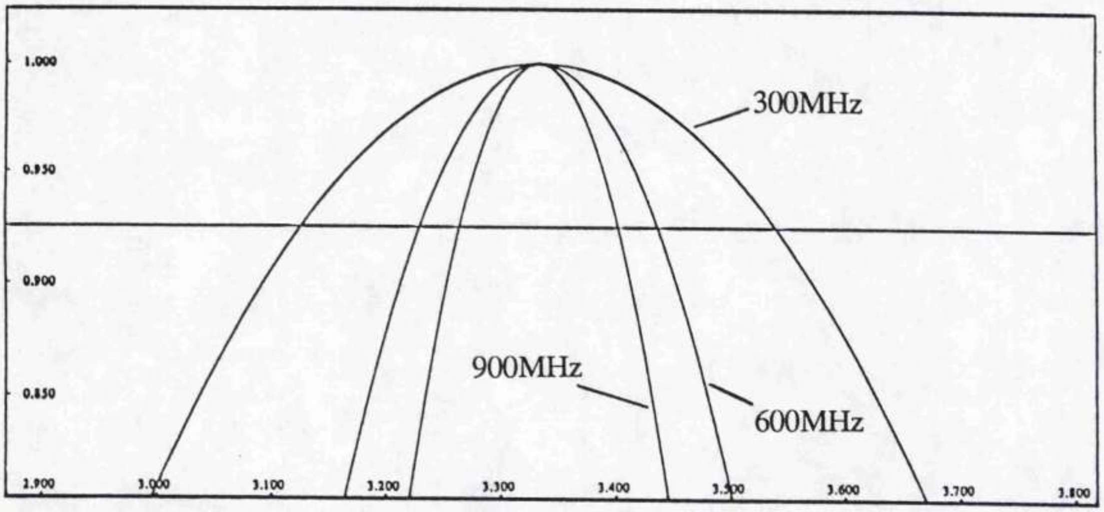

Figure 4.3 Gain window reduction by increasing the modulation frequency

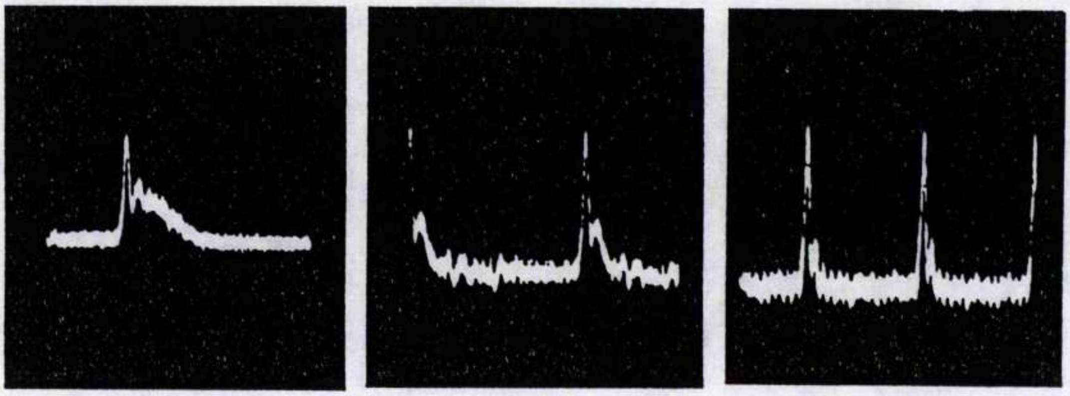

$f_m$ = 300MHz $f_m$ = 600MHz $f_m$ = 900MHz

Figure 4.4 Subpulse suppression by increased modulation frequency. The time base is 500ps in all cases.

As expected, for increased modulation frequency the proportion of total pulse energy in the main pulse becomes greater and the duration of the subpulse is reduced in accordance with the gain window constriction. The drawback with increasing the modulation frequency to affect subpulse suppression is that it becomes difficult to couple sufficient RF power into the diode amplifier and the associated electronics become both bulky and expensive. Also, and more importantly, the peak pulse power is significantly reduced as the modulation frequency is increased. The peak power can be found from the expression;

$$\begin{aligned}\text{Peak power} &= \text{Duty factor x Average power}\\ &= T_r/T_p \text{ x } P_{av}\\ &= P_{av}/\, T_p\, f_m\end{aligned}$$

where the modulation frequency $f_m=1/T_r$, and $T_p$ is the pulse duration.

The pulse durations from semiconductor lasers have been shown to be a weak function of frequency, tending to become constant at sufficiently high frequencies[132]. This is because the modulation depth decreases with frequency due to the bandwidth limitations imposed by the laser and its package. Moreover, the average output power is essentially constant as a function of frequency. This then leads to an approximately linear decrease in peak pulse power with increasing modulation frequency;

$$P_H \sim P_1/H$$

where $P_H$ is the peak power at the $H^{th}$ harmonic of the fundamental frequency $f_m$.

It may therefore be concluded that for optimum peak power pulse generation the modulation frequency must not be be excessively high, but the chosen frequency must be sufficiently high to limit the effect of subpulse generation. To this end it is attractive to develop a technique for eliminating subpulsing at relatively low modulation frequencies (eg 300-600MHz).

### 4.3.3 Zero DC bias operation

In this section a technique is described where the mode-locked pulse temporal envelope could be cleaned up to the extent that it consists of a single picosecond feature while employing relatively low-frequency modulation (see also section 3.6.4). This technique has been termed here as zero DC bias level operation or ZBO.

Consider the modulation signal of figure 4.5(a) which is comprised of a sinusoidal RF frequency modulation superposed on a subthreshold DC bias current level as is normally used for the mode-locking of semiconductor lasers. The gain window produced by this combination of bias signals as indicated in the figure can be seen to be quite long compared to the pulse durations expected (<10ps). It is therefore not surprising that gain recovery is significant and a large subpulse is generated following the desired ultrashort pulse. Figure 4.5(b) and (c) shows how the gain window behaves on reducing the DC bias current level used and at the same time increasing the RF signal intensity to give the same peak drive signal. Therefore the shortest possible gain window at any modulation frequency occurs when the DC current level is at a minimum. In practice the minimum DC bias level possible for the semiconductor laser is not in fact zero because no current is drawn on the negative part of the drive signal (the diode rectifies the signal). Hence the DC Fourier component of the drive signal is always positive. A DC current level which maintained a positive resultant modulation signal has always been traditionally applied because it was thought that biasing the diode amplifier negative would lead to damage or at least lifetime degradation. This has not been observed in this work where the InGaAsP semiconductor amplifiers have been operated under zero DC bias and large modulation signals for many hours with no failures and no observable decrease in performance.

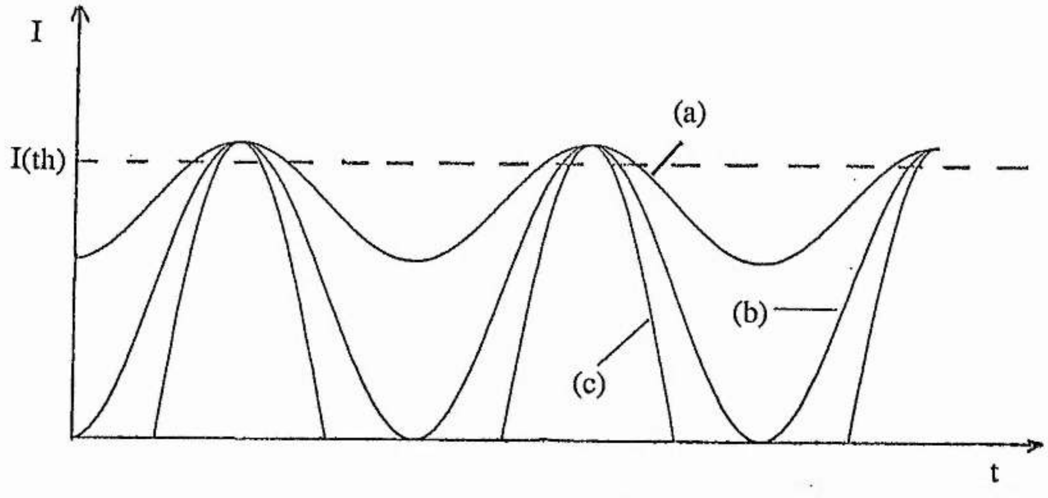

Figure 4.5 Subpulse suppression by reducing the DC component of the laser drive signal.

This technique was applied to the balanced, grating-tuned cavity configuration illustrated in figure 4.6(a). The pulse profiles recorded using a synchroscan streak camera arrangement are reproduced in figures 4.6(b) and (c) where figure 4.6(b) indicates the temporal calibration of the recorded data (obtained over an integration time of 3.3s). The single pulse profiles of figure 4.6(c) show that clean, single-feature pulses can readily be obtained using the ZBO technique. Although it is noted that the trailing edge of the pulse has a slower gradient than the leading edge.

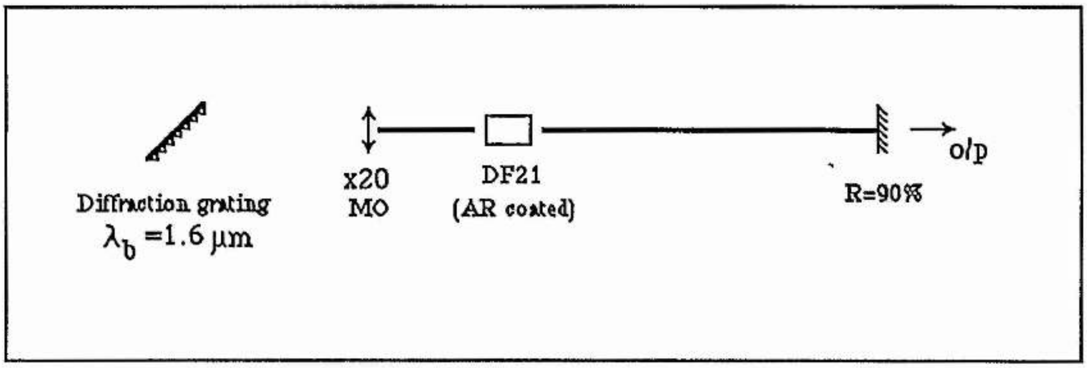

Figure 4.6 (a) Balanced, grating-tuned, semiconductor laser configuration.

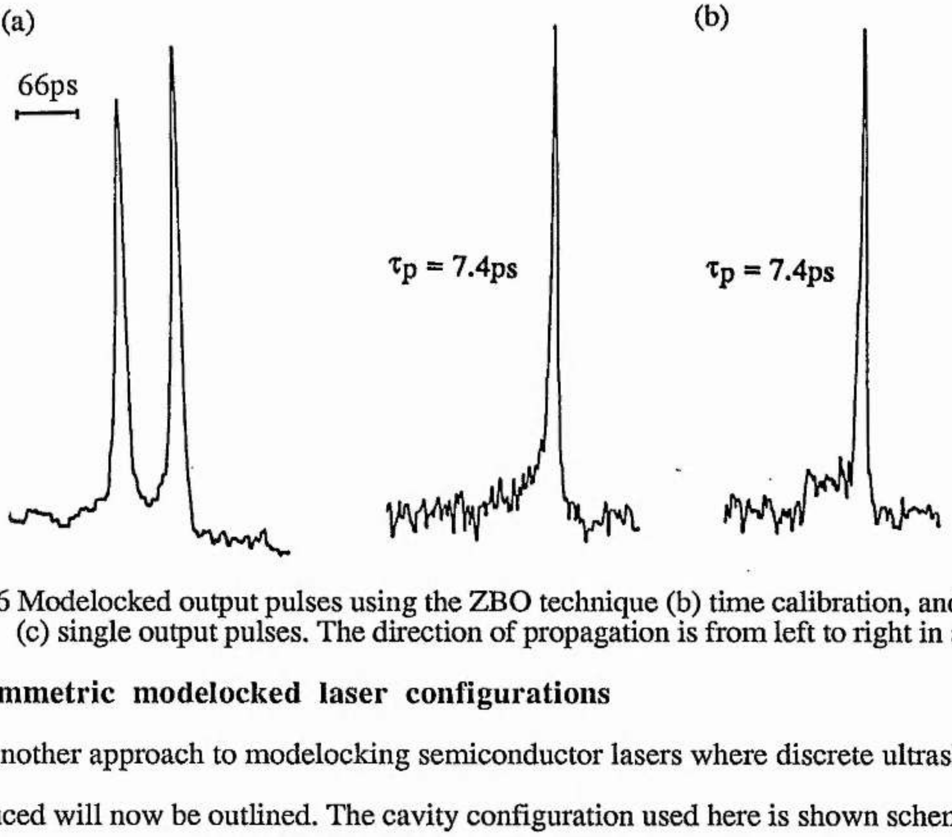

Figure 4.6 Modelocked output pulses using the ZBO technique (b) time calibration, and (c) single output pulses. The direction of propagation is from left to right in all cases

## 4.4 Asymmetric modelocked laser configurations

Another approach to modelocking semiconductor lasers where discrete ultrashort pulses are produced will now be outlined. The cavity configuration used here is shown schematically in figure 4.7. This asymmetric cavity consists of an anti-reflection coated semiconductor amplifier which is coupled onto a bulk diffraction-grating tuning element via a short (~10cm) length of microlensed fibre and a collimating x20 microscope objective. As is evident there are two output coupling ports, namely the collimated output taken directly from the semiconductor laser facet, and the zeroth-order specular reflection from the diffraction grating. In what follows these outputs are termed 'output 1' and 'output 2' respectively.

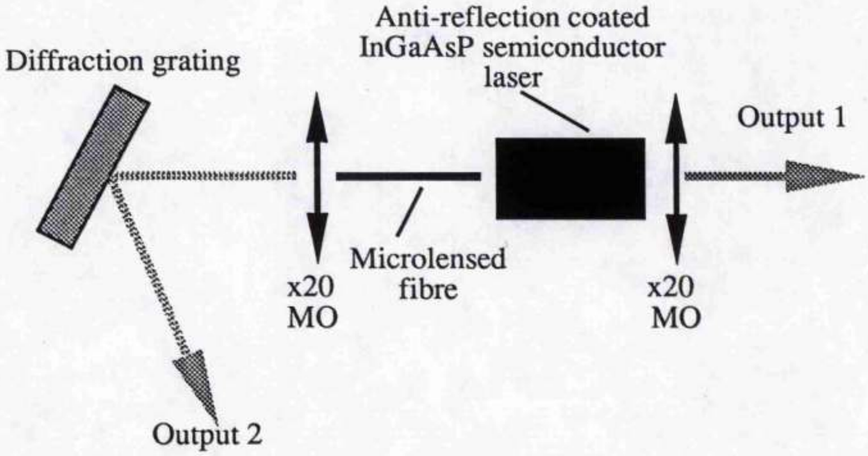

Figure 4.7 Asymmetric external cavity semiconductor laser

As before, the composite RF and DC modulation signal was applied to the diode chip and the laser output was continuously monitored using a synchroscan streak camera. For low DC bias levels the output, in terms of pulse duration and minimal subpulsing at output 1, was optimised. Increasing the DC bias led to an increase in the amplitude and duration of the noisy subpulse at output 1 without significant change in the main pulse duration and intensity. The main pulse simply shifts forward in time relative to the modulation signal and thus experiences essentially no change in the condition of the gain (this follows directly from the discussion of dynamic detuning presented in section 3.8). Such features are again closely related to the temporal envelope of the initial gain-switched transient. The pulse duration is slightly longer (~8ps) in this case than for the balanced-cavity configuration, and this is attributed to the absence of the enhanced gain saturation of the coherent interaction obtained in the active medium within symmetrical cavities. Despite the slightly longer pulses there is an increase in the laser output power, and the simplicity of the cavity configuration is an attractive advantage.

The grating efficiency was ~70-80% at the laser operating wavelength and significant output coupling in the zeroth-order diffracted beam could be obtained. To obtain more information about the pulse-shaping processes involved in the diode chip this output was also monitored by the streak camera. Hence with this laser system pulses emerging from both facets of the amplifier could be simultaneously monitored. One pulse has experienced a single pass through the amplifier (ie output 1), whereas the other is the reflected component of the first pulse and hence experiences a second transit of the amplifier. With the output optimised with respect to the pulses emitted from output 1 the other output pulse sequence was found to be almost identical (see figure 4.8(a)) which implies that the pulse-shaping processes for both pulses are essentially equivalent. On increasing the DC bias component of the electrical drive signal applied to the amplifier a marked difference in the profiles of the output pulses was observed, and these are included as figures 4.8(b) and (c). The main difference related to the formation features of the trailing subpulse because in one case an intensity increase was seen, but in the other a decrease. At sufficiently high current levels complete elimination of the subpulses attending the pulses emitted from output 2 was observed.

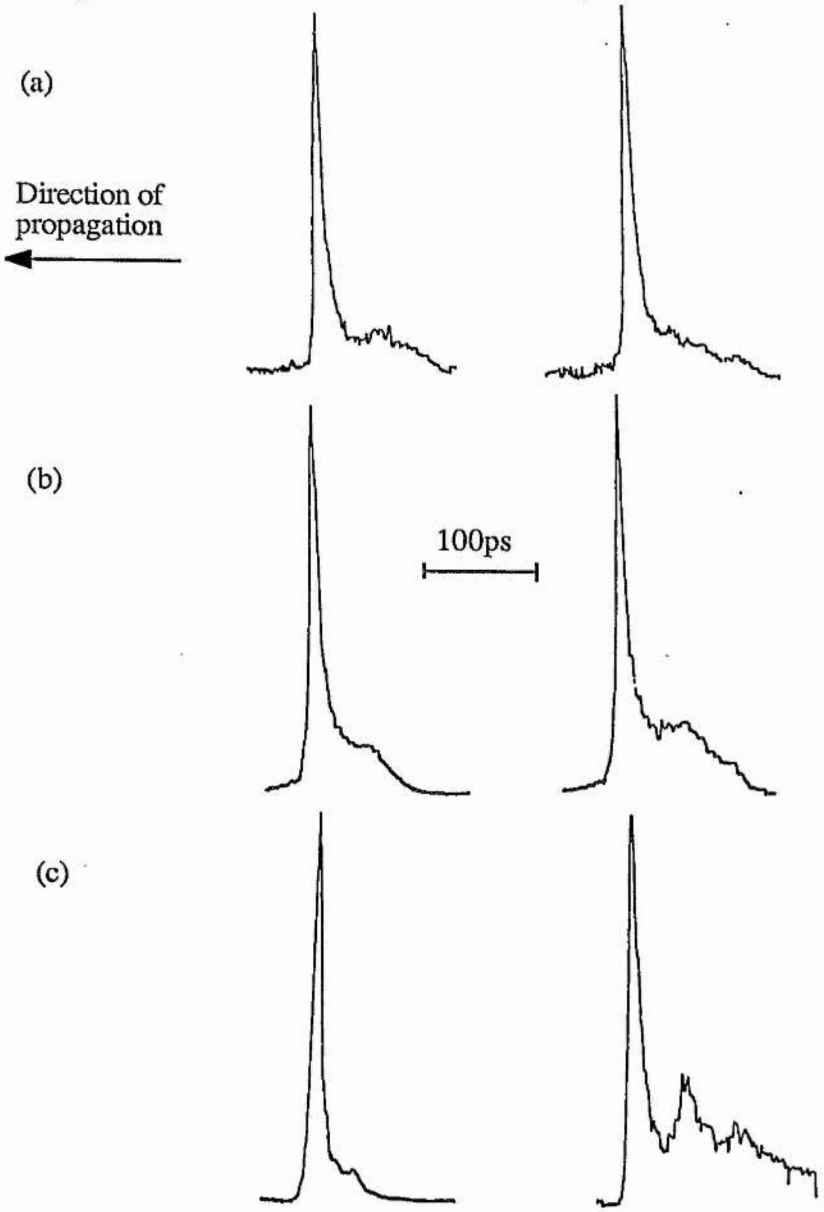

Figure 4.8 Pulse intensity profiles at (a) 70mA (b) 80mA, and (c) 127mA DC bias. Pulses from output 1 are shown on the right, and output 2 on the left.

This intriguing situation implied that the gross (or in other words, the pulse envelope) shaping processes were dependent upon the number of passes that the pulse made through the gain medium. In the case of optimised, subpulse-free emission from output 2 the large, long subpulses on output 1 are generated on a single transit of the discrete pulse through the amplifier. The question that arises here is, why is the reflected component of the subpulse not preserved on the pulses emitted from output 2? A series of experiments will now be described which were undertaken to gain some insight into the phenomena involved in producing the effects explained above.

### 4.4.1 Output pulse properties of asymmetric external-cavity laser configurations

The first measurements recorded were the dependence of the output pulse profile from output 2 with DC bias current. With the laser tuned to 1.5μm, data for the pulse evolution on increasing the DC bias current were obtained and are shown in figure 4.9(a). The measured FWHM pulse durations of this sequence of streaks was also plotted in figure 4.9(b). At low injection current levels the output consists of an intense short leading feature followed by a lower intensity subpulse. [It should be noted that the streak camera measurements were all obtained using a long accumulation time of 3.3s therefore the pulse durations are overestimated (by inherent pulse timing jitter) by up to 3-4ps.] On increasing the DC component of the drive signal the subpulse moves towards the main pulse and is eventually eliminated at approximately 110mA. [Note that the CW laser threshold was ~80mA]. During this process the pulse duration is roughly constant at ~14ps. Further increments of the DC current leads to both a reduction in the intensity and duration of the clean output pulse until at a current around 145mA the output pulse is quenched. The shortest pulse durations obtained were ~8ps at 135mA, but this was balanced by a reduction in the peak output power by about half. The location of the subpulse relative to the main pulse peak was also plotted with increasing DC current (see figure 4.10) and it was evident that the pulse envelope compression process was linear with increasing current.

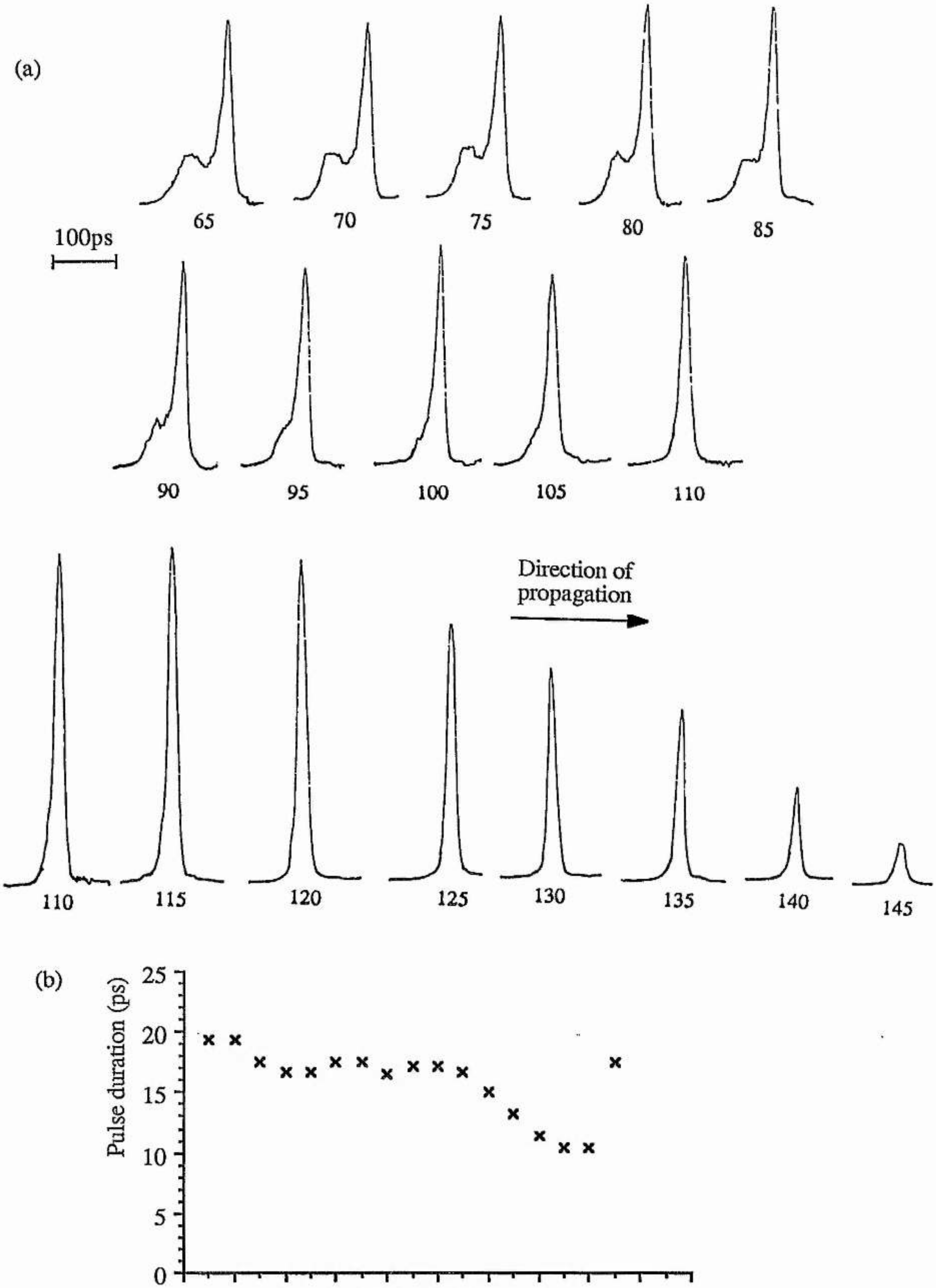

Figure 4.9 (a) Pulse profiles from output 2 as a function of the DC drive current component, and (b) the measured FWHM pulse durations.

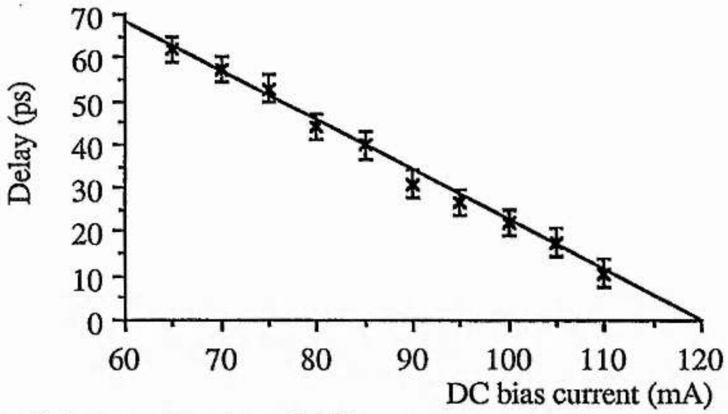

Figure 4.10 Subpulse delay as a function of DC current

Similar measurements were taken at the longer wavelength of 1536nm (see figure 4.11). Again the details of the pulse sequence were as before, although the intensity of the subpulse at low currents was markedly reduced. Complete subpulse elimination occurred at a current of ~60mA, where this reduced value reflects the smaller magnitude of the initial subpulse. The maximum in pulse peak power was obtained at a current 10-20mA higher than that required for complete subpulse suppression, and also the pulse quenching at yet higher currents is substantiated.

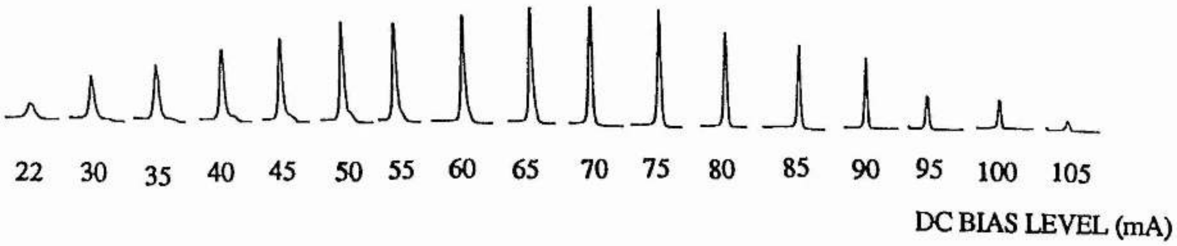

Figure 4.11 Pulse profiles from output 2 as a function of the DC current at λ=1536nm

To investigate the effect of external-cavity feedback on this subpulse suppression mechanism an optical attenuator was inserted into the laser cavity when the applied current to the amplifier chip was 90mA. Figure 4.12(a) shows that on insertion of the attenuator the output pulse is transformed from a single-feature pulse to one having a substantial subpulse. In figure 4.12(b) the DC current applied has been increased to 125mA such that the single-featured pulse output is restored. This then suggests that the maximisation of the feedback fraction from the external cavity will serve to minimise the current required to generate subpulse-free ultrashort pulses.

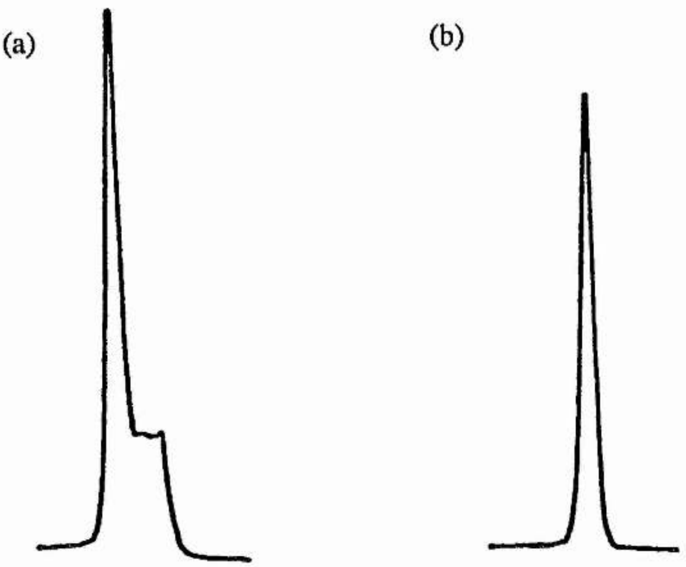

Figure 4.12 (a) Output pulse profile at 90mA after insertion of an optical attenuator, and (b) the recovery of a subpulse-free output by increasing the DC current to 125mA

The DC current component of the modulation signal required to achieve subpulse-free generation was recorded across the available tuning range of the laser system (see figure 4.13). These results clearly show that the DC current required decreases with increasing wavelength, and further there is a distinct modulation superimposed onto this characteristic. [Also included in figure 4.13 is a data set obtained when the RF component of the drive signal was increased. The effect of this was to increase the required DC current without significantly changing the previously detailed trends.]

The higher DC currents necessary at short wavelengths is most probably due to the lower efficiency of the diffraction grating, and as has been shown this leads to an increased DC current requirement. The spectral modulation can be linked directly to the gain modulation induced through external-cavity feedback into both cladding and active regions of the semiconductor waveguide. The period was measured to be ~10nm and increases significantly with wavelength, and both of these features agree well with the measurements obtained for this phenomenon which was described in section 3.5.2..

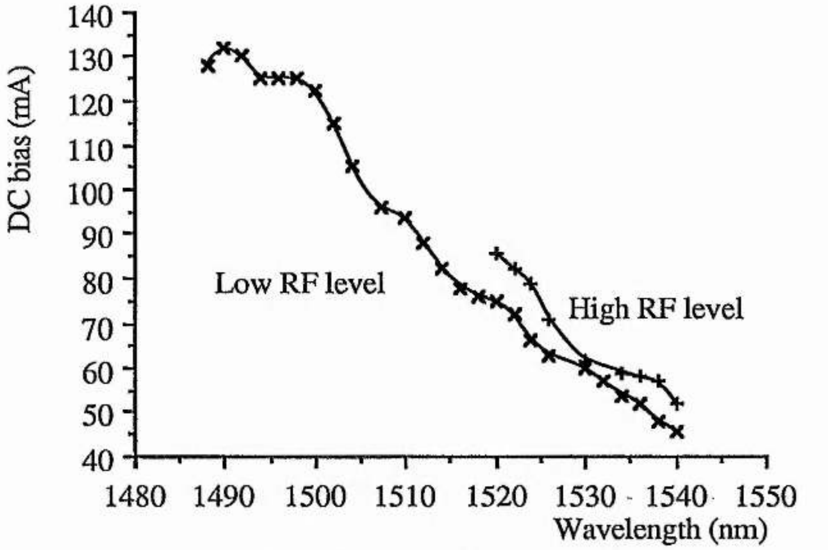

Figure 4.13 Subpulse elimination as a function of laser wavelength

### 4.4.2 Subpulse suppression mechanism in the asymmetric laser

The collated experimental details presented in the previous section provide the necessary evidence required to describe the pulse-shaping process present in the asymmetrical external-cavity laser system. The following mechanism is proposed to be that which determines the large-scale pulse envelope of this modelocked laser configuration. Since the only difference in the pulses emerging from outputs 1 and 2 is that one does not have an attendant subpulse then it suffices to explain how on a second passage through the semiconductor laser the subpulse is eliminated. Therefore this situation can be represented by figure 4.14 where the input pulse to the amplifier has a trailing subpulse which is eliminated after one transit through the device.

It appears that the main feature of pulse 3 can become sufficiently intense to saturate the gain of the amplifier to such an extent that a region of relatively large attenuation is created at the output facet (RHS facet in figure 4.14) of the amplifier. At low DC currents the gain is insufficient to amplify the pulse that is retroreflected from the facet of output 1 to the required intensity such that an attentuating region can be formed. By raising the current, and hence the gain, the pulse can begin to create the attenuating region which will increase with yet higher pumping levels. Therefore this picture can adequately explain the current-induced subpulse suppression mechanism. Furthermore, it is clear that if the feedback fraction from the external cavity is reduced then a higher DC level is required to amplify the pulse intensity to a degree sufficient to establish the attenuating region. Also the external-cavity feedback induced spectral modulation of the laser gain profile will affect the laser performance since higher DC currents will be required at the troughs of the gain spectrum to provide the pulse intensity necessary for the suppression process. The pulse is eventually quenched since the attenuating region becomes so extensive that most of the pulse evolution is frustrated. The laser then produces rather longer pulses of low intensity because the effective cavity gain is substantially reduced.

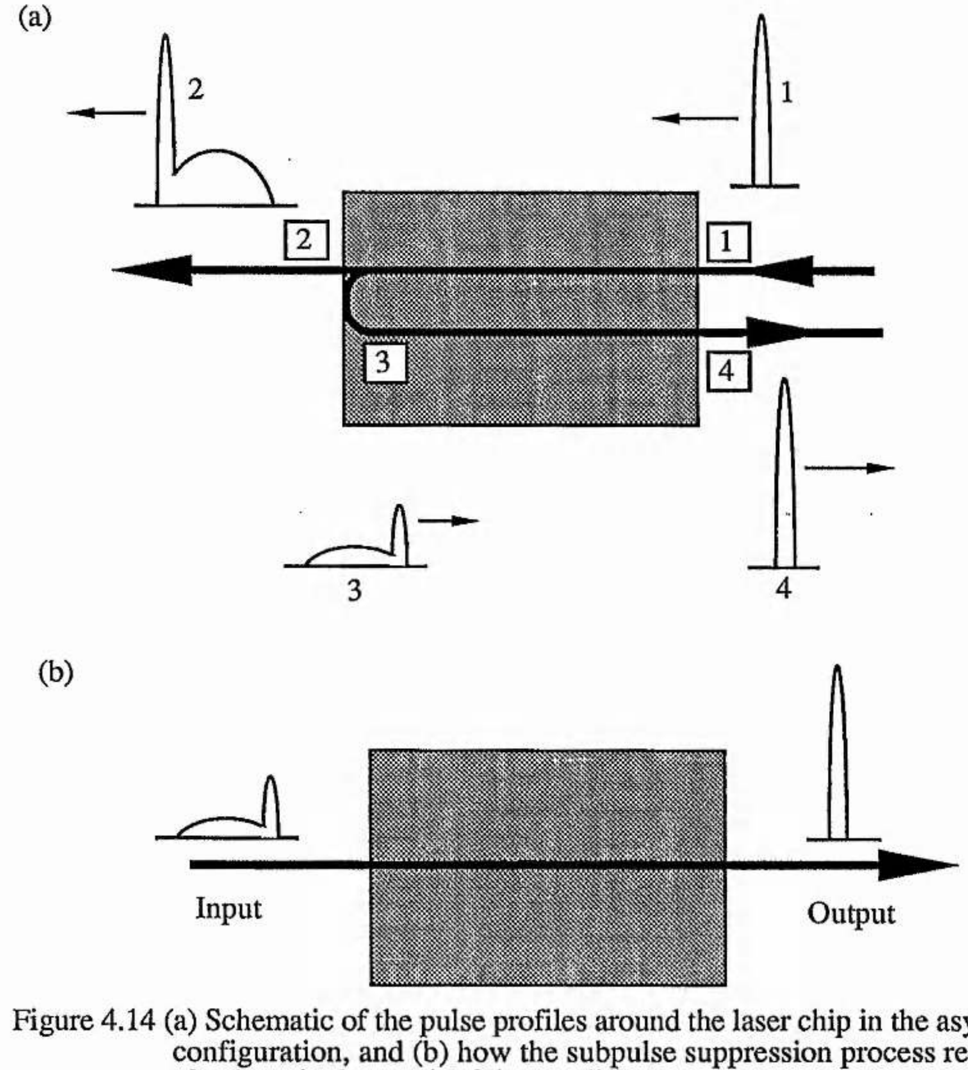

Figure 4.14 (a) Schematic of the pulse profiles around the laser chip in the asymmetric cavity configuration, and (b) how the subpulse suppression process requires consideration of only a single transit of the amplifier.

A similar effect has been demonstrated by Lomax et al[133] by using a gain switched pulse (with an attendant subpulse) incident on a travelling-wave semiconductor amplifier. This situation is analogous to that shown in figure 4.14(b) and indeed it was found that significant subpulse suppression was obtained when the amplifier was operated under high current conditions.

## 4.5 Summary

Low-frequency (<1GHz) modelocked semiconductor lasers are attractive since they provide a convenient source of wavelength tunable ultrashort pulses of moderately high peak power. The problem of subpulse generation from sinusoidally modulated semiconductor lasers has been addressed in this work, where the synchronously operating streak camera was extensively used to monitor and record these low optical intensity features. Various methods have been described which allow subpulse-free pulse production from these systems, and two useful techniques have been described in this chapter. The first technique utilises a minimal DC component to the driving signal to effectively reduce the applied 'gain window' thus eliminating subpulse generation.

Asymmetric laser configurations prove to possess their own particular pulse-envelope shaping processes, and data has been presented where clean, single-feature pulse generation from these sources has been confirmed. A simple, explanatory phenomenological model was proposed for the main long-term, pulse-shaping mechanism.

# CHAPTER 5

# PHASE NOISE MEASUREMENTS ON AN ACTIVELY MODELOCKED InGaAsP SEMICONDUCTOR LASER SYSTEM

## 5.1 Phase noise in modelocked lasers

Phase noise on modelocked pulse sequences is manifest as variations in the pulse-to-pulse temporal separation, or in other words fluctuations of the pulse repetition rate. A quantitative characterisation of phase noise can therefore identify where improvements should be made to modelocked laser sources, and can lead to better specifications for particular laser systems that should be capable of meeting the demands of selected applications. Such applications may involve rather stringent laser timing prerequisites with high-resolution, electro-optic sampling of integrated optical components[134] being an important example.

In passively modelocked lasers the pulse repetition rate is determined principally by the cavity round-trip time, and so a measurement of the phase noise will indicate the stability of the laser cavity length. In this case amplitude (or intensity) noise on the intra-cavity pulse may induce phase noise through associated refractive index changes. These are most likely to arise in the gain medium through gain saturation and also in the saturable absorber material where saturable absorption is involved. Instantaneous nonlinear effects such as self-phase-modulation (SPM) occuring from the optical Kerr effect will not affect the relative pulse positions. Although SPM will aid in modifying the pulse duration and this could in turn magnify the amplitude noise present. Hence for passively modelocked lasers either passive or active cavity stabilisation[135] is essential to ensure good phase noise characteristics. And also a high quality, 'quiet' pump laser is needed so that amplitude-to-phase noise conversion can be minimised. The situation is somewhat different in actively modelocked lasers where the output pulse repetition rate largely follows that of the modulation signal used to induce modelocking. Here cavity length perturbations will result in fluctuations of the pulse duration and these may of course couple through gain saturation effects to exacerbate the phase noise content in the output pulse sequence. Assessment of synchronously pumped colour centre lasers[136] and, as will be discussed here, modelocked semiconductor lasers tend to indicate that the latter source of phase noise can be ignored.

In the discussion that follows a sensitive technique for the measurement of phase noise of modelocked laser output will be described. Its application to the actively modelocked InGaAsP semiconductor laser source will be especially highlighted within the context of this thesis.

### 5.2 Technique for the measurement of phase noise

The phase-noise measurement technique used here was developed by von der Linde[137] and Rodwell et al[138] and utilises a frequency domain analysis of the Fourier components of the optical pulse train as recorded by a fast photodetector/spectrum analyser configuration. The key points of the theoretical development of this approach will now be outlined, but for a more comprehensive treatment of this topic the reader should see references **137** and **138**.

The intensity of a periodic train of short Guassian optical pulses can be described by the expression,

$$P(t) = P_{av}\, T.(\,1 + N(t)).\ \sum_{n=+\infty}^{n=-\infty} \Big[ \frac{1}{\sqrt{2\pi}.\sigma_t}\ .\exp\Big(-\frac{(\,t - T_0 - nT_l - J(t)\,)^2}{2\sigma_t^2}\Big)\Big]$$

where $P_{av}$ is the average intensity of the beam, $T_l$ is the repetition period, $\sigma_t$ is the rms pulse duration, N(t) is the normalised pulse intensity variation, J(t) is the timing fluctuation of the pulse train, and $T_0$ is the static timing offset of the pulse train. Taking the Fourier transform of this function the power spectral density (approximated to second order in terms of $n\omega_l\sigma_t$) is,

$$S_p(\omega) = P_{av}^2\, .e^{-\omega^2\sigma_t^2} \sum_{n=+\infty}^{n=-\infty} \Big[(1 - n^2\omega_l^2\sigma_J^2)\, 2\pi\, \delta(\omega - n\omega_l) + (1 - n^2\omega_l^2\sigma_J^2)\, S_N(\omega - n\omega_l) + n^2\omega_l^2 S_J(\omega - n\omega_l)\Big]$$

$\omega_l = \frac{2\pi}{T_l}$, $\sigma_J$ is the standard deviation of J(t), $S_N(\omega)$ is the power spectral density of N(t), and $S_J(\omega)$ is the power spectral density of J(t). The three components of the spectral intensity function represent; (i) a sequence of delta functions at frequencies harmonically related to the pulse repetition rate. (ii) amplitude-noise sidebands which accompany each delta function. The amplitude noise at each harmonic is directly proportional to the intensity of the delta function defining each Fourier component. (iii) phase-noise sidebands which attend each Fourier component. Note that the phase-noise intensity increases as the square of the harmonic number n.

It follows that by measuring $S(\omega)$ the attendant noise on the pulse train can be completely defined. Amplitude noise can be obtained by examination of low-frequency harmonics, because the phase-noise term here is negligible. At high harmonics phase noise dominates, and so for a full description of pulse sequence noise a photodetector/spectrum analyser measurement system with a large bandwidth must be employed. It should be noted that each Fourier component has a constant intensity, therefore on increasing n the increase in phase noise results in a decrease in the intensity of the delta function component of $S(\omega)$ (and hence a proportionate decrease in the amplitude-noise sidebands). The approximations used in the above analysis become weak when applied to pulse trains with a large degree of phase noise. A common criterion used to define the small deviation regime is that the integrated deviation over each frequency decade, (ie. $\Delta\phi(f,10f)$) is less than 0.2 rads[139].

In the experimental measurements the spectrum analyser displays the spectral power density integrated over the resolution bandwidth (B). Within a specific frequency range the rms amplitude fluctuation is given by:

$$\sigma_A[f_l,f_h] = \sqrt{<A(t)^2>} = \sqrt{\frac{P_{sb}}{P_c}}$$

$$\text{where } P_{sb} = \int_{nf_o+f_l}^{nf_o+f_h} \frac{2P(f)}{1.2xB}\, df$$

The factor of 1.2 in this expression is included to normalise the filter response of the spectrum analyser to a rectangular function. The phase-noise content is found in a similar way and is given by:

$$\sigma_J[f_l,f_h] = \sqrt{<J(t)^2>} = \frac{1}{2\pi nf_o}\sqrt{\frac{P_{sb}}{P_c}}$$

Since the noise spectrum of modelocked lasers varies with the frequency offset from the carrier then it is useful to plot the single-sideband noise power spectrum which is given by:

$$L_f = 10\log_{10}\left[\frac{P(f)}{1.2xBxP_c}\right]$$

On linearising this curve the phase-noise spectral density function can then be plotted;

$$L_j(f) = 10\log_{10}\left[\frac{10^{\frac{L_n(f)}{10}} - 10^{\frac{L_1(f)}{10}}}{n^2-1}\right]$$

Finally the pulse timing jitter can be obtained by direct integration under this curve, and recasting the result into the following expression;

$$\sigma_J[f_l,f_h] = \frac{1}{\sqrt{2}\pi f_o}\sqrt{\left[\int_{f_l}^{f_h} 10^{\frac{L_j(f)}{10}}\,df\right]}$$

By using these expressions the noise content of the laser source can be determined by examining the frequency-domain data for a range of Fourier components using the photodiode/spectrum analyser arrangement. This technique has been applied to investigate the phase-noise characteristics of modelocked InGaAsP semiconductor lasers.

### 5.3 Phase noise in an actively modelocked semiconductor laser system

The pulse sequence from an actively modelocked InGaAsP semiconductor laser was focussed onto an InGaAs PIN photodiode with a 3dB bandwidth in excess of 22GHz. The output signal was recorded using either a Hewlett-Packard HP8562B spectrum analyser with a frequency range of 0.1-22GHz and a minimum resolution bandwidth of 100Hz, or a higher resolution (10Hz) type HP70900 analyser with a frequency range of 2.7GHz. The phase noise content was initially studied when the RF drive source to the laser was a tunable Marconi 2019 frequency synthesiser. The data represented in figure 5.1 show the close-in sidebands attending the 1st, 20th, and 50th harmonics of the pulse train Fourier comb.

Indeed, the noise sidebands are seen to increase with the harmonic number n. This is indicative of a substantial amount of timing jitter in the optical pulse train. Also shown in figure 5.1 is the spectrum of the RF drive signal. It can be seen that the noise of the drive signal has been transferred directly onto the laser pulse train and no other noise components are evident in this case. The data obtained from these spectrum analyser records were plotted in figure 5.2 in terms of single-sideband noise power (relative to the power of the carrier). The data thus obtained violate the small deviation regime, on which the theoretical development was based, at frequencies below 1kHz and so the extraction of quantitative information from this noise distribution plot is severely limited. However, from knowledge gained using the streak camera the relative timing jitter in the range 30Hz to 1MHz was estimated to be ~2-3ps.

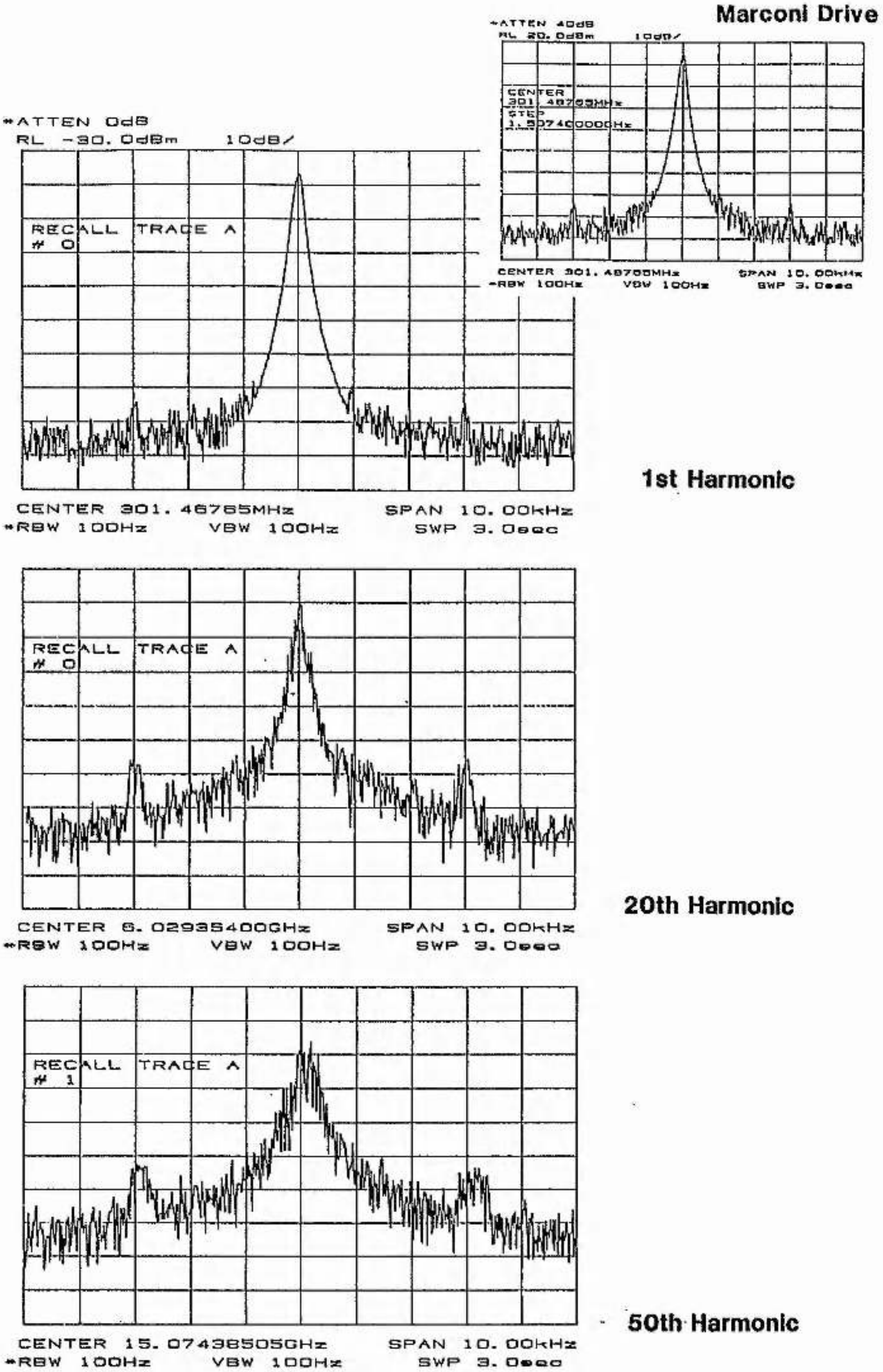

Figure 5.1 Close-in noise sidebands of (a) 1st (b) 20th and (c) 50th harmonics of the Fourier comb derived from the modelocked semiconductor laser, where the RF modulation source was a Marconi 2019 frequency synthesiser.

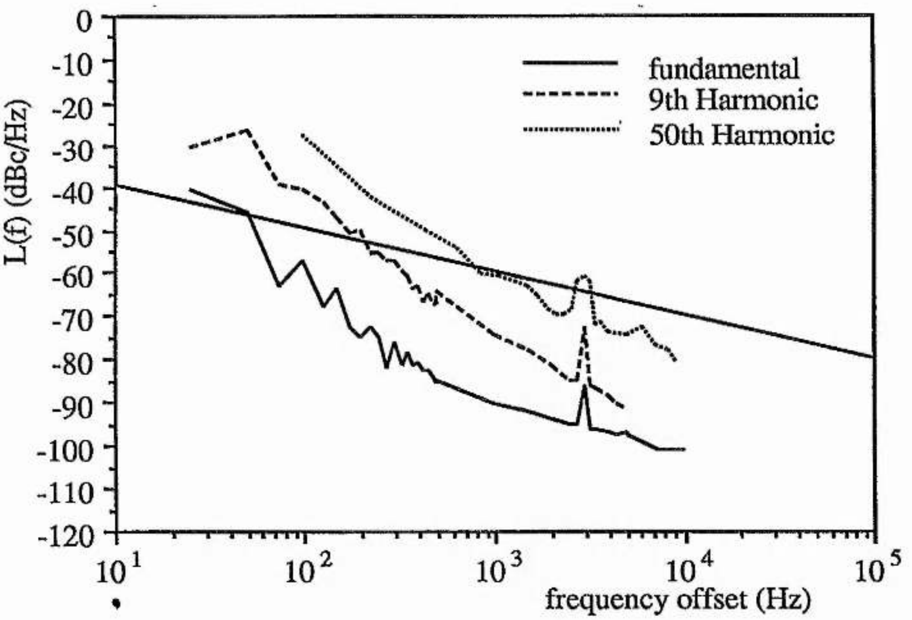

Figure 5.2 Single sideband noise content of a modelocked InGaAsP semiconductor laser with Marconi 2019 synthesised RF drive source. [The solid line indicates the small signal deviation criterion]

## 5.4 Optimisation of phase noise performance of the semiconductor laser system

The relatively poor noise performance of the laser pulse sequence detailed above was seen to be due mainly to the quality of the current modulation signal applied to the laser. It is perhaps worth explaining here that the Marconi synthesiser was not of especially poor quality and it is merely the fact that synthesisers in general tend to have inferior noise performance compared with fixed frequency crystal oscillators. This arises essentially because an error signal is required to sustain the phase-locking between the free-running, tunable, voltage-controlled oscillator and the internal crystal oscillator derived frequency reference. Indeed, of all the synthesisers tested the Marconi was found to have the lowest phase-noise content.

In an attempt to improve the laser noise performance an inhouse-designed and constructed fixed frequency crystal oscillator was employed. The crystal oscillator used had a frequency of 150MHz and its output power was split into two components. One was used to drive the streak camera diagnostic and the other was frequency doubled and amplified before being applied to the semiconductor laser. The corresponding noise sidebands measured for this laser configuration are shown in figures 5.3(a), (b).

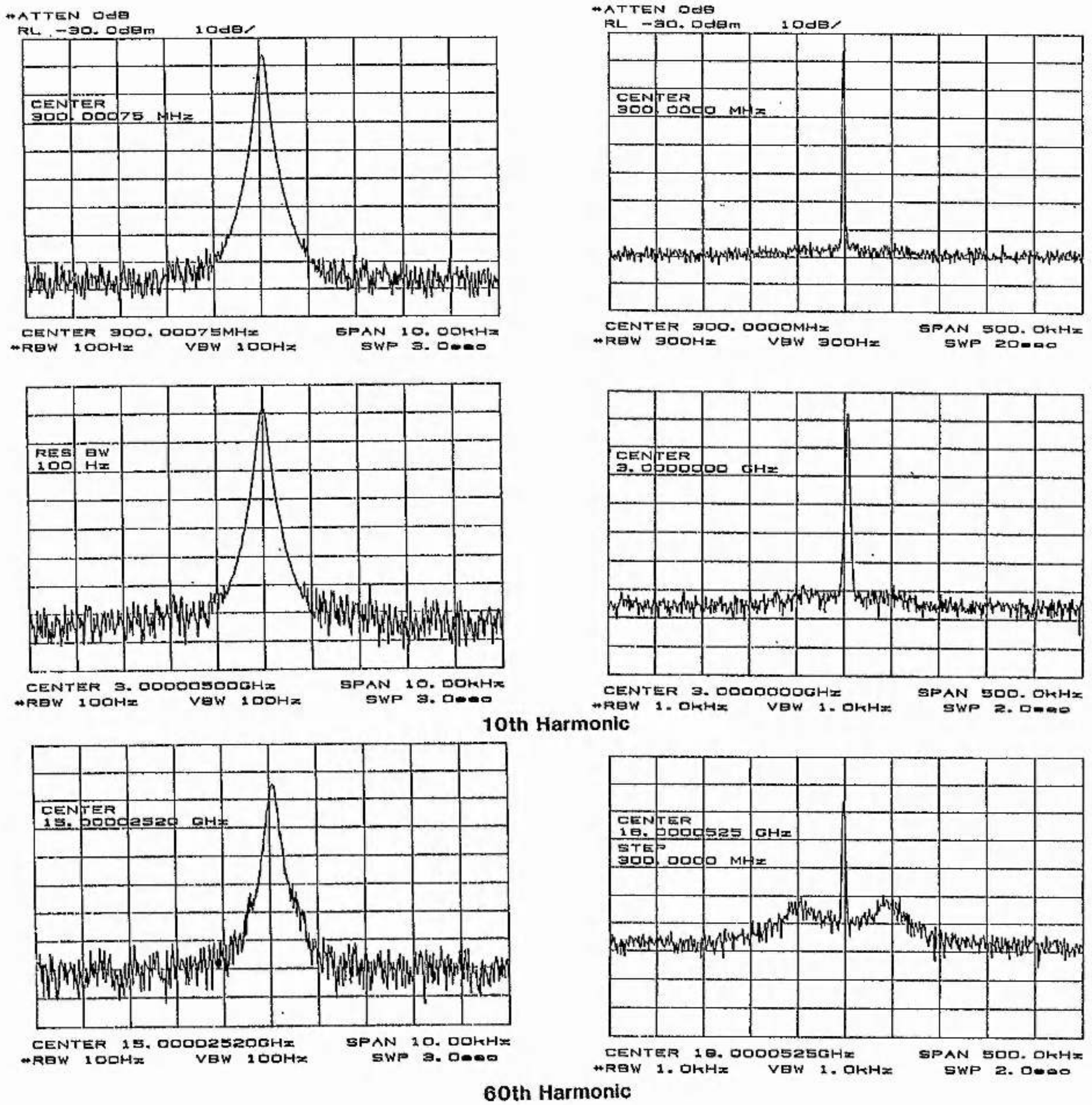

(a) (b)

Figure 5.3 Close-in noise sidebands of 1st, 10th and, 60th harmonics of the Fourier comb derived from the modelocked semiconductor laser for (a) 10kHz and (b) 500kHz frequency spans. The RF modulation source to the laser was a 'home built' crystal oscillator.

From this latter assessment it is clearly evident that the noise on the laser pulse train has been dramatically improved. It is, however, recognised that some residual noise components exist at large frequency offsets from the carrier (see figure 5.3(b)). These were attributable to noise on the power supply to the crystal oscillator and were readily removed by improved smoothing as confirmed by the data included as figure 5.4.

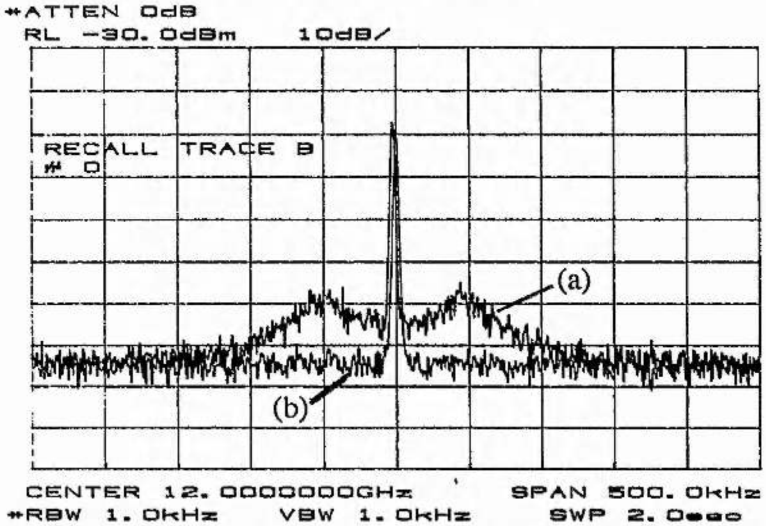

Figure 5.4 (a) High frequency noise components arising from the crystal oscillator power supply, and (b) their subsequent elimination with improved power supply

Single-sideband noise spectra were derived from these measurements as illustrated in figure 5.5. The noise associated with the oscillator power supply is shown separately in figure 5.6 for the fundamental and the 7th, 14th, and 60th harmonics. In the earlier analysis it was stated that the phase-noise sidebands increased in power as $n^2$, and so for these harmonics the relative power for the four chosen harmonics should be 1:49:196:3600. When transferred into decibels relative to the fundamental noise power the relative values become 0:17:23:36. At the peak of the noise sideband around 25kHz the noise powers of the harmonic components were found to be 0:11:17:30. The increments between the highest three components agree with that of pure phase noise. The discrepancy between the first and the seventh harmonics is due to the noise on the fundamental being so small that it is buried within the noise floor of the measurement equipment. In figure 5.6 the asterisk indicates the extrapolated phase noise level of the fundamental component. When the predicted fundamental noise component is added to the noise floor level the increase is only some 0.6dB.

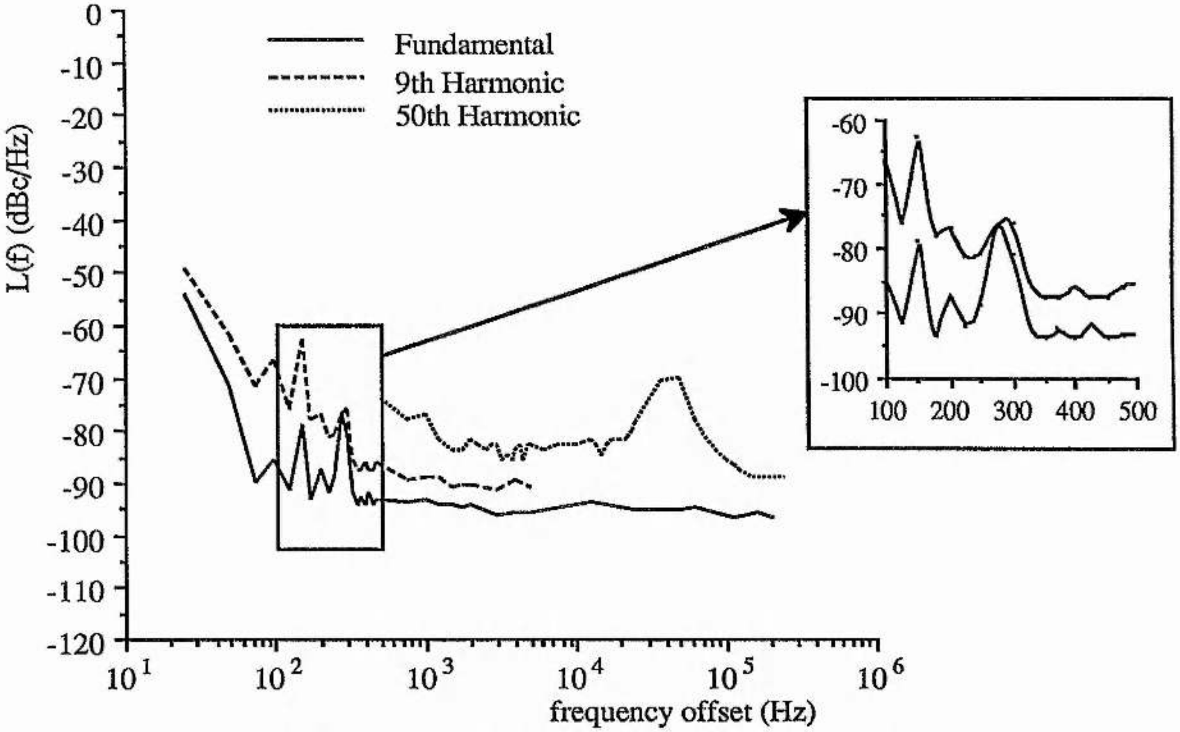

Figure 5.5 Single sideband noise spectra for laser with crystal oscillator drive source.

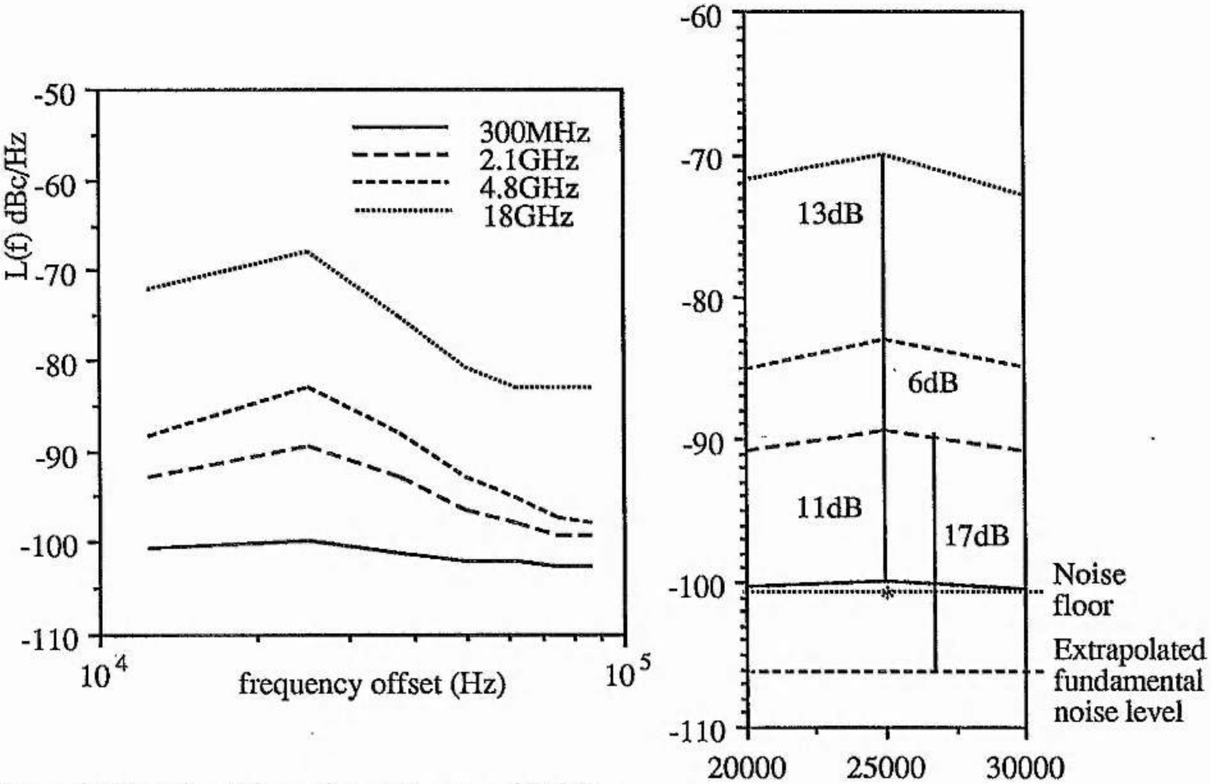

Figure 5.6 Details of the noise peak around 25kHz.

These results confirm both the validity of the theoretical development detailed previously, and the requirement for high-frequency Fourier component analysis when the phase noise becomes very small. It is also evident that the noise floor of the measurement system must be as low as possible, otherwise low power noise components can easily be unidentified with consequent errors in the calculations to which the timing jitter is deduced.

The phase-noise power spectrum Lj(f) was extracted from the curves of figure 5.5 (see figure 5.7) and values for the phase noise could be obtained as described previously. The measured values of pulse timing jitter for this laser were; $\sigma_J$[50Hz,500Hz] = 450fs, $\sigma_J$[500Hz,5kHz] = 130fs.

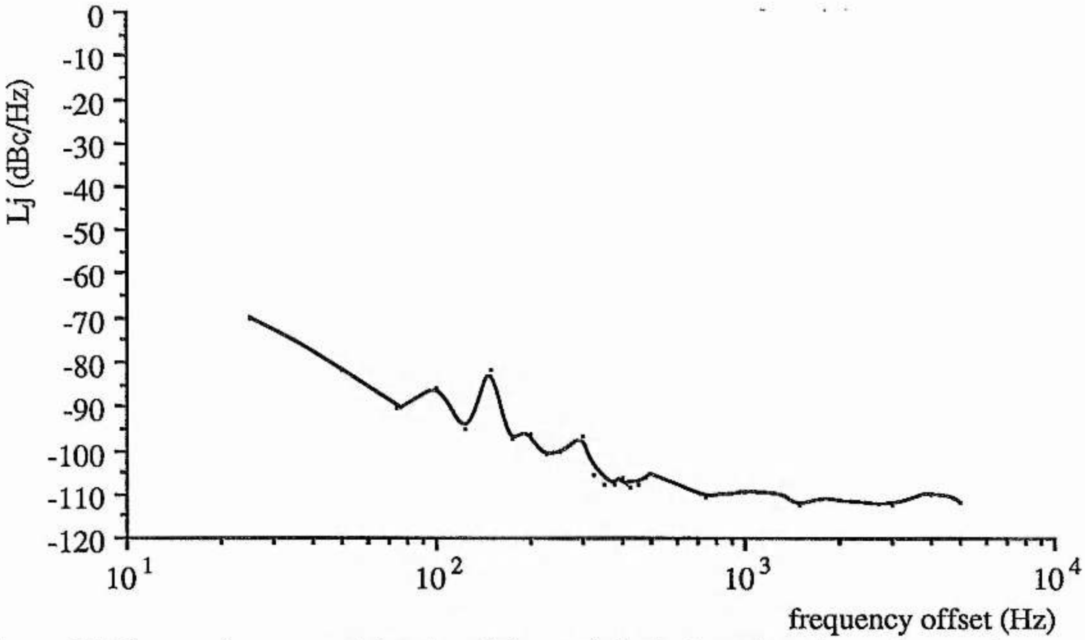

Figure 5.7 Phase noise spectral density of the modelocked semiconductor laser, where the modulation drive signal was derived from a crystal oscillator.

The insert to figure 5.5 clearly shows the existence of a strong amplitude-noise sideband around ~270Hz. The amplitude-noise character is evident because the increase in noise power does not scale with the square of the harmonic number. The origin of this feature was not clear, but it could indicate for example a beat between the applied modulation frequency and the cavity-mode separation. Since the details of the carrier noise (i.e. the phase noise of the internal oscillator within the spectrum analyser) were unknown then there is difficulty in quantifying the amplitude noise of the laser output. In fact, this technique is not the most amenable to the extraction of amplitude noise. A better method would entail some form of envelope detection. This can be implemented quite straightforwardly by monitoring the output of the laser using a photodiode-oscilloscope combination of suitable bandwidth. Examination of the intensity fluctuations for a range of timebase speeds should reveal the pertinent amplitude noise information in a more direct manner. For the laser described here this figure was found to be less than 1% in the frequency range considered.

On the basis of these measurements it can be seen that by using a crystal oscillator as the drive source for the modelocked laser the timing fluctuations of the optical pulse train have been reduced to well below 1ps. Also, the phase noise imposed on the pulse train from the drive oscillator was sufficiently low that some features intrinsic to the laser could be revealed. To further improve the phase noise of the laser a Hewlett-Packard crystal oscillator (f=300MHz) was used to generate the RF laser drive signal. As expected the phase noise of the laser was reduced in accordance with this high purity oscillator (see figure 5.8), and the associated timing jitter values from the laser were now reduced to; $\sigma_J$[50Hz,500Hz] = 150fs, $\sigma_J$[500Hz,5kHz] = 60fs.

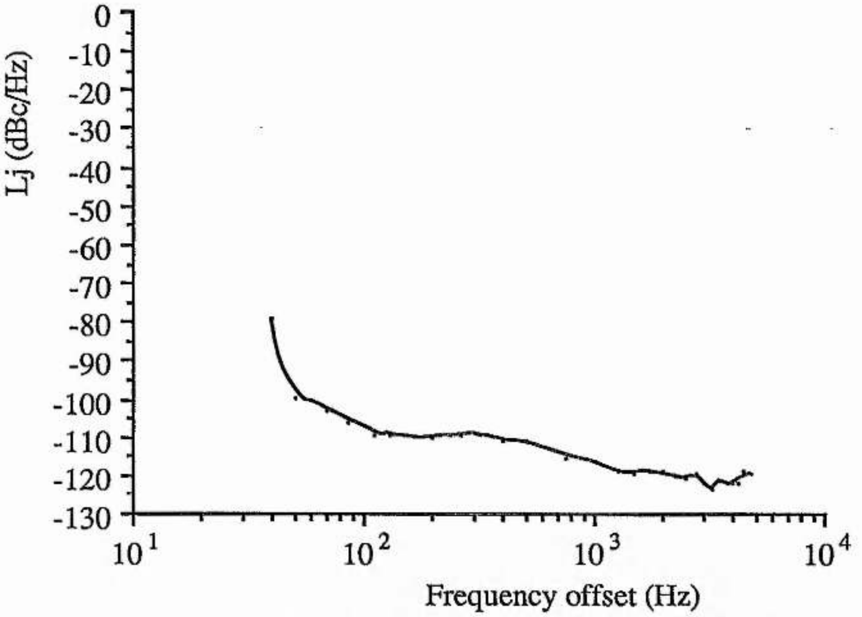

Figure 5.8 Phase noise spectral density associated with the Hewlett-Packard oscillator drive to the modelocked laser.

These values are close to that expected for the resolution of the measurement system and hence cannot be considered to be a sufficiently high fidelity result. In fact for a pulse sequence having a small phase-noise content the result obtained is only an upper bound of the timing jitter. It can therefore be concluded that this powerful measurement technique can reveal quantitative timing jitter information with better than 100fs resolution.

## 5.5 Summary

In this chapter a versatile technique for the quantitative measurement of timing jitter in modelocked pulse sequences has been described. This scheme which involves high-speed photodiodes and correspondingly high-bandwidth spectrum analysers, has allowed the development of a modelocked semiconductor laser source with greater than x10 improvement in the pulse timing jitter as compared to standard synthesiser driven systems. Timing jitter values of less than 200fs have been obtained in the frequency range 50-500Hz, and are as low as 60fs in the 500-5000Hz regime. These values are the lowest yet reported from any modelocked laser configuration and are a direct consequence of the compact nature of the laser and the stability of its drive oscillator. These values imply that such laser sources would be highly desirable for various laser timing experiments and in the evolving field of electro-optic sampling of high-speed electronic components.

# CHAPTER 6

# AMPLIFICATION OF ULTRASHORT PULSES USING AN ERBIUM-DOPED FIBRE AMPLIFIER

## 6.1 Introduction

At present the peak pulse powers from modelocked semiconductor lasers are typically limited to a few hundred milliwatts. This is obtained with low-frequency modulated systems such as those described previously. Whereas tens of milliwatts is more typical of lasers in which the current is modulated at high frequencies[140]. In this chapter the amplification of modelocked semiconductor laser pulses using optical amplifiers is considered where particular attention is given to the erbium-doped fibre amplifier. Due to the enhanced pulse powers thus produced such laser/amplifier systems should find applications as, for example, signal sources for non-linear soliton communications systems[141], or as compact probes for electro-optic characterisation of ultrafast electronic devices[142].

## 6.2 Optical amplifiers

In this section the characteristics of optical amplifiers will be described where an emphasis has been placed on amplification procedures for the 1.5μm spectral region. These amplifiers are usually termed as telecommunications amplifiers. Consideration will only be given to the characteristics of these amplifiers when used as single-pass or travelling-wave devices because although double-pass and regenerative amplifiers exhibit their own particular attributes they are more complex and are so far less suited to optical fibre communications systems. The latter schemes would perhaps be preferable for certain laboratory applications where complexity can be traded against features such as improved power extraction efficiency and saturation characteristics.

The operation of an optical amplifier is straight-forward in that on propagating through the device an initially weak optical signal grows in intensity resulting in a larger signal at the amplifier output. (The details concerning the actual amplification process will be discussed later since a variety of amplifier schemes will be dealt with.) The growth of intensity in the amplifier is exponential and can be characterised by the equation;

$$G=G_0\exp\left(\frac{I_{out}-I_{in}}{I_{sat}}\right)$$

G is the resultant gain, $G_0$ is the small signal, or unsaturated gain, $I_{in}$ and $I_{out}$ are the intensities of the input and the output of the amplifier respectively, and $I_{sat}$ is the saturation intensity of the amplifier medium. The saturation intensity can be physically interpreted as the intensity such that one photon is incident within the amplification cross-section of each atom per recovery time. When high input signals injected into the amplifier, or if the signal inside the amplifier builds up to a high level, then the increase in signal intensity no longer grows in an exponential fashion and the amplifier is said to be saturated. This provides a useful performance characteristic often quoted for amplifiers where, for example, the 3dB saturation output power is defined as the output power obtained for a 3dB decrease in the small signal amplifier gain (ie the point at which the gain is halved). Such parameters along with details of small signal gain, efficiency, and bandwidth will be detailed for each amplifier.

### 6.2.1 Gain

In a discussion of amplifiers (whether optical or electrical) the gain can often be usefully expressed in deciBels (dB) with the conversion from gain to gain in dB being;

$$G_{dB}(\omega)= 10 \log_{10} G(\omega)$$

If L is defined as the length of the amplifier then $G(\omega)$ can be expressed as;

$$G(\omega) = \exp[\ \omega L/c\ (\chi''(\omega))]$$

The imaginary part of the atomic susceptibility, $\chi''(\omega)$, includes all the details of the atomic lineshape. Using the expression for $G(\omega)$, the function $G_{dB}(\omega)$ becomes;

$$\begin{aligned} G_{dB}(\omega) &= 4.34 \log_e G(\omega) \\ &= 4.34\ (\omega L/c)\ \chi''(\omega) \end{aligned}$$

The power gain measured in dB's has the same lineshape as the atomic susceptibility. Therefore measurement of the fluorescence spectrum, which also has this shape, will give the gain spectrum of the amplifier in dB's, but at least two values of gain must be known to calibrate the gain axis.

### 6.2.2 Semiconductor amplifiers

Semiconductor amplifiers are essentially semiconductor lasers with some form of facet reflectivity suppression[143]. Since this topic was discussed in relation to external cavity lasers in chapter 2 only some typical operating parameters will be highlighted here. Internal gain values of greater than 25dB have regularly been obtained from semiconductor amplifiers[144], and multiple amplifier packages have been employed to give fibre-to-fibre gains of >30dB[145]. 3dB gain bandwidths in excess of 50nm[68] and saturation output powers exceeding 10dBm[146] are also typical. The main drawbacks with semiconductor amplifiers relating to their use in optical fibre systems are; diode/fibre coupling losses (typically in the range 3-5dB, although dependent on device structure), polarisation sensitivity, and general alignment sensitivities. All of these drawbacks can be overcome by using an amplifying medium which is more compatible with the optical fibre transmission medium, and indeed the most desirable optical amplifier is in fibre form.

### 6.2.3 Fibre amplifiers

There are various nonlinear processes that occur in silica fibres which can be exploited to transfer energy from a strong pump field to the transmitted information signal, and hence provide optical gain. Two amplifiers based on intrinsic nonlinear processes which involve standard low-loss transmission fibres will now be briefly outlined. Subsequently, the details of an alternative fibre amplifier type which utilises fibre core doping of laser active ions which provide gain at the transmission wavelength will be discussed.

### 6.2.4 Fibre Raman amplifiers

Raman amplifiers[147] utilise the gain created by the scattering of a strong pump beam by optical phonons. The resultant broadband Raman gain spectrum for a germano-silicate fibre is shown in the figure 6.1, where the pump wavelength was 1µm. (The form of the curve does not alter with different pump wavelengths, apart from some rescaling.) Fibres with different core dopant compositions can affect the shape of the gain spectrum significantly with $SiO_2$-$GeO_2$ being preferred. These amplifiers can exhibit very large gains (of up to 50dB) and have good saturation characteristics ($P_{-3dB}$>10mW).

Raman amplification can be used to compensate for the intrinsic fibre loss of a transmission system, where the whole transmission line is essentially a distributed amplifier operating at transparency. Pump light can be injected into the system every few kilometres such that the requirement for a high power pump laser is circumvented[148]. Nevertheless, Raman amplifiers still require rather high pump powers to compete with alternative optical amplifier schemes. Despite this, there is still a considerable research effort being devoted to improved Raman amplifier configurations[149].

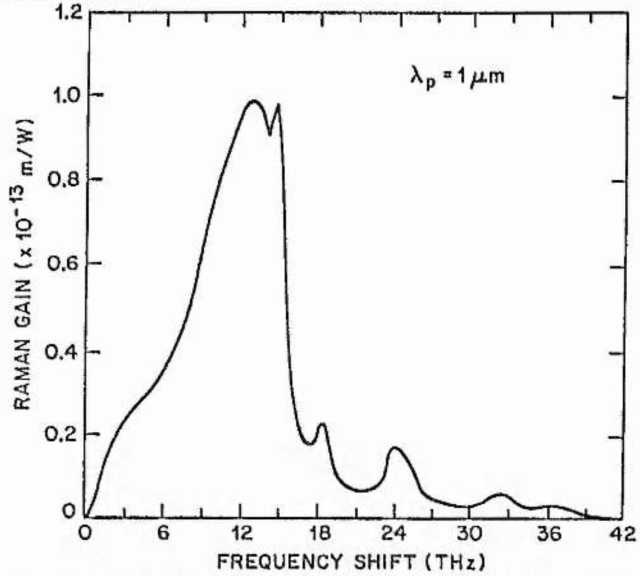

Figure 6.1 Raman gain spectrum for germano-silicate optical fibre. [After reference147.]

### 6.2.5 Brillouin fibre amplifiers

Brillouin amplification has some similarities with Raman amplification but in this case the gain is created by acoustic phonon scattering and this leads to the radically different gain characteristics observed. The gain spectrum is narrow (20-150MHz) and exists ~12GHz above the pump frequency[150]. It is required that the pump source must be of very narrow linewidth for significant Brillouin scattering. Although the gain can be very large (>30dB) and the pump requirements are modest (efficiencies of 4.3dB/mW demonstrated) the restrictive nature of the characteristics mentioned above has resulted in limited interest in the Brillouin amplifier as a telecommunications amplifier.

### 6.2.6 Doped-fibre amplifiers

Doped-fibre amplifiers[151] comprise standard fibre which has been doped with a laser active atomic species at the preform fabrication stage. By inducing a population inversion of the dopant ions with optical pumping gain can be created within the bandwidth of the atomic transition, in a similar fashion to any conventional laser material. The two doped-fibre amplifiers which are of some interest with respect to optical fibre systems have either neodymium[152] or erbium[151] dopants and their respective trivalent ionic species exhibit gain at ~1.3μm and around 1.55μm, (ie. the two low-loss windows of silica fibre.) Neodymium-doped fibres are of limited use as communications amplifiers (at least when incorporated into silica fibres as will be discussed further in chapter 8), and so only erbium-doped fibre amplifiers will be considered in the present context.

### 6.3 The erbium-doped silica optical fibre amplifier

Erbium-doped fibre amplifiers have been a prime topic of optical communications research for the past few years. Significant developments have been made in doping and co-doping techniques thus ensuring good homogeneity and device efficiency can be achieved[153]. This together with studies relating to optimal pumping wavelengths has enabled gains of up to 45dB[154] and efficiencies of 11dB/mW to be demonstrated[155]. The 3dB saturation output power can also be large (>10dBm) although this is usually achieved at the expense of efficiency. Such features, along with, low noise characteristics, robustness, polarisation insensitivity, the capability of semiconductor laser pumping, imply that erbium-doped fibre amplifiers may well dominate as the optical amplifier for future telecommunications systems.

There are basically two approaches in designing erbium fibre amplifiers whereby either long (>100m)[156] or short (~10m)[151] lengths of fibre are employed. The dopant concentration is altered such that the total number of dopant ions are essentially constant in both cases. The latter approach is more attractive but presents problems relating to the homogeneity of the doping profile within the fibre because at high concentrations quenching of laser action can occur due to the formation of aggregates. However, this can be prevented by introducing suitable co-dopants, eg. $Al_2O_3$, into the core during the fabrication of the fibre. More recent developments have indicated the possibility of ultralong erbium-doped amplifiers with transparency being obtained with pump powers of 1.5mW/km[157]. These distributed amplifiers can only be effectively pumped at a wavelength where the intrinsic fibre loss is also very low and this can be realised using the 1.48μm pump band (see section 6.5.2).

### 6.4 Ultrashort pulse amplification using an erbium fibre amplifier

It is of some interest to evaluate the amplification of picosecond duration optical pulses with erbium-doped fibre amplifiers, since any introduction of distortions onto a short pulse data stream would limit the potential usefulness of the amplifier. To this end an erbium amplifier was employed to amplify the ultrashort pulse output from a modelocked InGaAsP laser. Such an oscillator/amplifier source would allow for the generation of usefully high-peak power optical pulses for implementation in nonlinear transmission systems[158], for example, as pump sources for Kerr switches[159] and a range of other nonlinear devices. The potential amplification achievable would also allow for large fan-out factors for optical clocks in digital optical circuits and networks.

The experimental configuration used is shown in figure 6.2. The mode-locked laser oscillator is similar to that described previously in section 4.4. The modulation frequency used was generally ~600MHz which corresponded to a pulse period of ~1.67ns. Emission from the uncoated diode facet was collimated and refocussed into the input arm of a fused-fibre directional coupler. This enabled the oscillator launch power and wavelength to be monitored on one output port while the other port was fusion spliced to a 3.5 m length of germano-silicate erbium-doped fibre. This erbium-doped fibre had a core radius of 2.3μm, NA=0.24 and a dopant concentration of $6x10^{18}$ $cm^{-3}$. The amplified 1.5 μm signal was demultiplexed from the launched, counter-propagating pump by a second dichroic fused-fibre coupler at the amplifier output. A counter-propagating pump geometry was employed to increase the saturation output power thereby increasing the amplification factors obtained with large signal inputs.

The pump source for the fibre amplifier was an acousto-optically mode-locked, frequency-doubled, Nd:YAG laser which provided an average power in excess of 500mW at 532nm. A consequence of the long time constants of the erbium system is that the gain is impervious to high frequency pump laser fluctuations, and so the pulsed nature of the Nd:YAG laser (figure 6.3) does not effect the fibre amplifier in any way, since only the mean power level is of significance. Powers in excess of 100mW could be launched into the amplifier which exhibited small signal gains of >20dB at 1.536μm. Since the amplifier fibre was multimode at the pump wavelength of 532nm the gain observed was sensitive to the modal distribution of the pump within the fibre, and this was clearly a drawback with this short wavelength pumping because it reduced the efficiency of the device. The signal gain was determined by measuring the mean power at the amplifier input and output.

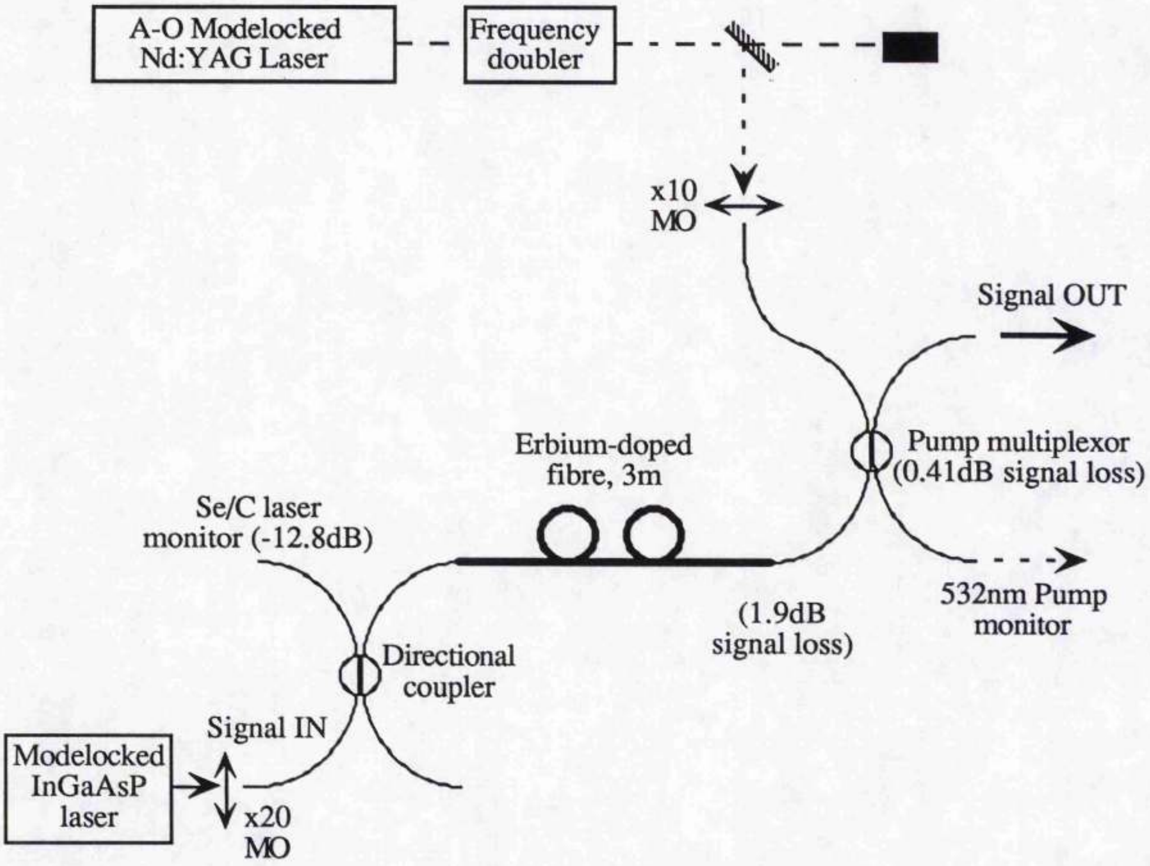

Figure 6.2. Experimental arrangement for ultrashort pulse amplification.

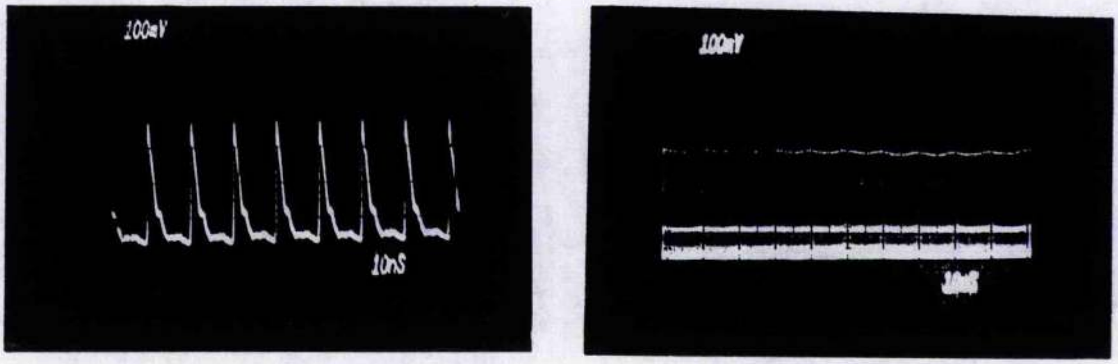

Figure 6.3 Oscilloscope traces of Nd:YAG pump laser output

The durations of the input 1.536µm modelocked pulses were determined by using an S1-type Photochron IIA streak camera which had a spectral sensitivity extending beyond 1.5µm. The amplified pulse train was also simultaneously monitored by the streak camera to determine whether any pulse reshaping had occurred. The modelocked single-arm external cavity InGaAsP laser system produced pulses of duration <10ps (figure 6.4(a)) at a repetition rate of 600MHz and at an average power of up to 500μW. The wavelength of the modelocked pulses was adjusted such that it was coincident with the 1.536μm spectral peak (4nm FWHM bandwidth, figure 6.5) of the erbium-doped fibre amplifier gain characteristic. The laser spectra were observed to be stable with a bandwidth of less than 1 nm, a typical example is shown in figure 6.4(b).

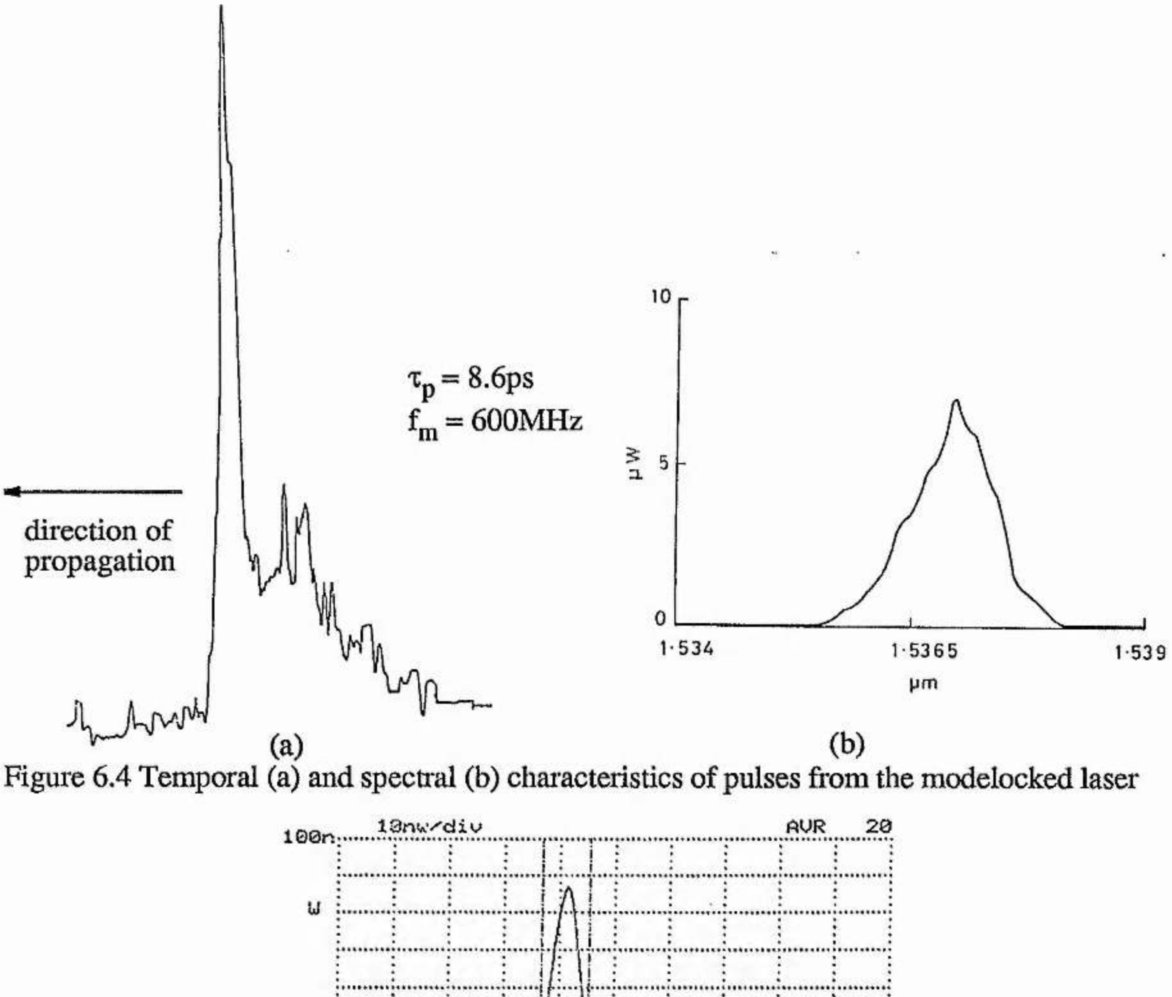

(a) (b)

Figure 6.4 Temporal (a) and spectral (b) characteristics of pulses from the modelocked laser

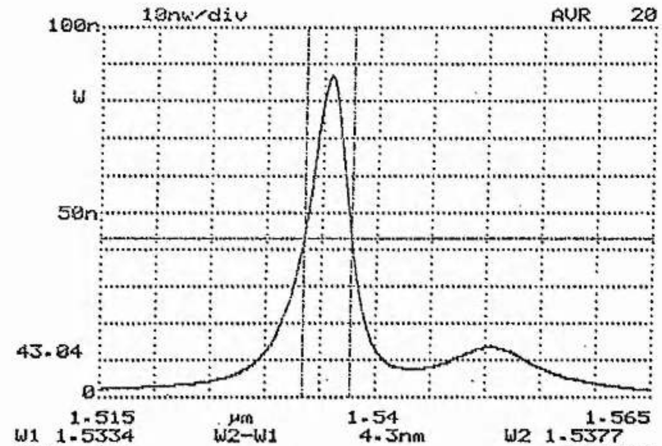

Figure 6.5 Fluorescence spectrum of the erbium-doped fibre amplifier.

Gain characteristics of the erbium amplifier were recorded by varying the input signal power and monitoring the output from the device at a constant pump power (figure 6.6). Because the output loss of the amplifier included both a 1.9dB splice loss, which was high due to the dissimilar nature of the fibres, and also a 0.4dB loss at the output multiplexor, then this 2.3dB figure can be added to the measured values to give the actual fibre gain. The launch monitor consisted of a calibrated photodiode/amplifier which directly gave the actual signal power launched into the fibre amplifier, and the output power was measured using a power meter. The 3dB saturation output power for the arrangement was found to be about 7dBm for typical launched pump powers in the 100mW range.

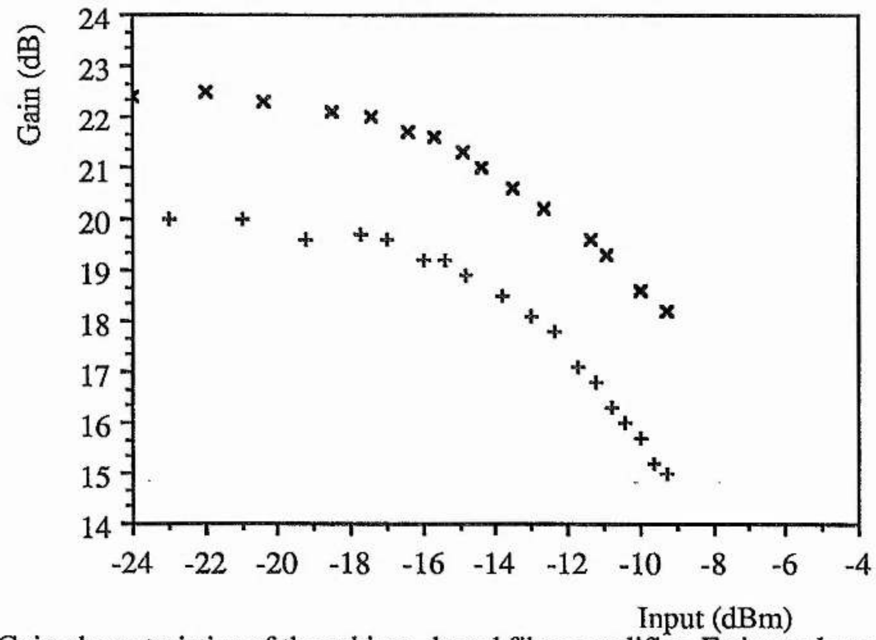

Figure 6.6 Gain characteristics of the erbium-doped fibre amplifier. Estimated pump powers were x=100mW, +=50mW.

For input signal powers up to 300μW (~-5dBm) gain saturation was observed and this reduced the available gain to 13dB. Associated typical streak profiles of the amplified pulse trains recorded in this regime are shown in figure 6.7. The output average power was ~6mW which corresponds to 0.58W peak pulse power when the power in the background subpulse was subtracted. By comparison of figures 6.4 and 6.7 it can be deduced that, within the resolution (< 5ps) of the streak camera, no profile reshaping of the main pulse occurred during the amplification process. The subpulse appears to be suppressed but this is more likely to be due to the increase in the signal-to-noise ratio of the measurements for the higher power pulses.

The capability of the amplifier, despite being strongly saturated, to amplify ultrashort pulses without distortion is attributed to the large number of erbium ions in the fibre core (~ 3 x $10^{14}$). It has been demonstrated by Pettitt and coworkers[160] that for pulse repetition rates above 100kHz the gain is unable to 'track' intensity variations of the signal. This is due in part to the large total erbium population in the fibre, but also to the slow up-pumping rate from the ground state to the upper laser level. A quasi-steady state equilibrium between up-pumping and stimulated emission rates determines the population inversion and hence the gain parameters. This interpretation applies to these results where the energy in a single output pulse cannot significantly deplete the population inversion on the timescale of a single pulse. The amplifier therefore saturates according to the mean power level and not the pulse peak power. This linearity of the gain is very attractive for use as a telecommunications amplifier.

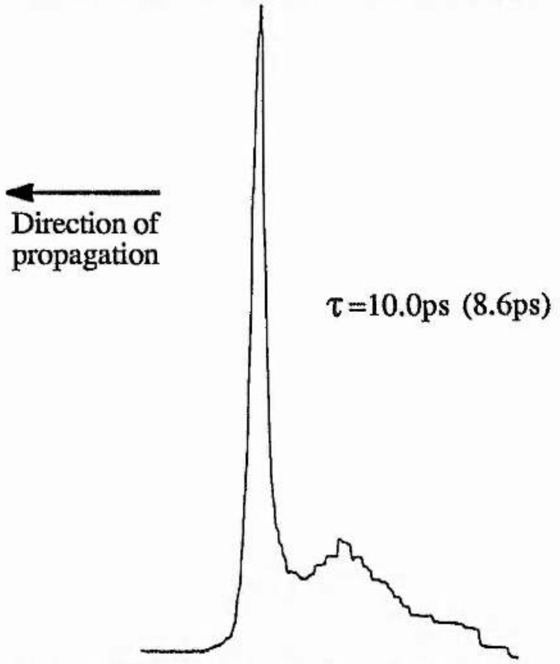

Figure 6.7 Amplified pulse profile with $P_{av}$=6mW, $P_p$(main peak)=0.58W.

To obtain higher peak power pulses the output derived from the specular reflection from the grating in the semiconductor laser was used, which when operated under the conditions as detailed in chapter 4, produced subpulse-free pulses with durations below 10ps. The repetition rate was also reduced to 300MHz, therefore since the average output power was ~1mW the launched power to the amplifier was effectively doubled but the peak power was actually increased by a factor of 8. With increased amplifier pumping improved amplifier gain could be obtained and stable average amplified powers of up to 14mW (G~14dB) were measured, corresponding to amplified peak pulse powers in excess of 5W (figure 6.8). It is believed that these are the highest peak power pulses to be generated from a modelocked semiconductor system. Further optimisation of the amplifier in terms of gain and saturation parameters would further enhance the pulse peak power generated.

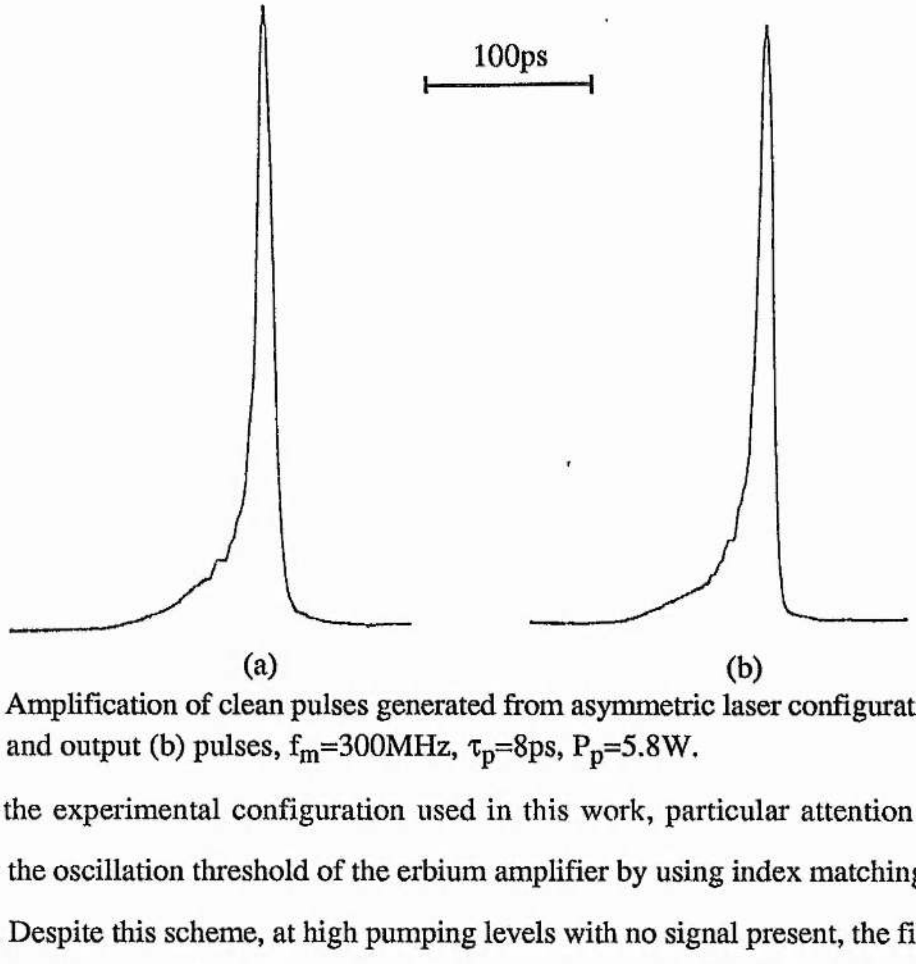

Figure 6.8 Amplification of clean pulses generated from asymmetric laser configuration, Input (a) and output (b) pulses, $f_m$=300MHz, $\tau_p$=8ps, $P_p$=5.8W.

In the experimental configuration used in this work, particular attention was paid to increasing the oscillation threshold of the erbium amplifier by using index matching cells on the fibre ends. Despite this scheme, at high pumping levels with no signal present, the fibre amplifier would self-oscillate as indicated by a noisy output spectrum. It was found (due to optimisation of the semiconductor launch power and the absence of optical isolation) that the fibre oscillation occurred off the diffraction grating in the semiconductor laser cavity. This might at first seem detrimental, but again due to the long time constants characteristic of erbium-doped fibre the presence of the semiconductor laser signal eliminated the fibre oscillation and only amplification took place. Therefore, for the application discussed here where a power amplifier for a continuously operating source laser is of interest this self-oscillation is unimportant. Of course, for use as a line amplifier for a modulated pulse stream which may have long sequences of zeros, then self-oscillation ought to be avoided, but would be dependent on the modulation scheme employed.

### 6.5 Semiconductor laser pump sources for erbium:fibre amplifiers

In this work the pump wavelength used to pump the erbium-doped fibre amplifier was 532nm, derived from a frequency-doubled acousto-optically modelocked Nd:YAG laser (modified Series 500 Control laser). The 532nm pump band although efficient requires the use of a large-frame laser for its generation. This, apart from being costly and inefficient, is useless with respect to any potential applications of erbium-doped fibre amplifiers and devices. Therefore it would be desirable to use a semiconductor laser as a pump source for erbium-doped fibres and with this objective in mind this section is devoted to potential applicability of semiconductor lasers as pump sources for erbium-doped fibre devices.

Fortunately, erbium-doped silica fibre has numerous pump bands throughout the visible and near-infrared regions of the electromagnetic spectrum[161] (see figure 6.9). Three of these pump bands can be accessed by already identified semiconductor lasers. These main pump bands occur at ~807nm, 1470-1490nm, and 980nm.

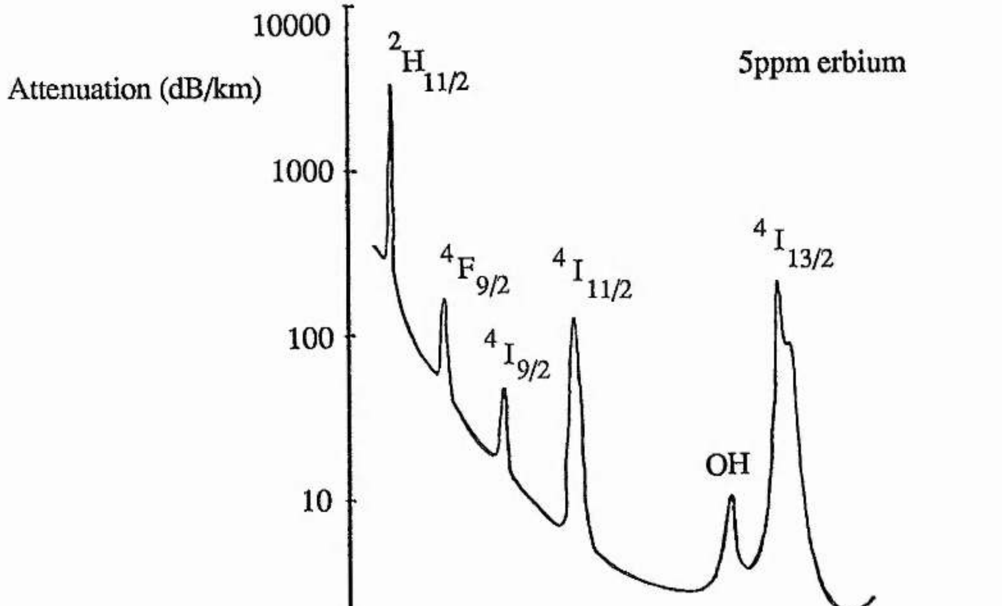

Figure 6.9 Absorption spectrum of erbium-doped, silica fibre. [Data provided by Robert Baker of STC Technology Ltd]

### 6.5.1 807nm semiconductor pump lasers

The 807nm pump band of erbium-doped amplifiers almost coincides with the wavelength that is of particular interest for semiconductor laser pumping of Nd:YAG microlasers[162]. These microlasers have received a lot of attention recently because of the significant advances that have been made in the manufacture of high-power GaAlAs semiconductor lasers[163]. Thus semiconductor pump lasers having CW output powers up to 1W are readily available and can thus be directly used for the excitation of erbium-doped fibre devices. Only one significant difference exists between a pump source for microlasers and fibre amplifiers which is that the output must be able to be efficiently coupled into the single-mode optical fibre of the erbium amplifier. Consequently, the higher power, multiple-stripe arrays (up to 1W) are unattractive, giving only ~5% coupling efficiency to lensed single-mode fibres. However, studies into injection locking and self-injection locking of high power arrays has enabled ~40% coupling efficiency to single-mode optical fibres to be demonstrated[164] because of their improved spatial beam quality. Also it has been shown that the good beam quality obtained from broad (3-5μm) single-stripe lasers can allow >40% pump coupling efficiency[165]. Although the total output power is relatively modest (~200mW) for broad-stripe devices[166], a factor of four increase in total coupled power can be achieved over an array with an output power of 0.5W.

The pumping efficiency of the erbium-fibre amplifier has been shown to be polarisation independent[167]. So fibre integrated polarisation multiplexors can be used to combine the output from two high-power semiconductor lasers to enhance the available pump power[154]. A further increase in the pump power will result from using both co- and counter-propagating pump sources and an example of such a high-power pumping scheme is illustrated in figure 6.10.

The commercial availability of high-power GaAlAs lasers make this pump source extremely attractive, although the existence of significant excited state absorption at ~800nm reduces the pumping efficiency and severely limits its applicability. Recently a marked improvement has been demonstrated by using long double-core fibres with a slightly higher pump wavelength of 820nm[168]. This combination goes some way to circumvent the problem of excited state absorption around 800nm.

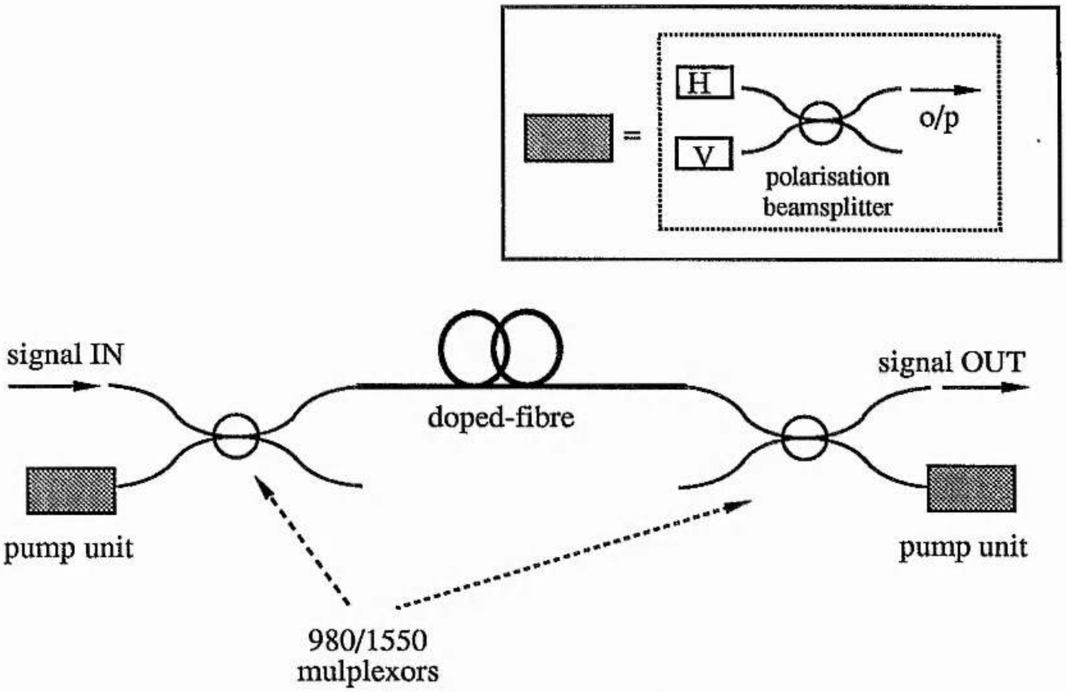

Figure 6.10 High power pumping scheme for doped fibre amplifiers. V and H denote vertical and horizontal launch polarisations. By using polarisation beamsplitters the power from many individual lasers can be coupled together to increase the available pump power.

### 6.5.2 1480nm semiconductor pump lasers

An alternative absorption band of erbium-doped fibres that is also accessible using semiconductor lasers occurs at ~1480nm. This corresponds to in-band pumping (see figure 6.11) and occurs within the compositional tuning range of InGaAsP/InP system semiconductor lasers[52]. Although the InGaAsP/InP system is a less mature technology than its GaAlAs/GaAs counterpart, the advances made with GaAlAs devices can be easily transferred to InGaAsP devices. Moreover, the extra degree of freedom owing to its quaternary nature generally results in higher performance and longer lifetime devices. InGaAsP diode arrays are uncommon, and most high power devices are of the broad-stripe type[166]. This is due mainly to the requirement of efficient optical coupling into single-mode fibres.

The incomplete inversion that accompanies in-band pumping affects both the maximum gain obtainable and also the detailed shape of the gain spectrum[170]. So that the spectrum will usually be broader and flatter. Another consequence of this pumping scheme is that the noise figure of the amplifier must always exceed the absolute value of 3dB which can, however, be obtained using other pump bands[171].

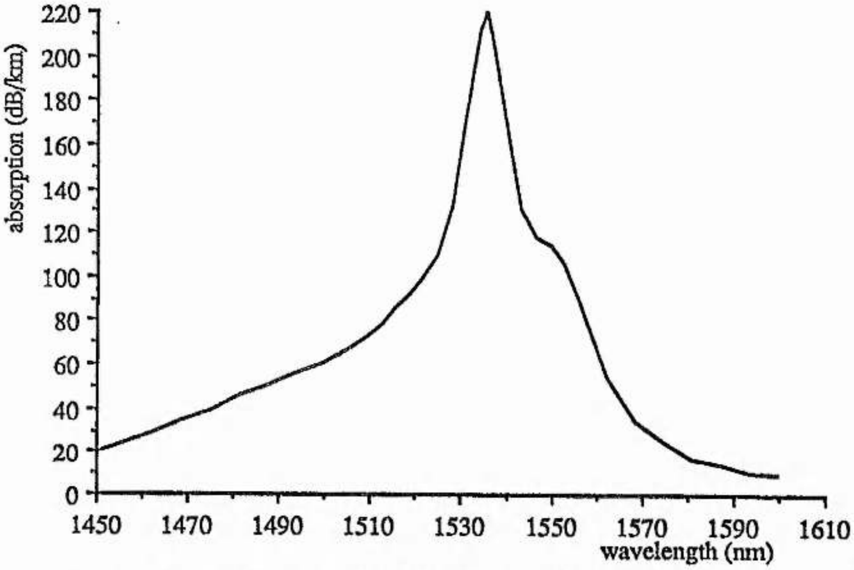

Figure 6.11 Ground-state absorption around 1.5μm in an erbium-doped, germano-silicate fibre.

InGaAsP semiconductor lasers are at this time the preferred pump source for erbium-fibre devices, because they already satisfy the necessary power, efficiency and lifetime requirements. For example, in one experiment[154] a gain of 46.5dB was achieved with an input pump power of 133mW within the wavelength range 1.45-1.51μm, supplied by four InGaAsP lasers. The measured gain coefficient was 0.76dB/mW and a saturation output power of 10.7dBm was obtained. Recently improvements in fibre production has enabled gain coefficients of up to 5dB/mW[155].

### 6.5.3 980nm semiconductor pump lasers

It has been shown that the wavelength of 980nm is the most efficient for pumping erbium-doped fibres[172] due to the absence of excited-state absorption at this wavelength, and reported efficiencies are as high as 11dB/mW[155]. Also recent advances in semiconductor laser technology has enabled the realisation of InGaAs laser sources operating within the 900-1100nm region[173] (ie. the region between GaAlAs and InGaAsP devices). Therefore, semiconductor laser oscillation from below 800nm to around 1600nm is now possible by the compositional tuning of only three semiconductor material systems.

The difficulty arising in the case of 980nm lasers is that the active region material cannot, as yet be lattice matched to a suitable substrate such that continuous oscillation can take place. By using strained-layer superlattices[174] this problem can be overcome. Although there are still doubts concerning the potential lifetimes of such strained-layer lasers typical devices operating continuously at >80mW output power have been demonstrated to operate for more than 1200 hours without a marked degradation in performance. It appears probable that these devices will fulfil even the most stringent applications lifetime requirement in the near future. It has also been claimed that strained layer devices could replace AlGaAs lasers due to the absence of the fast defect propagation along the **(110)** crystal axis which accounts for a significant proportion of failures in AlGaAs lasers[175]. Currently obtainable output power levels of around 100mW are perfectly adequate for most practical erbium-doped fibre based devices. Furthermore, by using multiple pumping geometries, compact, tunable, high output power erbium-fibre lasers can be produced, where only modest electrical inputs are required for their operation.

### 6.6 Soliton amplification

Amplification of short duration (~250fs) solitonic pulses has been observed in erbium-doped fibre amplifiers[176]. In one particular case this led to adiabatic pulse compression to produce output solitons of ~60fs by spectral enhancement due to the soliton self-frequency shift. At this time the necessary parameters of this soliton compressor seem unclear, and whether the process can be initiated by 1-10ps pulses appears doubtful. Even so, with correct choice of amplifier parameters such that the gain bandwidth is both broad and flat, then pulses with spectral bandwidths exceeding 60nm (equivalent to durations of ~40fs) could be amplified.

### 6.7 Summary

In this chapter amplification of optical signals around the 1.5μm spectral region has been considered. The discussion was centred on fibre amplifiers and in particular the erbium-doped fibre amplifier. Amplification of ultrashort pulses from an actively mode-locked semiconductor laser was outlined where significant peak output powers were achieved from this oscillator/amplifier system. The maximum power was limited by the available launch power to the amplifier from the oscillator and also by the low saturation power characteristics of the particular fibre used. It was also shown that as a consequence of the long upper-state lifetime and small gain cross-section of the erbium-doped fibre amplifier that the gain saturates only as a function of the avarage power and not as peak power. Therefore the amplification process is very linear and indeed no pulse shaping was observed as expected. This makes this type of oscillator-amplifier scheme very attractive and the further prospect of semiconductor laser pumping of the fibre amplifier will further add to its potential convenience, efficiency, and practicality.

# CHAPTER 7

# THE CONTROLLED AMPLIFIER MODULATOR

## 7.1 Introduction

### 7.1.1 Direct modulation of laser signals

Many devices have been developed for the purpose of laser signal modulation, and according to the effect produced these devices can be categorised as phase or amplitude modulators. In the former the frequency of the laser signal is altered in proportion to some driving signal, whereas in the latter it is the intensity of the laser signal that is changed. A brief account of a few typical laser modulators will now be given. In subsequent sections a novel modulator configuration based on a semiconductor laser amplifier will be described.

### 7.1.2 Phase modulators

A phase modulator is a device which effectively alters its optical path length under the influence of an applied electrical signal. The electro-optic (EO) phase modulator[177] is representative of a phase modulator and is operated in the following manner. An information signal is applied to the electrodes of the modulator which induces a change in the refractive index of the medium through the electro-optic effect. The refractive index change thus produced is directly related to the applied electric field strength. In this way the information is imposed onto the laser signal passing through the device in the form of a time-dependent phase variation of the laser frequency which is directly proportional to the amplitude of the applied information signal. Phase modulators have regularly been used as laser modelockers, and the term FM modelocking is generally used to describe this technique. A phase modulator can also be configured in, for example, a Mach-Zehnder interferometer arrangement[178] to affect amplitude modulation of the optical signal.

### 7.1.3 Amplitude modulators

Amplitude modulators are conceptually simpler than their phase counterparts in that a variation in the transmission of the device is affected by some externally applied drive signal. A representative example of an amplitude modulator is the acousto-optic (AO) modulator[179], and a schematic representation of a standing-wave device is shown in figure 7.1. When a signal is applied to the modulator an acoustic grating is formed which can scatter an incident laser signal into various diffraction orders. In effect, therefore, the undeflected beam is effectively attenuated. The attenuation is determined by the magnitude of the applied signal, and for typical acousto-optic modulators can be in excess of 60%. The deflection efficiency decreases with increasing modulation frequency, and the high frequency limit is in general less than 200MHz although improved transducer technology has permitted relatively efficient operation up to 500MHz to be demonstrated[180]. The AO modulator has also been frequently employed as a laser modelocking element, and is a standard component in many commercial systems.

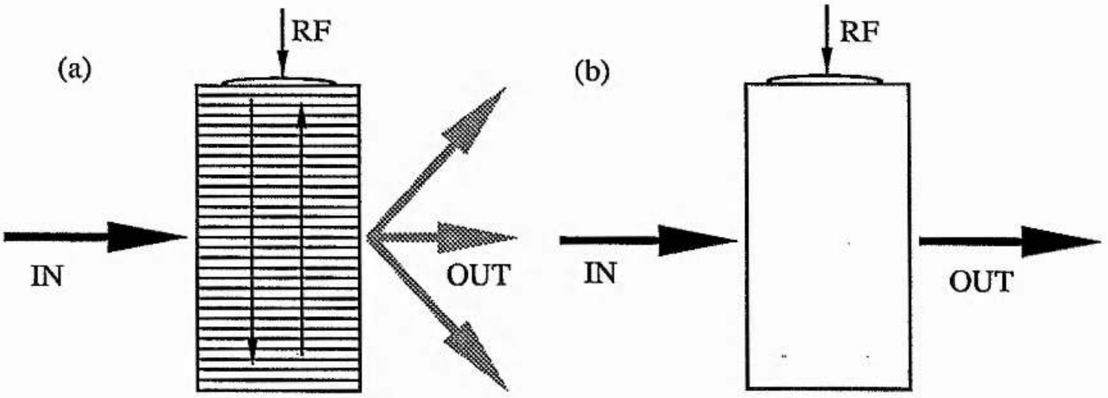

Figure 7.1 Schematic representation of an acousto-optic modulator. Incident and reflected acoustic waves add (a) constructively to form an index grating hence the undeflected beam is attenuated, and (b) destructively giving no resultant change in the optical beam.

### 7.1.4 The Controlled Amplifier Modulator

EO and AO modulators can be used as internal or external laser signal modulators. The modulator which is designated here as 'the controlled amplifier modulator', is intended primarily for incorporation into laser systems to facilitate more useful laser output properties than can be achieved otherwise. The application of the controlled-amplifier-modelocking (C.A.M.) to erbium-doped fibre lasers will be discussed in a later section. The principle of this type of modulator can be readily described by referring to figure 7.2. The semiconductor amplifier can be regarded as part of a laser cavity mirror structure and it is required that, the laser gain medium produces an output which falls within the wavelength range of the semiconductor amplifier gain curve. Initially, with no current injection, the semiconductor amplifier exhibits large attenuation to the fluorescence signal from the inverted laser gain medium.

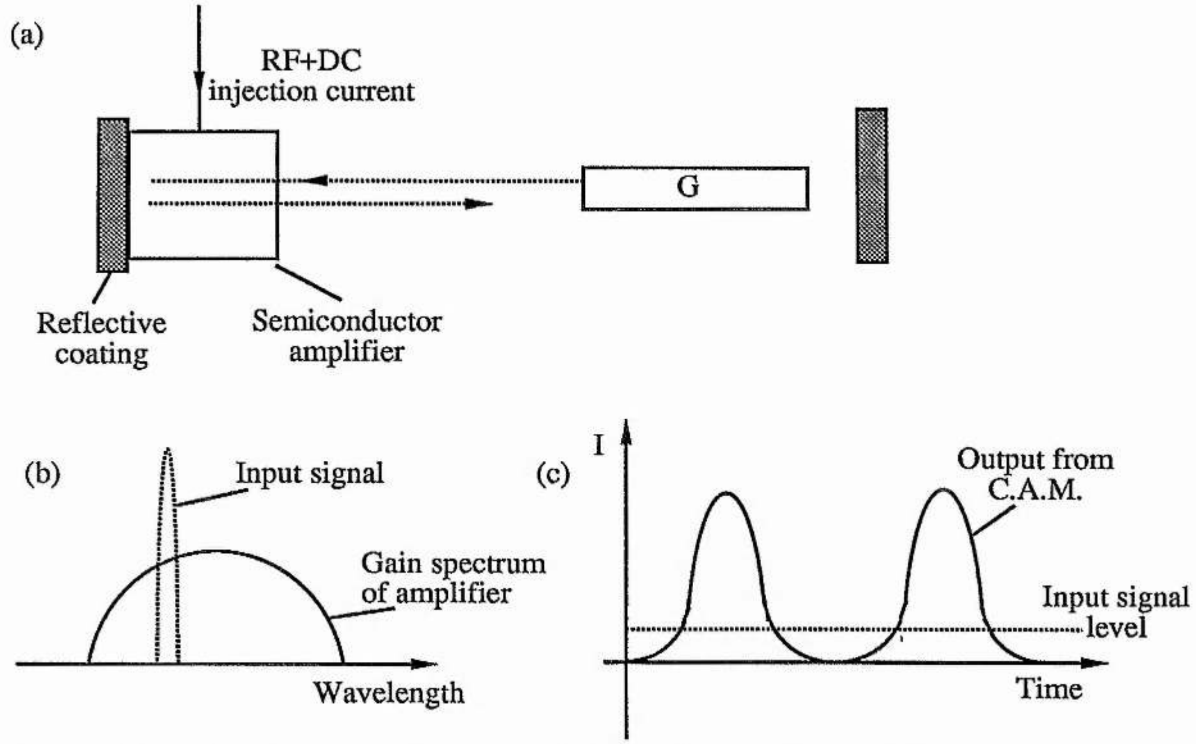

Figure 7.2 (a) A laser incorporating a controlled amplifier modulator. (b) The gain spectrum of the amplifier is selected to encompass the laser transition of the gain medium. (c) Modulated laser output through control of the modulator bias currents.

On increasing the DC bias applied to the amplifier the signal from the laser medium is amplified and retroreflected by the cavity reflector. At some DC bias level the amplifier gain is such that the cavity loss is reduced to a value at which laser oscillation can be established. In this manner the output from the laser is determined by the gain (and hence the bias level) of the semiconductor amplifier. Thus this amplifier configuration can be thought of as a complex mirror whose reflectivity is dependent upon the gain present in the amplifier. Therefore if a modulation signal is applied to the C.A.M. device at a frequency which is made equal to the laser cavity-mode separation then a modelocked pulse train will be produced. In the following sections the properties of such modulators will be examined under various operating parameters.

## 7.2 Operating characteristics of an InGaAsP modulator.

### 7.2.1. Direct current drive

The configuration as reproduced schematically in figure 7.3 was constructed to investigate the properties of the semiconductor amplifier under various current pumping schemes. The input signal source used was a ridge waveguide InGaAsP DFB laser[181] operating on a single-longitudinal mode at 1508nm. Drawn tapered fibre microlenses were employed for optical coupling to the semiconductor amplifier. The amplifier was an InGaAsP ridge waveguide device with the active region oriented at 7° to the facet normal in order to suppress the internal Fabry-Perot resonances. Both facets of the amplifier were coated with an $Al_2O_3$ anti-reflection coating to reduce the incident reflection loss to ~1%.

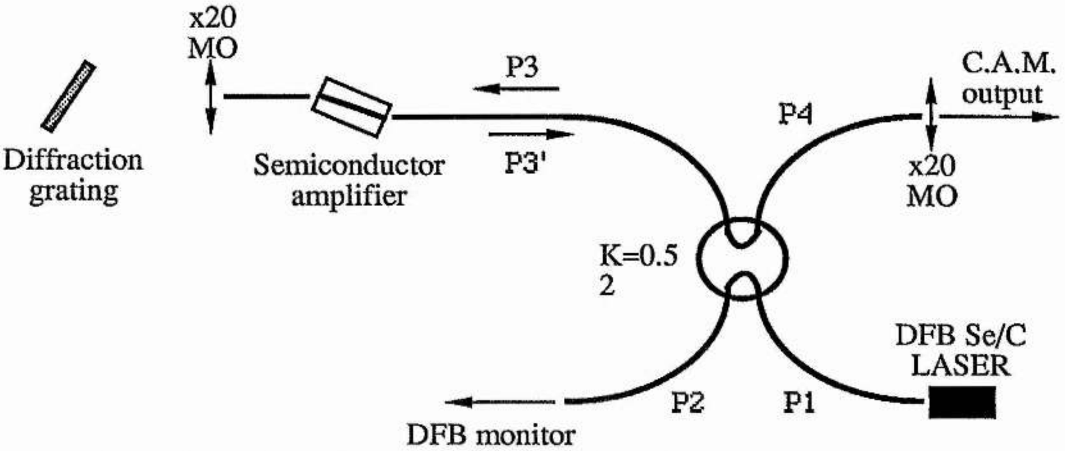

Figure 7.3 Experimental configuration of modulating scheme.

The diffraction grating used as a retroreflector limited the system amplification bandwidth to ~1nm. However, angular adjustment of the grating allowed tuning over the whole gain bandwidth of the InGaAsP amplifier. A broadband device could be constructed by using a high reflectivity mirror as the retroreflector, or alternatively the cleaved facet of a single facet reflectivity suppressed laser chip could be used. The latter device is particularly simple and interesting in view of its negligible modulation frequency sensitivity.

### 7.2.2. CW performance

The compound mirror reflection coefficient R(I) can be found from knowledge of the signal power levels at the two available monitor ports, 2 and 4 (as labelled in figure 7.3). The signal levels in any arm of the input directional coupler can then be deduced using the following set of relationships;

$$P_2 = (1-K)\,P_1$$
$$P_3 = K\,P_1$$
$$P_{3'} = R(I)\,K\,P_1$$
$$P_4 = (1-K)\,R(I)\,K\,P_1$$

K is the cross-coupling coefficient of the directional coupler, and was measured to be 0.52 at

1508nm. Since $P_2$, and $P_4$ are also measurable quantities the reflectivity function of the composite mirror can be evaluated experimentally by applying the relation,

$$R(I) = 1.92\, P_4 / P_2$$

The function R(I) was measured for various amplifier bias current levels and the corresponding data are included in figure 7.4. [The contribution to the output signal from spontaneous emission of the amplifier was also taken into account to ensure meaningful results.] The versatility of the device in terms of output signal level is evident, ranging from gains of ~15dB to very large input signal rejection levels, all possible over a modest current span. It should be possible to increase the peak gain value on optimisation of the device parameters, namely by using high-saturation, high-gain amplifiers[146], and by decreasing the retroreflection losses.

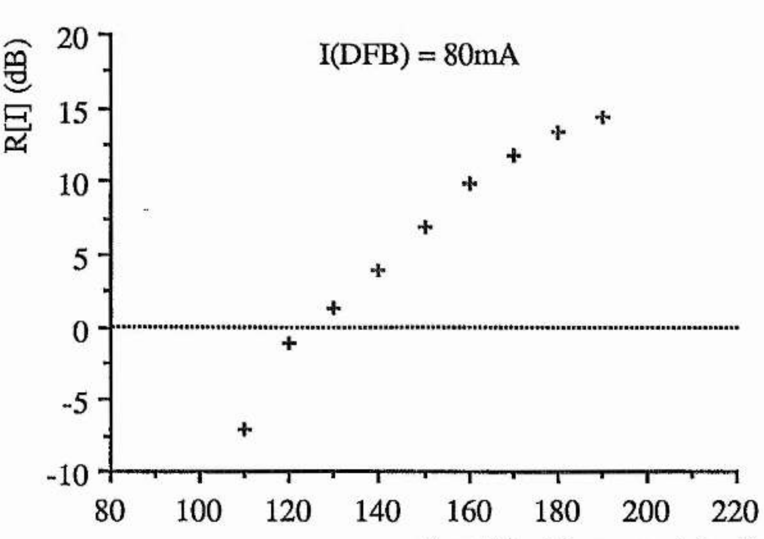

Figure 7.4 Effective reflectivity at 1508nm of composite mirror.

If amplifier saturation can be neglected the current-dependent reflection function may also be expressed as;

$$R(I) = 2G + L_g$$

where G is the single-pass fibre-to-fibre gain of the amplifier, and $L_g$ is the lumped value of the extended-cavity losses. From measurements of single-pass gain (see figure 7.5) an average value of ~4.5dB (~64%) was found for $L_g$. This value is quite high and is perhaps due to poor coupling back into the fibre pigtail on retroreflection from the grating. Also, the presence of two counter-propagating signals passing through the amplifier will lead to a reduction of the input signal level for the onset of gain saturation. This suggests that at the power levels used here negligible gain saturation cannot be assumed. However, a more realistic upper bound on the loss factor can be obtained when the effects of self emission saturation due to the homogeneous nature of the amplifier gain are considered.

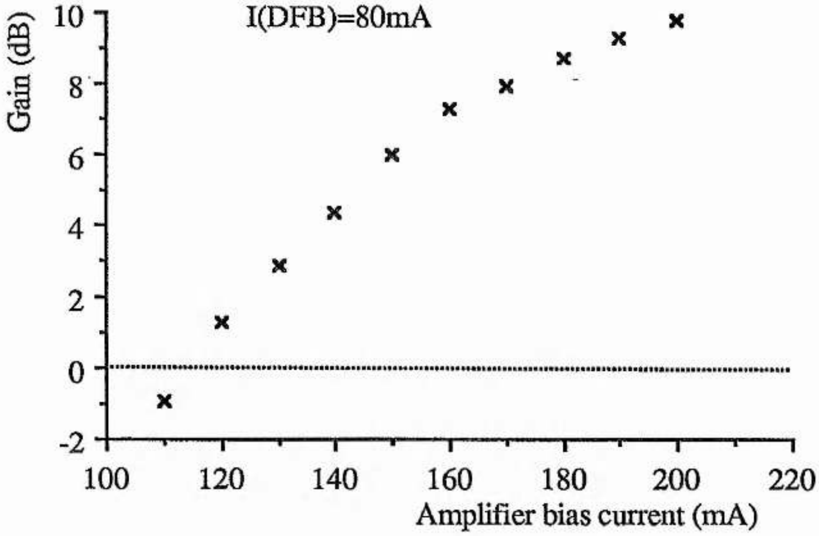

Figure 7.5 Single-pass fibre-to-fibre gain characteristic at 1508nm of $7^o$-angled amplifier

From figure 7.6 it is evident that the fluorescent output of the device is substantially reduced by the presence of the input DFB signal where the degree of self-emission saturation in this particular case is ~1/2. Because a constant self-emission had been assumed for the calculation of gain, so a knowledge of the degree of saturation is required for a more accurate calculation. The self-emission saturation is homogeneous and so the curve of figure 7.7 was obtained by monitoring the spectral intensity in a narrow wavelength band centred on 1520nm with and without the presence of the input DFB laser signal. From these measurements the R(I) values obtained from figure 7.4 were found to be underestimated by 1-1.6dB thus implying a more realistic value of around 3dB for $L_g$.

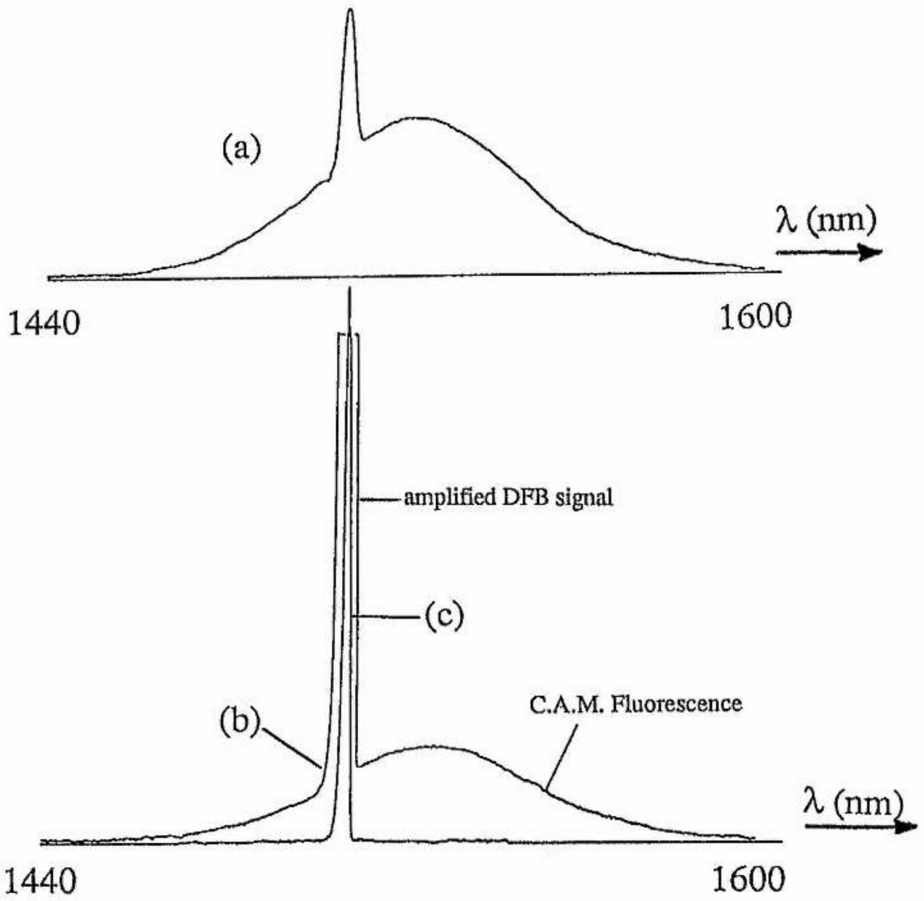

Figure 7.6 Spectral output of device for (a) no DFB signal present, and (b) with the input signal, where the current applied to the amplifier was 150mA. The vertical axes are the same for these two spectra. The spectrum (c) is the same as (b) but with the vertical scale changed.

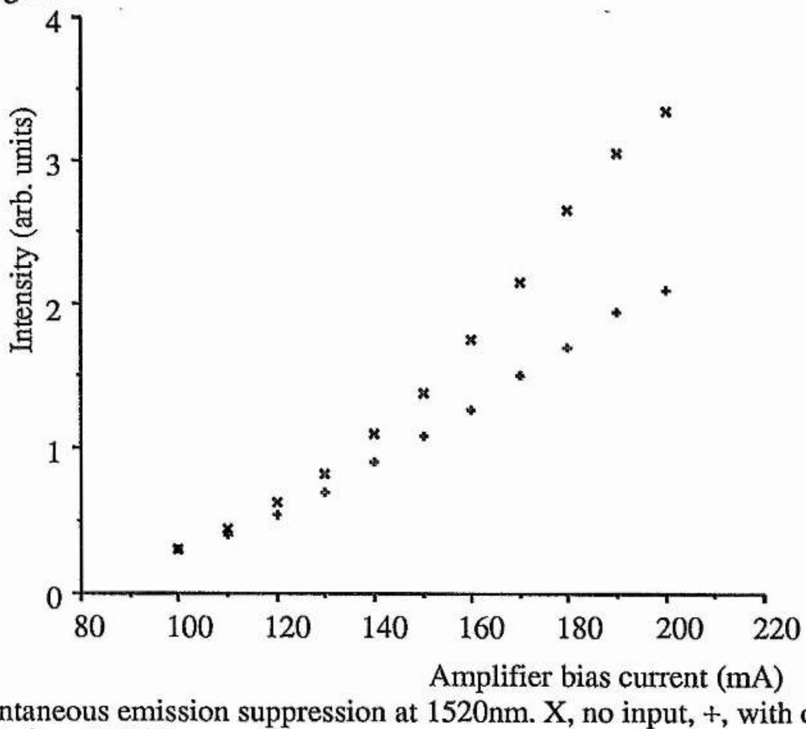

Figure 7.7 Spontaneous emission suppression at 1520nm. X, no input, +, with optical input from DFB laser.

### 7.2.3. Modulated drive current

It is apparent from figure 7.4 that this semiconductor modulator configuration should have desirable features when used in the intended mode of operation involving modulated drive current conditions. In this section the modulation characteristics will be outlined for the same experimental configuration as that discussed previously. The drive electronics were arranged to allow a combination of RF and DC bias current signals to be supplied to the amplifier.

The output signal from port 4 was focussed onto an InGaAs PIN photodiode from which the output was fed to a sampling oscilloscope arrangement to allow examination of the output optical waveform. The modulation frequency was chosen to be harmonically related to the reciprocal transit time of the extended resonator arrangement. Hence modulation frequencies of 312, 624, and 948MHz were used which related directly to the 0.48m external-cavity length. Deviations from the above criterion results in the retroreflected signal experiencing different gain conditions from the input signal and so significant attenuation and waveform distortion can take place. This is an obvious disadvantage of this form of extended modulator design but can be alleviated by using different configurations (as is demonstrated in sections 9.4 and 9.5).

### 7.2.4. Modulation performance

The output signal waveforms were recorded under various drive signal combinations (see figure 7.8). With small RF signal levels the output resembles that of the injection signal. On increasing the RF component of the drive signal the output becomes more intense and temporally narrowed, eventually resulting in a pulse-like output with strong RF pumping. It can thus be observed that on a single-pass the device is capable of amplifying and gating to <200ps an initially CW input signal (see figure 7.9).

By using low DC current levels coupled with large RF signal powers the output waveform duration is minimised, and this feature will result in fast ultrashort pulse build-up times when used in a mode-locked laser configuration. In figure 7.10 a sequence of oscillograms of the device output recorded for increasing modulation frequency is reproduced. The drive signals were arranged such that the peak intensities were roughly equal in all cases. It can be seen that (apart from a somewhat noisy region on the trailing edge of the 312MHz waveform) the

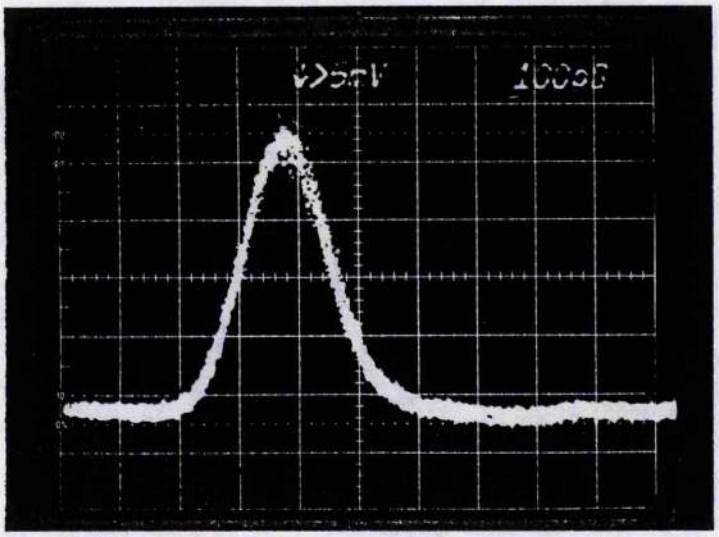

Figure 7.9 Gain window of C.A.M. device at 624MHz.

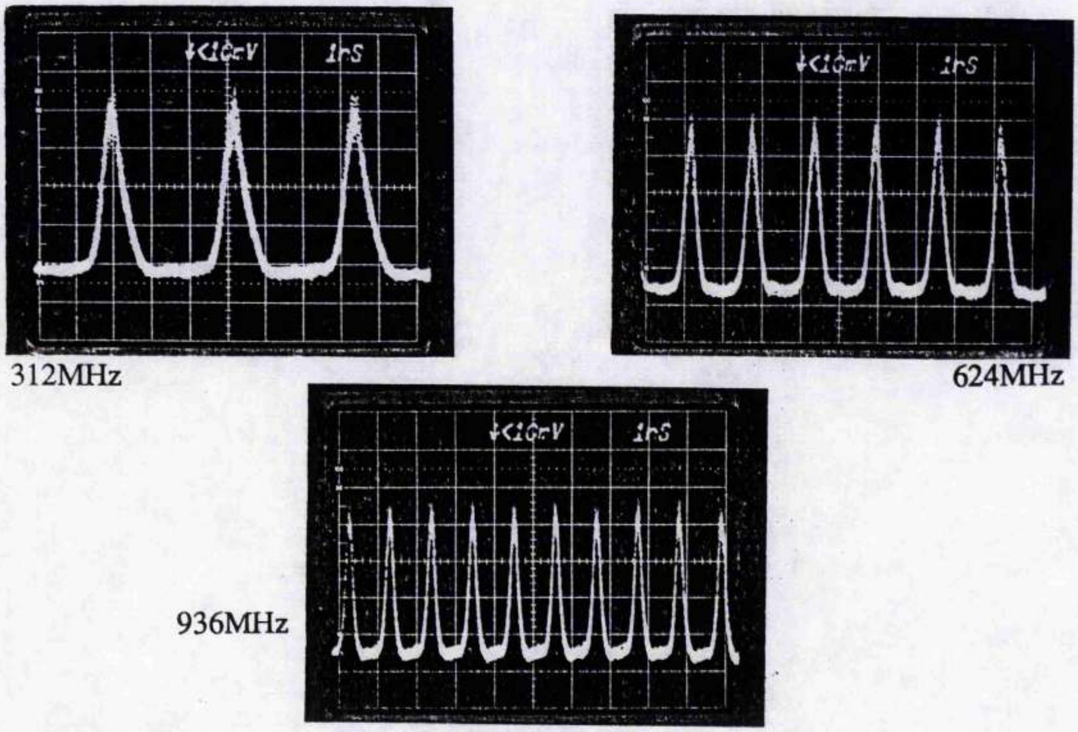

312MHz

624MHz

936MHz

Figure 7.10 Modulation responses at 312, 624, and 936MHz.

The response of the device was recorded with increasing launched power from the DFB laser, and a plot of peak output intensity of the resultant modulated waveform is shown in figure 7.11. For these measurements the modulation frequency was 624MHz and the amplifier was biased at 150mA with an applied signal power from the signal generator of -1dBm. It can be seen that the peak intensity saturates with increasing input optical signal power. The details of this response will be dependent on amplifier properties such as the gain levels present at the signal wavelength and the saturation output power level. Optimisation of this characteristic should lead to higher output powers from controlled amplifier modelocked lasers but this was not attempted in this phase of the work.

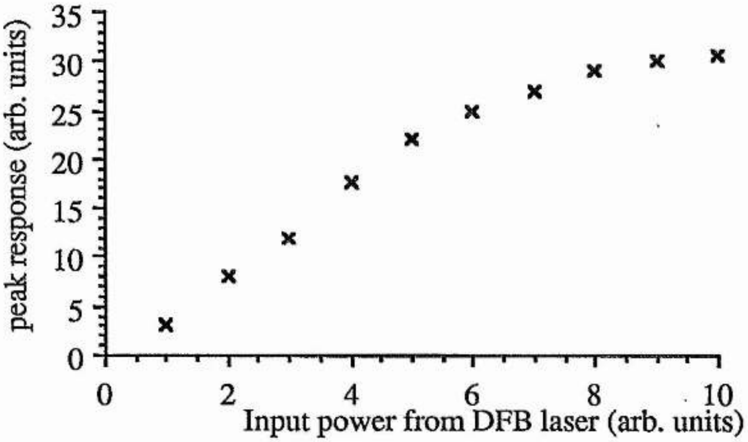

Figure 7.11 Peak intensity of output waveform versus input optical power.

## 7.3 Summary

The modulator described here is based on a semiconductor amplifier which essentially transforms a slow sinusoidal modulation signal into a fast pulsed response. This is advantageous since the electronic drive circuitry and matching networks can be simplified. Also, for modelocked lasers the system performance could be likened to that achieved with the synchronous pumping technique[182] and hence the deleterious features normally associated with sinusoidal modulation can be avoided. Moreover, the low input signal power for the onset of the nonlinear response to input optical power should aid mode-locked pulse production in low average power systems such as fibre lasers. Schemes have been devised for the application of the C.A.M. technique to high power laser systems and these will be addressed in a subsequent chapter.

# CHAPTER 8

# RARE EARTH, DOPED FIBRE LASERS

## 8.1 Introduction

A laser type that is receiving an increasing amount of scientific and technological interest is that which uses doped-optical fibres as the gain medium[183]. In general the active medium is a single-mode silica optical fibre with a rare-earth element dopant introduced into the fibre core region[184] during fibre preform production. Various resonator configurations from simple butted mirror Fabry-Perot cavities[185] to more complex wavelength tunable cavities[186] and ring resonators have been constructed using the doped-fibre active medium. In this chapter a review of the status of CW fibre lasers will be given with particular emphasis being placed on high-power laser configurations. In chapter 9 the modelocking of fibre lasers will be described where integrated semiconductor modulators have been employed to achieve high peak power ultrashort pulses.

The first reported fibre lasers utilised the commonplace neodymium ion dopant resulting in laser oscillation at ~1.07μm and the 3 level 940nm transition. Oscillation at 1.32μm is not possible in doped silica-fibre lasers unlike in, for example, YAG host crystals. This has been identified as being due to signal excited-state-absorption[186] (ESA) and has partly been overcome by using a fluorozirconate fibre host[187]. Other examples of doped-fibre lasers include erbium at 1.5μm[188] and 2.7μm[189], samarium emitting in the red[190], thulium[191], holmium[192] and ytterbium[193]. By far the most interesting with respect to optical fibre telecommunications applications is the erbium dopant with associated laser emission 1.53μm. Advances in production techniques[194] combined with investigations into operational parameters, such as optimal pumping wavelengths[172], has enabled researchers to produce a wide variety of efficient high-gain amplifiers and laser devices using erbium-doped fibres.

The energy level diagram of the trivalent erbium ion is shown in figure 8.1 (see also figure 5.9 in chapter 5). Laser action is possible on the $^4I_{13/2}$ to $^4I_{15/2}$ transition in the silica-fibre host. [Oscillation at 2.7-2.8μm on the $^4I_{13/2}$ to $^4I_{11/2}$ transition has been demonstrated[189] for erbium in a fluorozirconate fibre host, and thus should be applicable in the important field of medical lasers. Also, oscillation at 850 and 1µm have been observed from these lasers[195].]

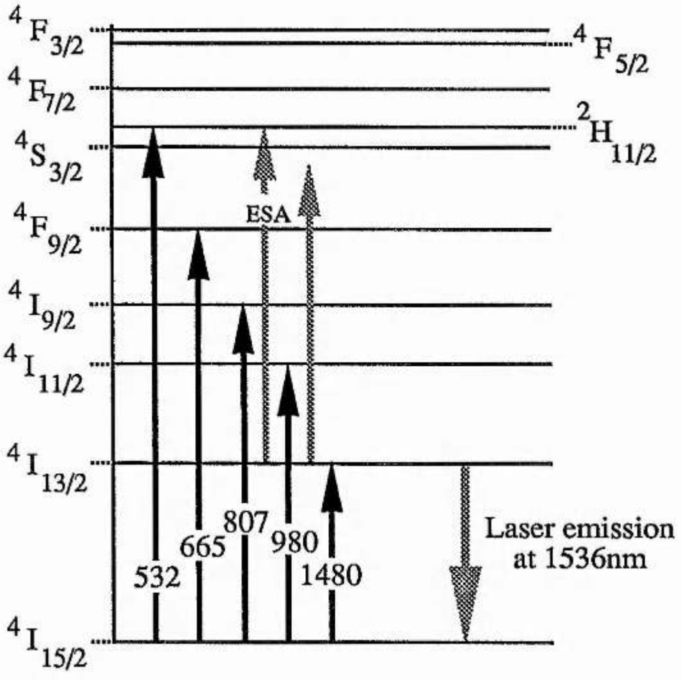

Figure 8.1 Energy level diagram for the trivalent erbium ion.

Whereas many radiative transitions occur in bulk $Er^{3+}$:glass/crystal media[196], the absence of these in the fibre host indicate the existence of preferential non-radiative decay channels which ultimately populate the $^4I_{13/2}$ upper laser level[161]. The laser transition terminates on the $^4I_{15/2}$ ground state of the erbium ion, and so the erbium-doped fibre laser is essentially a three-level system. Due to the low intrinsic loss in the 1.5µm spectral region[22] long interaction lengths are possible. Also, the optical fields are effectively confined to the small core region of the fibre waveguide which allows efficient overlap between the laser signal and the inverted population. Therefore the three-level nature of the system does not inhibit low threshold, CW laser oscillation as in its bulk counterparts. In fact, the peculiarities of the fibre waveguide geometry make it an ideal host for the incorporation of three-level laser active species. For the erbium-doped fibre laser threshold can be achieved at milliwatt absorbed pump powers in suitably optimised cavity configurations[185].

Studies of the absorption and emission spectra of the laser transition have suggested that the upper laser manifold is composed of four Stark components with 5-6 such components in the ground state[197]. The energy and extent of each Stark level is varied and leads to the essentially smooth, broad, double-peaked emission spectrum which is characteristic of erbium-doped fibres. Variations in the overall shape of the emission spectrum can be produced by altering the fibre codopants. For example, alumina-codoped fibre[198] has a smoother spectrum without the marked dip between the peaks associated with germania/erbium fibres (see Appendix A). Consequently, broadband tunable oscillation should be obtainable from erbium-doped fibre lasers, and in fact greater than 60nm has previously been demonstrated[199]. The fibre length is also very important in defining the laser tuning characteristics since the laser is three-level and significant reabsorption can take place when over-long fibres are used. The peculiarities of the tuning characteristics of erbium fibre lasers, and in particular length tuning will be addressed in sections 8.6 and 8.7.

## 8.2 Low finesse doped fibre lasers

A technologically interesting feature of fibre lasers is that laser oscillation is possible without the usual requirement of high reflectivity cavity mirrors. This is possible due to the extremely high gains that can be achieved in such laser media using only modest pump powers[167]. The general cavity configuration employed for such low finesse fibre lasers is shown schematically in the figure 8.2(A) where the cleaved fibre end exhibits a Fresnel reflectivity of ~4% (-14dB) and acts as the output coupling cavity mirror. This cavity loss mainly determines the gain required for laser oscillation since the other cavity losses will normally not exceed 50% (-3dB). To introduce spectral control of the laser output a tuning element can be placed between the collimating objective and the back cavity mirror. Alternatively the mirror can be replaced by a diffraction grating oriented in autocollimation (figure 8.2(B)), where a standard anti-reflection coated microscope objective is used to collimate the beam into the grating-loaded cavity section. The objective normally used has a focal length of 14.5mm (working distance of 6.7mm) because the numerical aperture closely matches that of the fibre. With this lens there is appreciable space between the fibre and the objective such that angled index-matching cells can be used to suppress spurious fibre end reflections. Pumping and output coupling are usually achieved by using a dichroic mirror, but this could be readily substituted by a multiplexing fibre directional coupler to give the system extra flexibility (as shown in figure 8.2(C)).

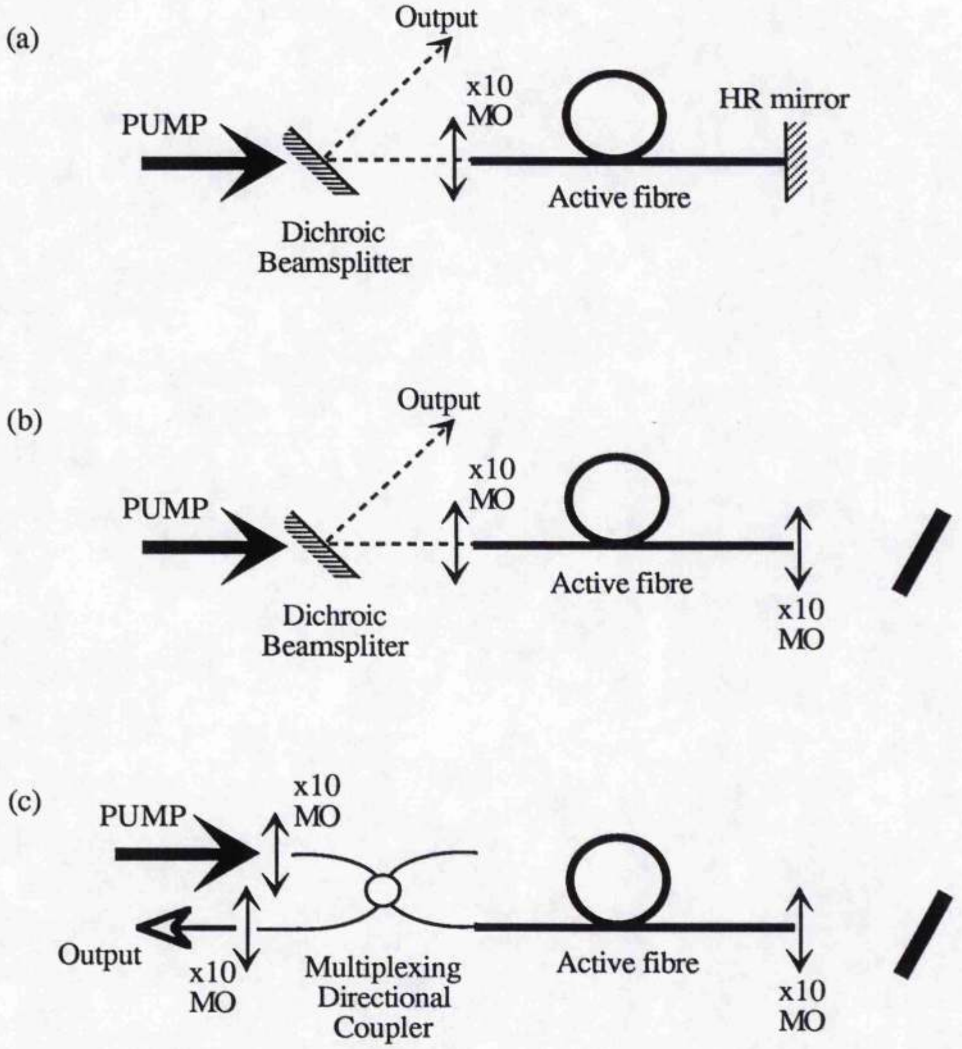

Figure 8.2 Low finesse fibre lasers; (A) standard cavity, (B) grating tunable cavity, and (C) a configuration using fibre multiplexor for input and output coupling

For these high-gain laser configurations the analysis developed by Rigrod[200] can be applied to reveal some very interesting features. A derivation of the efficiency of high-gain lasers following that of Rigrod will now be outlined.

## 8.3 Rigrod analysis of high-gain lasers

The analysis presented here is pertinent to the Fabry-Perot laser resonator configuration depicted in figure 8.3. However, the same technique can be applied to more complex cavities and also any specific features of, say, the gain medium used can be included. The simple arrangement that will be considered allows the most general results relevant to the laser configurations of figure 8.2 to be obtained.

Let $I_+(z)$ and $I_-(z)$ describe the intensities travelling to and from mirror $R_2$ of the laser respectively (see figure 8.3). These intensities grow with distance as;

$$\frac{dI_+(z)}{dz} = +2a_m(z)\, I_+(z) \qquad \text{........(8.1)}$$

$$\frac{dI_-(z)}{dz} = -2a_m(z)\, I_-(z) \qquad \text{.......(8.2)}$$

where $a_m$ is the gain coefficient.

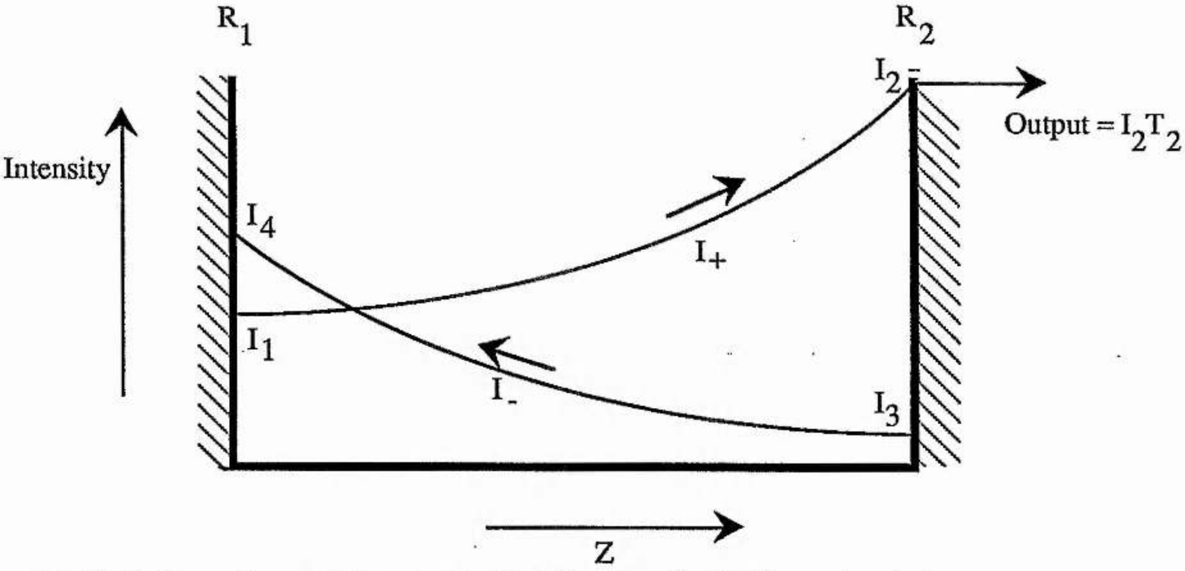

Figure 8.3. Definition of parameters used in the Rigrod analysis. The region between the cavity mirrors is assumed to contain a uniform gain medium.

For simplicity $I_+$ and $I_-$ are normalised to the saturation intensity of the medium. The gain coefficient $a_m(z)$ at any plane (z) then saturates according to the total intensity at that plane according to,

$$a_m(z) = \frac{a_{mo}}{1 + I_+(z) + I_-(z)} \qquad \text{........(3)}$$

where $a_{mo}$ is the small signal, unsaturated gain coefficient. On combining equations (1) and (2) the product of the intensities in the two directions at any plane can be found to be constant;

$$\frac{d}{dz}\{I_+(z)\, I_-(z)\} = I_+ . \frac{dI_-}{dz} + I_- . \frac{dI_+}{dz} = -2a_m I_+I_- + 2a_m I_+I_- = 0$$

So at any plane along the laser axis,

$$I_+(z)\, I_-(z) = \text{constant} = C.$$

Therefore the differential equation for $I_+(z)$ can be expressed as,

$$\frac{dI_+(z)}{dz} = \frac{2a_{mo}\, I_+(z)}{1 + I_+(z) + \frac{C}{I_+(z)}}$$

This can now be integrated over the length of the laser medium,

$$\int_{I_1}^{I_2} \{ 1 + \frac{1}{I_+} + \frac{C}{{I_+}^2} \}\, dI_+ = 2a_{mo} \int_0^L dz$$

The same procedure can be applied to the $I_-(z)$ wave, and the two equations can then be solved to give the expressions;

$$2a_{mo}L = \ln\{\frac{I_2}{I_1}\} + I_2 - I_1 - C\{\frac{1}{I_2} - \frac{1}{I_1}\}$$

$$2a_{mo}L = \ln\{\frac{I_4}{I_3}\} + I_4 - I_3 - C\{\frac{1}{I_4} - \frac{1}{I_3}\}$$

In addition, there are the boundary conditions that $I_1 = R_1I_4$, and $I_3 = R_2I_2$, and also the two product relations at the end surfaces, namely that $I_1I_4 = I_2I_3 = C$. On combining these relations an expression for $I_2$ can be obtained which is a simple function of the mirror reflectivities and the small signal gain coefficient;

$$I_2 = \frac{1}{\{(1+\frac{r_2}{r_1})(1-r_1r_2)\}} [\, 2a_{mo}L - \ln(\frac{1}{r_1r_2})]$$

where $r_1 = \sqrt{R_1}$ and $r_2 = \sqrt{R_2}$. Then useful output intensity from the laser is,

$$I_{out} = T_2I_2 = \frac{T_2I_{sat}}{(1+\frac{r_2}{r_1})(1-r_1r_2)} [\, \ln G_0 - \ln(\frac{1}{r_1r_2})]$$

where $G_0$ is the small signal gain. The maximum intensity that can be extracted from such a laser medium is,

$$I_{avail} = 2a_{mo}L_mI_{sat} = (\ln G_0)I_{sat}$$

and hence the power extraction efficiency or normalised output intensity can then be found to be;

$$\eta = \frac{I_{out}}{I_{avail}} = \frac{T_2}{(1+\frac{r_2}{r_1})(1-r_1r_2)} [\, 1 + \frac{\ln(r_1r_2)}{\ln G_0}]$$

The internal losses could be included in the differential equations for the laser but this would create difficulties with the integration and would in any case not significantly alter the end result. The general effects of small distributed losses in the cavity are thus best assessed by assuming them to be incorporated as part of the mirror reflectivity $R_1$.

The particular features of such lasers can now be discussed on examination of plots of the power extraction efficiency versus output coupler reflectivity (see figure 8.4). A few simple observations can be made from these graphs. For instance, the trend towards larger output coupling required for output power optimisation with increasing single-pass unsaturated gain is obvious (figure 8.4(a)). Secondly, for any gain level and output coupling value the output power is maximised by using a higher reflectivity mirror $R_1$ (as shown in the figure 8.4(b) and (c)). This is basically the usual statement that all the cavity losses apart from the output coupling loss should be minimised. Nevertheless, with high output coupling, as the case for 'mirrorless' fibre lasers, the output power becomes a weak function of the internal mirror reflectivity.

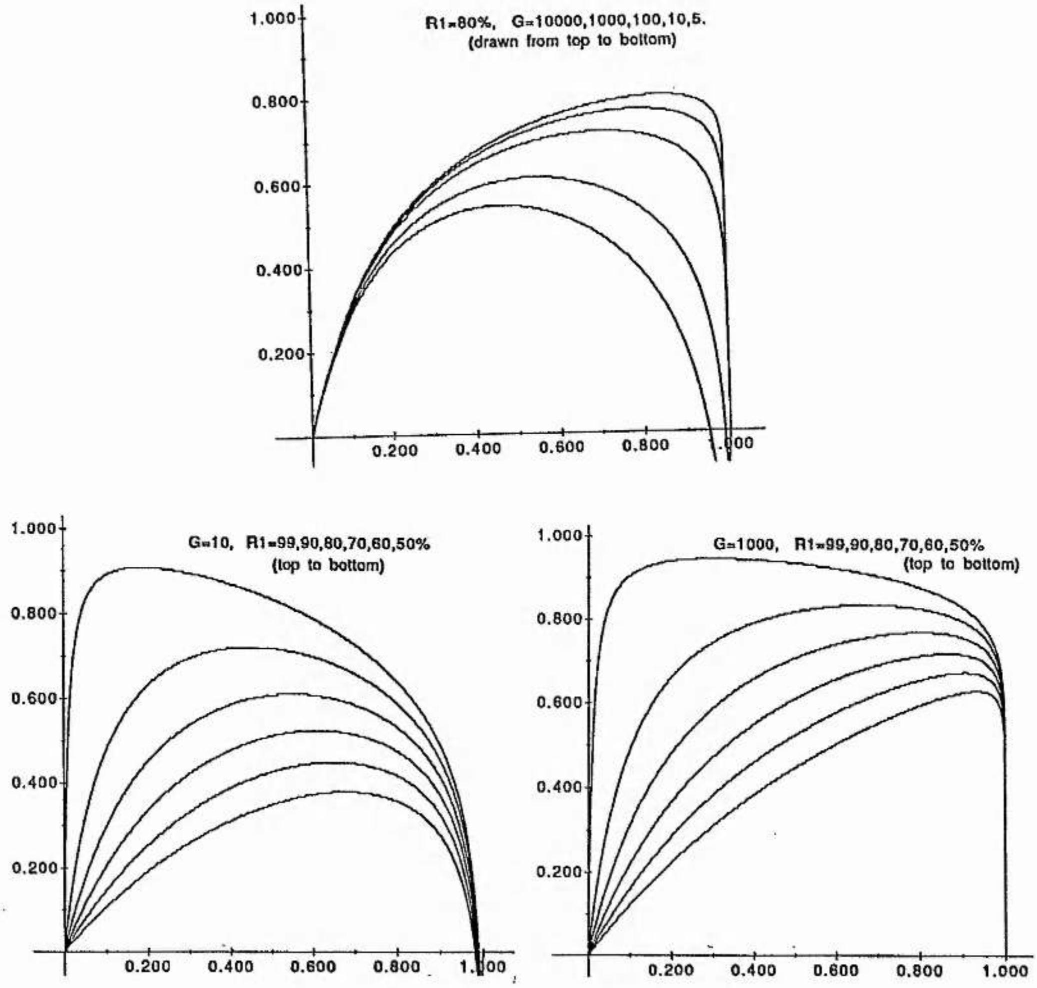

Figure 8.4 Extraction efficiency versus output coupler transmission for various combinations of unsaturated single-pass gain values and internal mirror reflectivities.

In general it can be seen that with higher values of unsaturated gain then the optimum output power occurs for low rather than for high values of output coupler reflectivity. Another feature of high-gain lasers is that the higher the unsaturated single-pass gain the less critical the output power is with respect to the output coupler reflectivity. For example for the case shown in figure 8.4(c), assuming $R_1$=90% then the difference in output power resulting between a 4% and the optimum ~37% reflectivity is less than 10%. This is fortunate since it is far easier in practice to utilise the Fresnel reflectivity of a cleaved fibre end as the fibre laser mirror than to a use butted, bulk dielectric mirror, or to directly apply a coating onto the fibre end. Furthermore, the use of a dielectric mirror as an output coupler will only result in the introduction of extra cavity loss. Such dielectric coatings can also be cumbersome and prone to damage at the high power densities normally encountered.

## 8.4 High-power, neodymium-doped fibre lasers

As a representative example of a low-finesse, high-gain, fibre laser the configuration of figure 8.2(b) was employed with an active fibre doped with neodymium. The fibre had the following characteristics; Nd concentration=300ppm, core diameter=5μm, and cutoff wavelength ~1μm. Initially a 90% reflectivity plane mirror was used instead of the diffraction grating. As a test of the previous analysis a variable attenuator was placed between the objective and the mirror which allowed the effective reflectivity of the internal mirror to be varied. The laser output power was then recorded for various effective internal mirror reflectivities (see figure 8.5). Overlaid on the graph is a curve obtained from the Rigrod treatment of such a configuration with a single-pass unsaturated gain of 10000 (40dB). The experimental data were corrected at low values of the internal mirror reflectivity for the attendant (and often large) ASE component and it can be seen the fit is very good. The assumed gain of 40dB is reasonable taking account of the oscillation threshold and the degree of pumping above threshold that was used. Thus it can be concluded that the high-gain, Nd-doped fibre laser behaves according to that expected from the simple Rigrod analysis.

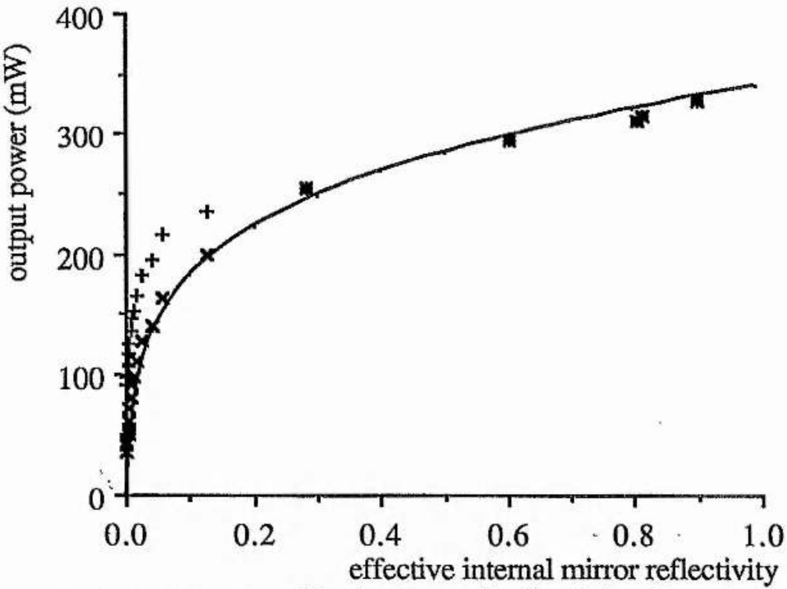

Figure 8.5 Laser output power versus effective internal reflectivity. Experimental points are indicated by +'s. x's indicate ASE corrected values

This provides confirmation that by using the cleaved-fibre end as an output coupler of the laser is a near-optimum cavity configuration. In the sections that follow the characteristics of low-finesse fibre lasers will be detailed. The properties of the neodymium-doped fibre lasers will first be outlined, and this will be followed by the corresponding data for erbium-doped fibre lasers.

## 8.5 High-power, tunable, neodymium-doped fibre lasers

The conversion of pump power into useful Nd-doped laser power is plotted in figure 8.6. The slope efficiency was measured to be 48% by assuming a pump launch efficiency of 65%. The coupling efficiency of 65% was assumed by comparison to those obtained using undoped fibres of similar dimensions. The deviation from the ideal quantum efficiency of 74% is mainly due to the difference in pump and signal mode-field distributions in the active fibre, and also the radiative transitions at 920 and 1320nm serve to reduce this value. There is also some evidence of excited-state absorption processes which lead to emission at shorter wavelengths and this results in a weak 'whitish' sidelight.

The measured fluorescence spectrum obtained from the $Nd^{3+}$:fibre is shown in figure 8.7(a). As expected, the spectrum is much broader than that obtained with $Nd^{3+}$:crystal/glass lasers[201]. The broad gain spectrum suggests that a large tuning range should be possible and to study this tuning range the mirror was replaced by a diffraction grating (see figure 8.2(b). The increased loss introduced by the grating reduced the total output power by ~10%. This reduction is consistent with the earlier Rigrod analysis on inclusion of the ~70% reflectivity of the grating. Finally the tuning range was recorded by rotating the grating about its vertical axis (see figure 8.7(b)).

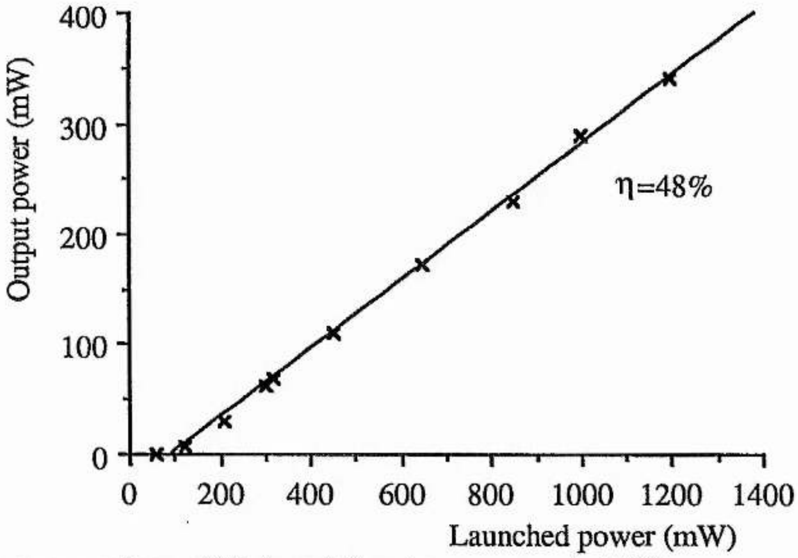

Figure 8.6 Output power from a Nd-doped fibre laser pumped at 810nm

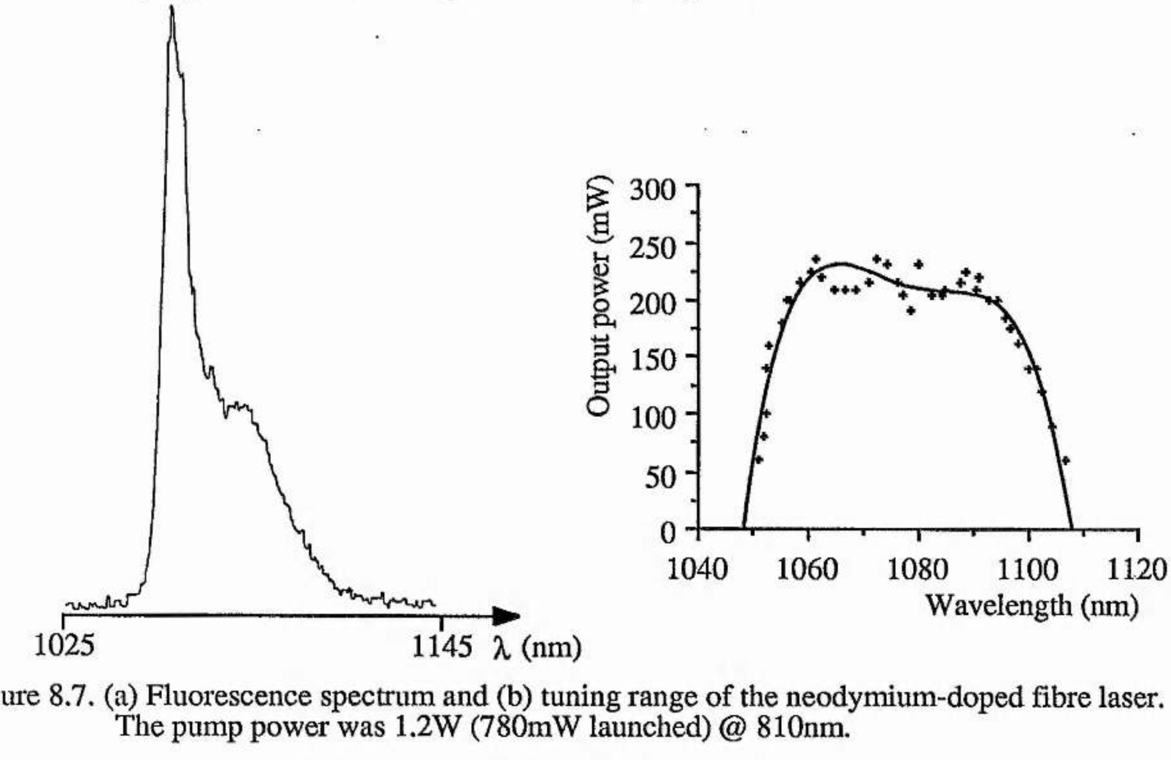

Figure 8.7. (a) Fluorescence spectrum and (b) tuning range of the neodymium-doped fibre laser. The pump power was 1.2W (780mW launched) @ 810nm.

The tuning range is characterised by a rapid increase to high power output at short wavelengths, a broad plateau region, then a gradual decrease in power to longer wavelengths. In total a tuning range of 57nm was obtained. The fluctuations within the plateau region have been identified as originating from the effects of the inherent birefringence of the active fibre[202]. When the grating was blocked significant channelling was observed on the amplified spontaneous emission (ASE) spectrum. On manipulation of the fibre position the internal polarisation state could be altered, and this caused variations in the details of the channelling. Specific manipulation resulted in an unmodulated ASE spectrum, and under these conditions a flat laser tuning curve was obtained. Hence for optimal performance some form of fibre polarisation controller[128] should be included in this type of laser.

An integrated fibre-grating device[90] was also incorporated as the $Nd^{3+}$:fibre laser internal mirror (see section 2.8.2 in chapter 2). The fibre grating had a reflectivity of >90% and a bandwidth of less than 1nm centred on 1080nm. This reflector restored the output power decrease which occurred for the bulk grating, and figure 8.8 summarises the laser output characteristics for all of the Nd:fibre laser cavity configurations considered.

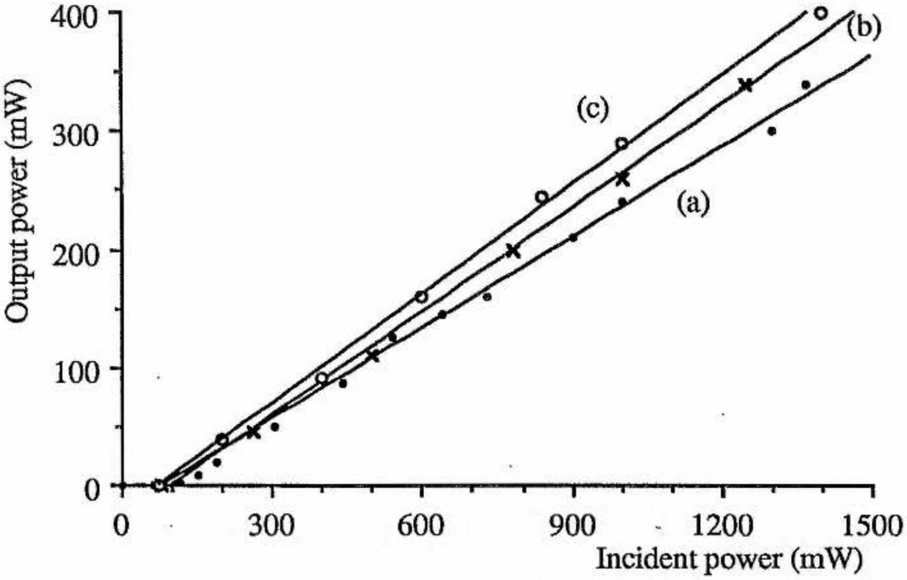

Figure 8.8. Power transfer characteristics $Nd^{3+}$:fibre lasers where the internal reflector was (a) diffraction grating ($\eta_s$=44%), (b) a 90% reflective mirror ($\eta_s$=48%), and (c) an integrated fibre grating ($\eta_s$=51%).

Further experiments were undertaken using a cavity with a highly reflecting internal mirror and a 50m length of doped fibre to maximise pump absorption. The excess unpumped portion of fibre was essentially transparent to the generated laser signal apart from a small additional loss due to intrinsic fibre absorption. This configuration did not significantly alter the laser performance although the increased pumping level of ~2.25W (1.5W launched) enabled an output power of >800mW to be obtained. An interesting feature of this laser was that >100mW output power could be obtained over a pump wavelength tuning range of some 130nm (720-850nm). This range included five obvious peaks with another existing below 720nm. The longest wavelength used (850nm) was due to the optics-related tuning range of the Ti:Sapphire pump laser, and would be expected to increase significantly from examination of the fibre absorption spectrum.

### 8.6 High-power, tunable, erbium-doped fibre lasers.

The high-power $Nd^{3+}$:fibre laser described in section 8.5 is a representative example of a four-level laser system. Now the operational characteristics of similarly configured three-level erbium-doped fibre lasers will be detailed. Again the laser cavity of figure 8.2(b) that afforded frequency tunability was used for high-power operation of the erbium-doped fibre laser. The diffraction grating used in this case had a blaze wavelength of 1.6μm and an efficiency of approximately 80%. The pump light was coupled into the doped fibre using a x10 microscope objective which was anti-reflection coated for the pump wavelength of 980nm. The dichroic mirror used to allow access to the generated laser signal was a highly reflecting mirror at 1.5μm which had a high transmissivity around 1.0μm.

#### 8.6.1 Erbium-doped, germanosilicate fibre lasers

The fibre used initially was of the germanosilicate type[203]. This fibre had a high germania doping in its core for which the radius could be reduced and the numerical aperture increased whilst still maintaining single-mode propagation at the laser wavelength. The values of erbium concentration, core radius, core/cladding refractive index difference (Δn), and numerical aperture of this fibre were $6 \times 10^{18} cm^{-3}$ (300ppm), 2.3μm, $20 \times 10^{-3}$, and 0.24 respectively. These features are desirable for fibre amplifier configurations but not necessarily so for the high-power fibre laser configurations considered here.

The fluorescence spectrum of germanosilicate erbium-doped fibres has two distinct peaks centred on 1536 and 1552nm (see figure A.5). These peaks clearly dominate the laser tuning spectrum (see figure 8.9(a)) for a laser incorporating a 5m length of active fibre used. The tuning range was obtained for a pump power (measured just before the launch objective) of 300mW.

The laser tuning range was continuous and extended from 1528 to 1560nm. The FWHM of the two peaks were 8nm and 15nm respectively. With stronger pumping, tuning to longer wavelengths could be achieved. However, this was limited because of gain saturation due to competition from amplified-spontaneous-emission (ASE). When the laser is tuned to long wavelengths the ASE output at ~1536nm increases and eventually dominates to the extent that further tuning is inhibited. In contrast, the tuning to shorter wavelengths is limited by the large ground state absorption and does not usually extend much below 1530nm.

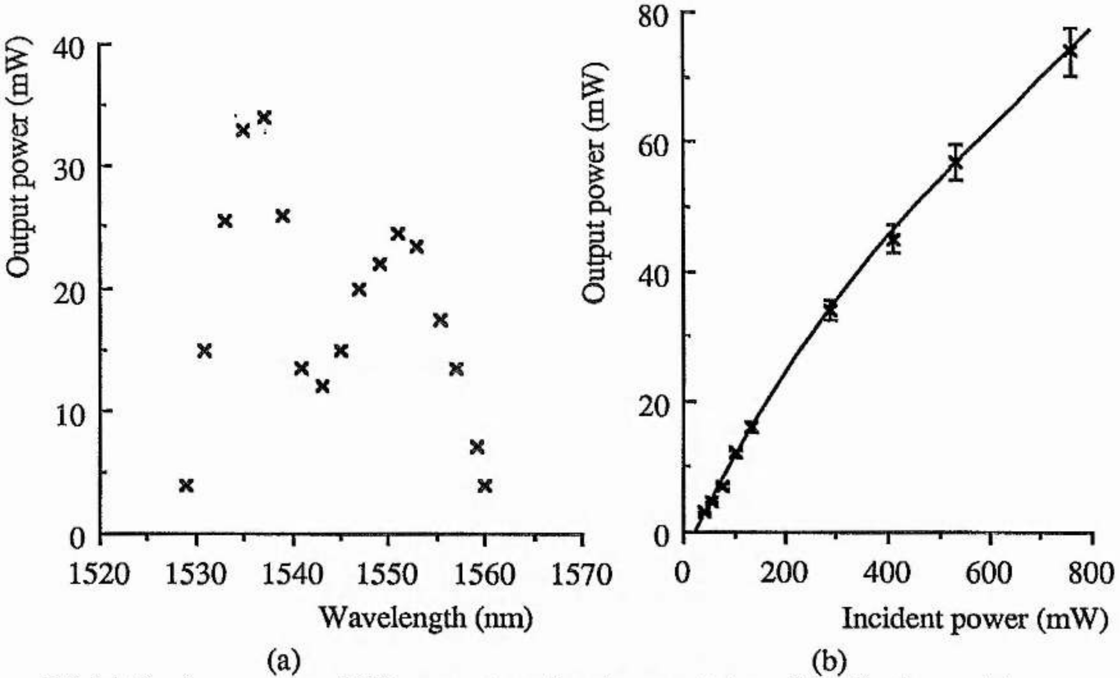

Figure 8.9 (a) Tuning range and (b) power transfer characteristics of the 5m long erbium-doped/germania fibre laser.

Included in figure 8.9 is the fibre laser output power versus pump power characteristic for the same laser. The measured slope efficiency was 22.3% in the low pump power region. The coupling coefficient to the fibre was estimated to be 65%, again by comparison to similar undoped fibres. The slope efficiency quoted here (and in all other cases) is related to the launched pump power and not the absorbed power. This was considered a more practical measure of the laser efficiency in such a three-level laser system. The curve obtained is far from being the expected straight line but is composed of two distinct regions each of which can be accurately fitted to straight lines. This was believed to be due to the changing mode quality of the argon ion laser used to pump the titanium sapphire laser. At low current levels the argon laser beam was in a single transverse mode ($TEM_{00}$) but the mode quality deteriorated markedly at high plasma currents. This affected the Ti:sapphire laser beam quality with a corresponding compromise in the coupling efficiency to the erbium fibre laser.

The maximum output power achieved was 78mW for ~750mW incident pump power. A longer fibre length would have been required to increase pump absorption so that the output power could have been optimised. Due to the small core and the shape of the gain spectrum the potential for high output powers and wide tuning range is limited with this type of fibre-laser design. Therefore attention will now be paid to a system which is capable of dramatic improvements on the results obtained here.

### 8.6.2 Erbium-doped, aluminosilicate fibre lasers

Recently erbium-doped fibres have been fabricated with an alumina codoped core region[204] instead of the more usual germania codoping. The power transfer characteristic for an erbium-doped aluminosilicate fibre laser comprising 5m of active fibre in the grating tuned cavity configuration is shown in the figure 8.10. [The fibre parameters were; erbium concentration=$6\times10^{18}cm^{-3}$ (300ppm), $\Delta n=7\times10^{-3}$, r=4.4μm, mode-field radius 5.3μm.] The slope efficiency was measured to be 32% (for an assumed 85% coupling efficiency), and output powers of up to 300mW for a pump power of ~1W (850mW launched) were readily obtained from this laser. The threshold for laser oscillation occurred for 23mW of incident pump power. The output was very stable and alignment tolerance into the large core fibre was more relaxed. Also the problem of damage to the fibre end which often occurred with small core germania fibres was not observed with the alumino-silicate counterpart even when high power beams of up to 3W were 'walked' across the fibre end. Consequently, with this laser system improvements in efficiency by a factor of ~3 over the previously described system have been described. The primary reason for this is simply that the fibre core cross-section is now larger.

The alumina codoping only influences the system when the laser tuning range is considered. The tuning curve from this laser that is shown in figure 8.12 follows closely the shape of the fluorescence spectrum obtained from the same fibre, and is in marked contrast to that of germania codoped fibres. The tunable output extended from 1512 to 1578nm with an almost flat region from 1528-1563nm.

Because a significant amount of the pump radiation was not absorbed within the fibre the 5m length of active fibre was replaced by a 20m length of identical fibre. With this laser a maximum output power of 700mW (see figure 8.10) was obtained for 1.65W incident pump power (1.4W launched). The slope efficiency increased to 52% and the laser threshold was found to be 43mW. The laser tuning range of the 20m laser is shown in figure 8.11 where an almost flat curve extending over 72nm from 1528 to 1600nm was obtained. The tuning range was now limited at long wavelengths by ASE generated around 1540nm which restricts the gain and inhibits oscillation in this low gain region. Similar effects occur when tuning to shorter wavelengths where higher laser thresholds exist due to the larger ground-state absorption. The whole tuning curve is thus shifted to longer wavelengths and this would continue to do so with further increase in the length of the active fibre.

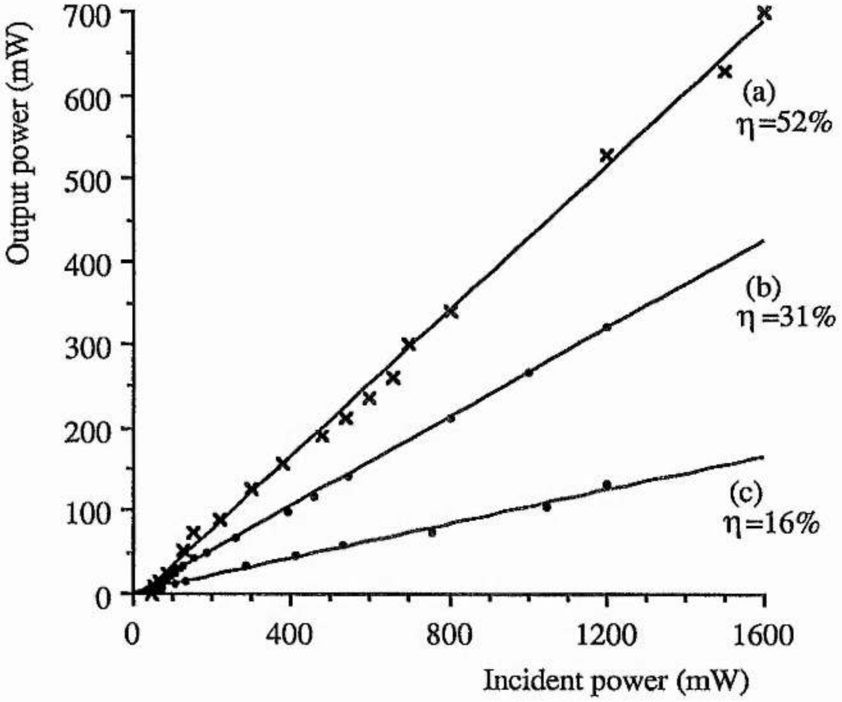

Figure 8.10 Power transfer characteristics for low-doped, high-power, erbium-doped fibre lasers for (a) 20m and (b) 5m aluminosilicate and (c) 5m germanosilicate host fibres.

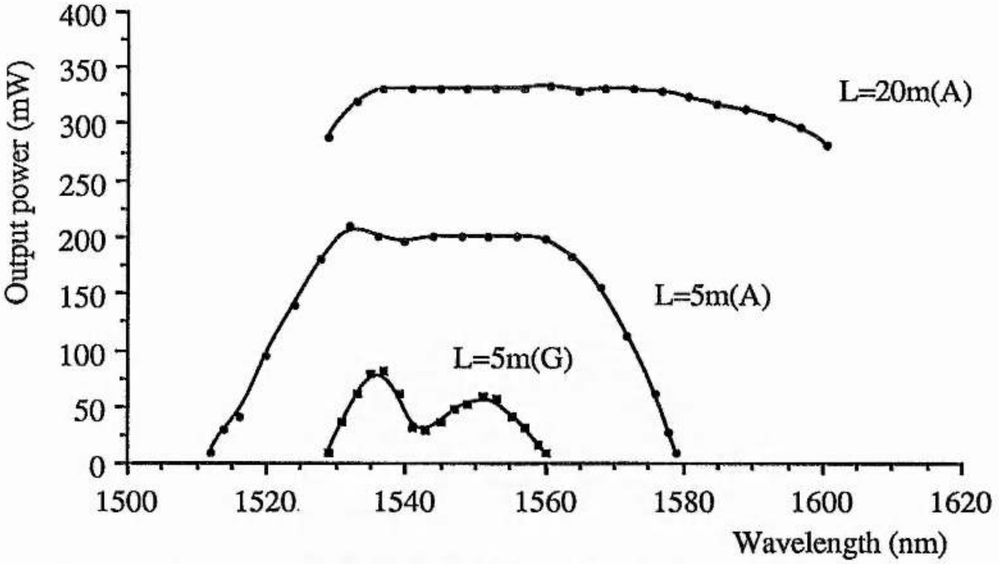

Figure 8.11 Tuning ranges of low doped erbium fibre lasers. A-alumina codoped, G-germania codoped. (Incident power of 800mW in all cases)

It follows from these observations that optimised short wavelength lasers would have short fibre lengths, whereas optimised long wavelength lasers will be long. These characteristics are typical of any three-level laser system which exhibits a spectral shift in its absorption and emission bands. This is because at longer wavelengths the laser behaviour becomes progressively more like that of a four-level system. In this longer wavelength region the gain becomes essentially dependent on absorbed power and not on the fibre length due to the absence of reabsorption within the laser band. This quasi-four-level nature can be accentuated by cooling the laser fibre, for example to 0°C by immersing the fibre in water and then freezing using dry ice (see figure 8.12).

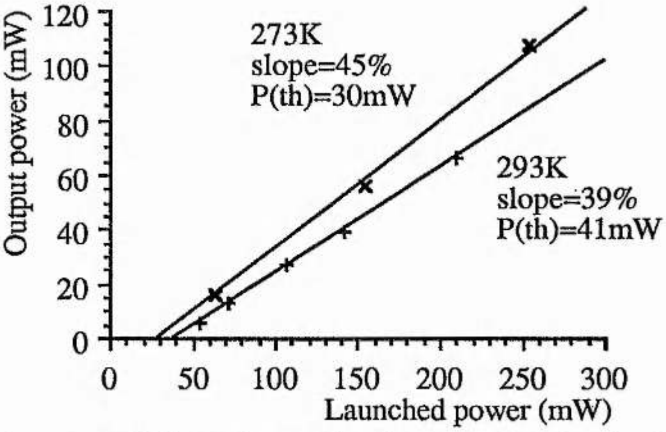

Figure 8.12 Enhanced output efficiency by cooling the quasi-four level erbium:fibre laser.

Although by far the most efficient pump wavelength for erbium-doped fibre devices is 980nm, the pump wavelength around 800nm is also easily accessible using the broadly tunable Ti:sapphire laser system. Therefore, in passing, the power transfer characteristics were recorded for pumping within the 800nm band (see figure 8.13). Despite the severe excited-state-absorption (ESA) problem[205] erbium:fibre lasers are capable of producing output powers in excess of 0.25W around 1.54µm when pumped with up to 2.5W at 810nm. The green sidelight emission that usually accompanies the ESA also becomes quite intense at such high pumping levels.

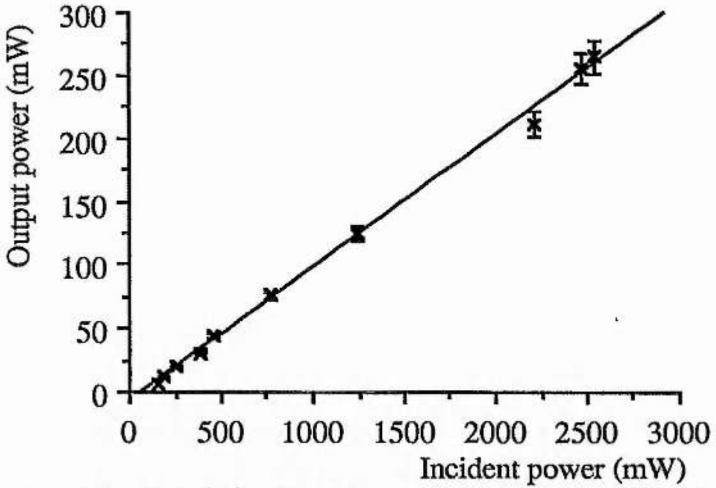

Figure 8.13 Output power characteristic of a 20m erbium:fibre laser pumped at ~810nm

### 8.7 Length tuning of erbium fibre lasers

In an attempt to maximise the tuning range of the erbium fibre laser the technique of 'length-tuning' was employed[206]. The active fibre used in this series of measurements had an erbium dopant concentration of 2500ppm which was approximately eight times larger than that of the fibres used previously. The reason for this was to reduce the total length of laser fibre used. Therefore the longest laser which consisted of 30m of highly-doped fibre corresponds to a 240m length of the previously described low-doped fibre. Thus no difference would be expected in the power transfer and tuning curves of these more heavily doped lasers as compared to their low-doped counterparts (as long as the length-dopant concentration product is constant).

The laser configuration used previously was again employed where the power transfer characteristics and the laser tuning ranges (see figure 8.14 and 8.15) were obtained for lasers incorporating 0.5, 2, and 7.5m lengths of active fibre. Also included in figure 8.15 is the tuning range obtained for a laser with a 30m length of this highly doped erbium fibre where the crosses indicate a region of self-Q-swiching (this will be discussed in section 8.8.3).

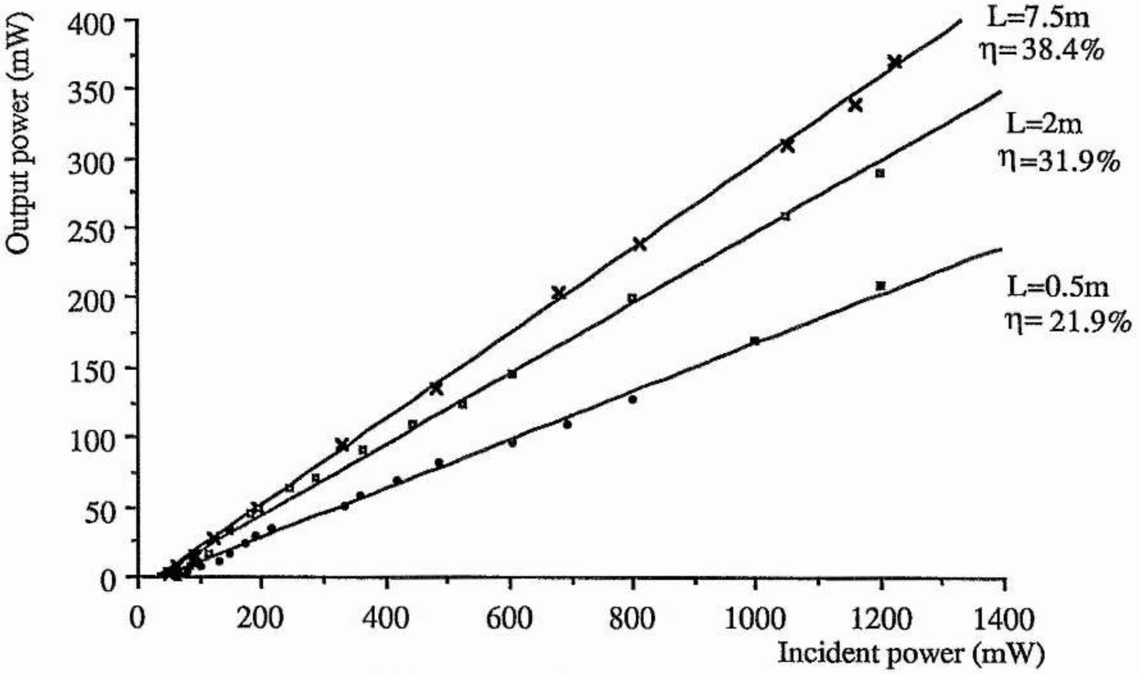

Figure 8.14 Power transfer characteristics for high-doped, erbium fibre lasers. The pump coupling efficiency was ~80% in this case.

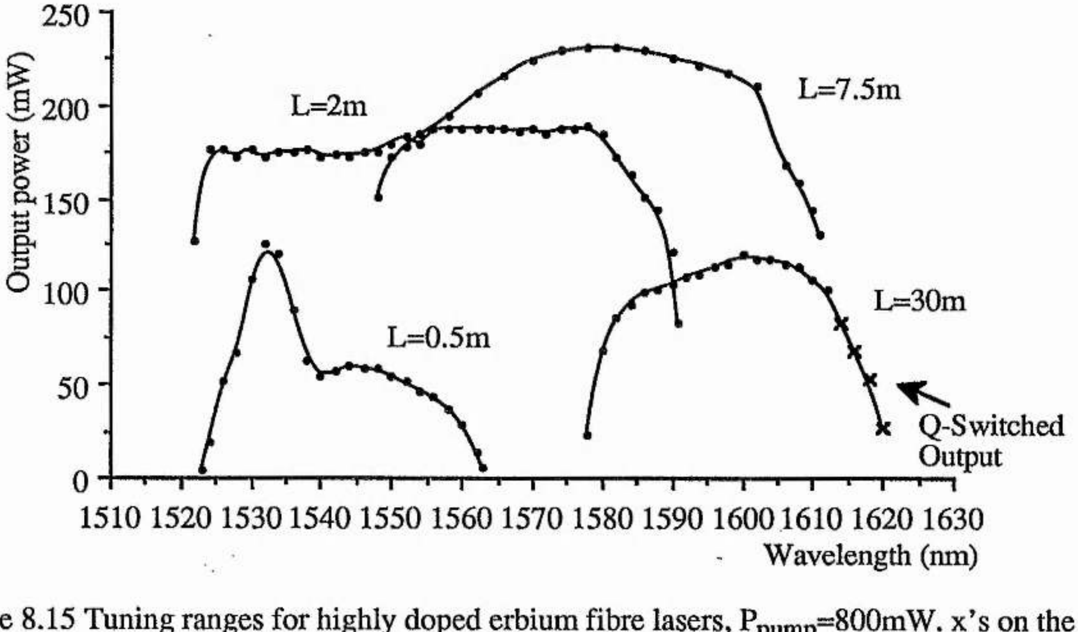

Figure 8.15 Tuning ranges for highly doped erbium fibre lasers, $P_{pump}$=800mW. x's on the 30m curve indicate the region of self Q-switching

On comparison of figure 8.14 with 8.10 it is evident that the lasers incorporating the more heavily doped fibre are only ~70% as efficient as those using the lower dopant concentration. The reason for this is that at high dopant concentrations aggregates of laser active ions are formed during fibre fabrication[207]. Thus an excited ion can exchange energy with a neighbouring ion and this then acts as a non-radiative decay channel for the inverted population. Care must therefore be taken in preparing doped-fibres to ensure a homogeneous distribution of dopant ions. However, the potential tuning range of these fibre lasers is not compromised due to this failing. Indeed a 100nm total tuning range was obtained (see figure 8.15) using only three fibre lengths. The tuning range was ~70nm for the 2m laser, and in excess of 60nm for the 7.5m laser. Furthermore it is interesting to note that the highest output power was obtained around 1580nm. This is because with this particular laser length (7.5m) all the pump radiation is absorbed in the fibre. Also at this wavelength the laser system behaves more like a four-level system and so the unpumped, or lightly pumped section at the end of the fibre does not absorb a significant fraction of the laser radiation. ASE within the high-gain regions at lower wavelengths (<1550nm) does not impose a limit to the long wavelength tuning due to the presence of the large ground-state absorption of the unpumped section of fibre. A clearer understanding of this technique can be gained on examination of the fluorescence spectra of these fibres, and Appendix A is dedicated to a consideration of this topic.

## 8.8 Long erbium-doped fibre lasers

### 8.8.1 Optimal pumping wavelengths for overlong fibres.

The technique of increasing the fibre length such that the laser tuning range can be enhanced leads to a variety of interesting observations all of which have their explanation in the form of the ground state absorption present. Firstly, when oscillation threshold is attained the fibre slope efficiency was essentially constant and independent of the laser wavelength since all the pump power is absorbed, but to minimise the laser threshold it was necessary to tune the pump laser away from the absorption peak at 980nm. For example, for a 30m long laser the minimum threshold occurs at 948nm, some 32nm from the peak of the absorption (see figure 8.16). Since the Ti:sapphire laser could not be tuned above 995nm (due to the available pump power and the bandwidth of the laser optics) the wavelength of the minimum threshold on the long wavelength tail of the absorption could not be established, but it can be assumed that one is present, as is evident for the 7.5m laser.

The shift in the optimum pump wavelength indicates that the laser prefers an inversion to be established over a large portion of its length. Since at the wavelength of peak absorption the pump is extinguished in the first few metres and so the majority of the fibre is unpumped and absorbing at the laser wavelength due to the residual ground-state absorption (GSA). [If the fibre was cooled to eliminate the long wavelength GSA then the above phenomena would not be as apparent]. Therefore a long moderate inversion level is more desirable than a short length high inversion with a long length of significant signal absorption.

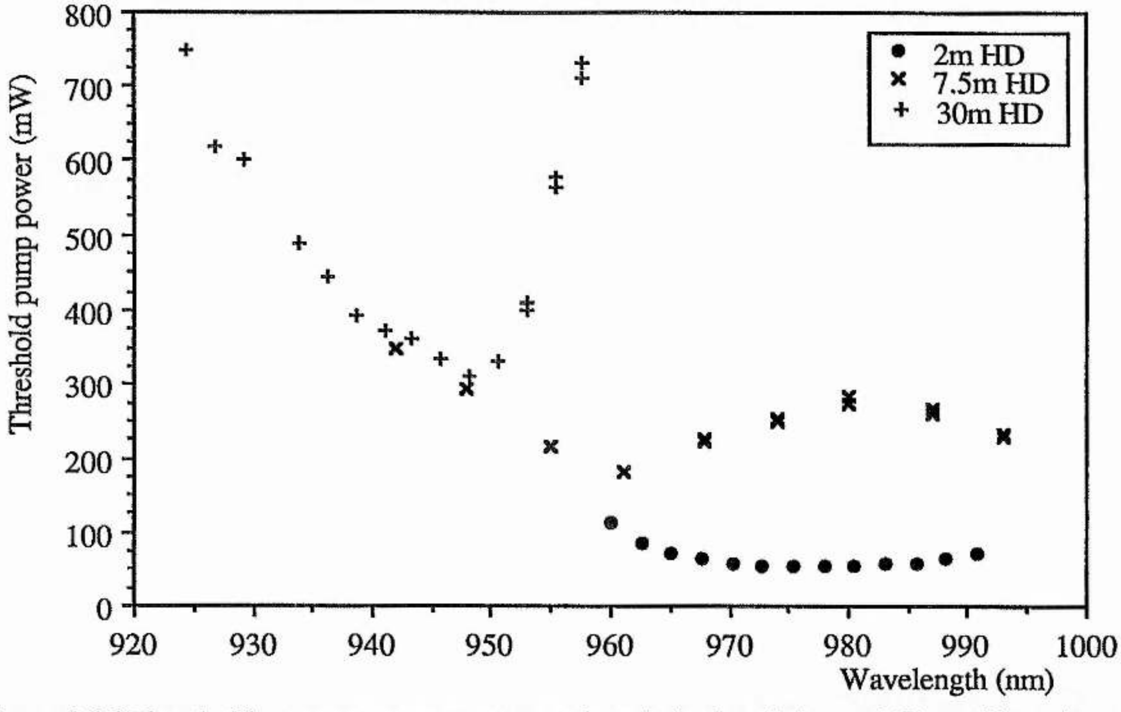

Figure 8.16 Threshold power versus pump wavelength for 2m, 7.5m and 30m erbium-doped fibre lasers. [HD; High dopant concentration of 2500ppm.]

### 8.8.2 Observation of optical bistability in erbium-doped fibre lasers

On tuning the pump laser away from the wavelength of minimum threshold towards the absorption peak the threshold increases dramatically and a hysteresis is observed around this threshold (hence the double points in figure 8.16). This phenomenon was evident with both 7.5 and 30m lasers (see figure 8.17). The degree of bistability was dependent on the pump wavelength, the effect increasing with tuning towards line centre and was accompanied by a marked threshold increase. A mechanism will now be suggested for this type of bistable operation.

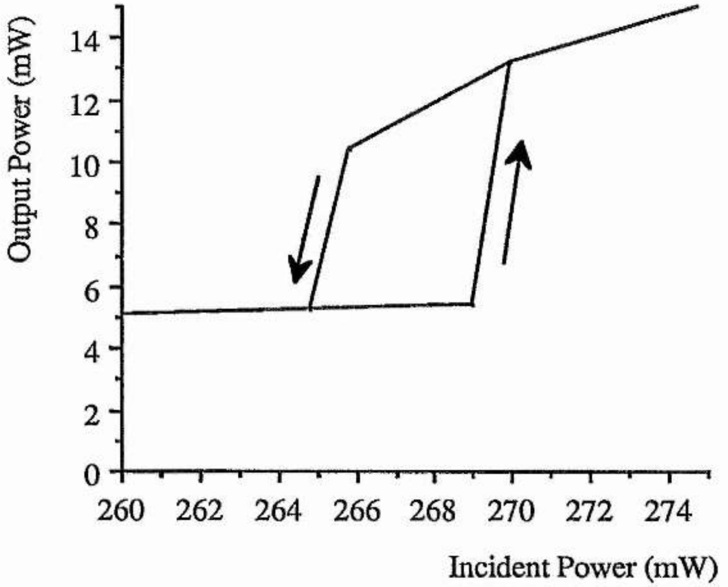

Figure 8.17 Power transfer characteristic of a 30m laser for $\lambda_p$=957nm. Insert: Detail of threshold region for a 7.5m laser ($\lambda_p$=980nm)

For a long laser pumped close to the absorption peak a large inversion is created at the beginning of the fibre, whereas the end of the fibre is unpumped and exhibits absorption at the laser wavelength. Therefore the laser can be considered as two essentially distinct parts (this represents a gross over simplification but should not significantly alter the physical interpretation involved). This situation of an inhomogeneously pumped laser is shown in figure 8.18. Section 1 presents large gain since it is highly pumped and hence fluoresces strongly. The fluorescence is coupled into section 2 and is reabsorbed thereby reducing the GSA.

When the gain in section 1 is increased through external pumping such that it equals the loss of the unpumped section the laser begins to oscillate. And the increase in intensity at the laser wavelength reduces the ground state absorption of section 2. The decrease in the cavity loss leads to a further increase in the laser output which in turn reduces the loss. This avalanche process is repeated until the saturable loss component of section 2 is bleached. As this sequence of events occurs rapidly the output is observed to undergo a light jump from a low intensity fluorescent signal to a higher power laser emission. The details of this process are illustrated in figure

8.19(b) on a plot of total cavity gain versus pump power (where the assumption that the gain is linear with pump power is used). Included in figure 8.19 is a similar plot of the characteristics of a traditional laser, and also a sketch of the (probable) loss function of section 2 versus laser intensity.

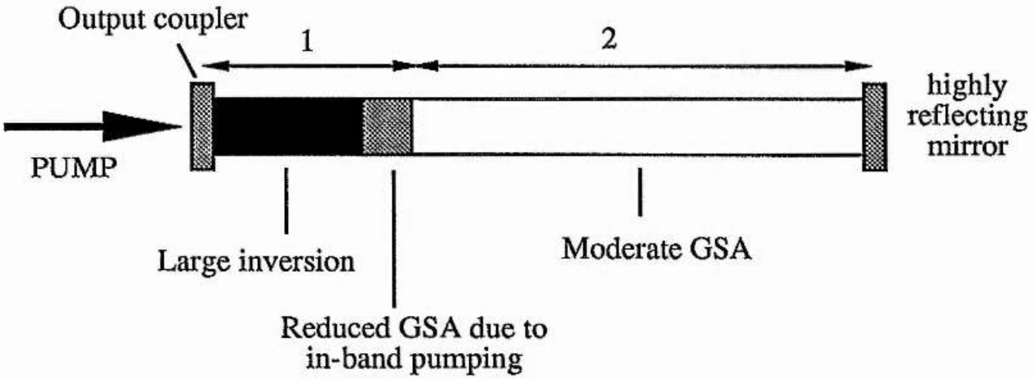

Figure 8.18 Inhomogeneously pumped fibre laser.

With increasing pump power the laser output follows the curve relating to a traditional laser with a loss equal to $L_{unsat}$. At threshold the process described above forces the output to jump onto the trajectory relating to that of a laser with $L=L_{sat}$. The output is then linear with further increases in pump power. As the pump power is reduced from a high level the output decreases linearly until the intracavity intensity reaches $I_2$ (as indicated in figure 9.19(c). At this point the avalanche process previously described is repeated but this time in reverse. That is, as the intensity decreases the loss increases, which further reduces the intracavity flux..... Thus the laser is abruptly switched off.

The magnitude of the hysteresis loop can then be described in terms of the difference between the unsaturated and saturated loss components ($\Delta L$) of section 2 of the laser cavity, and the value of the saturation intensity $I_2$ (see figure 8.20). It is clear that larger regions of unpumped fibre result in larger values of $\Delta L$ and hence more exaggerated hysteresis, and also the light jump will be correspondingly larger. Using a simple geometric argument it can be shown for the situation described here that: $I_1=\eta\Delta L$, $I_2=\eta\frac{\Delta L}{2}$ therefore implying that $I_1=2I_2$ and $P_2=\frac{P_1+P_2}{2}$.

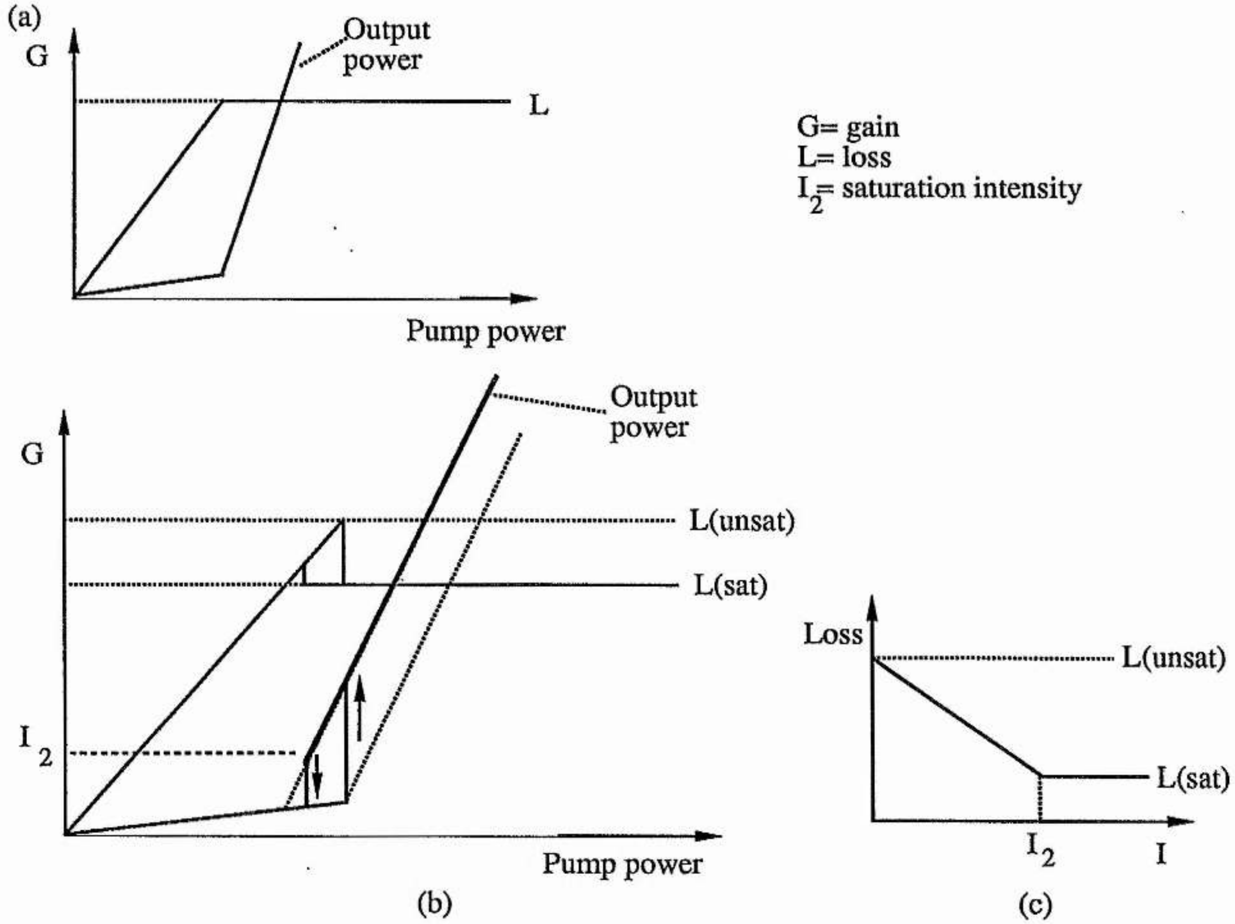

Figure 8.19 Characteristics of (a) a traditional laser, and (b) a laser exhibiting saturable absorption optical bistability. (c) Loss characteristic for (b).

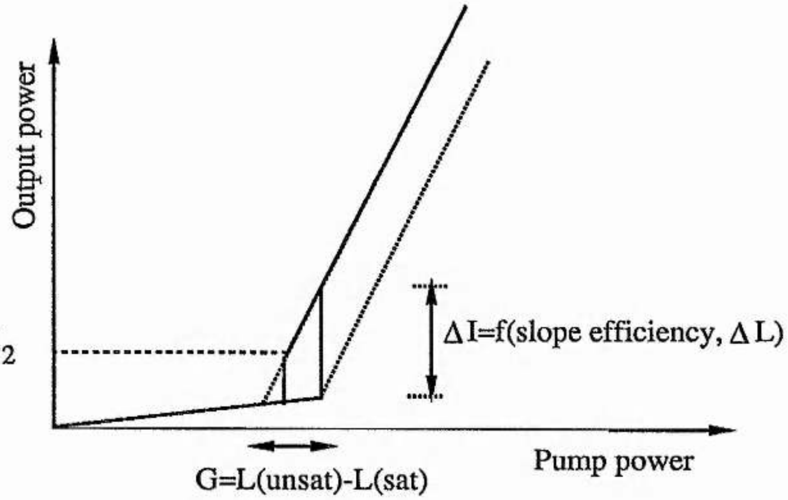

Figure 8.20 Magnitude of hysteresis.

Further work is still required to obtain the timescales involved in switching between the two output states, but due to the influence of the upper-state lifetime (~8ms) of the erbium system such values would be expected to be quite long.

### 8.8.3 Self Q-switching

The longest oscillation wavelengths were obtained using the 30m length of fibre in the laser. At wavelengths above 1612nm the output of the laser consisted of a sequence of pulses. This pulse sequence was very stable as evidenced in figures 8.21(a) and (b), where the duration of the pulses was typically 8µs (see figure 8.21(c)) with a 90µs interpulse separation. On close examination a modulation is apparent on the pulses, and the measured period was about 300ns. This modulation can be identified as mode-beating between the longitudinal cavity modes which are separated by 3.3MHz, with this corresponding to a round-trip time of 300ns. The interpulse separation was observed to decrease with increased pumping in a similar way to the spiking oscillations associated with laser turn-on[26].

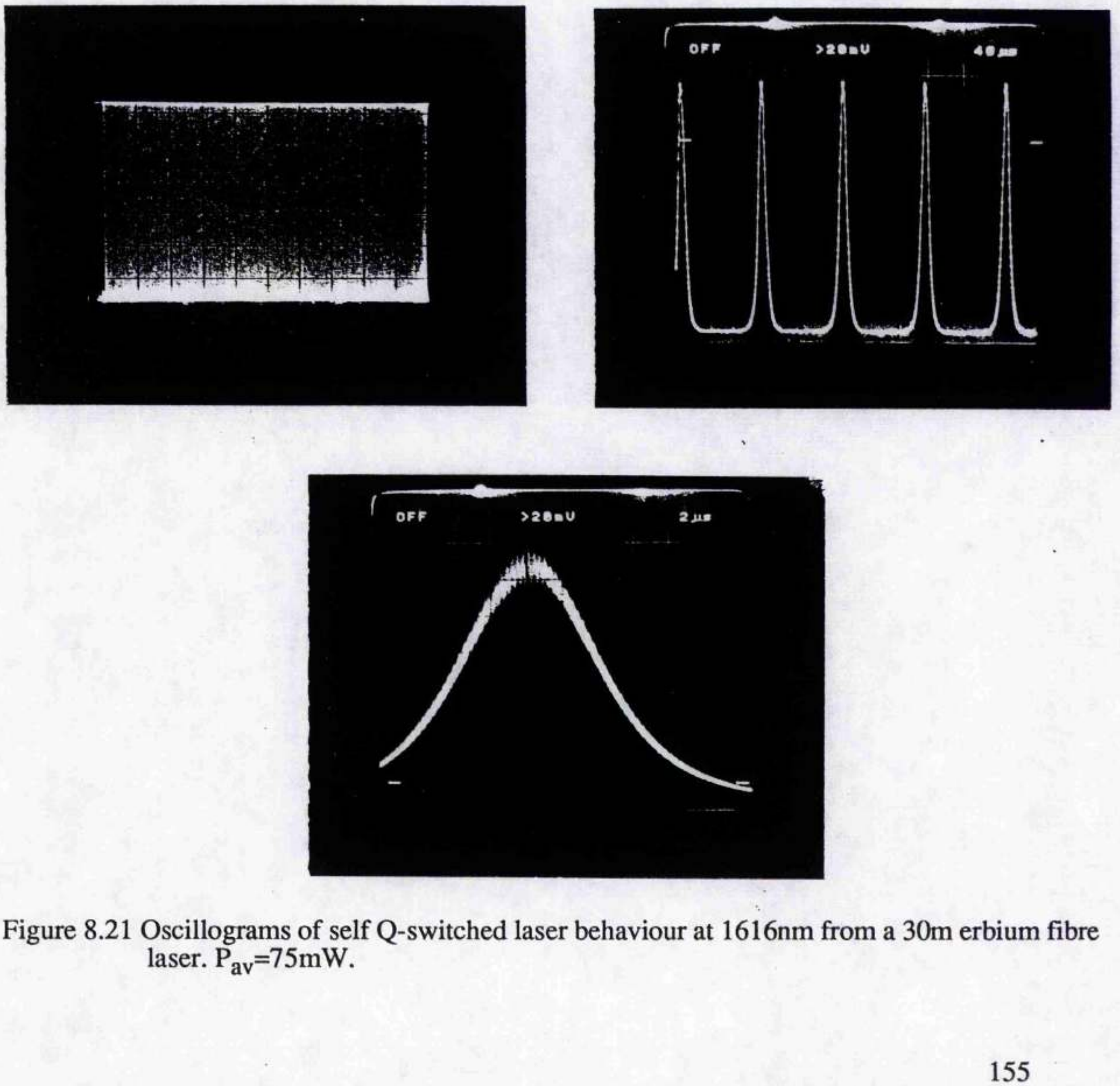

Figure 8.21 Oscillograms of self Q-switched laser behaviour at 1616nm from a 30m erbium fibre laser. $P_{av}$=75mW.

This effect can be explained in the following way. A rapid build-up of the laser signal occurs due to saturation of the residual ground-state absorption present at the long wavelength tail of the gain spectrum. The optical pulse produced forces the laser to turn off due to a depletion of the inverted population. The whole process is repeated after a characteristic time when the laser has recovered sufficiently. This time constant will be similar to that which controls spiking and relaxation oscillations. With stronger pumping the pulse build-up is faster and thus the delay to the next pulse is accordingly reduced.

The CW tuning range of the erbium:fibre laser system studied here is limited by the onset of this self-driven Q-switching. Although this phenomenon may be avoided by using different cavity configurations, and in particular those employing bidirectional pumping geometries. The enhancement in the peak power of the laser was only a factor of about ten for the situation described above. Therefore an attempt to obtain higher peak power pulses from erbium-doped fibre lasers using a more conventional form of Q-switching will now be described.

## 8.9 High power pulse generation using mechanical Q-switching

The long upper-state lifetime (~8ms, see Appendix A) of the erbium ion in the silica-fibre host implies that large energy storage is possible since there is little radiative decay within a characteristic time determined by this lifetime. This would allow a large inversion to be established leading to high peak power pulses through the process of Q-switching. Q-switching[208] is the technique where initially the cavity losses are made very high (ie. low cavity 'Q'), and hence a large inversion can be created before laser threshold is achieved. The loss is then reduced to a low value rapidly (high Q state), and the laser output that results is in the form of a giant pulse. The cavity Q can be switched by various methods where one of the simplest involves a mechanical chopper wheel.

Q-switching of fibre lasers has led to pulses of 200ns duration and 8.8W peak power at 1.08μm, and 70ns pulses of a few watts peak power at 900nm, both from a neodymium fibre laser[209]. Tunable erbium-doped fibre lasers with 32ns pulses of 120W peak power have also been demonstrated using an acousto-optic Q-switch[210].

Because the duration and hence peak power of Q-switched pulses are determined by the ratio of the inversion established in the low Q-state to that of the high Q-state (commonly referred to as 'r'), it was decided to use a mechanical chopper as the Q-switch since a larger initial population inversion could be maintained. The cavity configuration employed was as illustrated in figure 8.22. The chopper was inserted to traverse the beam where it is focussed to a small spot by the pair of intracavity microscope objectives, thus minimising the opening time of the Q-switch and hence inhibiting multiple-pulsing. When the chopper was at full speed the opening time was estimated to be around 200ns. The chopping rate used was 400Hz (period= 2.5ms), and the chopping window was reduced to about 30μs by using a ~1mm slit. The chopping rate was well in excess of the upper laser level lifetime therefore the average output power of the Q-switched laser would be expected to be equal to the CW output power. However, this was not the case for this laser where the average CW power was 80mW for 250mW pump power, and the average Q-switched power was only 14.7mW. The effective decrease in the upper-state lifetime is attributed to lifetime shortening due to amplified spontaneous emission.

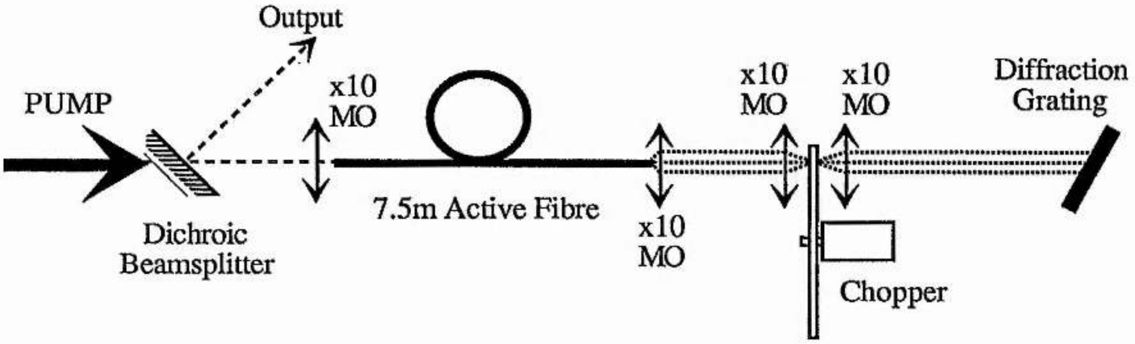

Figure 8.22 Mechanically Q-switched, erbium-doped fibre laser.

A plot of the pulse duration and peak power as a function of wavelength is shown in figure 8.23, for a pump power of 250mW (ie. r=5). The shortest pulse duration of 120ns was recorded at 1560nm but the maximum in the peak power did not coincide with the minimum in the pulse duration. The results obtained are shown again in figure 8.24 along with the CW power tuning curve of the laser with 800mW pump for comparison. The Q-switched peak power is some three orders of magnitude greater than the average CW power even though the CW laser is pumped more than three times higher.

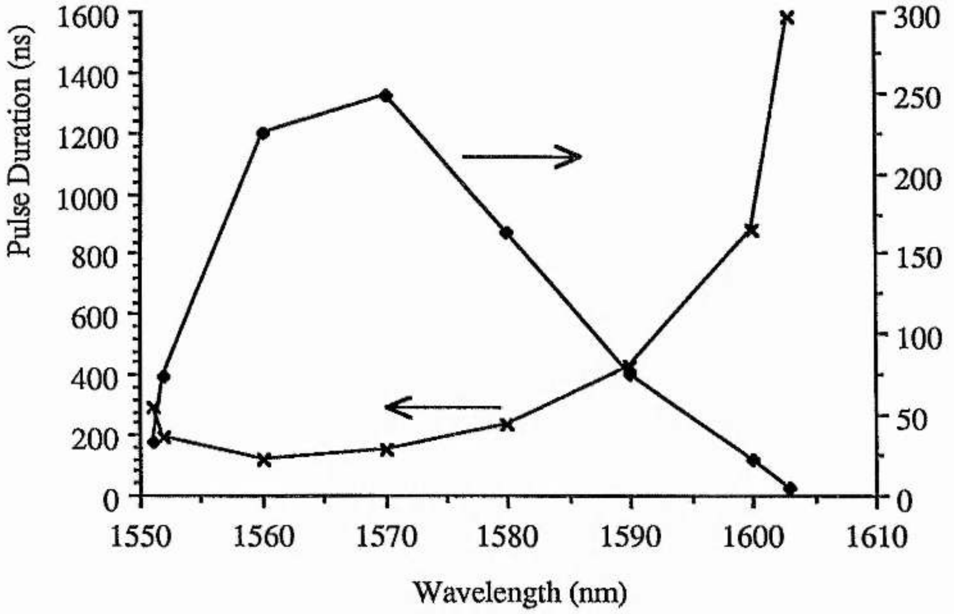

Figure 8.23 Pulse duration and peak power as a function of wavelength for a 7.5m Q-switched erbium fibre laser, $P_{pump}$=250mW (threshold=50mW, r=5).

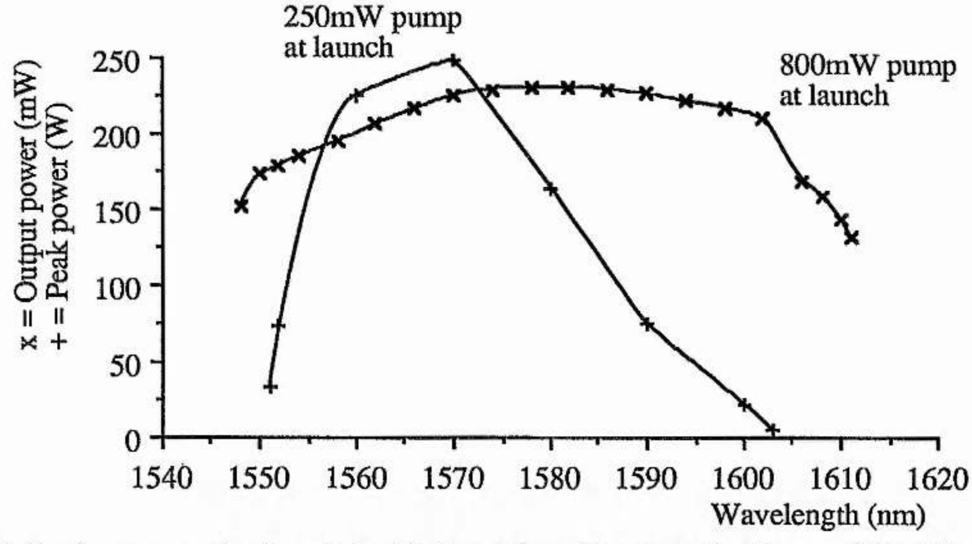

Figure 8.24 Tuning range of a Q-switched 7.5m erbium fibre laser for $P_{pump}$=250mW, and CW tuning curve for $P_{pump}$=800mW.

On increasing the pump power to 750mW the Q-switched pulse durations at 1575nm decreased to 90ns with an average power of 29mW which corresponded to a peak pulse power of 805W (73μJ). By tuning the laser to 1560nm the pulse duration was further reduced to 78ns with 25mW average output power and so the peak power was 800W (see figure 8.25(a) and (b)). The pulse energy was calculated to be approximately 62μJ at this operating point.

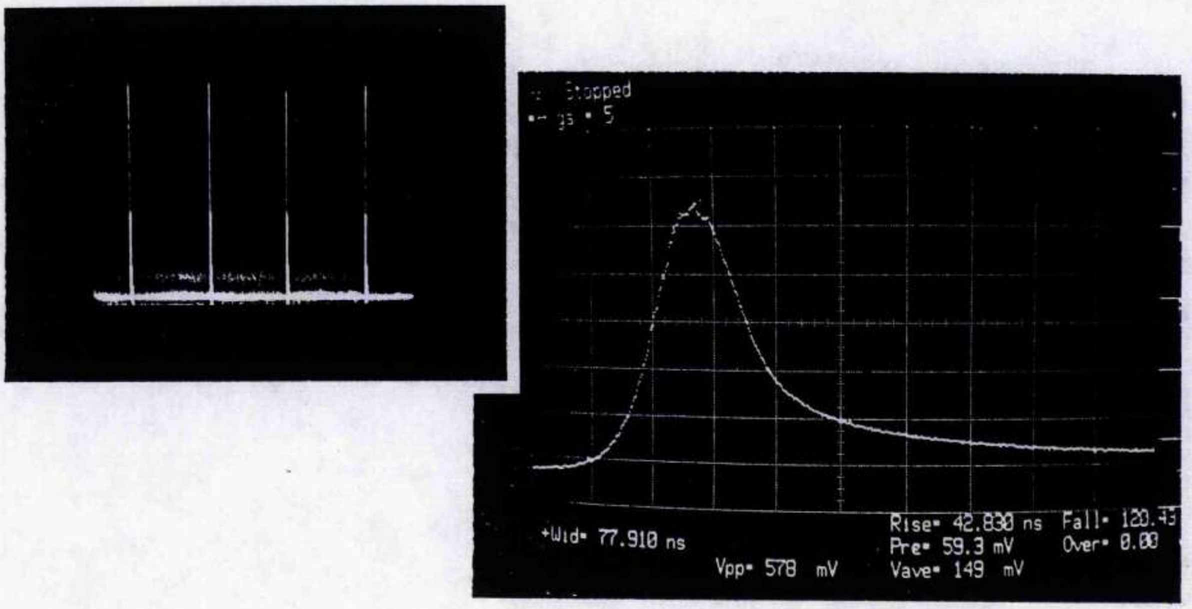

Figure 8.25 Oscillogram of output of the 7.5m Q-switched fibre laser; (a) 78ns duration pulses with a peak power of 800W, $\lambda$=1560nm. (b) Longer term oscillogram of the 50µJ Q-switched pulses at a repetition rate of 400Hz.

The observed pulse asymmetry of the Q-switched output pulses is attributable to the very large initial inversion, where the risetime of the leading edge is mainly governed by the inversion parameter r. The trailing edge of the pulse is determined by a time constant equivalent to the cavity decay rate which in this case was ~25ns. In a similar laser which had a 30m length of active fibre, and a correspondingly longer cavity decay rate, the pulse did indeed have a longer tail with a characteristic decay of around 100ns (see figure 8.26).

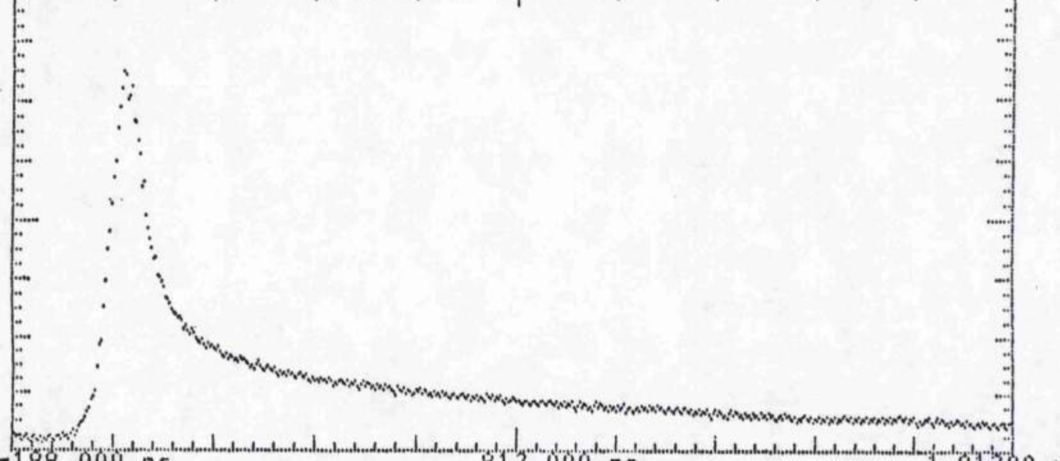

Figure 8.26 Output pulses from 30m Q-switched fibre laser, $\tau_{FWHM}$=86ns.

Figure 8.27 shows three spectra of the Q-switched laser tuned to different wavelength regions. The spectrum of figure 8.27(b) also shows the ASE spectrum when the cavity was blocked. Therefore as the laser was tuned to longer wavelengths the ASE component of the output are larger such that the inversion was reduced and the pulsewidth increased. It is believed that it is the effect of the ASE that determines the wavelength where the shortest pulses are obtained, and hence this is not necessarily the wavelength of maximum output power, as indicated in figure 8.24 above.

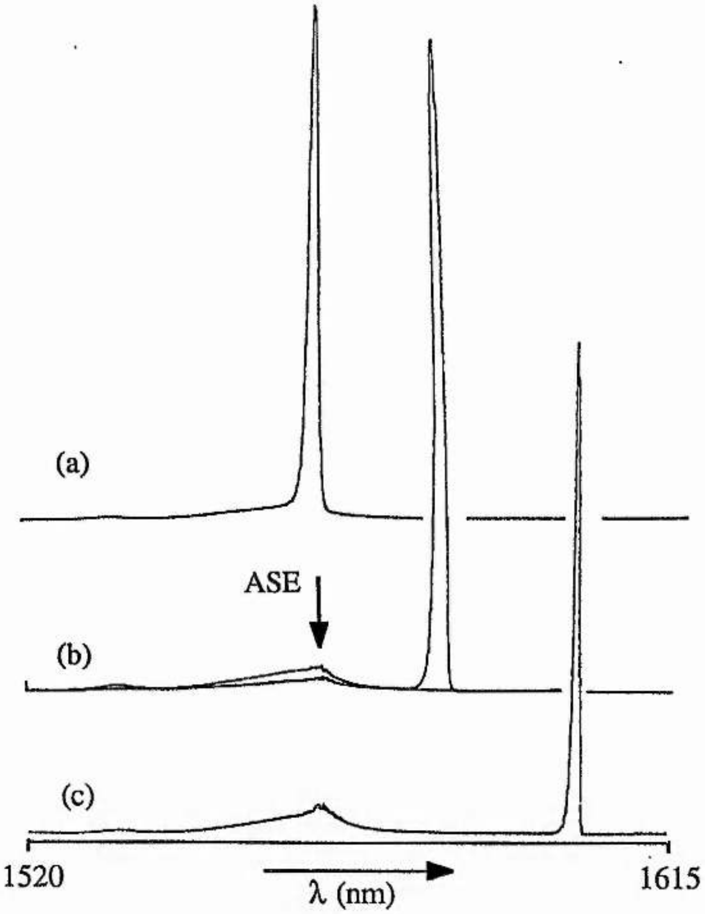

Figure 8.27 Spectra of the tunable, Q-switched, erbium-doped fibre laser (L=7.5m)

This laser source represents a significant improvement in peak power from previously developed Q-switched and/or modelocked erbium-doped fibre lasers. Indeed, the peak output power level of 800W is the highest yet reported for any fibre laser device. It is expected that this figure could be significantly improved through decreasing the fibre length. The result of this would be twofold; firstly the shorter cavity would emit shorter pulses with the extent of the trailing edge being reduced. The threshold pump power for the onset of multiple pulsing would also be increased due to the reduced ASE build-up within the laser. The large hold-off possible with the mechanical chopper is attractive, however, the opening time will always be limited. A Pockels effect modulator[211] featuring both good hold-off and speed could therefore represent the ideal candidate for the laser Q-switch. Using such techniques the potential of an order of magnitude improvement in the Q-switched laser performance seems likely.

## 8.10 Summary

A low-finesse, neodymium-doped fibre laser has been shown to be adequately described by a simple high-gain laser analysis developed by W.W. Rigrod. These lasers utilise a simple cavity geometry and are capable of high power operation. It is believed that the value of 800mW output power obtained is the highest yet reported value for Nd:fibre lasers. Furthermore by using a diffraction grating as a tuning element an essentially flat tuning range of 57nm has been demonstrated. The inherent stability of the fibre format should allow these lasers to compete with miniature diode-pumped rod lasers

The same cavity geometry was applied to erbium-doped fibres. Output powers of up to 700mW were obtained and again this represents the highest output power levels yet reported for a 1.5μm single-mode fibre laser. An enlarged tuning range of erbium-doped fibre lasers has been exploited using a 'length tuning' procedure. Where a total tuning range of 100nm from 1520-1620nm has been obtained from only three different lengths of fibre. The limit to the long wavelength tuning was 1620nm which is well above the previously reported longest wavelength of 1603nm[206].

A variety of nonlinear phenomena have also been shown to result from very long erbium:fibre lasers, namely self-Q-switching and optical bistability. A tunable, Q-switched, erbium-doped fibre laser was constructed using a mechanical chopper as the Q-switch. This laser produced stable pulses of 78ns duration with unprecedented peak powers in excess of 800W (~60-70μJ). The peak power value obtained is the highest yet reported from any doped fibre device to date. Such a laser source could be applicable within the field of medical lasers due to the large water absorption present at this wavelength[212].

# CHAPTER 9

# CONTROLLED AMPLIFIER MODELOCKED LASERS

## 9.1 Introduction

In this chapter a modelocking technique utilising the semiconductor modulator principle which was detailed in chapter 7 will be described. This has been applied to fibre lasers similar to those discussed in chapter 8. In the first section the CW operating characteristics of an erbium-doped fibre laser configuration controlled via the current applied to an intracavity semiconductor amplifier is discussed. In the subsequent sections the modelocking performance of this, and of more refined configurations are outlined.

## 9.2 The electrically controlled erbium-doped fibre laser

The fibre laser configuration incorporating a semiconductor amplifier as shown in figure 9.1 was constructed. The cavity consisted of a 3.5m length of germano-silicate, erbium-doped fibre which was spliced at both ends to fibre directional couplers. One coupler allowed optical pumping (at $\lambda$=532nm) of the active fibre whereas the coupling coefficient of the other was 3dB at the signal wavelength of ~1.53$\mu$m. A x10 microscope objective and a 63% reflecting plane mirror terminated one end of the laser cavity. A tunable semiconductor amplifier mirror arrangement similar to that discussed in chapter 7 was used to complete the configuration.

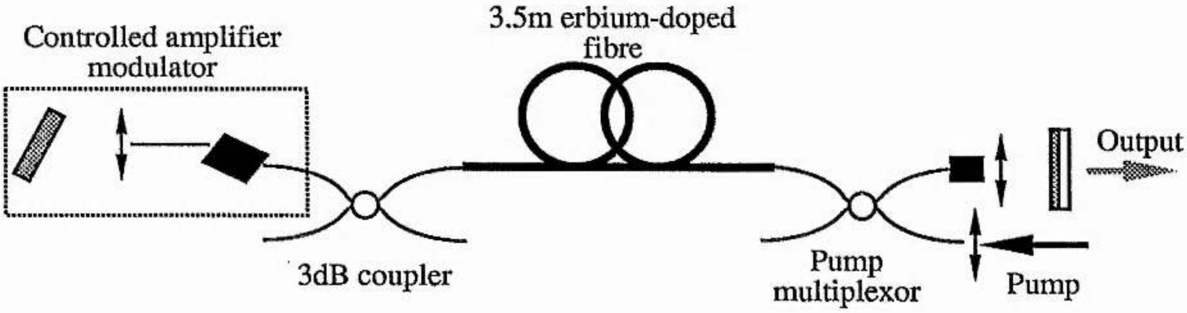

Figure 9.1 Fibre laser configuration with a semiconductor amplifier incorporated into one cavity mirror.

The output power from the 63% reflecting mirror was recorded as a function of the DC current applied to the amplifier. The curve obtained (see figure 9.2) was as expected apart from a peculiar feature around the laser threshold current. This feature could only be removed by a misalignment that increased the laser threshold. To find the source of this effect the diffraction grating was removed and the output through the diode was directed onto a monochromator.

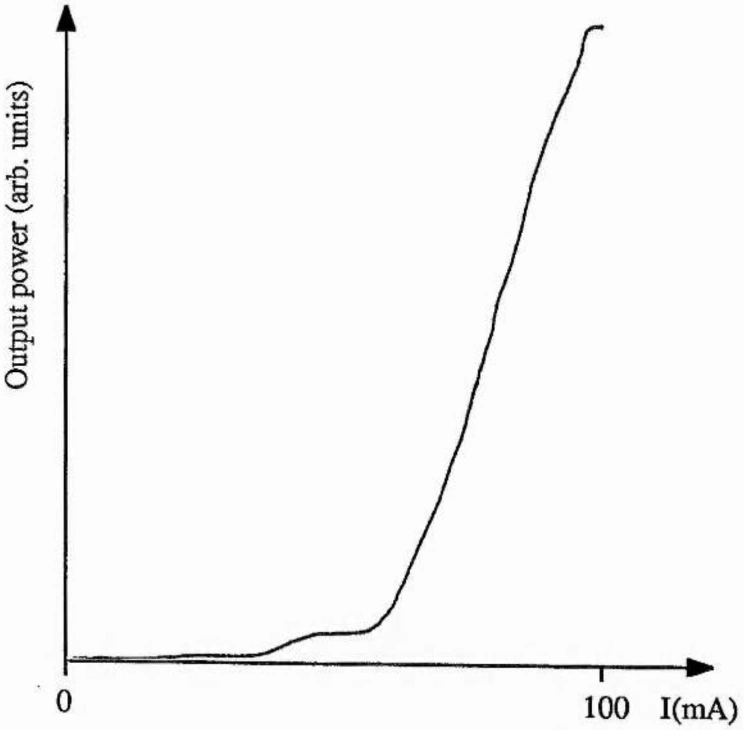

Figure 9.2 Output characteristics of the diode-current controlled fibre laser.

From the fluorescence spectra obtained (see figure 9.3) it became evident that the origin of this feature was due to amplification of the 1.55μm fluorescence peak from the erbium-doped fibre. At low currents the peak gain of the semiconductor amplifier is provided around 1.55μm. The gain peak shifts progressively to shorter wavelengths with increasing current thereby allowing amplification of the fluorescence peak at 1.536μm. The emission at 1.536μm then dominates at the expense of the weaker 1.55μm signal. Consequently, the feature observed in figure 9.2 can be explained as the onset of laser oscillation at 1.55μm. Since the gain at this wavelength is fixed with respect to that at 1.536μm the gain of the semiconductor amplifier solely defines the output wavelength. This is consistent with the observation that the 1.55μm emission was absent for high threshold currents because gain saturation due to the 1.536μm signal reduces the gain at 1.55μm below its oscillation threshold. Also in a similar way the output at high injection currents only consists of the 1.536μm signal, as evidenced in figure 9.4.

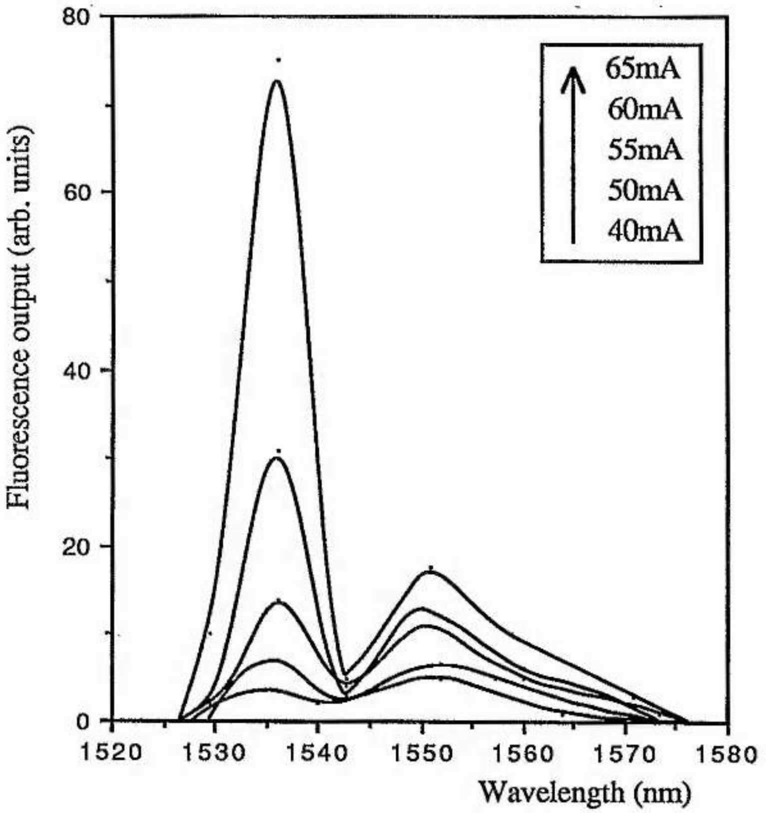

Figure 9.3 Fluorescence spectra obtained with increasing current applied to the semiconductor amplifier

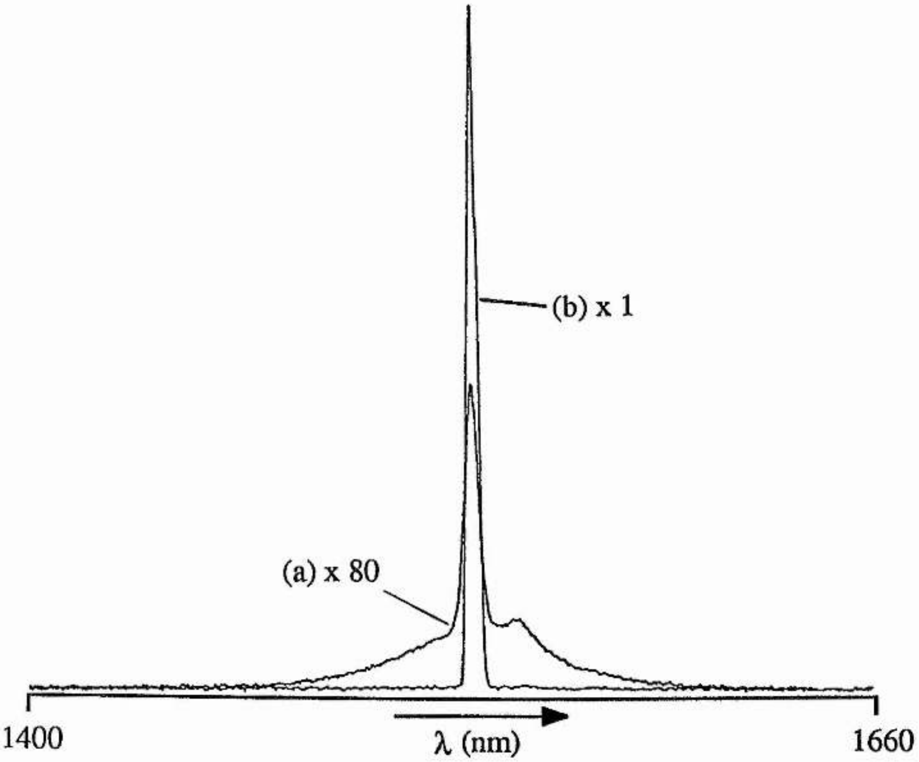

Figure 9.4 Laser output for (a) grating cavity blocked, and (b) unblocked.

The output power from the laser was roughly an order of magnitude higher than the equivalent laser configuration not having the erbium-doped fibre section ($P_{out}$~3-5mW). Therefore the laser discussed here effectively combines the controllability of the semiconductor amplifier with the higher output power capability and low-noise features of the erbium-doped fibre laser.

### 9.3 Modelocking of erbium fibre lasers

The erbium fibre laser has the potential of producing ultrashort pulses owing to its very large bandwidth. Although due to the relatively long upper-state lifetime (see section A.4) and small stimulated emission cross-section modelocking of erbium fibre lasers is not as straightforward as with other laser systems. For instance, the modelocking technique of synchronous pumping is not applicable because the laser is impervious to pump fluctuations at frequencies above ~100kHz. This is unfortunate since a frequently used, and efficient pump source is the frequency-doubled modelocked Nd:YAG laser. Also, the laser gain saturates with the mean power level in the fibre and not over the duration of a single pulse so no pulse shaping due to gain saturation can be expected.

There are also difficulties encountered with acousto-optic modelocking of the 'mirrorless' laser configuration, because the laser signal is insensitive to the internal mirror reflection coefficient (see figure 8.5 in chapter 8), and so the effective modulation depth of the modulator is very much reduced and the resultant pulsewidth is very long. The modulation depth can be increased by attenuating the signal incident on the modelocker and this does lead to somewhat shorter pulses but at the expense of reduced output power. Even though reasonably short pulses (~200ps) can be produced by this technique it does not lead to a proper exploitation of the inherent characteristics of this laser medium. Therefore different techniques must be employed to produce shorter pulses from erbium-doped fibre lasers. In general it can be said that for modelocking erbium fibre lasers either a pulse-shaping nonlinearity must be included in the resonator or a technique that accesses the intrinsic nonlinearity of the fibre host must be used. In the subsequent sections of this chapter such techniques will be assessed with particular emphasis on the use of the nonlinear controlled-amplifier modulator discussed in chapter 7.

### 9.3.1 The controlled amplifier modelocked erbium-doped fibre laser

The fibre laser incorporating the semiconductor amplifier modulator of figure 9.1 was operated in the modelocked regime by applying a radio-frequency component to the drive current of the modulator. Since the resonant frequency of the modulator was known to be a multiple of ~312MHz the only other criterion requiring consideration was the length of the erbium fibre cavity section. By applying a 312MHz RF signal onto a subthreshold DC bias current the position of the 63% reflecting output mirror was translated until a pulsed output was observed. An InGaAs PIN photodetector/sampling oscilloscope arrangement was employed to monitor the output from the laser during the alignment procedure. The duration of the pulses were minimised by adjustments of the electrical drive signals and the relative positions of both cavity mirrors such that the pulses collided within the semiconductor amplifier which enhanced the degree of gain saturation produced. A typical example of the output pulses produced from this laser is illustrated by the oscillograms in figure 9.5.

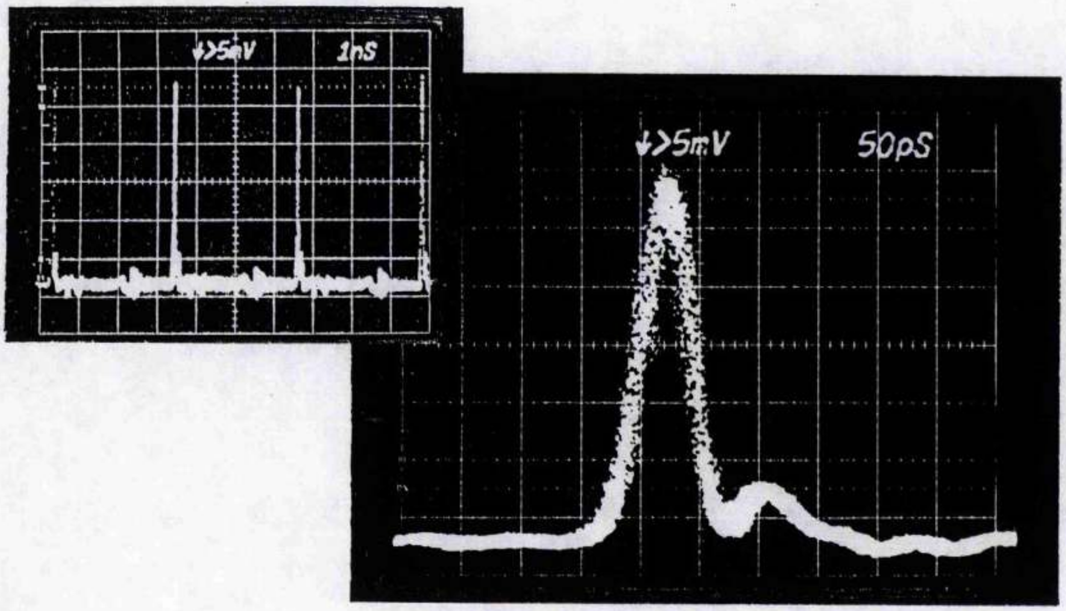

Figure 9.5 Output pulses from the modelocked laser at $f_m$=312.6624MHz

It was evident that the resultant pulse durations were significantly less than the resolution limit of the sampling oscilloscope and so a synchronously operating steak camera system was employed for complementary pulse analysis. In figure 9.6 the intensity profile recorded using the streak camera is reproduced for typical modelocked pulses from this laser configuration. The measured pulse duration was 6.9ps and the average output power was usually around 4mW (for approximately 100mW launched pump power at 532nm). The peak power of the pulses were thus consistently in the region of 1.4-1.8W. The fact that no subpulsing is evident in this laser is due to the enhanced peak power of the intracavity pulses which can sufficiently saturate the available gain present in the semiconductor amplifier such that no gain recovery or re-emission is possible.

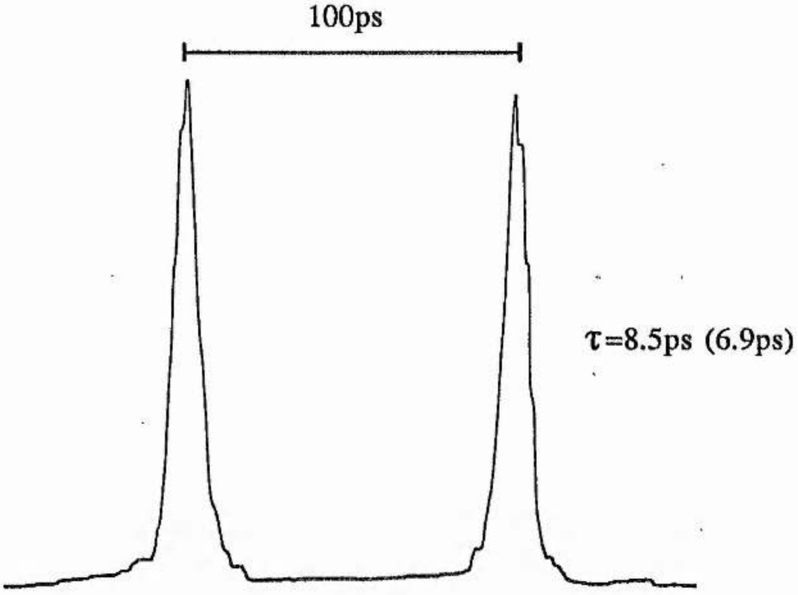

Figure 9.6 Streak intensity profiles of modelocked laser pulses.

The laser performance varied slightly with modulation frequency. With negative detuning the pulse peak diminished until a signal resembling the modulation response of the amplifier was produced. With positive frequency detuning the pulsewidth slowly increased until at 312.76MHz (that is 100kHz above the optimum frequency) the output suddenly behaved as indicated in figure 9.7. Although this output is difficult to interpret from the sampling oscilloscope data, it appears that the laser is pulsing with a duration somewhat greater than 100ps, but this is also rapidly turning on and off. As no other diagnostic was available to give additional direct insights the following explanation is put forward. When the intracavity pulse steadily phase-lags the detuned modulation signal applied to the semiconductor amplifier a situation arises where the gain thus created has dissipated due to fluorescent emission or CW oscillation. The pulse then experiences loss on propagation through the amplifier and is effectively extinguished. Another pulse can then build up, and will be extinguished after a characteristic time, and the whole process of creation and annihilation of pulses can then be repeated.

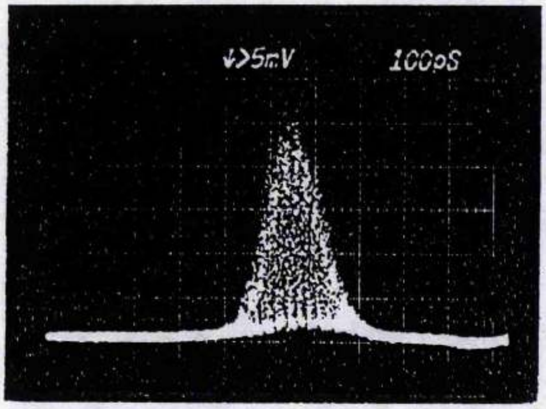

Figure 9.7 Output pulse profile characteristic at ~100kHz positive frequency detuning.

For these results the DC component of the bias signal was kept small, and in some instances was reduced to zero. It was found that the output pulses were not particularly sensitive to this parameter, but it became apparent that the best quality pulses were generated when the measured direct current level (as monitored by a milliammeter) was at a specific value. The current indicated by the ammeter gives a measure both of the direct current applied from the power supply and of the rectified component of the RF modulation signal during its negative excursion. For the amplifier chips used in this work this value was between 50-55mA and varied little with modulation frequency or the pumping conditions of the erbium-doped fibre. As the modulation frequency was increased, and the RF power coupled to the amplifier decreased (due to imperfect impedance matching) so the applied DC current had to be increased accordingly to sustain the current criterion.

The modulation frequency applied to the modulator was then doubled to 625MHz, and again clean output pulses were produced with no evidence of the subpulsing associated with the passive fibre cavity configurations discussed in chapter 3 (see figure 9.8). From streak camera measurements the pulse duration was found to be 8ps as illustrated in figure 9.9. On deconvolution of the temporal resolution of the streak camera system a value of 6.2ps was obtained. Under these conditions the output power was 3.5mW and the peak pulse power was calculated to be 0.9W. The spectrum of the laser was measured to have a FWHM bandwidth of 1.0nm. For the corresponding duration-bandwidth product of ~0.8 this implies that appreciable chirp existed across the pulse envelope. This is not too surprising given that the primary pulse shaping effect is gain saturation within the semiconductor amplifier which causes a frequency chirp due to the carrier density dependant refractive index of the medium. And indeed the ΔνΔt product is typical of conventional modelocked semiconductor laser systems. The peaks on the laser spectrum are separated by ~0.66nm which is commensurate with the value obtained for the Fabry-Perot resonances of the amplifier subcavity. The modulation depth is low due to the use of the angled-ridge amplifier, although weak reflections from the surface of the microlensed fibres would act to exacerbate the spectral modulation.

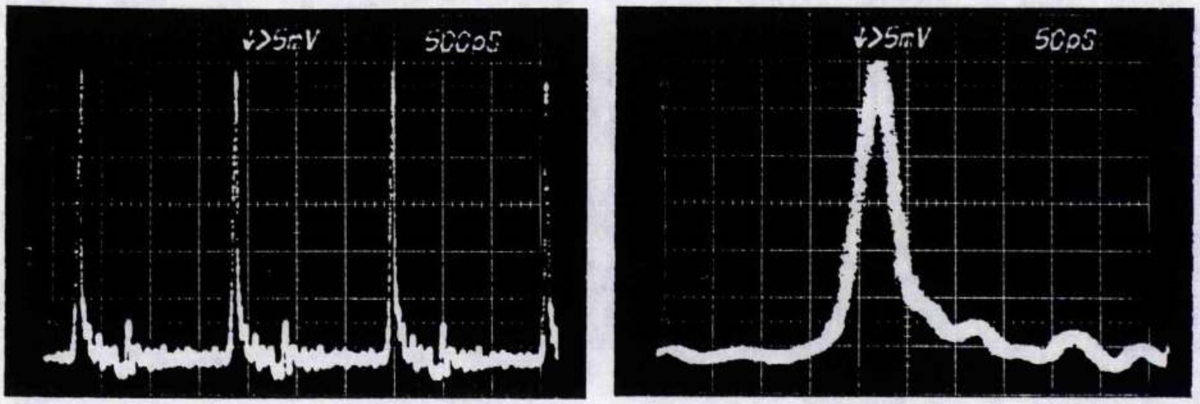

Figure 9.8 Oscillograms of modelocked output pulse sequence at a 625MHz repetition frequency.

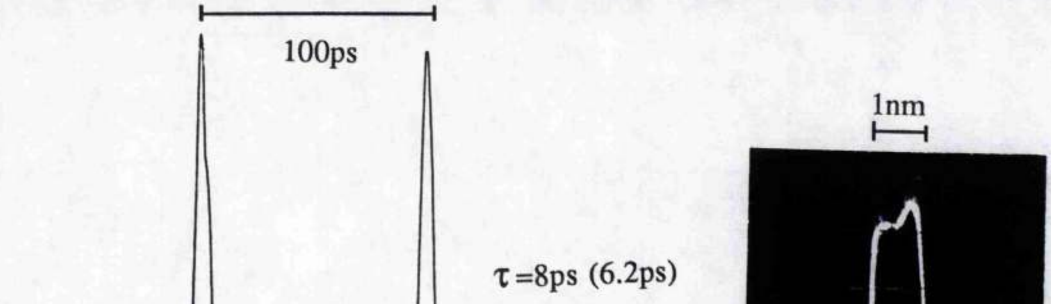

Figure 9.9 Streak intensity profiles of modelocked laser pulses at a 624.79MHz repetition frequency. (Insert: spectrum of the laser output).

These optimised pulses were again directed onto the InGaAs PIN photodetector and as illustrated in figure 9.10 the pulse duration was sufficiently short that the oscillogram effectively shows the impulse response of this measurement equipment. Again with a positive modulation frequency detuning, which in this case was 110kHz, a sustained dropout mode of operation could be accessed (see figure 9.11). Two states could be clearly resolved; one being of a single pulse of ~75ps duration and the other was of low intensity with multiple peaks. This observation agrees with the explanation previously proposed, and the clarity of the two states suggests that the transition from one to the other is very fast although no technique was available to further examine this effect.

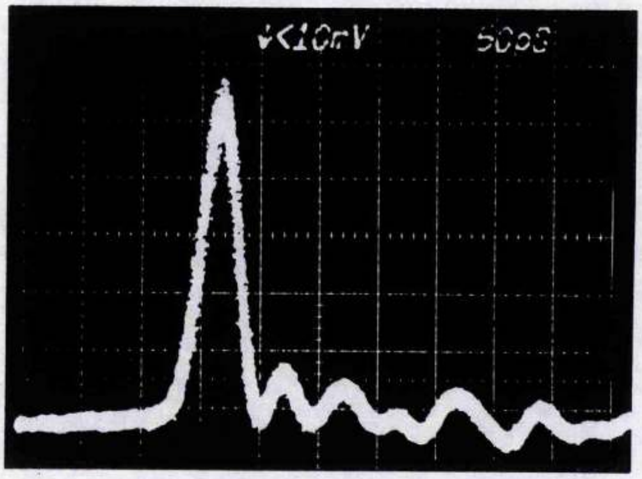

Figure 9.10 Impulse response of the InGaAs PIN photodetector/sampling oscilloscope arrangement obtained on illumination with optimised laser pulses.

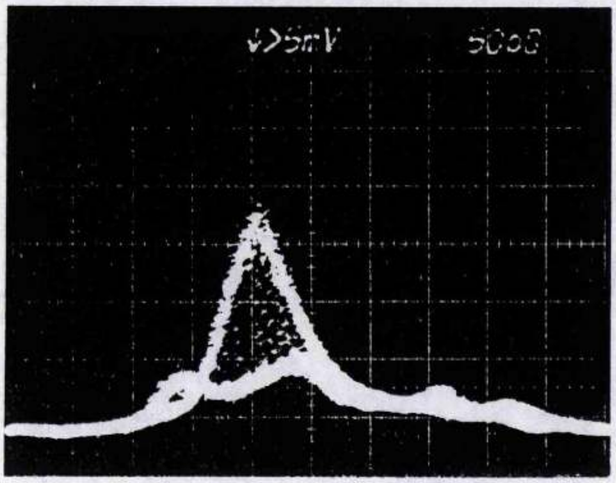

Figure 9.11 'Dropout' mode for 110kHz positive detuning from the optimum frequency

After initial laser alignment and subsequent coupling to the streak camera system an output state as shown in figure 9.12 was frequently observed. This streak record indicates an output consisting of two pulses of unequal intensity and separated by ~150ps. In all observations the trailing pulse intensity never exceeded $\sim\frac{1}{5}$ that of the leading, or main pulse.

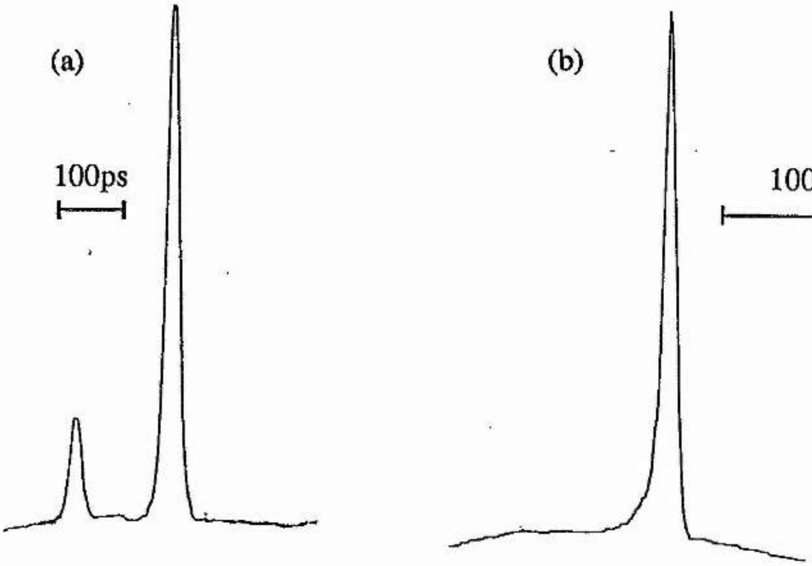

Figure 9.12 (a) Double pulse output. (b) Optimised output pulse.

The existence of a double pulse output was a feature of the long modelocked erbium fibre lasers investigated by Schlager et al[213]. They found that the two pulses were in orthogonal polarisation states and the time delay was simply due to the polarisation dispersion of the fibre cavity. In most instances the trailing pulse could be extinguished by affecting the polarisation state within the laser cavity. In very long (>1km) laser cavities the two pulses were of roughly equal intensity and a single pulse output could not be produced. In the laser detailed in this work the secondary pulse only existed when the cavity alignment was poor, and by optimisation of the pulse duration the trailing pulse could be easily extinguished. This was mainly due to the different gains of the amplifier for the two polarisation states, and also because as the first pulse becomes sufficiently intense the amplifier gain is depleted and any secondary pulses present will be severely attenuated.

### 9.3.2 Amplitude noise suppression in C.A.M. erbium-doped fibre lasers

The beam derived from the Nd:YAG pump laser was quite noisy (see oscillograms of figure 9.13) so an investigation of the amplitude noise properties of both the pump laser and the erbium-doped fibre laser was undertaken. The oscillograms of figure 9.14 summarise the results of noise measurements on both the pump (bottom trace) and the erbium:fibre laser (top trace).

The bottom right trace indicates the background level for the two laser signals. Therefore it is evident that on very long timescales the erbium:fibre laser follows that of the pump laser but suppresses the magnitude of the fluctuations. Alternatively on timescales shorter than ~20μs the erbium:fibre laser does not respond to fluctuations of the pump intensity. Or in other words, fluctuations of the pump intensity of frequency greater than ~50kHz are not coupled onto the erbium:fibre laser output.

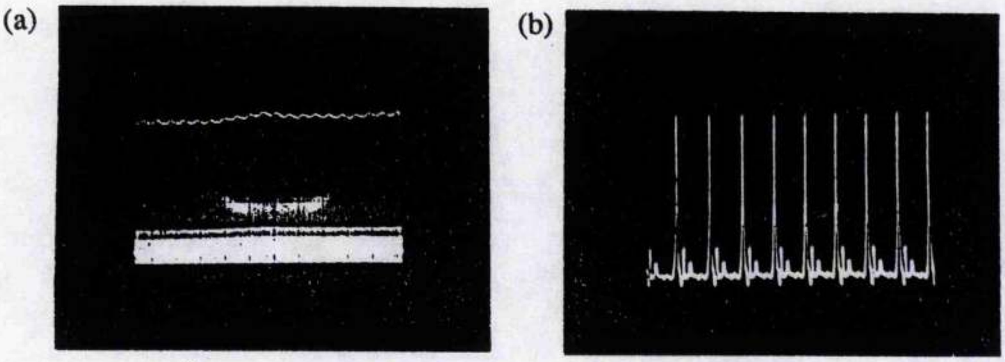

Figure 9.13 Nd:YAG pump laser noise for (a) 20μs/div (b)10ns/div.

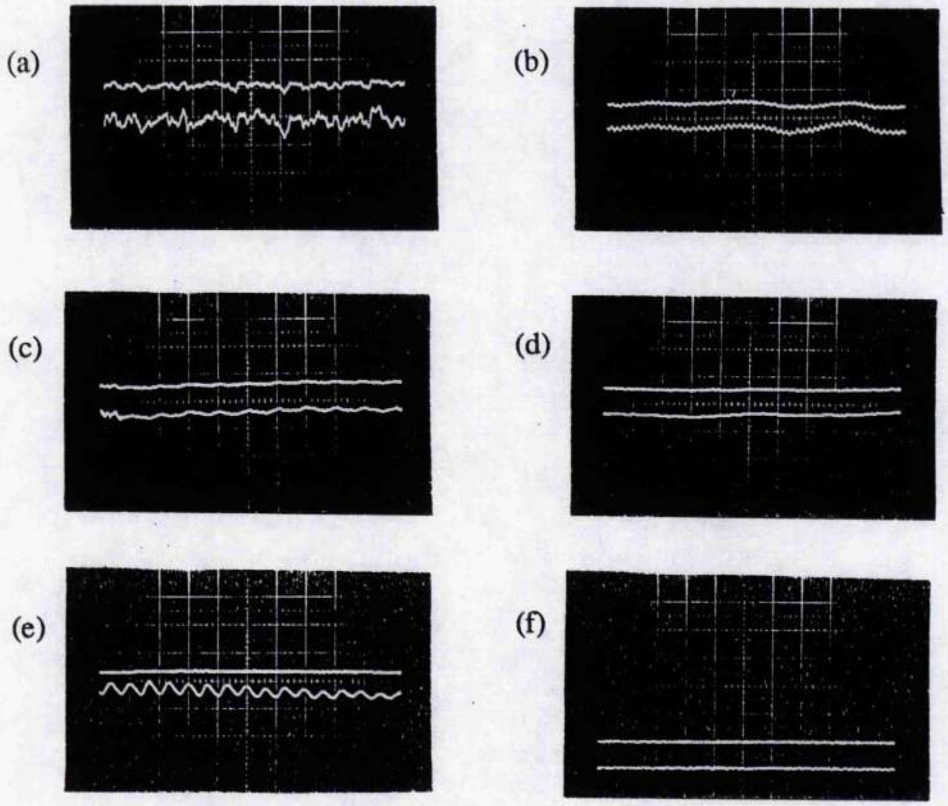

Figure 9.14 Modelocked erbium fibre laser (top trace) and pump laser output noise (lower trace) for (a) 0.5s/div, (b)100ms/div, (c) 10ms/div, (d) 2ms/div, and (e) 20μs/div. The oscillogram (f) indicates the zero level for both laser signals.

This suppression of pump laser noise is attractive and is due mainly to the long upper state lifetime and the small cross-section of the laser active erbium ion. A large reservoir of inverted ions can therefore be maintained and the fluctuations of the pump laser cannot couple effectively to the signal field through the population inversion. The quality of the pump laser is thereby relaxed for these laser systems.

### 9.4 Actively modelocked erbium-doped fibre ring laser

The cavity configuration discussed previously utilised the coherent collision of counterpropagating pulses within the semiconductor amplifier to enhance the gain saturation, and hence minimise the output modelocked pulse durations. This was achieved by iterative adjustments of the modulation frequency and the resonator length at each side of the modulator. A more obvious configuration which automatically satisfies this condition is a ring resonator and so such a cavity was constructed as detailed in figure 9.15.

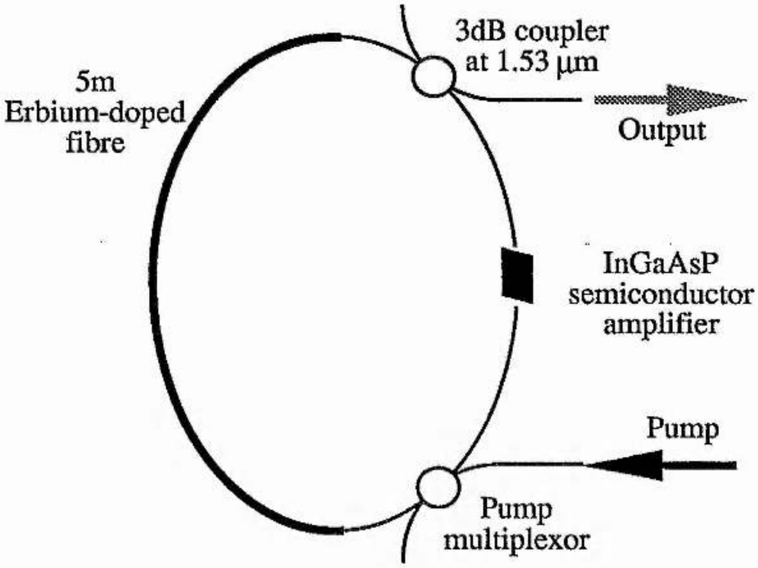

Figure 9.15 C.A.M. erbium-doped fibre ring laser

The pump multiplexor allowed efficient coupling of the pump radiation into the erbium-doped fibre, but was of low loss at the operating wavelength of the ring laser. The erbium fibre was again 5m long and identical in composition to that used in the linear cavity arrangement described in section 9.2. The output coupling fibre directional coupler was 3dB around 1.54μm and was configured such that the un-absorbed pump radiation exited the cavity before reaching the semiconductor amplifier. The ring laser output was chosen to be the portion of the beam which had just propagated through the erbium-doped section rather than that from the semiconductor device. This output was more intense since it had just undergone amplification, whereas the other beam intensity was smaller due to the coupling losses experienced on propagating through the semiconductor modulator cavity section. The pump wavelength used in this experiment was 980nm and was derived from an argon ion laser pumped titanium:sapphire laser. This wavelength is particularly efficient for erbium-doped fibres since no pump excited-state-absorption exists and the quantum defect is reduced compared to the other efficient pump band at 532nm. Pump powers between 50-100mW could be effectively coupled into the erbium-doped fibre section of the ring laser.

With only direct current applied to the semiconductor amplifier the laser output was coupled onto an InGaAs PIN photodetector. On application of an RF drive component the modulation frequency was adjusted until a pulsed output was observed using the sampling oscilloscope. An example of the pulsed laser output is shown in figure 9.16(a). In this manner a number of resonant frequencies of the laser were obtained which were separated by 21.25MHz. The corresponding cavity length and round-trip time were therefore 9.5m and ~47ns respectively. The frequency of ~615MHz (29th harmonic) was used in all further measurements since this was within the frequency range of the streak camera system used.

The output pulse sequence from the laser was directed onto the streak camera via a calibrated optical delay line which was adjusted to provide a temporal separation of 66ps between the pulses travelling in the two arms. An optimised-resolution limited streak intensity profile of the pulses from the ring laser configuration is included as figure 9.16(b). Although the minimum pulse duration could not be determined from these measurements it was evident that the pulses were extremely stable, and that negligible interpulse noise was present on the pulse train.

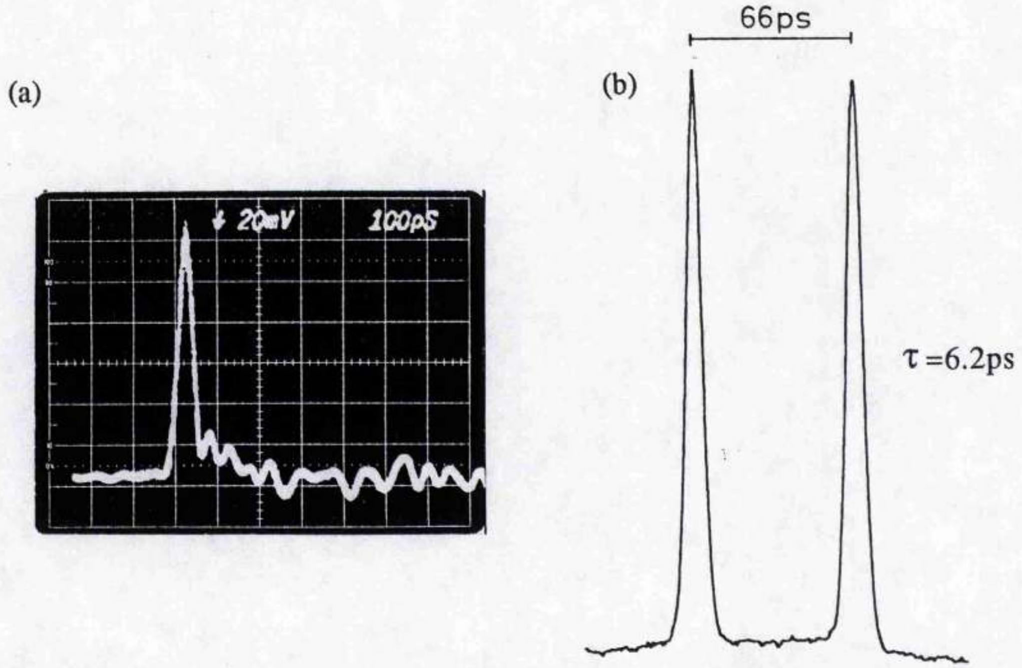

Figure 9.16 Output pulses from the modelocked ring laser as monitored by (a) an InGaAs PIN photodiode/sampling oscilloscope arrangement, and (b) by the streak camera.

The average output power at 1536.5nm was 6mW with fluctuations of less than 5%. The pump laser stability was ~10% over a time of 50ms (see figure 9.17(a)). This is not typical of the output from the titanium:sapphire laser, and it was found that the source of the instability was feedback of pump radiation from the fibre laser arrangement. (The inclusion of an optical isolator would eliminate this source of pump laser noise but such a device was not available during the course of this work.) As previously described the damping effect of the long upper-state lifetime of the erbium system influences the fibre laser such that the output exhibits a reduced amplitude-noise content as is evident in figures 9.17(b) and (c). During a period of 50ms the intensity fluctuations were measured to be less than 3%, and <6% over a 5s interval. Hence the noisy pump does not prove to be a serious problem, and with the potential advantages of semiconductor laser pump sources an exceptionally low-noise laser source could be realised (see section 6.5 in chapter 6).

The modulation frequency detuning characteristics of the modelocked ring laser were recorded and are detailed in figure 9.18. The crosses indicate the measured streak durations and the dashed line represents the true pulse durations obtained after deconvolution of the instrumental function of the streak camera system. Sub-10ps pulse durations could therefore be obtained over a frequency range of >15kHz. Again positive frequency detuning from the optimum modelocking frequency is characterised by a slow, but steadily increasing pulse duration. The pulse duration increased much more rapidly on negative detuning, with a fivefold pulse broadening occuring for only 3kHz of detuning.

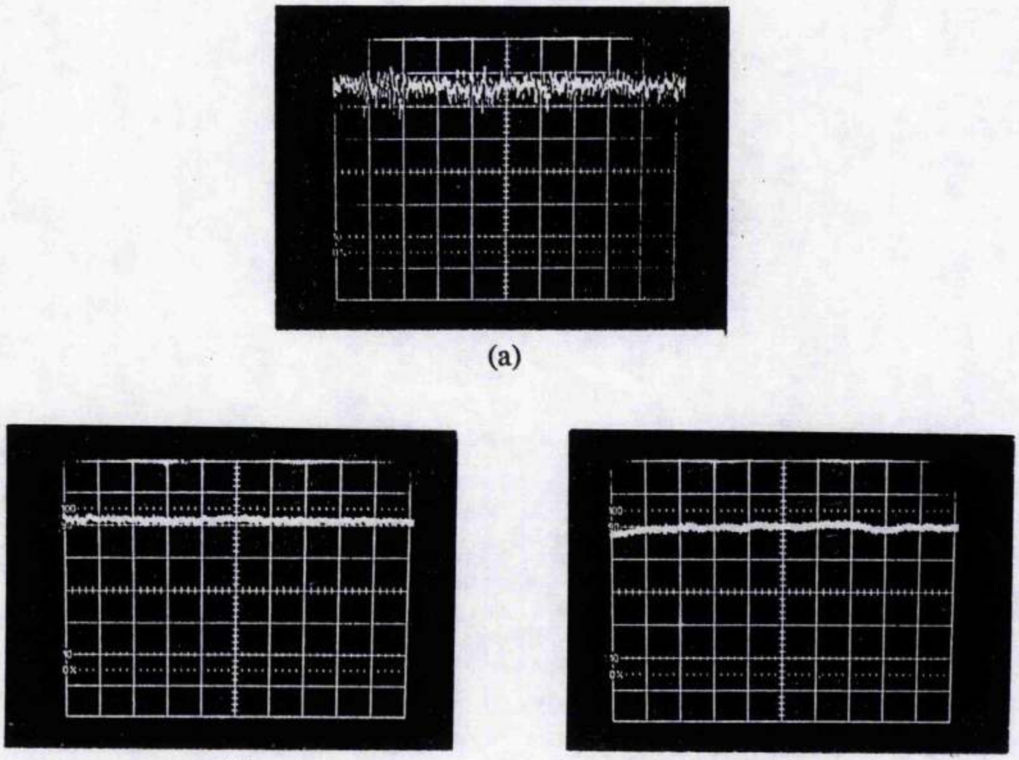

(a)

(b)

(c)

Figure 9.17 (a) Titanium:sapphire pump laser stability (5ms/div), and modelocked ring laser stability for timescales of (b) 5ms/div, and (c) 0.5s/div.

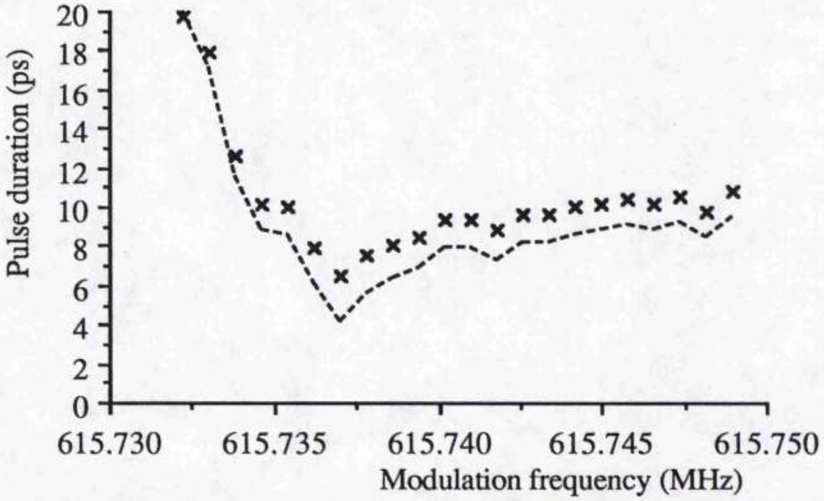

Figure 9.18 Frequency detuning characteristics of the modelocked ring laser

The modulation frequency giving the shortest pulse duration could only be confirmed by using the increased temporal resolution provided by the streak camera. Examination of the output laser spectrum can also provide a useful indication of the required operating parameters (see figure 9.19). The spectrum of figure 9.19(a) was obtained before final optimisation using the streak camera. The bandwidth was ~1.5nm and the corresponding pulse duration was in the range 15-20ps. Note the strong modulation features which are indicative of a subcavity within the laser resonator. The modulation period of ~0.7nm is commensurate with that expected for the semiconductor amplifier which had a length of 500μm. After detailed cavity alignment to obtain the shortest duration pulses the spectrum was transformed to that shown in figure 9.19(b). The bandwidth increased to 2nm and the output power was improved by roughly a factor of two. For this reduced pulse duration the effect of the subcavity is decreased and so there is minimal interference between the main pulse and any reflected components within the subcavity. This would imply that the pulse duration is below 4ps as obtained from the deconvolved streak camera data.

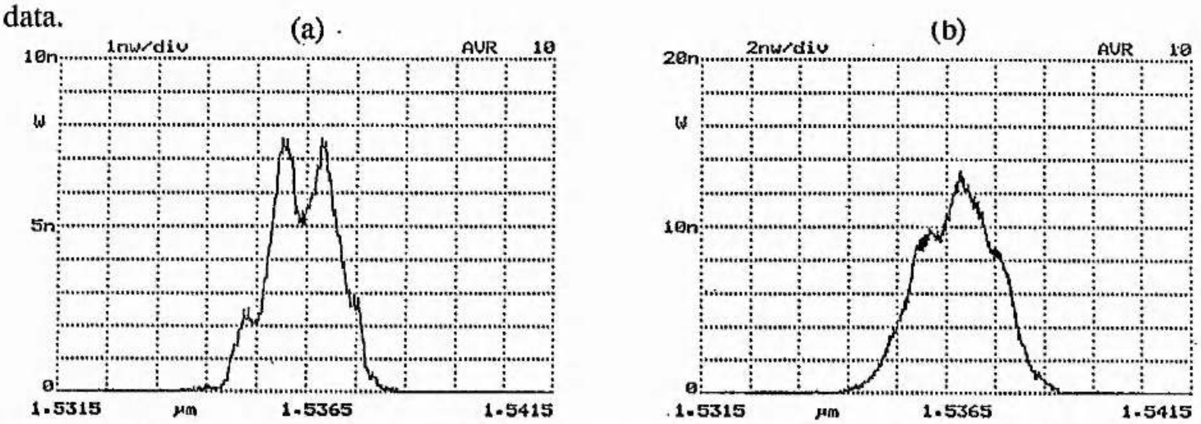

Figure 9.19 Modelocked ring laser spectrum (a) before, and (b) after optimisation using the streak camera.

To obtain an unambiguous value for the duration of the pulses from the modelocked ring laser a diagnostic with better temporal resolution was therefore required. To this end an autocorrelator utilising second harmonic generation in a 2mm crystal of lithium niobate was employed. (At 1.5μm the temporal resolution of the system is better than 100fs.) Using this technique the second-order autocorrelation function of the modelocked pulse train was obtained (see figure 9.20). The 3:1 contrast ratio implied good modelocking and by assuming a hyperbolic secant squared ($\mathrm{sech}^2$) pulse intensity profile a pulse duration of 3.5ps was deduced. (Also included in figure 9.20 is the average output power level. Note that this trace is inverted, with the ground level being the top line of the oscillogram).

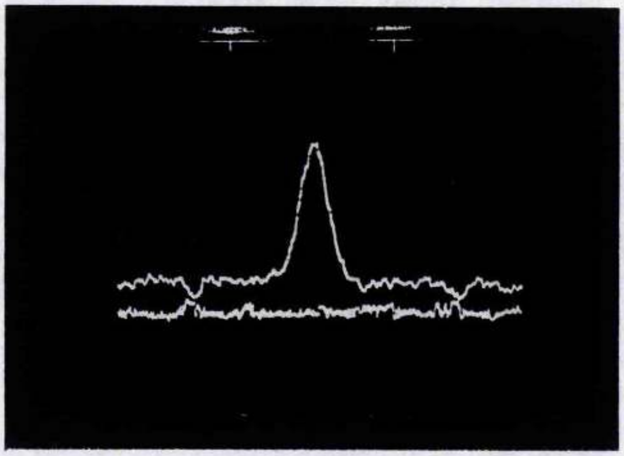

Figure 9.20 Autocorrelation function of the modelocked erbium fibre ring laser

In the autocorrelation process the intensity fluctuations of the average power of the pulse train are highlighted so a low-level signal averaging of the autocorrelator data was justified. The uncorrupted autocorrelation function of the modelocked pulses could thus be obtained (see figure 9.21(b)). Indeed the noise was of such low frequency that only four accummulations were generally required to yield the function. In this way a pulse duration of 3.4ps was consistently obtained. For the measured average power of 6mW the corresponding peak pulse power was found to be 2.9W. The associated output spectrum is shown in figure 9.21(a) and hence the duration-bandwidth product of 0.86 was calculated.

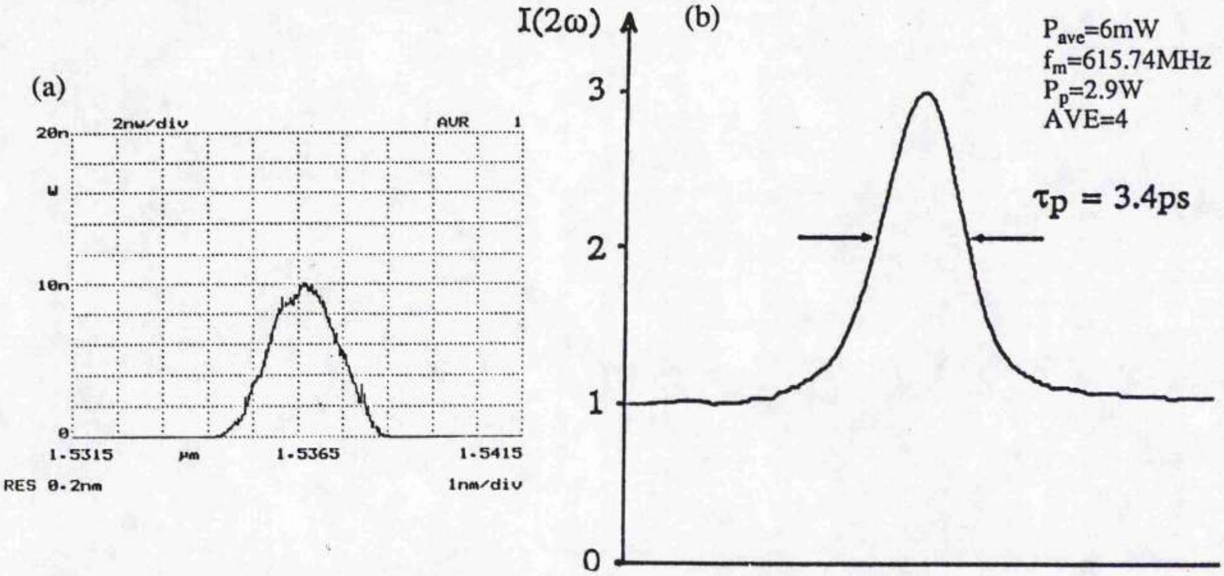

Figure 9.21 (a) Spectral and (b) temporal details of the output from the modelocked ring laser.

Again these results, in terms of pulse duration, are not far removed from that obtained for a modelocked semiconductor laser system with a passive fibre external cavity. Moreover, the frequency chirping due to gain saturation within the semiconductor amplifier still appeared to be dominating the features of the output pulses.

## 9.5 Modelocked 'mirrorless' hybrid InGaAsP/erbium-doped fibre laser

The principle of controlled amplifier modelocking was extended to include the attractive 'mirrorless' doped fibre lasers which were detailed in the previous chapter. The laser configuration was particularly simple and included only the semiconductor modulator, a 5m length of germano-silicate, erbium-doped fibre and a fibre directional coupler (see figure 9.22). A directional coupler conveniently allowed coupling of the semiconductor amplifier to the active fibre and also provided access for optical pumping. In this configuration the pump beam was directed away from the modulator thereby alleviating the risk of damage to the facet of the semiconductor amplifier.

The semiconductor modulator used here was based on a buried heterostructure laser which had an antireflection coating applied to one facet. The reflectivity of the coated facet was approximately $1.2 \times 10^{-3}$. This modulator scheme does not impose any restrictions on the modulation frequency used to modelock the laser, and hence it is ideal for the mirrorless fibre laser geometry.

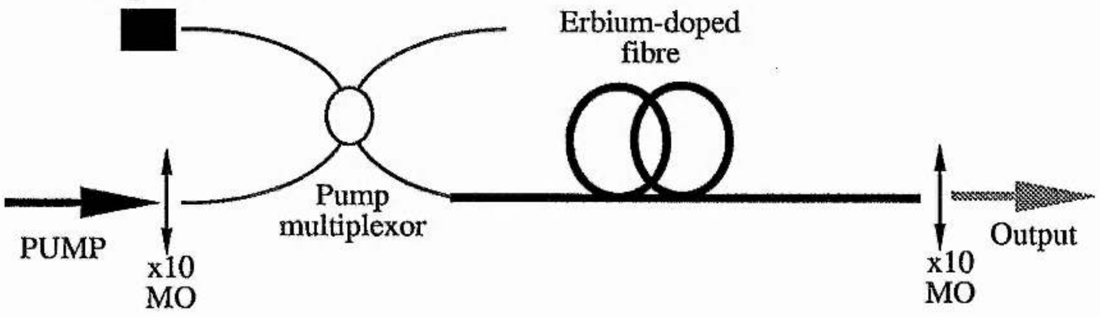

Figure 9.22 Hybrid InGaAsP/erbium-doped fibre laser geometry.

A combination of DC and RF modulation signals was supplied to the semiconductor modulator and a photodetector/oscilloscope was used to examine the laser output. At a resonant frequency of ~640MHz a typical example of the output pulses as monitored on a sampling oscilloscope is shown in figure 9.23. A more detailed examination of the modelocked laser output was obtained using the streak camera system described previously. The streak intensity records obtained suggested a pulse duration of 10ps, which when corrected for the system resolution became 8.7ps (see figure 9.24(a)). The pulse peak power was 1.98W at the highest average power of 11mW. Spectral measurements of the laser output indicated an oscillation bandwidth of 0.54nm which implies that the duration-bandwidth product was 0.59.

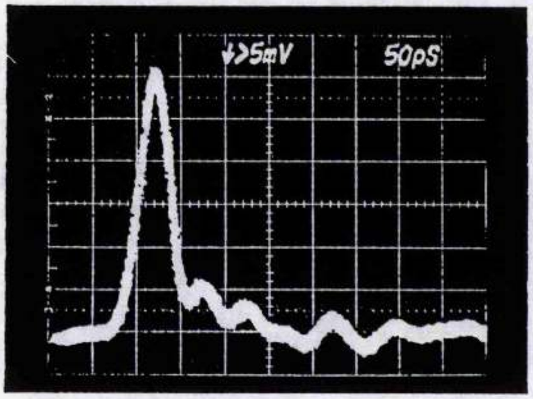

Figure 9.23 Modelocked output from a ‘mirrorless’ laser

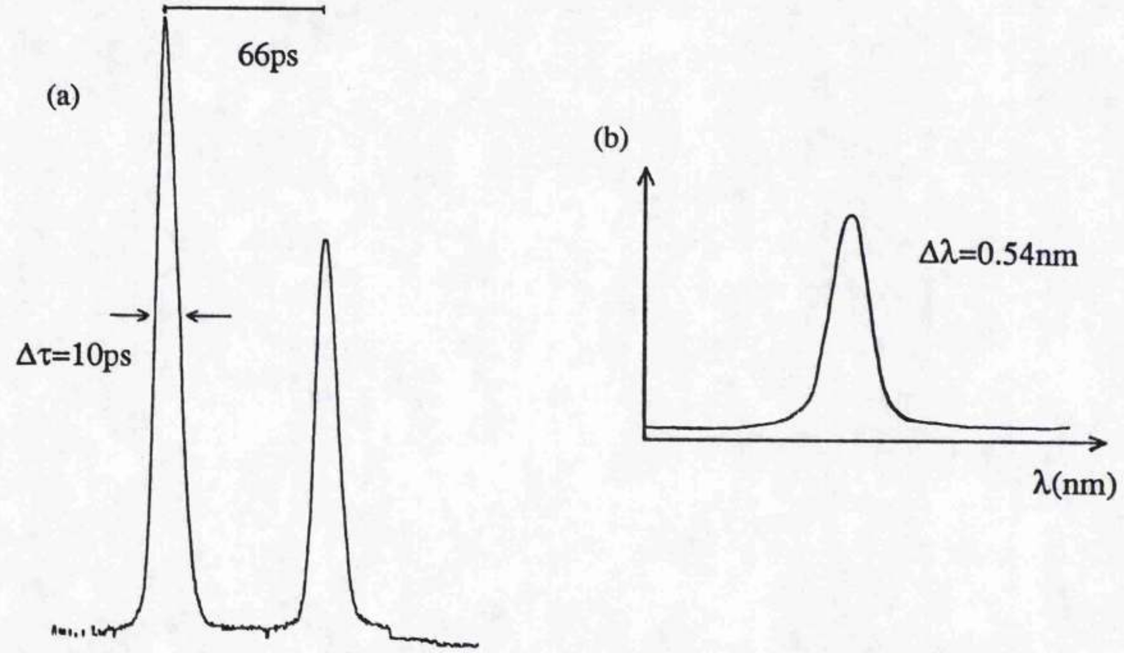

Figure 9.24 Temporal (a) and spectral (b) output from the hybrid laser configuration.

Although this laser emits longer pulses the performance can be considered superior to the ring laser for the following reasons. (i) This simple cavity design results in a very straightforward alignment procedure, (ii) the pumping geometry allows higher pumping levels to be maintained without the fear of damage to the semiconductor modulator. Incident pump powers of up to 200mW at $\lambda$=980nm were used in this experiment where the launch efficiency was estimated to be >65%. With such pumping the average modelocked output was as high as 11mW as illustrated in figure 9.25. This output power is comparable with the 20mW obtained under the same pumping conditions from a similar grating-tuned CW fibre laser configuration (see section 8.6.1 in chapter 8). (iii) Since the facet reflectivity was only $10^{-3}$ there was a significant spectral modulation of the semiconductor amplifier gain spectrum. In this case this proved advantageous since it provided a degree (although weak) of limitation on the oscillating laser bandwidth. For this reason, a clean unmodulated spectrum which basically consists of one Fabry-Perot mode of the semiconductor modulator subcavity was obtained (see figure 9.24(b)). Because of the weak nature of this effect the spectrum was difficult to stabilise but through judicious combinations of the drive signal components the spectrum could be stabilised. Improved spectral selectivity could be induced by using a modulator with a larger gain ripple, but this would of course compromise the minimum pulse duration achievable.

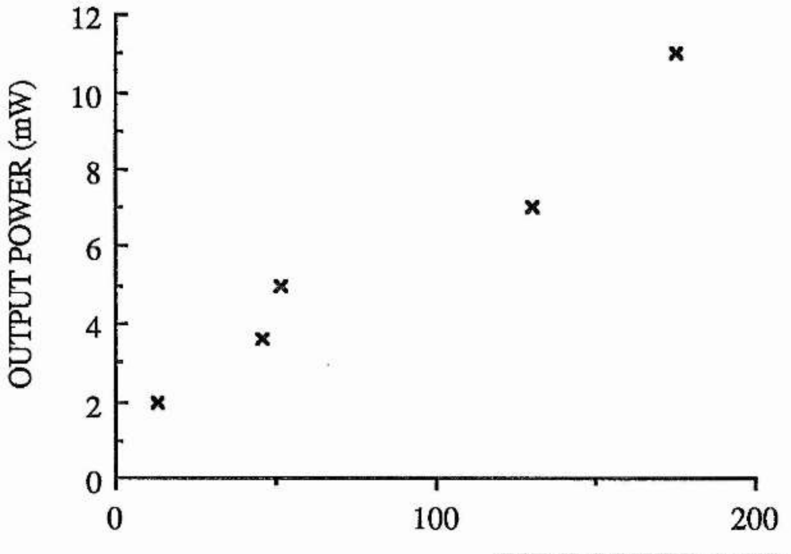

Figure 9.25 Output power characteristic of the modelocked mirrorless laser

## 9.6 Application of CAM to other laser types

To extend the applicability of the C.A.M. technique cavity configurations must be designed that allow ultrashort pulse generation from higher power lasers. One such arrangement is to use a cavity configuration similar to that used by Foster et al[214] to modelock the HeNe laser. Recently such laser configurations have received a lot of interest where the secondary resonator contains a nonlinear element[215], and this approach has been successfully demonstrated using an InGaAsP semiconductor amplifier in conjunction with a KCl:Tl colour-centre laser[216]. Although the amplifier was driven with direct current only it is believed that the addition of an RF component should extend the operational parameters of this laser. In particular, high frequency pulse sequences could be accessed due to the high-speed capability of the semiconductor amplifier where shorter and more compact cavity configurations could be used.

In principle, the C.A.M. technique could be applied to any laser medium where the emission falls within the gain bandwidth of the semiconductor amplifier. A few typical examples are indicated in Table 9.1. Since the advent of the semiconductor laser new materials have been investigated and developed to extend the wavelength coverage attainable, and although particular emphasis has been paid to near-infrared lasers from 0.7-1.6µm significant advances have been made in the demonstration of visible and far-infrared semiconductor lasers.

TABLE 1 Some potential C.A.M. laser systems

| LASER MEDIA | SEMICONDUCTOR AMPLIFIER | WAVELENGTH (µm) |
|---|---|---|
| KCl:Tl | InGaAsP | 1.45-1.57 |
| $Ti:Al_2O_3$ | GaAlAs | 0.80-0.87 |
| | InGaAs/GaAs strained layer | 0.9-1.1 |
| Nd:YAG | InGaAs/GaAs strained layer | 1.064 |
| | InGaAsP | 1.32 |

## 9.7 Summary

Various erbium-doped fibre laser configurations have been modelocked using an intracavity InGaAsP semiconductor amplifier modulator. This technique has been designated 'controlled amplifier modelocking' (C.A.M.). The modulation frequencies used in this work were compatible with those used in chapters 3 and 4 for modelocked passive fibre external-cavity semiconductor lasers therefore a direct comparison could be drawn between the two system approaches. It was clearly evident that significant improvements in average output power, peak pulse power, and pulse quality have been achieved using this C.A.M. technique.

Both ring and 'mirrorless' fibre cavity arrangements were investigated and this illustrates the degree of flexibility in resonator design afforded by using such high gain laser media. Pulse durations ranging from 3.5-10ps were produced at peak power levels around 2W. The amplitude noise performance of these lasers was also investigated revealing that the transfer of pump laser noise to the modelocked laser was minimal above ~50kHz, and significantly suppressed at lower frequencies. This feature relaxes the specification required of the pump laser for low-noise performance of the modelocked laser.

Higher power modelocked lasers could be configured using the C.A.M. technique by applying the popular coupled resonator approach. Alternatively, by employing higher power handling amplifiers the simpler linear and ring lasers described here could easily be extended to higher output power levels.

The modelocking technique described in this chapter utilises gain saturation of the semiconductor amplifier as the principal pulse-shaping nonlinearity. A different method that accesses the intrinsic nonlinearity of the optical fibre could also be applied as demonstrated by Kafka and Baer[217], and Smith et al[218]. By invoking the solitonic pulse-shaping mechanism similar pulse durations to those produced in this work have been readily achievable. It is proposed that by utilising the high-speed capability and short pulse gain-switching characteristics of a semiconductor laser with a stable, high power, erbium-doped fibre regenerative amplifier system that such soliton generation could be obtained in a rather straightforward manner. In this system a short (<50ps) gain switched pulse derived from a solitary semiconductor laser is injected into a highly-pumped, 'mirrorless', erbium-doped fibre laser. Selective amplification and subsequent solitonic pulse-shaping would then transform the output to a frequency tunable stream of high power ultrashort pulses.

## CHAPTER 10

# GENERAL CONCLUSIONS

### 10.1 Modelocked semiconductor lasers

In this thesis the experimental appraisal of active modelocking of InGaAsP semiconductor lasers emitting at 1.5μm has been described. Various cavity configurations have been employed with particular emphasis being given to optical fibre-based external resonators. External fibre cavities allow excellent mode control to be obtained without seriously compromising the inherent compactness of the semiconductor laser.

The problem of subpulsing in modelocked semiconductor lasers that have been current modulated at low frequencies has been addressed. Two techniques have been devised and evaluated for the generation of subpulse-free picosecond pulses from these lasers. The first method effectively reduces the temporal extent of the gain window produced by the externally applied modulation signal by a judicious combination of both RF and DC current levels. It has been shown that by combining a large RF signal with a small, or indeed zero direct current injection level that the induced gain window reduction leads to the desired subpulse suppression. As an alternative approach, subpulse elimination has been affected through a completely distinct mechanism in assymetric external-cavity configurations. In this type of configuration the large-scale pulse envelope shaping processes are quite distinct because the intracavity pulse undergoes two transits through the gain medium. It has been proposed that this leads to an attenuating region being established close to the internal semiconductor laser facet. The pulses exiting the laser cavity from either end therefore undergo different shaping processes and thus under certain conditions of a high DC current component subpulse elimination can be achieved. The presence of significant frequency chirp within the pulses generated by semiconductor lasers requires further study since shorter pulses could be accessed through its compensation, and also this would result in a highly desirable digital optical source.

The phase-noise content of an asymmetric-cavity modelocked laser was measured to follow that of the oscillator from which the modulation signal was derived. By employing low phase noise crystal oscillators the rms timing jitter of the laser could be reduced to 150fs in the range 50-500Hz and 60fs between 500-5000Hz. These performance figures represent the best obtained to date for any modelocked laser system, and provide evidence of the potential for modelocked semiconductor lasers in, for example, electro-optic sampling of integrated optical components.An enlarged range of applicability can therefore be envisaged for these low-phase noise, discrete pulse, modelocked laser sources although the low (<1mW) average output power may represent a serious drawback at present.

Amplification of output from the modelocked lasers using an erbium-doped fibre amplifier was also demonstrated, and peak pulse powers in excess of 5W were readily obtained. With the technological advances made since this work was undertaken scope exists for markedly improving upon the results obtained here. It was also pointed out that the long upper-state lifetime and the small gain cross section of the active fibre results in a variety of attractive features, namely (i) suppression of amplitude fluctuations of the pump laser, (ii) low crosstalk between different channels in a wavelength multiplexed communication system, and (iii) negligible gain saturation on a timescale of a single pulse (the gain saturates with the mean power level in the amplifier). All these observations confirm the very good linearity of the erbium:fibre amplifier system.

## 10.2 The Controlled-Amplifier Modulator

A new modelocking technique was developed called 'Controlled-Amplifier Modelocking' and has been applied in the generation of ultrashort pulses from erbium-doped fibre lasers. The flexibility in resonator design afforded by the high gain erbium-doped fibre medium resulted in the construction of very simple modelocked lasers without the usual requirement of high reflectivity cavity mirrors. The stability and quality of the ~4ps pulses obtained at enhanced average power levels by these lasers compares favourably with the modelocked oscillator/amplifier configurations used in earlier work.

This scheme represents the first example of active modelocking using a modulator possessing optical gain. The contrast ratio between the on and off states can be very high ranging from >10dB gain to being highly attenuating for the two states respectively. The on-state gain will be reduced due to gain saturation by the high peak power of the intracavity pulses, and this serves as the primary pulse shaping nonlinearity in the case of the erbium fibre lasers discussed in chapter 9. It is proposed that the CAM technique could be applicable to many other laser systems affecting more desirable output pulse properties than would otherwise be produced. Furthermore, by employing a semiconductor amplifier in a nonlinear external-cavity arrangement it has been shown by Grant et al that ~200fs pulses can be obtained from a KCl:Tl laser. Therefore much scope still exists for generating ultrashort laser pulses by incorporating semiconductor laser amplifiers into other laser systems. In particular two semiconductor laser amplifiers could be employed where one represents the gain medium of an external-cavity laser with the other being used within a separate, but coupled external resonator. A study of this type of system would initially entail bulk or optical fibre cavity arrangements with a view to the construction of monolithically integrated versions.

## 10.3 Ultra-high repetition rate lasers

The techniques for laser modelocking described in this thesis should apply equally well in lasers designed to access a higher repetition frequency output. The method of harmonic modelocking (used extensively in this work) can be applied to increase the output pulse frequency or alternatively the laser cavity length can be reduced. A fairly familiar query is 'can the output of the solitary diode laser chip be modelocked?' For active modelocking this would require modulation frequencies between 80-120GHz for most standard laser lengths, or ~40GHz for a longer ~1mm laser. Alternatively, integrated extended-cavity lasers employing, for instance, distributed Bragg reflectors[219] could be utilised although it is uncertain as to how long the total length can be made.

Microwave modulation at frequencies of 10's of GHz presents some problems not only in terms of cost but in the coupling of the signal to the laser. One suggestion would be to mount the laser in a resonant microwave cavity to which the output from a Gunn-diode oscillator[220] (itself in a resonant cavity) using a suitable waveguide. In this way the impedance matching problem is remote to the laser and by simply adjusting the resonator size would be sufficient to maximise the coupling. Also, the effects of contact impedance is circumvented. It still remains to be seen whether sufficient microwave power can be coupled into the laser in this manner and indeed if it is possible to establish modelocking.

Recently a modelocked semiconductor laser has been demonstrated where the pulse duration was 2.4ps and the repetition frequency was 108GHz[221]. This was achieved through saturable absorption passive modelocking using a two-section multiple quantum well laser. By combining these two approaches a hybrid modelocked laser system could be developed where the microwave modulation would introduce improved phase-noise performance due to the stabilisation of the repetition frequency. Also the average output power could be significantly increased over that of the pure passive modelocking case.

Another attractive method of achieving a high repetition source would be to time-division multiplex the output from an array of lower frequency modelocked lasers (alternatively the multiplexing could be performed in the wavelength domain. The outcome is essentially the same, although in communications systems the WDM technique is probably preferable.) Fibre directional couplers and erbium:fibre amplifiers could be employed to combine these lasers (each operated at a few gigahertz) to produce a high frequency pulse stream. For optical communications applications the multiplexing approach is desirable since the individual pulse streams could be encoded before multiplexing to alleviate the use of very high speed modulators.

## 10.4 Erbium-doped fibre amplifiers

The applicability and practicality of erbium-doped fibre amplifiers is becoming dramatically improved due to the availability of semiconductor laser pump sources. At present 1.48μm InGaAsP pump lasers are commercially available with fibre-coupled output powers as high as 50mW. It is believed that these powers will increase significantly and also that 980nm lasers of similar, and probably higher powers[222] will be commercially available in the near future. Such amplifier units when coupled to integrated modelocked lasers sources should provide compact low budget sources for optical telecommunications systems. Indeed such a source has been employed in a >12000km soliton propagation experiment at 2.4Gbit/s where the loss of the transmission line was compensated by discrete erbium amplifier packages[223].

One interesting application of erbium-doped fibre amplifiers which still requires further study is that of a soliton pre-amplifier. Here the output from a modelocked laser is launched into the amplifier and adiabatic soliton compression occurs due to the presence of gain. This topic has been studied by Nakazawa et al[176] but the full operating range of this device has yet to be determined. in view of the basic simplicity of this scheme its implementation may provide the most convenient, and perhaps the only, route to the femtosecond pulse regime using fibre integrated devices.

### 10.5 Erbium-doped fibre lasers

The study of continuous-wave rare-earth doped fibre lasers (see chapter 8) has shown that highly efficient laser oscillation can be achieved for a number of different active dopants. The main emphasis was on the erbium-doped silica optical fibre system although some data were presented for their neodymium counterparts, and output powers of up to 700 and 800mW were obtained respectively from these two systems. The potential tuning range of the erbium-doped fibre laser was demonstrated to extend from 1510nm to 1620nm, [the long wavelength tuning limit obtained was ~17nm greater than previously reported results] and was obtained by employing a length-tuning technique. As with erbium-doped fibre amplifiers the potential of fibre lasers will be greatly improved on incorporation of semiconductor laser pump sources. Here the pump power requirements are increased and in most cases greater than any single semiconductor laser. Therefore some form of pump beam combining is necessary to produce high power pump modules. Schemes to couple the output of two semiconductor lasers have been implemented (see 6.5) using fibre-based polarisation beamsplitters. By using two injection-locked pump lasers[224] the coherently combined output could be converted back to a linear polarisation state, and this is then suitable from combining with the output from an identical pump unit. Through coherent beam combining the output power from many individual pump lasers could be added until the required total power is achieved. Also due to the low locking power necessary many individual lasers could be injection locked from one moderate power, mode stabilised laser.

The effect of co-dopants on the fluorescence spectrum (and also the laser tuning range) was investigated. The system containing an alumina codopant was found to dramatically extend and smooth the fluorescence features compared to those of the germania codopant. For this and other related work it can be concluded that alumina codoped erbium-doped fibres are preferable for most potential applications. Nevertheless, for high gain, high numerical aperture amplifiers the most advanced erbium-doped fibres currently available utilise the dual codopant system of alumina/germania. Basically the alumina defines the spectral properties with the germania being added to reduce the core size whilst still maintaining a high fidelity single-mode waveguide.

By using long fibre lengths to obtain enhanced wavelength tuning a number of nonlinear effects became apparent. The first was self Q-switching which occurred at wavelengths between 1614 and 1620nm and so the CW tuning range was limited to <1614nm. It is believed that this self pulsation was related to saturation of the residual ground-state-absorption (GSA) in the unpumped section of the (quasi-four level) erbium-doped fibre. The repetition frequency was clearly related to the relaxation oscillation frequency of the laser but the exact mechanism for this effect remains the subject of further study. Another phenomenon also originating, we believe, in the effect of residual GSA of an unpumped section of the fibre was optical bistability. This was revealed as a hysteresis loop around the oscillation threshold of these relatively long lasers. From experimental observations an explanation based upon saturable absorption in an inhomogeneously pumped laser was advanced. Again further study of this phenomenon is required to justify this proposed mechanism. In particular, investigation of the effect at different oscillation wavelengths would be expected to change the form of the hysteresis feature due to the variation in the GSA with wavelength. Also, the practicality of this device requires some study with reference to the speed of the effect and if scaling to lower operating powers is possible.

Finally, the technique of Q-switching to produce high peak power pulses of ~tens of nanoseconds duration was applied to the low finesse erbium fibre laser. For this purpose a mechanical chopper was inserted into the laser cavity at the focal point of two microscope objectives such that the opening time of the switch was minimised. In this way pulses with durations of <80ns and peak powers of up to 800W were obtained. [The maximum pulse energies obtained were ~73μJ.] These extracavity peak powers represent the highest yet reported from any fibre laser device. Further improvements in the Q-switch opening timeshould enable shorter, higher peak power pulses to be generated.

The presence of the first overtone of the hydroxyl ion resonance at ~1.4μm[225] [the fundamental stretching vibration peak occurs at ~2.72μm] leads to significant absorption in the body around the emission wavelengths of erbium fibre lasers. Therefore Q-switched erbium fibre lasers could be effectively employed in the field of medical lasers[212], where the flexible nature of the fibre host lends itself to insertion into the body for internal microsurgery purposes. The 2.8μm emission observed from erbium-doped fluorozirconate fibre lasers[226] further extends the potential of fibre lasers in biomedical applications.

# APPENDIX A

# ERBIUM-DOPED FIBRE FLUORESCENCE MEASUREMENTS

## A.1 Fluorescence spectra

To demonstrate the effects that the ground state absorption (GSA) has on the erbium-doped fibre gain spectrum when the laser length is increased, an experiment involving the set-up shown in figure A.1 was carried out. Fluorescence spectra were recorded using a computer-controlled scanning monochromator for two different 1m long erbium-doped fibre samples. One fibre was an alumina codoped fibre with a high erbium concentration (2500ppm), whereas the other was codoped with germania and had a lower erbium doping concentration of 300ppm.

In figure A.2(a), (b) the spectral progression of the active fibre fluorescence is reproduced for a range of pump powers. These curves clearly indicate the effects of the GSA on the fluorescence output and hence the gain of the fibre. The output of the $GeO_2$ codoped fibre saturates much more quickly because the erbium concentration is some 8 times less than in the $Al_2O_3$ codoped sample. By normalising these spectra (see figure A.3) the differences can be dramatically portrayed. If the optical coupling efficiency of the pump radiation is considered to be equal in both cases then the two data sets can be compared, in terms of length of fibre that is pumped, by dividing the pump power in figure A.3(a) by a factor of ~18. This factor takes into account both the relative dopant concentration and the differences in fibre core radii.

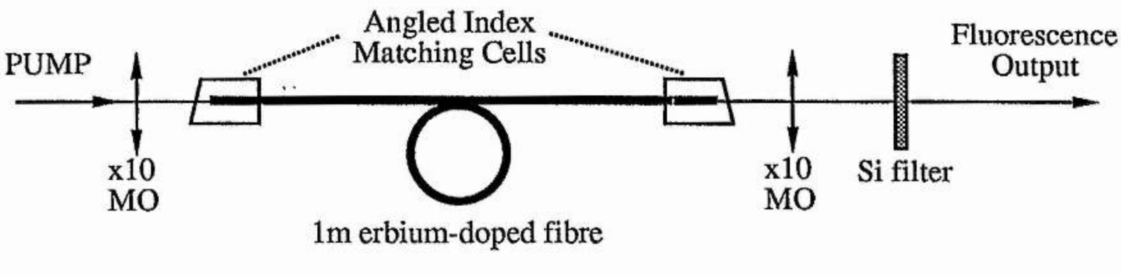

Figure A.1. Experimental configuration.

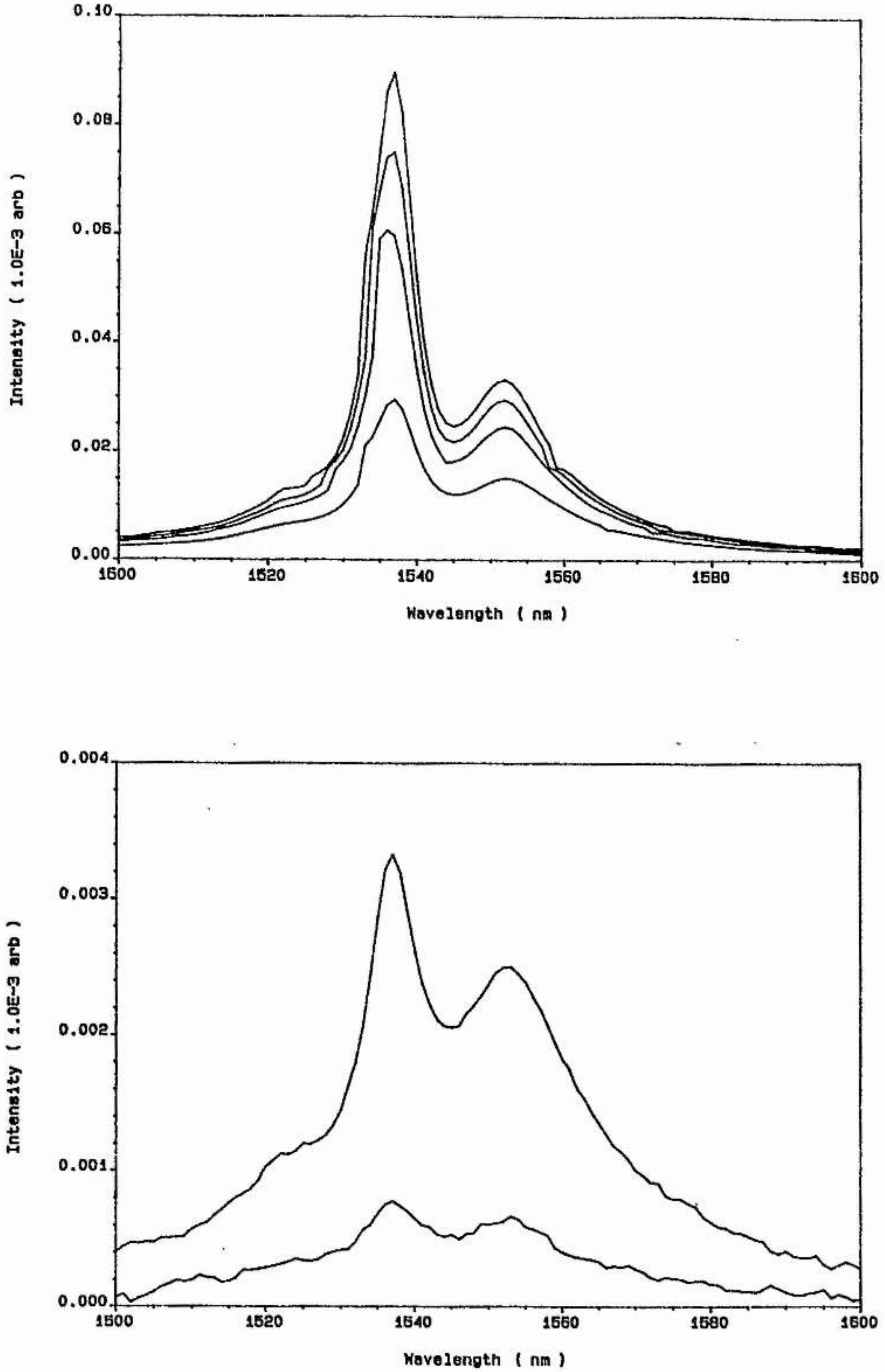

Figure A.2(a) Spectral progression for the germania co-doped fibre sample

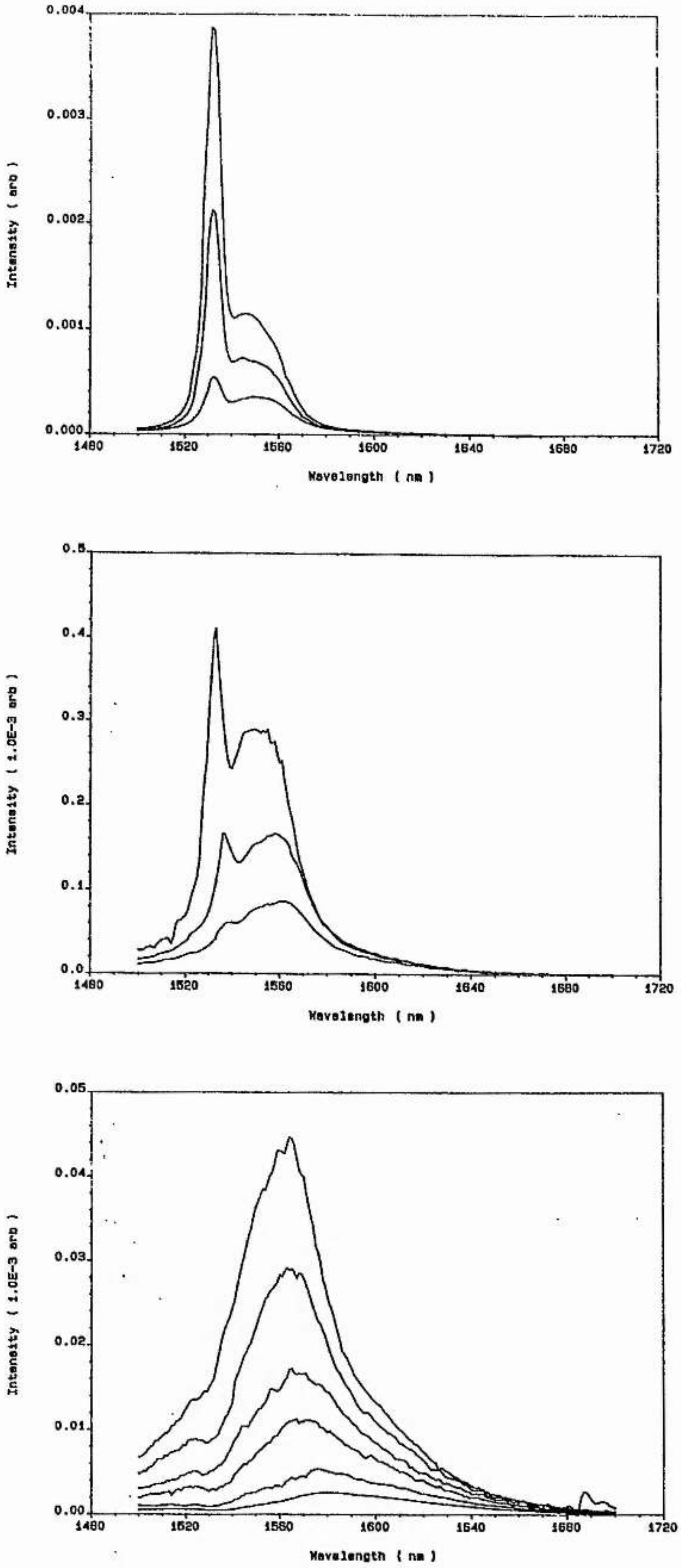

Figure A.2(b). As A.2(a) but for the alumina co-doped fibre sample

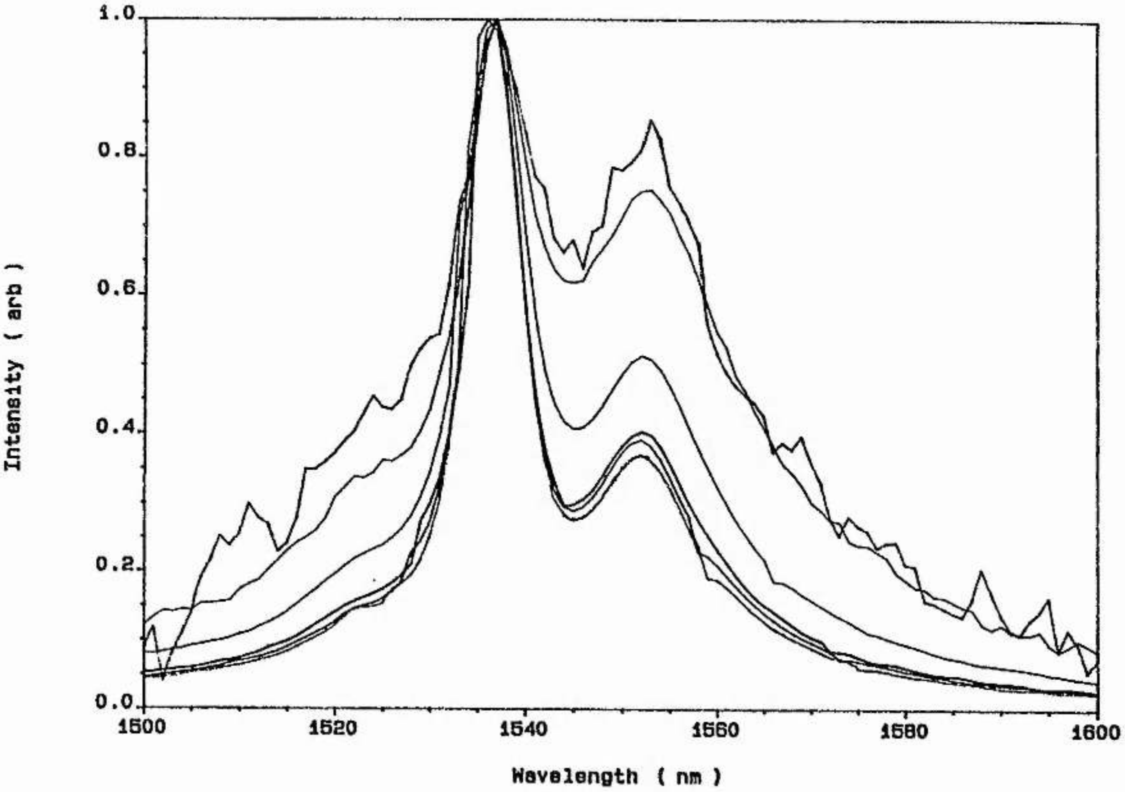

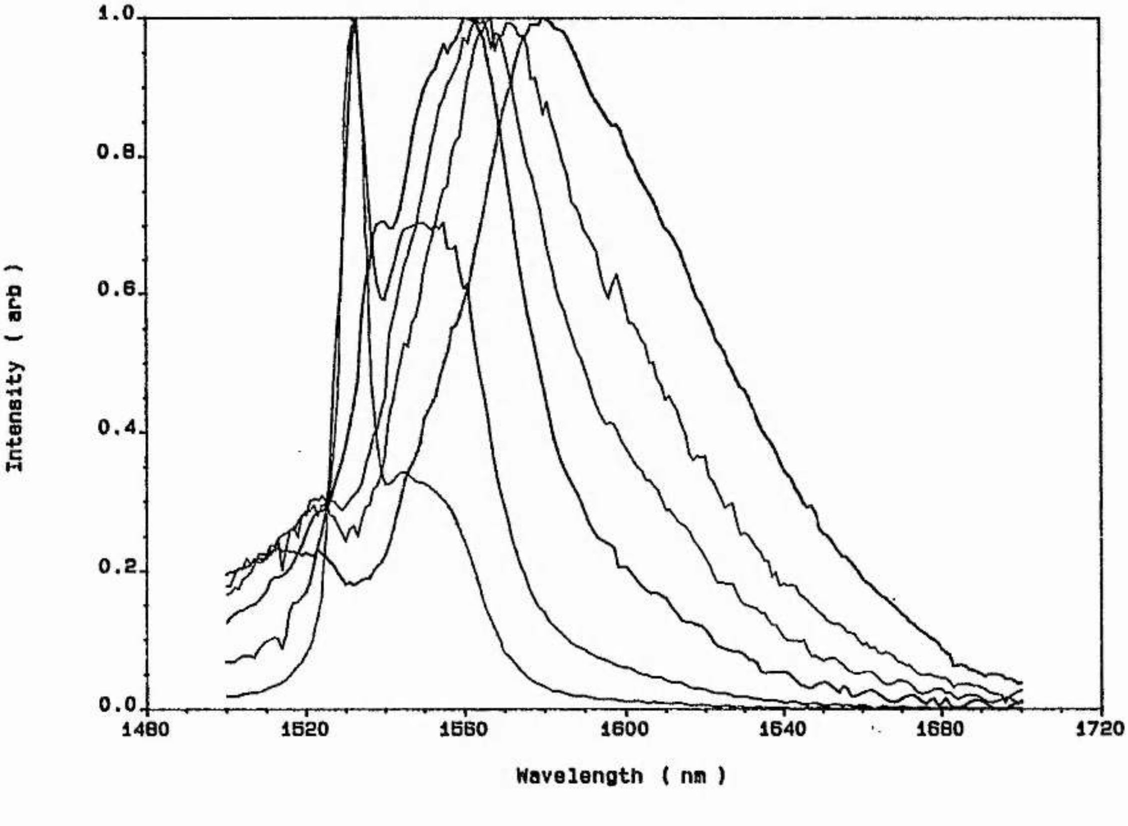

Figure A.3 Spectra of figures A.2 after normalisation. (a) germania co-doped, (b) alumina co-doped

In figure A.4 the fluorescence power saturation is shown for the $GeO_2$ fibre sample. Note the emergence of the peak at ~1520nm which occurs for very high pumping levels due to the saturation of the large GSA in this spectral region. This feature would be evident at lower pump powers if either a very short fibre was used or if the sidelight spectrum was monitored. Since this was not practical, this feature only becomes apparent at high pump levels such that complete inversion of the full fibre length was obtained.

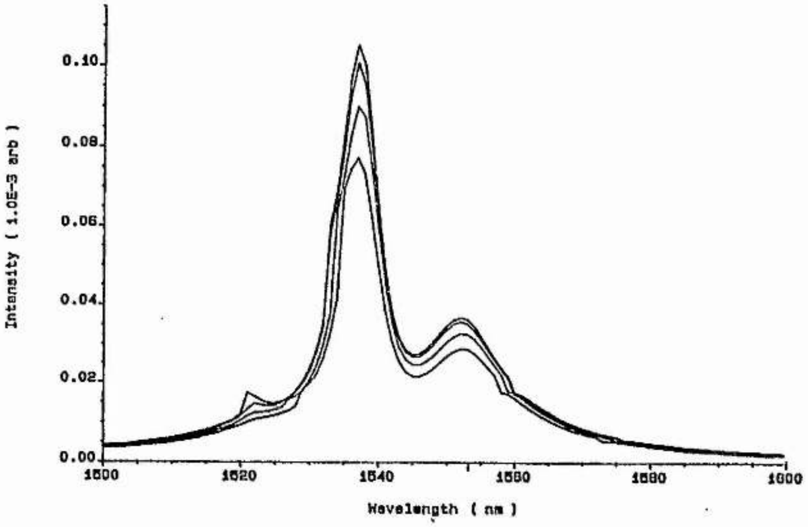

Figure A.4(a) Fluorescence spectra of $GeO_2$ co-doped fibre sample with high pumping

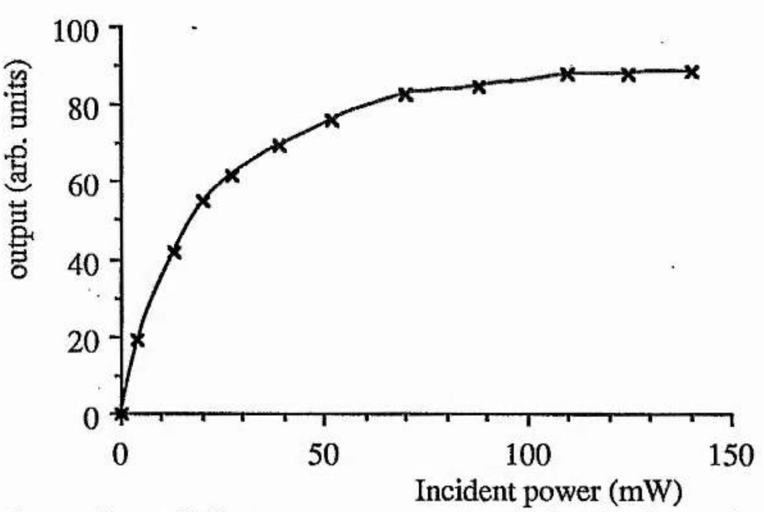

Figure A.4(b) Saturation of fluorescence output of the $GeO_2$ codoped fibre sample, for $\lambda_p$=980nm.

Although in these figures the variable parameter was the pump power, since the shape is solely dependent on the residual GSA (which varies with $\lambda$) then similar results would be obtained by varying the fibre length and using a constant pump intensity[206]. It is this effect which primarily determines the shape of the laser tuning curves observed in practice as described in chapter 8.

## A.2 Fibre laser length tuning

The laser tuning range is related to the power gain spectrum (in dB's) which in turn has the same shape as the fluorescence spectrum. For long fibre lasers the tuning is shifted to longer wavelengths, and since all the pump power is absorbed in the first few metres then the laser has high efficiency. At these long wavelengths the GSA is small so moderately overlong fibres can be tolerated. However, the oscillation threshold is increased because the gain-per-metre at such wavelengths is quite low.

For short fibre lasers the tuning curve is essentially that of the high pump (or saturated) fluorescence spectra of figure A.2, since only at these wavelengths does the fibre have sufficient gain-per-metre to permit oscillation. Here the threshold is low but complete pumping of the total fibre length is essential since the GSA is also very large and thus considerable pump power can exit the fibre unabsorbed. Thus the laser efficiency is reduced and consequently the output power is limited.

Fibre lasers of intermediate length exhibit a steady shift to longer wavelengths with increasing length and the laser efficiency also increases and saturates when complete pump absorption is obtained. Further length increases enable the long wavelength tail of the gain spectrum to be exploited since the higher gain region at shorter wavelengths experience increasing GSA and this inhibits gain clamping due to amplified spontaneous emission (ASE). By exploiting this technique a total laser tuning range exceeding 100nm has been demonstrated using three fibre lengths (see section 8.7).

## A.3 Saturated fluorescence spectra in $Al_2O_3$ and $GeO_2$ fibre media

Saturated fluorescence spectra of both alumina and germania codoped fibre samples are shown in figure A.5. There is a clear short wavelength shift of the main peak in the alumina spectrum, and also the curve is also much smoother and broader than its germania counterpart.

On close examination structure within the emission band of the $GeO_2$ trace can be resolved, and the long wavelength tail is seen to be compromised.

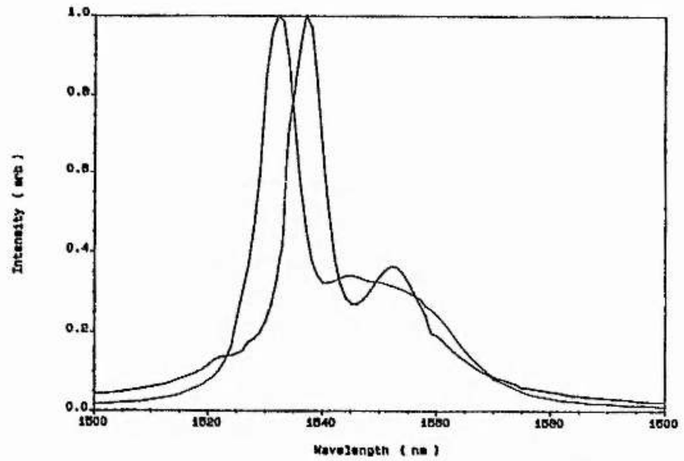

Figure A.5 Saturated fluorescence spectra of the two doped fibre samples. (Traces have been normalised)

## A.4. Fluorescence lifetime of erbium-doped fibres

The fluorescence decay of the germania codoped fibre was obtained by chopping the input pump beam using a mechanical chopper. The fluorescence output is shown in figure A.6 for the pump wavelengths of 810 and 980nm. The 980nm-related trace can be accurately fitted to an exponential function with a 1/e time of 7.8ms. As a consequence of the large excited state absorption (ESA) at ~810nm the corresponding fluorescence decay is non-exponential[207]. A non-exponential decay is typical of laser media with significant pump ESA because this results in a delay in the emission of a fraction of the inverted atoms. Since these atoms are further excited into high energy levels and must undergo a series of non-radiative decays before being available to decay radiatively from the upper laser level (see figure A.7). The decay will tend towards the exponential form in a time dependent upon the non-radiative decay processes involved. The absence of this phenomena for the 980nm pump band confirms the absence of ESA at this pump wavelength.

The green emission (broad-band around 547nm) which accompanies ~800nm pumping was observed to increase during the pumping cycle, because the population inversion steadily increases in this period and the probability for ESA increases. Also, the decay time for the green emission was found to be very fast (limited by detector bandwidth to <20μs).

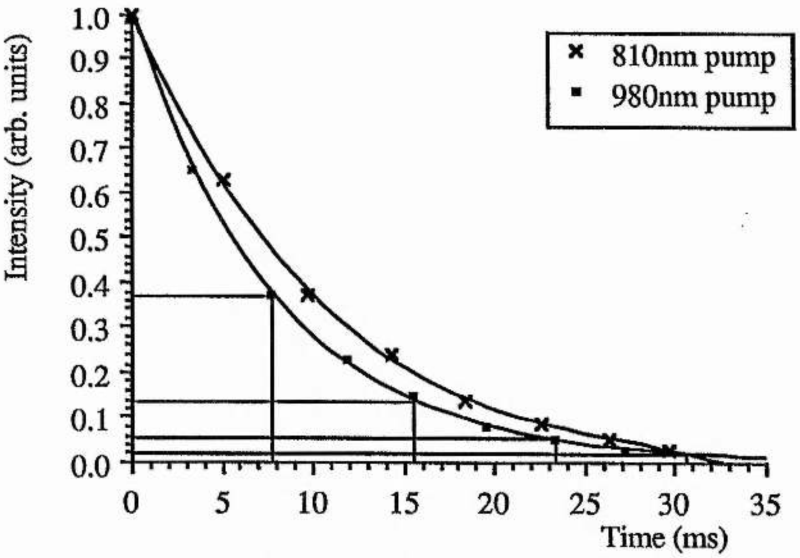

Figure A.6 Fluorescence decay of erbium-doped fibre ($GeO_2$)

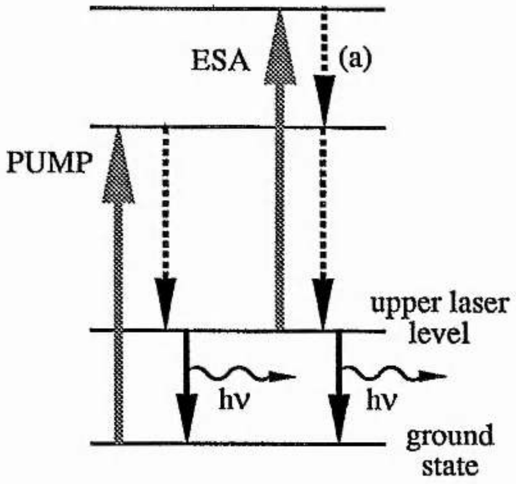

Figure A.7 Fluorescence delay via pump ESA. Relaxation of excited state to pump level (transition (a)) may involve many energy levels.

## References

1. C. Kittel. 'Introduction to Solid State Physics', Wiley, Hew York, 1971

2. J.M. Ziman. 'Principles of the Theory of Solids', Cambridge, 2nd ed., 1972

3. R. Dupuis. IEEE J. Quantum Electron., 23, p659+the following four papers, 1987

4. R.N. Hall, G.E. Fenner, J.d. Kingsley, T.J. Soltys, R.O. Carlson. Phys. Rev. Lett., 9, p366, 1962

M.I. Nathan, W.P. Dumke, G. Burns, F.H. Dill, G.J. Lasher. Appl. Phys. Lett., 1, p62, 1962

T.M. Quist, R.H. Rediker, R.J. Keyes, W.E. Krag, B. Lax, A.L. McWhorter, H.J. Zeiger. Appl. Phys. Lett., 1, p91, 1962

N. Holonyak, Jr, B.F. Bevacqua. Appl. Phys. Lett., 1, p82, 1962

5. M.G.A. Bernard, G. Duraffourg. Phys. Status Solidi, 1, p699, 1961

6. R.J. Phelan, R.H. Rediker. Appl. Phys. Lett., 6. p70, 1965;

C.B. Roxlo, M.M. Salour. Appl. Phys. Lett., 38, p738, 1981;

B. Valk, M.M. Salour, G. Munns, H. Morkoc. Appl. Phys. Lett., 49, p549, 1986

7. G.P. Agrawal, N.K. Dutta. 'Long Wavelength Semiconductor Lasers', Van Nostrand Reinhold, New York, 1986

8. W.P. Dumke. Phys. Rev., 27, p1559, 1962

9. I. Hayashi, M.B. Panish, P.W. Foy. IEEE J. Quantum Electron., 5, p211, 1969;

Zh. I. Alferov, V.M. Andreev, E.L. Portnoi, M.K. Trakan. Sov. Phys. Semicond., 3, p1107, 1970

10. L.A. D'Asaro. J. Luminescence, 7, p310, 1973

11. I. Hayashi, M.B. Panish, P.W. Foy, S. Sumski, Appl. Phys. Lett., 17, p81, 1970;

Zh. I. Alferov, V.M. Andreev, D.Z. Garbazov, Yu. V. Zhilyaev, E.P. Morozov, E.L. Portnoi, V.G. Trofim. Sov. Phys. Semicond., 4, p1573, 1971

12. J.E. Ripper, J.C. Dyment, L.A. D'Asaro. T.L. Pauli. Appl. Phys. Lett., 18, p155, 1971

13. W.T. Tsang. Appl. Phys. Lett., 38, p204, 1981

14. R. Dingle, W. Wiegmann, C.H. Henry. Phys. Rev. Lett., 33, p827, 1974

15. T.R. Chen, L. Eng, B. Zhao, Y.H. Yhuang, S. Sanders, H. Morkoc, A. Yariv. IEEE J. Quantum Electron., 26, p1183, 1990

16. M. Bagley, R. Wyatt, D.J. Elton, H.J. Wickes, P.C. Spurdens, C.P. Seltzer, D.M. Cooper, W.J. Devlin. Elecrton. Lett., 26, p269, 1990

17. M. Asada, Y. Miyamoto, Y. Suematsu. IEEE J. Quantum Electron., 22, p1915, 1986

18. G.H.B. Thompson. 'Physics of Semiconductor Laser Devices', John Wiley & Sons, 1980;

19. I.P. Kaminow, L.W. Stulz, J.S. Ko, A.G. Dentai, R.E. Nahory, J.C. DeWinter, R.L. Hartman. IEEE. J.Quantum.Electron., p1312, 1983;

S. Turley. IEEE. J.Quantum.Electron., p1186, 1983

20. G.P. Agrawal. J. Lightwave Tech., LT-2, p537, 1984

21. D. Renner, A.J. Collar, P.D. Greene, G.D. Henshall. Electron. Lett., 21, p1007, 1985

22. T.Y. Miya, T.Terunama, T. Hosaka, T. Migoshita. Electron. Lett., 15, p106, 1979

23. A. Sugimura, K. Daikoku, N. Imoto, T. Miya. IEEE J. Quantum Electron., 16, p215, 1980

24. K.J. Blow, N.J Doran. IEEE Proc., 134, pt J, p138, 1987

25. 'Picosecond Phenomema', Edited by C.V. Shank, E.P. Ippen, S.L. Shapiro. Springer, Berlin, 1978

26. A.E. Siegman. 'Lasers', Oxford University Press, 1986

27. A.J. DeMaria, D.A. Stetser, H. Heynau. Appl. Phys. Lett., 8, p174, 1966

28. H.A. Haus. IEEE J. Quantum Electron., 11, p323, 1975

29. P.T. Ho, L.A. Glasser, E.P. Ippen, H.A. Haus. Appl. Pyhs. Lett., 33, p241, 1978

30. L.A. Glasser. Electron. Lett., 14, p725, 1978
31. G. Eisenstein, R.S. Tucker, U. Koren, S.K. Korotky. IEEE. J. Quantum. Electron., 22, p142, 1986
32. E.P.Ippen, D.J. Eilenberger, R.W. Dixon. Appl. Phys. Lett., 37, p267, 1980
33. J.P. van der Ziel, W.T. Tsang, R.A. Logan, R.M. Mikulyak, W.M. Augustyniak. Appl. Phys. Lett., 39, p525, 1981
34. P.W. Smith, Y. Silberberg, D.A.B. Miller. J. Opt. Soc. Am. B, 2, p1228, 1985
35. H.A. Haus. J. Appl. Phys., 51, p4042, 1980
36. N.A. Olsson. M.G. Oberg, L.D. Tzeng, T. Cella. Electron. Lett., 24, p569, 1988
37. W. Rideout, R. Holmstrom, J. LaCourse, E. Meland, W. Powazinik. Electron. Lett., 26, p37, 1990
38. D.G. Parker, P.G. Say, A.M. Hansom, W. Sibbett. Electron. Lett., 23, p527, 1987
39. Tektronix product guide
40. D.J. Bradley, B. Liddy, W.E. Sleat. Opt. Comm., 2, p391, 1971
41. W. Sibbett. Proc. XVth int. conf. on high speed photography and photonics, SPIE 21, p226, 1982
42. A. Finch, Y. Liu, H. Niu, W. Sibbett, W.E. Sleat, D.S. Walker, Q.L.Yang, H. Zhang. Ultrafast Phenomena IV, Springer Series in Chem. Phys., 48, p159, 1988
43. A. Finch, Y. Liu, W.E. Sleat, W. Sibbett. Rev. Sci. Instrum., May, 1989
44. K.L. Sala, G.A. Kenny-Wallace, G.E. Hall. IEEE J. Quantum Electron., 16, p990, 1980
45. J.-C.M. Diels, J.J. Fontaine, I.C. McMichael, F. Simoni. Appl. Opt., 24, p1270, 1985
46. G. Chanin, J.C. Lecuillier. Infrared Phys., 18, p589, 1978
47. R.P. Salathe. Appl. Phys, 20, p1, 1979.
48. H. Kogelnik, C.V. Shank. Appl. Phys. Lett., 18, p152, 1971
49. H. Kawanishi, Y. Suematsu, Y. Itaya, S. Arai. IEEE J. Quantum Electron., 15, p701, 1979
50. S. Akiba, M. Usami, K. Utaka. J. Lightwave Tech., LT-5, p1564, 1987
51. S. Wang. IEEE J. Quantum Electron., 10, p413, 1974
52. N.K. Dutta, R.J. Nelson. Appl. Phys. Lett., 38, p407, 1980
53. M.W. Fleming, A. Mooradian. IEEE. J. Quantum. Electron. 17, p44, 1981
54. N.A. Olsson, J.P. van der Ziel. J. Lightwave Tech., LT-5, p510, 1987
55. L.A. Glasser. Electron. Lett., 14, p725, 1978
56. F.K. Rienhart, I. Hayashi, M.B. Panish. J. Appl. Phys 42, p4466, 1971
57. T. Ikegami. IEEE J. Quantum. Electron. 8, p470, 1972
58. R.H. Clarke. Bell Sys. Tech., 62, p2885, 1983
59. T. Saitoh, T. Mukai. Electron. Lett. 23, p219, 1987
60. G. Eisenstein, L.W. Stulz. Appl. Opt., 23, p161, 1984
61. B. Mersali, G. Gelly, A. Accard, J-L Lafragette, P. Doussiere, M. Lambert, B. Fernier. Electron. Lett., 26, p124, 1990
62. I.P. Kaminow, G. Eisenstein, L.W. Stulz. IEEE J. Quantum Electron., 19, p493, 1983
63. E. Mohn, R.F. Broom, Ch. Deutsch, J. Hatz. Phys. Lett. 24A, p561, 1967
64. D. Marcuse. J. Lightwave Tech., LT-7, p336, 1989
65. J.T.K. Chang, PhD Thesis, Imperial College London, 1988
66. C.E. Zah, J.S. Osinski, C. Caneau, S.G. Menocal, L.A. Reith, J. Salzman, F.K. Shokoohi, T.P. Lee. Electron. Lett., 23, p990, 1987
67. C. Armistead. Private Communication
68. P.E. Barnsley, J.J. Isaac, D.J. Elton. Electron. Lett., 26, p825, 1990
69. J. Chen. PhD Thesis, Imperial College London, 1985
70. C.E. Zah, J.S. Osinski, C. Caneau, S.G. Menocal, L.A. Reith, J. Salzman, F.K. Shokoohi, T.P. Lee. Electron. Lett., 23, p990, 1987

71. The Optometrics Group product guide
72. Quantex Infrared Sensor Model No. Q-32-R
73. J.O. Binder, G.D. Cohen, L.A. Coldren. IEEE J. Quantum. Electron., 26, p1200, 1990
74. R. Wyatt, W.J. Devlin. Electron. Lett., 19, p110, 1983.
75. R. Lang, K. Kobayashi. IEEE J. Quantum. Electron., 16, p347, 1980
76. K.-Y. Liou, Y.K. Jhee, G. Eisenstein, R.S. Tucker, R.T. Ku, T.M. Shen, U.K. Chakrabarti, P.J. Anthony. Appl. Phys. Lett., 48, p1039, 1986
77. C.H. Henry. J. Lightwave Tech., LT-4, p288, 1986
78. N. Schunk, K. Petermann. IEEE J. Quantum. Electron., 24, p1242, 1988
79. R.G. Harrison, D.J. Biswas. Progress in Quantum Electronics, 10, 1985
80. W. Ruhle, P. Brosson. J. Appl. Phys., 51, p5949, 1980
81. F.R. Nash, W.J. Sundbury, R.L. Hartman, J.R. Pawlik, D.A. Ackerman, N.K. Dutta, R.W. Dixon. AT+T Tech. J., 64, p809, 1985
82. M. Fuchs, W. Hoppe. Appl. Phys. Lett., 52, p1936, 1988
83. J. Mellis, S.A. Al-Chalabi, K.H. Cameron, R. Wyatt, J.C. Regnault, W.J. Devlin, M.C. Brain. Electron. Lett., 24, p988, 1988
84. Kindly provided by W. Devlin of BTRL
85. M.C. Farries, J. Buus, M. Kearley. Electron. Lett., 26, p1626, 1990
86. M.C. Farries. Private communication
87. D. Mehuys, M. Mittelsen, A. Yariv. Electron. Lett., 25, p143, 1989
M. Mittelsen, D. Mehuys, A. Yariv, J.E. Ungar,R. Sarfaty. Appl. Phys. Lett., 54, p1092, 1989
88. G. Wenke, Y. Zhu. Appl. Opt., 22, p3837, 1983
89. H. Kuwahara, M. Sasaki, N. Tokoyo. Appl. Opt., 19, p2578, 1980
90. I. Bennion, D.C.J. Reid, C.J. Rowe, W.J. Stewart. Electron. Lett., 22, p341, 1986
91. W.V. Sorin, S.A. Newton. Optics Lett., 13, p731, 1988
92. C.A. Park, C.J. Rowe, J. Buus, D.C.J. Reid, A. Carter, I. Bennion. Elctron. Lett., 22, p1132, 1986
93. P.N. Kean, K. Smith, B.D. Sinclair, W. Sibbett, C.J. Rowe, D.C.J. Reid. Electron. Lett., 23, p1241, 1987
94. S. Enochs. Photonics Spectra, p119, Sept. 1987
95. T. Bricheno, A. Fielding. Electron. Lett., 20, p230, 1984
96. T. Bricheno, V. Baker. Electron. Lett., 21, p251, 1985;
S.K. Sheem. J. Appl. Pyhs., 52, p3865, 1982
97. I.D. Miller, D.B. Mortimore, W.P. Urquhart, B.J. Ainslie, S.P. Craig, C.A. Millar, D.B. Payne. Appl. Opt., 26, p2197, 1987
98. K.J. Blow, N.J. Doran, B.K. Nayar. Opt. Lett., 14, p754, 1989;
A.G. Bulushev, E.M. Dianov, O.G. Okhotnikov. Opt. Lett., 15, p968, 1990
99. D.J. Kuizenga, A.E. Siegman. IEEE J. Quantum Electron., 6, p694, 1970;
H.A. Haus. IEEE J. Quantum Electron., 11, p323, 1975;
A.J. DeMaria, W.H. Glenn, jr., M.J. Brienza, M.E. Mack. Proc. IEEE, 57, p2, 1969;
P.W. Smith. Proc. IEEE, 58, p1342, 1970
100. J. C. AuYeung. IEEE. J. Quantum. Electron. 17, p398, 1981
101. A. Valster, L.J. Meuleman, P.I.Kuindersma, T.V. Dongen. Electron. Lett., 22, p16, 1986
102. P. Horowitz, W. Hill. 'The Art of Electronics', Cambridge University Press, 1980
103. D. Marcuse, T.P. Lee. IEEE J. Quantum. Electron., 19, p1397, 1983
104. R.S. Tucker, I.P. Kaminow. J. Lightwave Tech., LT-2, p385, 1984
105. S. Takamiya, F. Kitasawa, J,-I, Nishizuwa. Proc. IEEE. (Letters), 56, p135, 1968;
K.Y. Lau. Appl. Phys. Lett., 52, p2214, 1988

106. K.Y. Lau. Appl. Phys. Lett., 52, p257, 1988
107. A. Yariv. 'Quantum Electronics', 2nd ed. Wiley. New York. 1975
108. L. Hai-Feng, M. Fukazawa, Y. Kawai, T. Kamiya. IEEE J. Quantum Electron., 25, p1417, 1989
109. K. Otsuka. In 'Picosecond Optoelectronic Devices', C.H. Lee, Ed., New York:Academic, p34, 1984
110. M. Nakazawa, K. Sukuki, Y. Kimura. Opt. Lett., 15, p715, 1990
111. A. Takada, T. Sugie, M. Sarawatari. Electron. Lett., 21, p969, 1985
112. S. Taracha, K. Otsuka. IEEE J. Quantum Electron. 17, p810, 1981
113. J.T.K. Chang, J.I. Vukusic. IEEE J. Quantum. Electron. 23, p1329, 1987
114. R.S. Tucker, G. Eisenstein, I.P. Kaminow. Electron. Lett., 19, p553, 1983
115. D. Marcuse, J. Stone. J. Lightwave Tech., LT-4, p377, 1986
116. Philips Components, type OM335
117. C. Lin, T.P. Lee, C.A. Burrus. Appl. Phys. Lett., 42, p141, 1983
    A.S. Sudbo. IEEE J. Quantum. Electron., 22, p1006, 1986
118. J,-P. Hamiaide, Ph. Emplit. Opt. Lett., 14, p689, 1989
119. M. Osinski, M.J. Adams. Opt. Comm., 47, p190, 1983
120. E.B. Treacy, IEEE J. Quantum Electron., 5, p454, 1969
121. B.J. Ainslie, C.R. Day. J. Lightwave Tech., LT-4, p967, 1986
122. P.J. Delfyett, C.H. Lee, L. Florez, N. Stoffel, N. Andreadalis, T. Gmitter, G.A. Alphonse, J.C. Connelly. Ultrafast Phenomena, Monterey, 1990
123. G.P. Agrawal, N.A. Olsson. IEEE J. Quantum. Electron. 25, p2297, 1989
124. P.A. Morton, R.J. Helkey, S.W. Corzine, J.E. Bowers. IEEE J. Quantum Electron., 25, p1426, 1989
125. R. Fork, C.V. Shank, R. Yen, C.A. Hirlimann. IEEE J. Quantum. Electron. 19, p500. 1983
126. A. Olsson, C.L. Tang. IEEE J. Quantum. Electron. 17, p1977, 1981
    J. McInerney, L. Reekie, D.J. Bradley. Electron. Lett., 21, p117, 1985
127. R.M. Jopson, G. Eisenstein, M.S. Whalen, K.L. Hall, U. Koren, J.R. Simpson. Appl, Phys. Lett., 48, p204, 1986
128. H.C. Lefevre. Electron. Lett., 16, p778, 1980
129. R.M. Jopson, G. Eisenstein, M.S. Whalen, K.L. Hall, U. Koren, R.J. Simpson. Appl. Phys. Lett. 48, p204, 1986\
130. P.A. Morton, R.J. Helkey, J.E. Bowers, IEEE J. Quantum Electron., 25, p2621, 1989
131. J.C. AuYeung, A.R. Johnston. Appl. Phys. Lett., 40, p112, 1982
132. R.S. Tucker, G. Eisenstein, I.P. Kaminow. Electron. Lett., 19, p552, 1983
133. A.M. Lomax, I.H. White, W.J. Devlin, D.M. Cooper. Proc. IEEE Colloq. Dig. 1989/119, paper no. 12, 1989
134. K.J. Weingarten, M.J.W. Rodwell, D.M. Bloom. IEEE. J. Quantum. Electron. 24, p198, 1988
135. D. Walker, W. Sleat, J. Evans, W. Sibbett. 19th International Congress On High Speed Photography And Photonics, Cambridge, paper no. C56, Sept. 1990.
136. A. Finch, X. Zhu, P.N. Kean, W. Sibbett. IEEE J. Quantum. Electron. 26, p1115, 1990
137. D. von der Linde. Appl. Phys. B, 39, p201, 1986,
138. M.J.W. Rodwell, D.M. Bloom, K.J. Wiengarten, IEEE J. Quantum. Electron. 25, p817, 1989
139. Hewlett Packard Application note no. 207
140. G. Eisenstein, R.S. Tucker, U. Koren, S.K. Korotky. IEEE. J. Quantum. Electron., 22, p142, 1986

141. R.H. Stolen, E.P. Ippen. Appl. Phys. Lett., 22, p276, 1973
K. Iwatsuki, S. Nishi, M. Saruwatari, M. Shimizu. Electron. Lett., 26, p1, 1990
142. J.A. Valdmanis, G.A. Mourou, C.W. Gabel. Appl. Phys. Lett., 41, p211, 1982
143. S. Kobayashi, T. Kimura. IEEE Spectrum, p26, May 1984;
M.J. O'Mahony. J. Lightwave Tech. LT-6, p531, 1988
144. T. Saitoh, T. Mukai. IEEE J. Quantum Electron., 23, p1010, 1987
145. I.W. Marshall, P.D. Constantine. ECOC, Brighton, Paper MoB4-4, 1989
146. T. Saitoh, T. Mukai. Electron. Lett., 23, p218, 1987
147. Y Aoki.J. Lightwave Tech. LT-6, p1225, 1988
148. L.F. Mollenauer, K. Smith. Opt. Lett., 13, p675, 1986
149. K. Byron, D. Burns, R. Grant, G.T. Kennedy, C.I. Johnston, W.Sibbett. to be published in Electronics Letters.
150. D. Cotter. Electron. Lett., 18, p465, 1982;
N.A. Olsson, J.P. van der Ziel. Appl. Phys. Lett., 48, p1329, 1986
151. R.J. Mears, L. Reekie, I.M. Jauncey, D.N. Payne, Electron. Lett. 23, p1026, 1987;
152.M Brierley, S. Carter, P. France, J.E. Pederson. Electron. Lett., 26, p329, 1990
153. B.J. Ainslie, J.R. Armitage, S.P. Craig, B. Wakefield. IEE Conf. Publ. 292, Pt. 1, p62, 1988
154. Y. Kimura, K. Suzuki, M. Nakazawa. Electron. Lett., 25, p1656, 1989
155. M. Shimuzi, M. Horiguchi, M. Yamada, M. Okayasu, T. Takeshita, I. Nishi, S. Uehara, J. Noda, E. Sugita. Electron. Lett., 26, p498, 1990
156. M. Shimuzu, M. Yamada, M. Horiguchi, T. Takeshita, M. Okayasu. Electron. Lett., 26, p1642, 1990
157 S.P. Craig-Ryan, B.J. Ainslie, C.A. Millar. Electron. Lett., 26, p185, 1990;
S.T. Davey, D.L. Williams, D.M. Spirit, B.J. Ainslie. Electron. Lett., 26, p1149, 1990
158. L.F. Mollenauer, J.P. Gordon, M.N. Islam. IEEE J. Quantum Electron., 22, p157, 1987;
159. K.C. Byron. Electron. Lett., 23, p1324, 1987
160. M.J. Pettitt, A. Hadjifotiou, R.A. Baker. Electron. Lett., 25, p416, 1989
161. B.J. Ainslie, S.P. Craig, S.T. Davey. J. Lightwave Tech., LT-6, p287, 1988
162. D.L. Sipes. Appl. Phys. Lett., 47, p74, 1985
163. G.L. Harnagel, D.R. Scifres, H.H. Kung, D.F. Welch, P.S. Cross, R.D. Burnham. Electron. Lett., 22, p605, 1986
164. L. Goldberg, J.F. Weller. Appl. Phys. Lett. 50 (24), p1713, 1987
165. R.A. Baker, Private communication
166.B.S. Bhumbra, R.W. Glee, P.D. Greene, G.D. Henshall, C.M. Lowney, J.E.A. Whiteaway. Electron. Lett., 26, p1755, 1990
167. E. Desurvire, J.R. Simpson, P.C. Becker. Optics. Lett., 12, p888, 1987
168. M. Nakazawa, Y. Kimura, K. Susuki. Electron. Lett., 26, p548, 1990
170. C.G. Atkins, J.F. Massicott, J.R. Armitage, R. Wyatt, B.J. Ainslie, S.P. Craig-Ryan. Electron. Lett., 25, p910, 1989
171. R. Olshansky. Electron. Lett. 24, p1363, 1988
172. R.I. Laming, S.B. Poole, E.J. Tarbox. Opt. Lett., 13, p1084, 1988;
R.I. Laming, M.C. Farries, P.R. Morkel, D.N. Payne, P.L. Scrivener, F. Fontana, A. Righetti. Electron. Lett., 25, p12, 1989
173. M. Okayasu, T. Takeshita, M. Yamada, O. Kogure, M. Horiguchi, M. Fukuda, A. Kozen, K. Oe, S. Uehara. Electron. Lett., 25, p1563, 1989
174. W.D. Laidig, Y.F. Lin, P.J. Caldwell. J. Appl. Phys., 57, p33, 1985
175. R.G. Waters, J.J. Coleman. Tech. Dig. Conf. Lasers Electro-Opt. (CLEO), Anahiem, paper CMH1, 1990

176. M. Nakazawa, K. Sukuki, E. Yamada, Electron. Lett., 26, p2040, 1990;
K. Susuki, Y. Kimura, M. Nakazawa. Opt. Lett., 14, p 865, 1989
177. R.C. Alferness, S.K.Korotky, E.A.J. Marcatili. IEEE J. Quantum Electron., 20, p301, 1984
178. J.L. Jackel, J.J. Johnston. J. Lightwave Tech., LT-6, p1348, 1988
179. E.I. Gordon. Proc. IEEE, 54, p1391, 1966
180. U. Keller, K.D. Li, B.T. Khuri-Yakab, D.M. Bloom, K.J. Weingarten, D.C. Gerstenberger. Opt. Lett., 15, p45, 1990
181. L.D. Westbrook, A. W. Nelson, D.J. Fiddyment, J.S. Evans. Electron. Lett., 20, p225, 1984
182. P.G. May, W. Sibbett, J.R. Taylor. Appl. Phys. B., 26, p179, 1981
183. C.J. Koester, E. Snitzer. Appl. Opt., 3, p1182, 1963;
C.J. Koester. IEEE J. Quantum. Electron., 2, p580, 1966
184. S.B. Poole, D.N. Payne, M.E. Ferman. Electron. Lett., 21, p737, 1985
185. M. Shimitzu, H. Suda, M. Horiguchi. Electron. Lett., 23, p768, 1987
186. I.P. Alcock, A.I. Ferguson, D.C. Hanna, A.C. Tropper. Opt. Lett., 11, p709, 1986
187. W.J. Miniscalco, L.J. Andrews, B.A. Thompson, R.S. Quimby, L.J.B. Vacha, M.G. Drexhage. Elecron. Lett., 24, p29, 1988
188. R.J. Mears, L. Reekie, S.B. Poole, D.N. Payne, Electron. Lett., 22, p159, 1986
189. M.C. Brierly, P.W. France, C.A. Millar. Electron. Lett., 24, p539, 1988
190. M.C. Farries, P.R. Morkel, J.E. Townsend. Electron. Lett., 24, p709, 1988
191. L. Esterowitz, R. Allen, I. Aggarwal. Electron. Lett., 24, p1104, 1988
192. M.C. Brierly, P.W. France. Electron. Lett., 24, p539, 1988
193. D.C. Hanna, R.M. Percival, I.R. Perry, R.G. Smart, P.M.J. Suni, J.E. Townsend, A.C. Tropper. Electron. Lett., 24, p1111, 1988
194. J.E. Townsend, S.B. Poole, D.N. Payne. Electron. Lett., 23, p329, 1987
195. M. Monerie, J.Y. Allain, H. Poignant, F. Auzel. ECOC, Brighton, Paper TuB12-6, 1989
196. J.N. Sandoe, P.H. Sarkies, S. Parke. J. Phys. D: Appl. Phys., 5, p1788, 1972
197. E. Desurvire, J.R. Simpson. Opt. Lett., 15, p547, 1990
198. J.R. Simpson, J.B. MacChesney. Electron. Lett., 19, p261, 1983
199. R. Wyatt. Electron. Lett., 25, p1498, 1989
200. W.W. Rigrod. J. Appl. Pyhs., 36, p2487, 1965;
W.W. Rigrod. IEEE J. Quantum Electron., 14,, p377, 1978
201.W. Koechner. 'Solid State Laser Engineering', Springer-Verlag, Berlin, 1976
202. R. Ulrich, A. Simon. Appl. Opt., 18, p2241, 1979
203. S.B. Poole, D.N. Payne, R.J. Mears, M.E. Ferman, R. Laming. IEEE J. Lightwave Tech., LT-4, p870, 1986
204. E. Desurvire, J.R. Simpson. J. Lightwave Tech., LT-7, p835, 1989
205. C.G. Atkins, J.R. Armitage, R. Wyatt, B.J. Ainslie, S.P. Craig-Ryan. Opt. Comm., 73, p217, 1989
206. Y. Kimura, K. Suzuki, M. Nakazawa. Appl. Phys. Lett., 1988
207. J.G. Edwards, J.N. Sandoe. J. Phys. D: Appl. Phys., 7, p1078, 1976
208. C.J. Gaeta, M.J.F. Digonnet, H.J. Shaw. J. Lightwave Tech., LT-15, p1645, 1987
209. I.P. Alcock, A.C. Tropper, A.I. Ferguson, D.C. Hanna. IEE Proc. J., 134, p183, 1987
210. R.J. Mears, L. Reekie, I.M. Jauncey. Tech. Dig. Conf. Lasers Electro-Opt. (CLEO), Baltimore, Paper WD3, 1987
211. I.P. Kaminow, E.H. Turner. Appl. Phys., 7, p10, 1966
212. Q. Ren, K.J. Schomacker, T.F. Deutch, R. Birngruber, C.A. Puliafito. Tech. Dig. Conf. Lasers Electro-Opt. (CLEO), Anahiem, paper CTUH90, 1990

213. J.B. Schlager, Y. Yamabayashi, D.L. Fransen, R.I. Juneau. IEEE Photonics Technology Lett., 1, p264, 1989

214. L.C. Foster, M.D. Ewy, C.B. Crumley. Applied Physics Letters, 6, p6, 1965

215. J. Mark, L.Y. Liu, K.L. Hall, H.A. Haus, E.P.Ippen. Opt. Lett., 14, p48, 1989;

P.N. Kean, R.S. Grant, X. Zhu, D.W. Crust, D. Burns, W. Sibbett. Tech. Dig. Conf. Lasers Electro-Opt. (CLEO), Washington, DC, paper PD7-1, 1988

216. R.S. Grant, P.N. Kean, D. Burns, W. Sibbett. Tech. Dig. Conf. Lasers Electro-Opt. (CLEO), Anahiem, paper CTuH38, 1990

217. J.D. Kafka, T.M. Baer, D.W. Hall. Tech. Dig. Conf. Lasers Electro-Opt. (CLEO), Baltimore, paper FA3, 1989;

J.D. Kafka, T.M. Baer, D.W. Hall. Opt. Lett., 14, p1269, 1989

218. K. Smith, J.R. Armitage, R. Wyatt, N.J. Doran, S.M.J. Kelly. Electron. Lett., 26, p1151, 1990

219. Y. Suematsu. M. Seki, M. Yamaguchi, I. Mito, K.E. Kobayashi, K.O. Kobayashi. Electron. Lett., 19, p840, 1983;

R.S. Tucker, U. Koren, G. Raybon, C.A. Burrus, B.I. Miller, T.L. Koch, G. Eisenstein. Electron. Lett., 25, p621; 1989

220. G. Smith. PhD Thesis, University of St. Andrews, 1990

221. S. Sanders, L. Eng, J. Paslaski, A. Yariv. Appl. Phys. Lett., 56, p310, 1990

222. T.R. Chen, L. Eng, B. Zhao, Y.H. Zhuang, S. Sanders, H. Morkoc, A. Yariv. IEEE J. Quantum. Electron., 26, p1183, 1990

223. L.F. Mollenauer, B.M. Nyman, M.J. Neubelt, G. Raybon, S.G. Evangelides. Electron. Lett., 27, p178, 1990

224. G.P. Agrawal, N.A. Olsson, N.K. Dutta. Appl. Phys. Lett., 45, p119, 1984

225. M.L. Molbarsht. IEEE J. Quantum Electron., 20, p935, 1984

226. M.C. Brierly, P.W. France. Electron. Lett., 24, p935, 1988

227. W.J. Miniscalco. J. Lightwave Tech., LT-9, p234, 1991

## Publications

'Active modelocking of an external cavity GaInAsP laser incorporating a fibre-grating reflector', D. Burns, D.W. Crust, J.T.K. Chang, W. Sibbett, Electron. Lett., 24, p1439, 1988

'Enhanced moodelocking of colour-centre lasers using coupled-cavity feedback'
P,N. Kean, R.S. Grant, X. Zhu, D.W. Crust, D. Burns, W. Sibbett. Tech. Dig. Conf. Lasers Electro-Opt. (CLEO), Washington, DC, paper PD7-1, 1988

'Amplification of mode-locked semiconductor diode laser pulses in erbium-doped fibre amplifier', R.A. Baker, K.C. Byron, D. Burns, W. Sibbett, Electron. Lett., 25, p1131, 1989

'Modelocked InGaAsP semiconductor diode lasers', D. Burns, D.W. Crust, W. Sibbett, paper no. 146P , QE9, Oxford, 1989

'Modelocked external fibre cavity InGaAsP semiconductor lasers', D. Burns, R.A. Baker, D.W. Crust, K.C. Byron, W. Sibbett, Proc. IEEE Colloq. Dig. 1989/87, paper no. 11, 1989

'Active modelocking of an $Er^{3+}$:fibre ring laser', D. Burns, R.A. Baker, W. Sibbett, Tech. Dig. Conf. Lasers Electro-Opt. (CLEO), Anahiem, paper CFR5, 1990

'Controlled amplifier modelocked $Er^{3+}$ fibre ring laser', D. Burns, W.Sibbett, Electron. Lett., 26, p505, 1990

'Noise characterisation of a modelocked InGaAsP semiconductor diode laser', D. Burns, A. Finch, W. Sleat, W. Sibbett, IEEE J. Quantum Electron., 26, p1860, 1990

'Passive coupled-cavity, modelocked colour-centre lasers', R.S. Grant, P.N. Kean, D. Burns, W. Sibbett, Tech. Dig. Conf. Lasers Electro-Opt. (CLEO), Anahiem, paper CTuH38, 1990

'High-speed synchronously pumped Raman fibre amplification'
K. Byron, D. Burns, R. Grant, G.T. Kennedy, C.I. Johnston, W.Sibbett. to be published in Electronics Letters.

# Acknowledgements

I would like to thank my supervisor Professor Willson Sibbett for his patience and encouragement during my stay at St. Andrews. I would also like to thank Dr Kevin Byron for his enthusiasm and guidance with respect to the better curry houses in Bishop's Stortford area. Thanks are due to the many personalities at STL who have assisted me over the years. In particular, I am indebted to Robert Baker for his extreme patience and his everlasting supply of good humour.

I would also like to thank;

Dr Bill Sleat for his electronic wizardry,

Jimmy Lindsay, George Radley and Reg Gavine for 'turning' drawings into metal, and also for showing me 37 ways of killing myself on milling machines and lathes.

Margo and Babs.

Jegsy, Phil, Svitch, Rubin, Jonny, Dave, Dave, Dave, Dave, and all the 'W Squad' past, present and future.

Grand Master Stanners, Baggy, Shirls, Watty.

Mum, Dad and Bill.

Last, but in no way least, my wife Heather and wee Julie for putting up with me and cooking my dinner.